Numerical and physical modelling of bank retreat in gravel-bed rivers

Dissertation

submitted to and approved by the

Department of Architecture, Civil Engineering and Environmental Sciences
University of Braunschweig – Institute of Technology

and the

Faculty of Engineering
University of Florence

in candidacy for the degree of a
Doktor-Ingenieurin (Dr.-Ing.) /
Dottore di Ricerca in "Riduzione del Rischio da Catastrofi Naturali su Strutture ed Infrastrutture" *)

by
Laura Nardi
Born 29.07.1977
from Florence, Italy

Submitted on	18 March 2011
Oral examination on	10 May 2011
Professorial advisors	Prof. A. Dittrich
	Prof. M. Rinaldi

2011

*) Either the German or the Italian form of the title may be used.

ACKNOWLEDGMENTS

The following study was developed at the Dipartimento di Ingegneria Civile e Ambientale of University of Florence (Italy) and at Leichtweiß-Institut für Wasserbau of Technical University of Braunschweig (Germany) within the framework of the International Graduate College 'Mitigation of Risk due to Natural Hazards on Structures and Infrastructures'.

My best thanks to my Italian advisor Prof. M. Rinaldi for guiding me with his expertise through these years and for our fruitful discussions. He encouraged me to have the academic experience I always wanted to do when I had already abandoned this idea and he incited me to apply this Doctorate School.

In the same manner I would like to thank my German advisor Prof. A. Dittrich for supporting and giving me valuable feedback and helpful suggestions.

These results would have been impossible to achieve without the financial support of Prof. S. Lanzoni from the University of Padua. I am sincerely thankful for that.

I express thanks to Prof. S.E. Darby from School of Geography at the University of Southampton for providing me results of CSM tests and Dr. Jason W. Kean from the U.S. Geological Survey for helping me to better understand his model.

My students and friends, Serena Basile, Rosaria Scozzafava and Francesco Bonini deserve special thanks. They have largely contributed to this study.

My sincere gratitude to Lorenzo Campo for his practical help in programming and our stimulating discussions.

A huge thank to my family and friends and especially to Guido for his love, his imperturbable patience in accepting my absences and for supporting my decisions, always.

ABSTRACT

Bank erosion is a natural geomorphological process which affects a wide range of physical, ecological and socio-economic issues in the fluvial environment. Among the others, the impacts include loss of lands, damage to structure and infrastructures and dynamics of sediments, nutrients and contaminants. Hence, it is not surprising how riverbank retreat is closely related to the risk assessment.

Despite many progresses have been made in understanding and modelling bank erosion, further investigations are needed to better understand processes occurring on riverbank totally or partially composed of relatively coarse sediments. Therefore, the general aim of this study is to give a contribution in understanding and modelling processes, with particular focusing on gravel banks.

The study is organized to provide a general framework of analysis at different spatial scales, using as a reference study case the Cecina River (Pisa, Italy).

At the catchment scale, riverbank processes were studied with the specific aim to identify the variability of bank features (geometry and composition), the dominant mechanisms of retreat and their spatial distribution. Different methods to predict the lateral instabilities were also undertaken in order to pinpoint causes and factors which control the occurrence of different mechanisms of retreat.

At the reach scale, numerical models were employed with the aim of exploring methods for a combined analysis which couples different mechanisms of retreat, with particular focus on the inclusion of near-bank shear stresses. Moreover, based on results of the previous analyses, a framework for risk analysis due to bank erosion was developed.

The objective of the analyses carried out at the bank scale, was to better understand the basic processes occurring in relatively coarse bank sediments, in particular the occurrence of mass instability in the absence of fluvial erosion. In order to address the objective, a physical model of a bank composed by gravel and sand was built, and some experiments simulating the behaviour of the bank during a hydrograph were carried out. The tests allowed for the identification of different mechanisms of failure and for the analysis of the factor affecting non cohesive bank stability.

ZUSAMMENFASSUNNG

Die Ufererosion stellt einen natürlichen geomorphologischen Prozess in fluvialen Fließgewässern dar, der von großer Bedeutung für verschiedene ingenieurtechnische, ökologische und sozio-ökonomische Fragestellungen ist. Sie stellt einen wichtigen Prozess im Hinblick auf die Dynamik von Sedimenten, Nährstoffen und Schadstoffen in Fließgewässern dar und kann gleichzeitig aber auch zum Verlust von Land oder zur Gefährdung von Siedlungen und der Infrastruktur führen. Deshalb ist es nicht erstaunlich, dass der mit der Ufererosion verbundene Rückgang der Ufer in engem Zusammenhang mit der Risikobewertung steht.

Bis heute führten zahlreiche Untersuchungen zu einem verbesserten Verständnis der relevanten physikalischen Prozesse und somit zu einer verbesserten Modellierung der Ufererosion. Allerdings existieren, speziell im Hinblick auf die Erosion von relativ grobkörnigen Ufern, immer noch zahlreiche offene Fragestellungen. Das Ziel der Arbeit bestand deshalb darin, zum besseren Verständnis und zur verbesserten Modellierung der Erosion von Ufern aus kiesigem Material beizutragen.

Hierzu wurde anhand des Referenzgewässers des Cecina-Flusses in Italien ein übergeordneter Rahmen für die Analyse der relevanten Prozesse unter der Berücksichtigung verschiedener räumlicher Skalen geschaffen. Auf der Skala des Einzugsgebiets wurden die entsprechenden Prozesse mit dem spezifischen Ziel untersucht, die Variabilität der Ufereigenschaften (Geometrie und Zusammensetzung), die dominanten Mechanismen für den Rückgang der Ufer als auch deren räumliche Verteilung zu identifizieren. Mittels verschiedener Methoden zur Vorhersage lateraler Instabilitäten wurden die relevanten Faktoren und Prozesse aufgezeigt, welche die verschiedenen Mechanismen der Ufererosion kontrollieren.

Auf der Flussabschnittsskala wurden anhand numerischer Modellierungen Methoden untersucht, die zu einer adäquaten kombinierten Analyse der verschiedenen Erosionsmechanismen herangezogen werden können. Ein spezielles Augenmerk wurde hierbei auf die Schubspannungen in Ufernähe gelegt und es wurde ein Rahmen für die Risikoanalyse im Hinblick auf die Ufererosion entwickelt.

Auf der Uferskala stand die Untersuchung der relevanten physikalischen Prozesse im Vordergrund, welche die Erosion von grobkörnigen Ufersedimenten und insbesondere das Auftreten von Uferrutschungen dominieren, wenn kein Sedimenttransport im Gewässer vorliegt. Zu diesem Zweck wurde ein physikalisches Modell eines aus Kies und Sand bestehenden Ufers aufgebaut. Die Modelluntersuchungen, bei denen die Stabilität des Ufers infolge des Strömungsangriffs während eines Hochwasserereignisses unter Berücksichtigung der Ganglinie untersucht wurde, führten zur Identifikation verschiedener Versagensmechanismen und wurden zur Analyse von Faktoren herangezogen, die die Stabilität von nicht kohäsiven Ufern beeinflussen.

TABLE OF CONTENTS

LIST OF FIGURES

LIST OF TABLE

LIST OF SYMBOL

Variable	Meaning	Unit
A	Drainage area	[km^2]
A	Cross-sectional flow area	[m^2]
A	Plan view area of rough element	[m^2]
b	Wake thickness	[m]
B	Length of roughness element	[m]
c	Total cohesion	[N/m^2]
c_a	Apparent cohesion	[N/m^2]
c'	Effective cohesion	[N/m^2]
C	Coefficient of expansion	[-]
C_s	Chezy coefficient	[-]
C_D	Drag coefficient	[-]
D_{50}	Median grain size of sediment	[m]
F	Form drag	[N]
Fr	Froude number	[-]
FS	Factor of safety	[-]
F_w	Hydrostatic force exerted by the surface water on the vertical part of the slip surface	[N/m]
g	Acceleration of gravity	[m/s^2]
h_e	Energy head loss	[m]
H	Water depth	[m]
H	Bank height	[m]
H	Height of element roughness	[m]
H_{reg}	Height of element roughness of regular sequence	[m]
I_s	Vertical interslice shear forces	[N/m]
I_n	Horizontal interslice normal forces	[N/m]
k_d	Erodibility coefficient	[m^3 /N s]
k_s	Effective roughness	[m]
K	Channel conveyance	[m]
L	Channel length	[m]
L	Length of slip surface	[m]
L	Loss	[€/m]
L_{lob}, L_{ch} , L_{rob}	Reach lengths left, right and main channel	[m]
n	Manning's roughness coefficient	[$s/m^{1/3}$]
N	Total normal force per unit channel length	[N/m]

P	Wetted perimeter	[m]
P	Hydrostatic-confining force	[kN/m]
q	Flow discharge per unit width	[m^3/s]
Q	Flow discharge	[m^3/s]
Q_2	Flow discharge with return period 2 years	[m^3/s]
$\bar{Q}_{lob}, \bar{Q}_{ch}, \bar{Q}_{rob}$	Flow discharge in main channel, left and right overbank	[m^3/s]
r	Coefficient of slope reduction	[-]
R	Hydraulic radius	[m]
R	Risk	[€/m year]
s	Specific gravity	[-]
S	Shear force at the base of the failure block per unit channel length	[N/m]
S	Channel slope	[-]
S_0	Initial slope at upstream section	[-]
S_f	Friction slope	[-]
$\bar{S}_f$	Average friction slope	[-]
u_a	Pore air pressure	[kPa]
u_b	Velocity at the top of the wake	[m/s]
u_w	Pore water pressure	[KPa]
u_{ref}	Reference velocity	[m/s]
u_*	Shear velocity	[m/s]
u_{*IBL}	Shear velocity within internal boundary layer	[m/s]
u_{*T}	Shear velocity in the outer region	[m/s]
U	Depth-averaged velocity in x direction	[m/s]
U	Hydrostatic uplift force on saturated portion of block	[kN/m]
V	Depth-averaged velocity in y direction	[m/s]
$\bar{V}$	Averaged velocity	[m/s]
w	Channel width	[m]
W	Weight	[kN]
Y	Water depth	[m]
z	Distance from the boundary	[m]
z_{0SF}	Local roughness height without topographic element	[m]
z_{0T}	Local roughness height due to skin friction and drag form	[m]
Z	Elevation of the main channel inverts	[m]

α	Angle of failure plane	[°]
a_1, a_2	Velocity weighting coefficients	[-]
β	Bank angle (from horizontal)	[°]
γ	Unit weight of material	[N/m^3]
γ_w	Unit weight of water	[N/m^3]
γ_s	Unit weight of saturated material	[N/m^3]
γ_d	Unit weight of dry material	[N/m^3]
δ	Boundary layer height	[m]
ε	Fluvial erosion rate per unit time and unit bank area	[m/ s]
θ	Volumetric water content	[m^3/m^3]
κ	Von Karman's constant	[-]
λ	Spacing between crest	[m]
λ_{reg}	Spacing between crest of regular sequence	[m]
ϕ^*	Equivalent friction angle of material	[°]
ϕ'	Effective friction angle	[°]
ϕ^b	Angle expressing the increase of strength due to matric suction	[°]
ρ	Fluid density	[kg/m^3]
σ	Normal stress	[KPa]
σ	Stramwise length scale	[m]
σ_{reg}	Stramwise length scale of regular sequence	[m]
τ	Shear stress exerted by the flow	[N/m^2]
τ	Shear strength	[kPa]
τ_D	Shear stress due to Form drag	[N/m^2]
τ_{SF}	Shear stress due to Skin drag	[N/m^2]
τ_c	Critical shear stress	[N/m^2]
τ_{exc}	Excess shear stress	[N/m^2]
ω	Unit stream power	[Watt/m^2]
Ω	Total stream power	[Watt/m]

1. Introduction

1.1 Study rationale

With an ever-increasing emphasis on alluvial channel systems worldwide through the continuing encroachment of urban areas, a need exists for the assessment of channel conditions. Papanicolaou et al. (2008) estimated the damage in infrastructures to be nearly $1.1 billion in the Midwest during the last decade, while according to a technical report (Department of the Army U.S. Army Engineer District, Alaska, 2006), the city of Kenai has an average annual loss of $151,000 due to reduced value of lands, buildings, relocation of buildings and utilities caused by the erosion of banks along the river.

Bank erosion is a natural geomorphological process which occurs in dynamically stable systems as adjustments of channel size and shape are made to convey changes in discharge or sediment supply. Thus, it is a key process in fluvial dynamics affecting a wide range of physical, ecological and socio-economic issues in the fluvial environment. These impacts include the establishment and evolution of river and floodplain morphology and their associated habitats (e.g. Hooke, 1980; Millar and Quick, 1993; Darby and Thorne, 1996; Barker et al., 1997; Millar, 2000; Goodson et al., 2002), turbidity problems (e.g. Bull, 1997; Eaton et al., 2004), sediment, nutrient and contaminant dynamics (e.g. Reneau et al., 2004), loss of riparian lands (e.g. Amiri-Tokaldany et al., 2003), and associated threats to flood defence and transportation infrastructure (e.g. Simon, 1995).

Knowledge of spatial and temporal trends and dominant processes of channel adjustment is central to plan and implement maintenance or mitigation measures to reduce economic and environmental risk associated with the channel instability.

1.2 Aims and methods of the research

During recent years, progresses have been made in understanding and modelling bank erosion, as emphasized by the increasing number of bank erosion investigations; however several aspects are not jet understood.

Among the others, the knowledge of processes occurring on riverbank totally or partially composed of relatively coarse sediments requires further investigations In fact, the majority of studies dealing with mass failure focused on cohesive banks which are frequent on sandy rivers and tidal channels. In gravel-bed rivers, banks

are often composite, with a basal layer composed of granular sediments (gravel and cobbles mixed with sand). The complex behaviour of such type of banks is often oversimplified. In fact, morphodynamic models of river planform evolution traditionally considered fluvial entrainment and erosion as the dominant, if not exclusive, mechanisms of retreat. Nonetheless, field evidences suggest that processes on coarse sediments are extremely variable with a combination of fluvial erosion processes and small-scale mass failures. Therefore, the general aim of this study is to give a contribution in understanding and modelling processes, with particular focus on gravel banks. This study is organized to provide a general framework of analysis at different spatial scales, by exploring the potential of available methods and physical modelling. Indeed, riverbank retreat processes can be studied at different spatio-temporal scales. Couper (2004) found that there is a positive relationship between the time and space scale, as smaller spatial scale is commonly combined with shorter temporal scale. The spatial scale may vary from the single bank (e.g. Osman and Thorne, 1988) to the whole catchment network (e.g. Lawler et al., 1999), while the temporal scale may range from the single flow event up to centuries. Within the riverbank research, a nested hierarchy of scale, where each level contains the level below it, is often applied. Models, observations, data or field measurements are dependent upon the scale of investigation (Kirkby et al., 1996) and results derived at one scale cannot generally be transferred to another (Lam and Quattrochi, 1992). Moreover, different factors may play the dominant role in the analysis depending on the spatio-temporal scale.

For all the three spatial scales, the Cecina River was selected as a reference study case, due to various reasons, including: (1) the presence of actively eroding composite banks, consisting of a basal layer of packed and slightly cemented gravel, with a wedge of loose gravel and cobble at the bank toe, and an upper fine-grained (predominantly sandy silt) cohesive portion of the bank; (2) its relatively low degree of urbanization, and (3) existing research activity already completed in the last years on the riverbank processes (Rinaldi et al., 2008a; Luppi et al., 2009) and on channel adjustments over the last decades (Rinaldi, 2003; Surian et al., 2009).

At the catchment scale, riverbank processes along the entire length of the river were studied with the specific aim to identify the variability of bank features (geometry and composition), the dominant mechanisms of retreat and their distribution.

Different methods to predict the lateral instabilities were also undertaken in order to pinpoint causes and factors which control the occurrence of different mechanisms of retreat.

Moving to the reach scale, while it is well established the importance of interactions between processes (namely, weakening, mass failure and fluvial erosion processes), most of the studies tend to adopt reductionist approaches that focus on a single set of processes (Rinaldi and Darby, 2008). Recent researches on bank erosion modelling carried out by integrating different numerical models on a bank of the Cecina River (Rinaldi et al., 2008a; Luppi at al., 2009) represent some of the few exceptions. The focus was on the short time scale (single flow event scale) and bank dynamics modelling aimed to address specific questions regarding mutual role of different processes. However, modelling these processes at the spatial scale of a meandering reach and at a time scale of years or decades with the previous approach can be excessively difficult and not appropriate to address more general questions about spatial and temporal distribution of instability factors and causes. Therefore, the aim of the present research at the reach scale was to explore other possible modelling methods which are more suitable for a combined bank stability analysis and to address previous limitations, with particular focus on the inclusion of near-bank shear stresses. For this purpose a more straightforward approach has been used in this work, with the objective to develop and apply a rational framework of modelling interaction at the reach scale. The methodological framework is based on the following components: (1) application of hydrodynamic models to characterize the flow velocity pattern and to determine the values of shear stresses in the area adjacent to the banks of interest; (2) implementation of a near-bank shear stresses model for determining form drag on small-scale topographic bank features and quantifying the near-bank flow field; (3) fluvial erosion modelling based on the excess of shear stresses exerted by the flow on the bank surface and using specific erodibility parameters obtained via calibration; (4) bank stability analysis carried out by using specific algorithms developed for river banks which employ standard limit equilibrium methods. An example of coupling mass failure and erosion processes is also provided. Moreover, based on results of the previous analyses, a framework for risk analysis of land loss due to bank erosion was developed.

Turning to the perspective of bank erosion at the bank scale, although progresses have been made in understanding and modelling processes, however several

problems and aspects are not yet understood. As aforementioned, the mechanisms of bank instability in relatively coarse riverbanks (mainly composed by gravel) require further investigation. The objective of the present study at the bank scale was to obtain a better comprehension of the basic processes occurring in relatively coarse bank sediments, with emphasis on mass instability in the absence of fluvial erosion. In order to address this objective, a physical model of a bank composed by granular relatively coarse sediment was built, and some experiments simulating the behaviour of the bank during a hydrograph were carried out. The tests allowed for the identification of different mechanisms of failure and for the analysis of factors affecting non-cohesive bank stability.

1.3 Research outline

The present study is structured into 3 main parts following the general and specific aims aforementioned. Each part in turn, has been divided into chapters. Chapter 2 represents an exception: it is not included in any one of the part given that it provides an overview of riverbank processes and methods at the state of the art. Part I comprises Chapter 3, which describes the Cecina catchment and includes the analysis of riverbank retreat processes observed along the entire length of the river.

Part II deals with the analyses at the reach scale and consists of Chapter 4, 5 and 6. In details, Chapter 4 describes hydraulic, near-bank shear stress and stability models employed in further analyses. Chapter 5 provides a description of the selected reach along the Cecina River and collection of data required by the models. The methodological framework obtained by coupling different models, the results and their interpretation, together with the framework for risk analyses due to fluvial erosion are reported in Chapter 6.

Chapter 7 and Chapter 8 compose Part III, which illustrate the experimental analyses carried out in order to investigate processes at the bank scale. Specifically, Chapter 7 provides the description of the experimental setup, the preliminary and main tests, while results and their interpretation are stated in Chapter 8.

A general conclusion, in which all findings are combined and summarized, is finally presented in Chapter 9.

2. Key concepts in riverbank processes

2.1 Riverbank retreat in the risk context

[..] channel changes, such as meander migration, and bank erosion, may constitute a greater hazard than overbank flow in some areas. (Federal Emergency Management Agency, 1999)

2.1.1 Riverbank retreat in anthropized areas

Riverbank erosion is one of the major and most controversial management issues in alluvial corridors. Although many negative impacts of bank erosion were highlighted through extensive literature, whereas a reconsideration of its effect is taking place and the awareness of beneficial aspects is nowadays widely accepted.

The adverse impacts of bank retreat include loss of lands (e.g. Amiri-Tokaldany et al., 2003), damage to property and infrastructure (Piégay et al., 1997) as shown in Figure 2-1, turbidity problems (e.g. Bull, 1997; Eaton et al., 2004), and sediment, nutrient or contaminant dynamics (e.g. Reneau et al., 2004). Downs and Simon (2001) found bank erosion have also negative effects on channel morphology and flood carrying capacity further downstream by means of the supply of sediment and large woody debris.

The cost of protecting U.S. stream banks in 1981 was about U.S.$l billion (U.S. Army Corps of Engineers, 1983) and according to more recent technical reports (Department of the Army U.S. Army Engineer District, Alaska, 2006), the city of Kenai incurs an average annual loss of $151,000 due to reduced value of lands and buildings and relocation of utilities, caused by the erosion of banks along the rivers. Therefore, it is not surprising that bank erosion is considered as a natural hazard by the society (National Rivers Authority, 1994), even ‘greater than overbank flow in some areas’ (Federal Emergency Management Agency, 1999) although, due to its time-continuous nature, generally it does not imply human losses.

Hutton and Emdad Haque (2003), in their analysis on riverbank erosion-induced displacement in the floodplains of Bangladesh, pointed also to the need of integrating a social, cultural and psychological context into hazard analysis and mitigation studies.

Figure 2-1 Damage of fluvial erosion on (A) structure (Tarbuck and Lutgens, 2002), and (B) infrastructure (Pignone (SP), Italy, October 2011).

In contrast with previous aspects, in certain context bank retreat can be regarded as a positive phenomenon, being a key factor in the morphodynamic equilibrium of meandering or braiding rivers (Bravard et al., 1986; Church, 1992). Beneficial aspects mostly involve ecological issues (Piégay et al., 1997, 2005). For instance, Florsheim et al. (2008) found bank processes being a 'desirable attribute' of rivers, since they play an important role in promoting riparian vegetation and in creating dynamic habitats which are crucial for aquatic and riparian plants and animals. Furthermore, in incised rivers preservation of bank erosion can contribute to self-restoration by supplying coarse sediments (e.g. Bravard et al., 1999).

A reconsideration of traditional policies for managing river bank erosion is currently taking place driven by the increased awareness of the unsustainable nature

of some engineered bank protections (Piégay et al., 2005). In fact, besides the considerable economic costs of providing protections, by reducing the supply of sediment to the river (e.g. in the Sacramento River, for example, approximately 60% of the total sediment inflow is attributable directly to bank erosion, US Army Corps of Engineers 1983), such protections may either initiate local incision which, in turn, can undermine the structure and/or merely relocate bank erosion downstream (Odgaard, 1989; Thorne, 1992). Moreover, traditional bank protections (e.g. levees, rip-rap or armoring protections), by promoting incision, often cause the channels to be disconnected from their floodplains (Buijse et al., 2002) and induce impoverishment of biodiversity.

Aiming to take account also for ecosystem services and other benefits in the cost-benefit analyses of bank protections, new strategies were recently followed: river managers are increasingly adopting the idea of allowing rivers to migrate freely within a defined corridor, property rights within the corridor usually being obtained either by negotiation with land owners or by buying the land outright (Piégay et al., 1994, 1996a, 1996b, 2005). This solution appears a compromise between people's land use expectations and river dynamics.

The erodible corridor concept, defined as space of mobility, has been introduced in French legislation. Piégay et al. (2005) described the evolution of such legislation dealing with the areas located nearby the rivers. Particularly relevant is the décret 2002-202 (13 February 2002) which modifies the rules authorizing bank protection structures greater than 50 m (for rivers less than 7.5m wide) or 200 m (for rivers wider than 7.5 m) in length. The law indicates that bank protections must not significantly reduce the 'space of mobility' of the channel, the corridor being defined on the basis of a historical analysis of channel mobility (Piégay et al., 2005). It becomes clear how the definition of the extent of the erodible corridor is a crucial point in management issues.

A detailed overview of different geomorphic tools that are available to define the extent of the erodible corridor has been proposed by Piégay et al. (2005). These tools, based on geomorphological analyses, include simple rules of thumb such as evaluation of the equilibrium meander amplitude (Malavoi et al., 1998), analyses on historical maps and sequential aerial photographs based on GIS technology to overlay different time series (Downward et al., 1994, Marston et al., 1995;Wasklewicz et al., 2004), and 2D or 3D hydromorphological modelling (e.g.

Lane, 1998; Mosselman, 1998; Darby et al., 2002; Nagata et al., 2002; Olsen, 2003) to predict planform changes in alluvial plains.

Piégay et al. (2005) also recognized that the erodible corridor concept is not universally suitable, depending on the extent of fluvial erosion and on a cost-benefit analysis. Its applicability has to be verified in each particular case.

2.1.2 Risk management

Risk management represents an important strategy whenever a certain event with a certain probability of occurrence can lead to damages and losses of a system. The multidisciplinary nature of analysis and management of natural disaster often leads to misunderstanding within the scientific community. Pliefke et al. (2007) made an attempt to remove ambiguities and proposed a risk management framework which includes three main components, namely: risk identification, risk assessment and risk treatment. Each component, in turn, comprises different procedures, as described in Figure 2-2. In the following descriptions definitions of the elements composing the risk management chain of Figure 2-2 will be adapted to the context of the present study specific issue.

The *risk identification* represents the first phase of the procedure and consists in defining the spatial domain and identifying all the sources of events that are able to harm the system. Considering the channel migration issue, the spatial domain may range from a specific structure or infrastructure next to the river to an anthropized area encroached by the river at a certain reach or, in a wider perspective, to the entire system at the catchment scale. In the latter case, the analyses will interest unconfined valleys where the river is free to migrate. Once the boundaries that circumscribe the system are defined, the *Risk Assessment* phase may be undertaken. The first step of this analysis is the identification and quantification, in terms of intensity and frequency, of each *Hazard* affecting the system (*Hazard analysis*). The hazard is represented by a certain ranges of discharges flowing within the selected system which are able to produce net positive excess shear stress for prolonged periods. The frequency analysis of excess shear stress depends on the probability distribution function of flow discharge and from the relation between the latter and the shear stresses exerted on the riverbank.

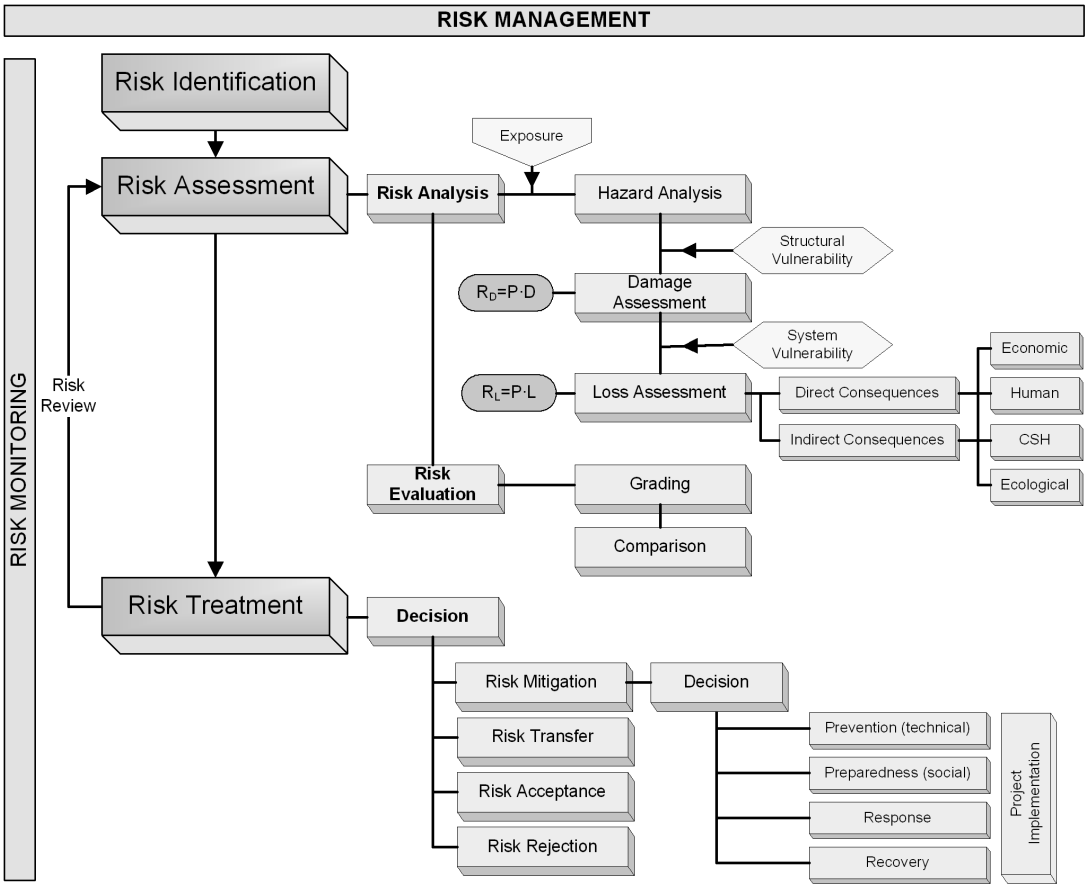

Figure 2-2 Overview of the whole risk management process (Pliefke et al., 2007).

As it will be described in Section 6, this relation is not monotonically increasing differently from what, in first rough approximation, can be assumed for the relation discharge-water stage when dealing with flood risk.

The *Damage* is defined and quantified by mean of the *Damage Assessment* procedure. Depending on the degree of anthropization of the system, the damage can be represented by the reduction of areas available for human activities, by harms to structures and infrastructures or damages to ecosystem. The latter can be due to (a) increasing turbidity or (b) release of nutrients and/or fertilizers present in the surrounding cropped lands. The relation between the hazard intensity and the resulting damage is called *Structural Vulnerability* and provides indications on the degree of susceptibility of an *Element at Risk* (EaR) towards the impact of the hazard. The elements at risk, represented by the land itself or by the structures and infrastructures adjacent to the river, are defined through the concept of *exposure*, represented by the distance of the element from the bank.

The structural vulnerability is represented by the geomorphological features of the bank subject to erosion, such as strength of the material represented by the

erodibility parameters and the shear strength of sediments (see following Sections). By means of the *Loss Assessment* the damage can be quantified in monetary terms providing the economic *Loss*. However, the loss is not exclusively related to monetary consequences. In fact, it can be divided into *direct* and *indirect consequences* which, in turn, may be further divided into sub-classes, e.g. economic, human, cultural or ecological. Not all these classes of loss may be quantified in tangible terms. Tangible losses, which are the economic consequences (as they can be referred to monetary value), can be estimated in fluvial erosion risk through (a) the price of lands or (b) harmed structures and infrastructure and (c) costs for the damaged structures relocation. Conversely to other natural hazards, such as floods or earthquakes, fluvial erosion does not necessarily occur in combination with extreme events (for extreme discharges the perspective of fluvial erosion risk is combined with flood risk), as it will be described in Chapter 6. Therefore human injuries and fatalities are rare.

If the only consequence of fluvial erosion is the reduction of land available for human activities, the *Structural Risk*, defined by the product of the annual probabilities of occurrence of the hazard and the damage, can be expressed in m^2/m (eroded area per bank length unit), whereas the *Total Risk*, represented through the product of annual probabilities of occurrence of the hazard and loss, may be quantified in terms of value of agricultural lands lost (€/m).

Subsequent to the completion of the risk analysis, the *Risk Evaluation* procedure, which consists of defining different classes of risk *comparable* and *grading* them, is undertaken.

Grading risks allows stakeholders to make *decisions* about how to handle the risk. This procedure is called *Risk Treatment*. Common decisions are *Risk Mitigation*, *Risk Transfer*, *Risk Acceptance* or *Risk Rejection*. Risk mitigation is generally addressed to the reduction of structural vulnerability. Channel migration can be mitigated through hard engineered bank protections, such as riprap armouring or rock gabions or bioengineering strategy, mostly based on vegetative coverage of riverbank in order to provide underground soil reinforcement and surface protection from scour. The aforementioned policy of negotiating lands within the potential erodible corridor, can be regarded as a risk acceptance strategy.

2.2 Riverbank processes

Riverbank retreat can be considered as the product of three interacting mechanisms, namely, subaerial weakening and weathering, fluvial erosion, and mass failure (Thorne, 1982; Lawler, 1992). Within a river basin downstream process, three processes/domains may be identified: subaerial processes dominating the upper reaches, fluvial erosion prevailing in the middle reaches, and mass failure prevailing in the lower reaches of the river (Lawler, 1992).

2.2.1 Subaerial processes

For long time sub-aerial processes have been thought only as preparatory mechanisms, weakening the bank face prior to fluvial erosion. More recent studies (Lawler, 1993; Prosser et al., 2000; Couper and Maddock, 2001) demonstrated that subaerial processes are underestimated as erosive agents.

Subaerial processes are the result of local climate and include wetting and drying or freezing and thawing. Wetting may occur as a consequence of high flows, groundwater rise, and infiltration of precipitation (Lawler et al., 1997). It results not only in an increase of the weight of the bank, but also in a positive pore water pressure. Both of these factors may reduce the bank stability with respect to the mass failure mechanism (Darby and Thorne, 1996).

Desiccation of the bank surface leads to soil cracking and exfoliation (Lawler et al., 1997). Thus, as well as the wetting process, it is responsible for a reduction in bank stability.

Lawler et al. (1997) recognize that freeze–thaw processes have the greatest influence on the erodibility of cohesive soils, as they affect porous structure, soil water content and soil composition (Gatto, 2000). These processes occur in streambank soils due to the freezing of soil moisture during cold nights and subsequent thawing from warmer daytime temperatures.

Although sub-aerial processes are recognized to be important in preparing bank material to erosion, as well as direct erosion (Couper and Maddock, 2001), few studies tried to quantify their impact; among these, Costard et al. (2003) proposed a one-dimensional model to estimate thermal erosion efficiency.

2.2.2 Fluvial erosion

Fluvial erosion corresponds to the detachment of grains, or breakdown of grain aggregates, from the bank surface and their subsequent removal by the flow (Thorne and Osman, 1988). In general, fluvial erosion rates depend on the near-bank flow intensity and physical characteristics (i.e., the erodibility) of the bank material.

Ikeda et al. (1981) assumed that the rate of bank retreat is proportional to the excess near-bank velocity, which is the difference between the near-bank depth-averaged velocity and the reach-averaged velocity. Consequently, the bank retreats when the excess near-bank velocity is greater than zero; otherwise, the bank advances. Variations in bend geometry and bank material properties are taken into account through a dimensionless coefficient. This method was adopted by Odgaard (1989), Crosato (1990), Larsen (1995), and Constantine et al. (2009). Odgaard (1989) explained the patterns of bend migration, combining the Ikeda model with a model for flow in bends with constant curvature. Constantine et al. (2009) used the Ikeda model attempting to clarify the extent to which the rate of bank retreat depends on physical characteristics of the channel boundary materials. The authors used measured data from the Sacramento River, obtained through jet-test apparatus. They found that the variability of the erodibility parameters explains much of the variability in the rates of retreat.

Hasegawa (1989) related the bank erosion rate to the excess velocity which was defined as the difference between near-bank and centerline depth-averaged flow velocity.

Duan (2005) proposed a method for calculating the rate of bank erosion for cohesive banks that integrates both basal erosion and bank failure processes. This approach suggests that bank erosion takes place when the rate of entrainment of bank surface particles is greater than their rate of deposition. Duan (2005) found that the entrainment rate is the product of a first term depending on bank material properties and lift coefficient, and a second term depending on the difference between friction velocity at the bank surface and critical friction velocity for entrainment. The latter term can include the effects of cohesive forces. However analytical expressions of these forces are not available and they should be determined by experimental and field data.

The excess shear stress model proposed by Partheniades (1965) and Arulandan et al. (1980) represents one of the most widely accepted models to estimate fluvial

erosion rates. It was used to predict channel erosion in models such as CONCEPTS (Conservational Channel Evolution and Pollutant Transport System), a model proposed by Langendoen (2000), in the Bank-Stability and Toe-Erosion Model (BSTEM) developed by Simon et al. (2000) or in the fully coupled fluvial erosion and bank stability analyses (Darby et al., 2007; Rinaldi et al., 2008a; Luppi et al., 2009).

According to the excess shear stress model, the fluvial erosion rate (ε) is proportional to the erodibility parameter of the sediments and to the difference between the shear stress exerted by the flow at the boundary and the critical shear stress that is characteristic of the bank material. Therefore, the fluvial erosion rate per unit time and unit bank area is defined as following:

$$\varepsilon = k_d(\tau - \tau_c)^a \tag{2.1}$$

where τ is the boundary shear stress exerted by the flow on the bank, τ_c is the critical shear stress, k_d is the erodibility parameter, and a is a dimensionless coefficient empirically derived and generally assumed equal to 1.0.

Factors influencing the erodibility depend on the bank material properties and, more specifically, whether the sediments are cohesive or non-cohesive (Lawler et al., 1997). In the case of cohesive material, the transport is governed not only by hydrodynamic forces (e.g., drag and lift), but also by electrochemical inter-particle forces (e.g., van der Waals bonding and Coulombic repulsion); thus, the resistance to the entrainment depends on several factors, including clay and organic content, pH and composition of interstitial fluids (Arulanandan et al., 1980; Grissinger, 1982). Due to the difficulties to take into account all these factors, there are few theoretical or empirical models and their use is limited. This explains why erodibility parameters for cohesive material are mainly measured through jet testing (Hanson, 1990; Hanson and Simon, 2001). Recently, the Cohesive Strength Meter (Tolhurst et al., 1999, Vardy et al., 2007) has been used to measure the critical shear stress (Darby et al., 2010).

By mean of submerged jet-test device, Hanson and Simon (2001) carried out 83 in-situ measures along several streams in Nebraska, Mississippi and Iowa and developed the following relation between critical shear stress (τ_c) and the erodibility coefficient (k) for cohesive silts, silt-clays and clays:

$$k = 2 \cdot 10^{-7} \tau_c^{-0.5} \tag{2.2}$$

The shear stress required to entrain non-cohesive sediments are in general lower than those necessary for cohesive material. In the case of non-cohesive material, such as sands or gravels, resisting forces are primarily dependent on the weight of the particles. For these sediments, the erodibility parameters are modelled with the same methods that are used to predict the entrainment of bed sediments, although with modifications to take into account the effect of the bank angle on the downslope component of the particle weight (Lane, 1955). Non-cohesive particles composing the bottom layer of composite banks often show some degree of packing and cementation due to the weight of the upper cohesive layer and to fluid circulation. In order to take account for these factors, Millar and Quick (1993) (Equation 2.4) and Millar (2000) proposed an empirical coefficient based on the analysis by Lane (1955). Bank composed of packed gravels can be stable with angles considerably higher than the angle of repose of the correspondent loose sediment.

$$\frac{\tau_c}{\gamma_w(s-1)D_{50}} = 0.048 tan\phi^* \sqrt{1-\frac{sin^2\beta}{sin^2\phi^*}} \tag{2.3}$$

In Equation (2.3), τ_c (Pa) is the critical shear stress for the bank sediments; s is the specific gravity of the sediment (2.65 assumed); γ_w (N/m^3) unit weight of water, assumed here to be 9810; D_{50} (m) is the median grain size of bank material; ϕ^* (°) is an equivalent friction angle of material, estimated from the steepest angle that the bank forms at the bankfull waterline and β (°) is the bank angle measured from the horizontal.

The knowledge of the boundary shear stress generally represents a challenging part of studies dealing with riverbank retreat. In fact, the near-bank shear stresses can largely vary both in space and in time, depending on such factors as the bank geometry (which is highly variable itself), cross-section size and shape, channel curvature, and flow stage. Moreover, direct measures are often impracticable due to the hazardous nature of collecting data during flow event responsible for the channel retreat (Rinaldi and Darby 2008). Thus, often, the only viable way to predict the shear stress is by means of hydraulic models. A rough estimation can be obtained by assuming near-bank shear stress distributions derived from laboratory channels experiments (e.g. Leutheusser, 1963; Kartha and Leutheusser, 1972; Simons and Senturk, 1977; Knight et al., 1984). These distributions have been coupled with one-dimensional hydraulic models (Rossi Romanelli et al., 2004;

Darby et al., 2007). Nevertheless, they have been derived from tests in flume, so they cannot represent complex geometries as those present in natural banks. Thus, they should be applied prudently. An alternative is represented by the application of CFD model. Several progresses have been achieved in the field of hydrodynamic modelling, as demonstrated by the increasing diffusion of a wide range of numerical codes. Two-dimensional models have been used for sediment routing (Wiele et al., 1996; Wiele and Torizzo, 2005), investigation of geomorphic processes (Miller, 1995; Rathburn and Wohl, 2003), and in the design of river restoration projects (Wheaton et al., 2004a, b). Several two-dimensional models are available. Among them, River2D developed by the University of Alberta (Steffler and Blackburn, 2002) is a finite element two-dimensional, depth-averaged hydrodynamic model. It was employed in restoration programs (Wu and Mao, 2007; Boavida et al., 2009; Lee et al., 2010) or to predict hydraulics with a partial or total ice cover (Katopodis and Ghamry, 2007). TELEMAC-2D represents another example of two-dimensional depth-averaged flow model which uses semi-implicit finite element techniques to solve St. Venant equations (Hervouet and Bates, 2000). Among the other applications, it was employed to simulate the transport of plume pollutant and to produce the quality indicator map (Awad and Darwich, 2009).

Although 2D codes overcome some of the physical constraints present in one-dimensional models, only 3D models are able to capture the flow field in the vertical and horizontal directions.

Wilson et al. (2003) compared the accuracy of the 2D depth-averaged code TELEMAC-2D with that of the 3D code SSIIM (Olsen, 2002) in the numerical simulation of free surface flows. For both codes a standard k-ε turbulence model was employed to simulate the flow field, and their assessment was based on the prediction of depth-averaged velocity traverses around a meander bend. Both codes predicted the lateral distribution of depth-averaged velocity in the main channel with reasonable accuracy at relatively low flow depth, with the 3D code predicting better than the 2D code. At a higher flow depth no extra accuracy in the prediction of depth-averaged velocity was gained from the 3D model with respect to the 2D model, although the 3D model predicted the correct location and direction of secondary currents.

A number of public domain or commercial 3D codes are currently available. To solve the Navier- Stokes equations which govern fluids flow, different CFD models apply different schemes of discretization. These available methods are alternatively

based on a (a) finite difference (e.g. TRIVAST by Cardiff University; Trim3D, Cassuli and Cattani, 1994); (b) finite volume (e.g. the commercial code FLUENT-3D); and (c) finite element (e.g. CCHE3D by the National Center for Computational Hydroscience and Engineering at the University of Mississippi).

The implicit finite difference scheme is employed by 3D hydrodynamic model Delft3D developed by Delft Hydraulics and Delft University of Technology. This model investigates the hydrodynamics, sediment transport and morphology, and water quality for fluvial, estuarine and coastal environments. Among the various studies, an example of application is represented by the study on the Cecina River (Rinaldi et al., 2008) where Delft3D was selected to characterize the flow distribution along the meander as required by fluvial erosion analysis.

Recent improvements have been performed in modelling the near-bank shear stress by coupling CFD models with the analytical model developed by Kean and Smith (2004, 2006a,b). This model allows to quantify the form roughness induced by the irregular topographic bank features and to partition the shear stress acting on the banks. Kean and Smith (2005) and Kean et al. (2009) combined this model with a 2D hydraulic model based on the ray-isovel approach, whereas in the recent study from Darby et al. (2010) it was coupled with the EIA 3D hydrodynamic model developed by Technical Research Centre of Finland and EIA Ltd. (Environmental Impact Assessment Centre of Finland).

2.2.3 Mass failure

Mass failure is related to the collapse of riverbank under the influence of gravity (Thorne, 1982; Lawler et al., 1997). In opposition to fluvial erosion, mass failure is a discontinuous and large-scale detachment process and it may occur through several mechanisms (Figure 2-3), including planar failure, rotational failure, cantilever failures of undercut banks, toppling of vertically arranged slabs, rotational slumping and wedge failures (Thorne et al., 1981, Thorne, 1982). The bank stability is defined through the safety factor (FS), which is expressed as the ratio between stabilizing and destabilizing forces. The resulting driving force consists of the weight component of the failure block, while the resultant resisting force is function of both cohesion and internal friction angle.

Different factors lead the bank to become unstable, such as the increase in the unit weight of soils, the decrease in the negative pore water pressure and consequently in

the apparent cohesion, or the loss of confining pressure during the drawdown phase of a flow event.

The type of failure usually reflects the degree of undercutting (if any) by fluvial scour or other sources, and the nature of the bank (Thorne and Osman, 1988, Darby et al., 2000). Different failures can be analyzed with specific models. Planar failures are associated with low and steep banks (Thorne and Osman, 1988, Darby and Thorne 1996) while rotational failures are associated with gently sloping cohesive banks. Composite banks are prone to cantilever given that lower granular layers are eroded to create overhangs in the overlaying cohesive soils (Lawler et al., 1997; Dapporto et al., 2003).

The mechanism of cantilever can be classified into beam, shear and tensile failure depending on the corresponding geometry (Thorne and Tovey, 1981). Sapping or piping are other common processes in composite banks (Thorne, 1982) due to the seepage processes occurring between different soils.

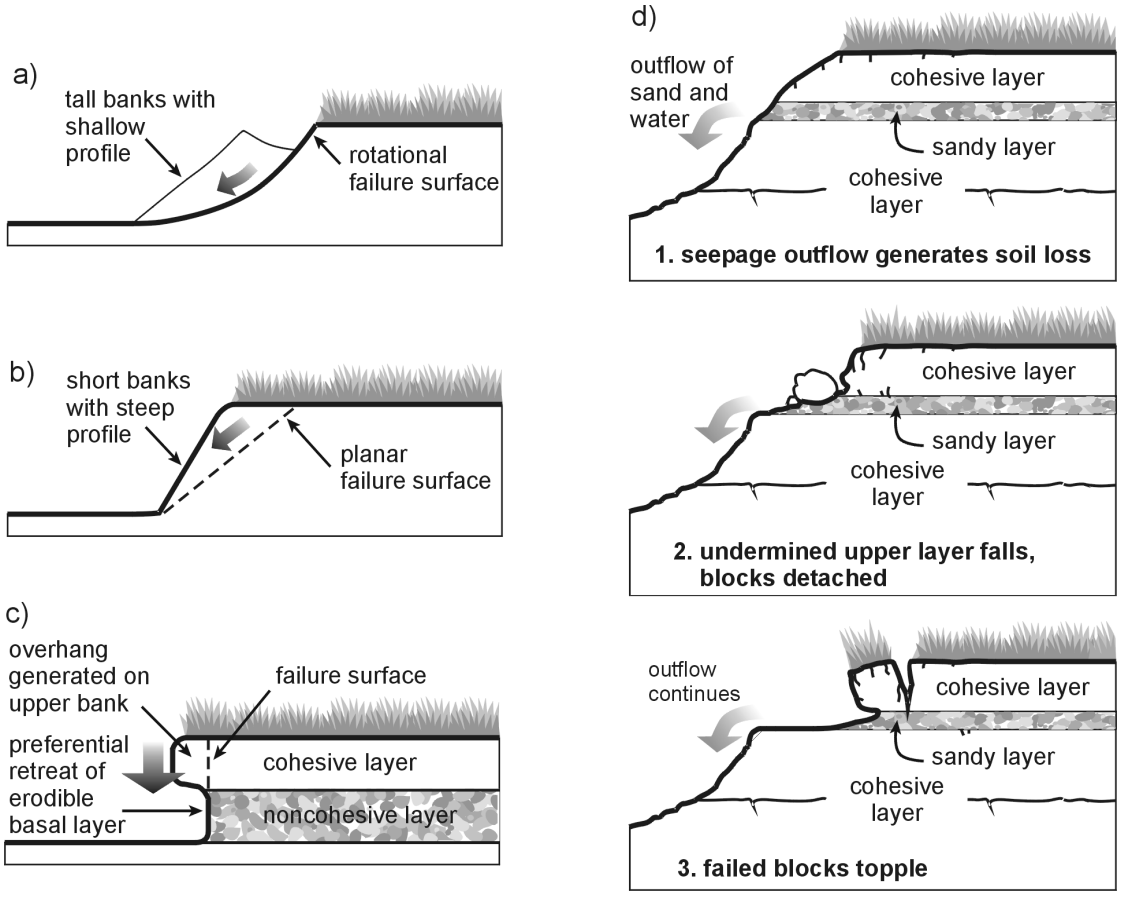

Figure 2-3 Bank failure mechanisms: a) Rotational failure, b) Planar failure, c) Cantilever failure, and d) Piping or sapping failure (modified from Langendoen, 2000).

Streambank stability can be analyzed using Limit Equilibrium Methods (LEM) based upon static equilibrium of forces and moments. This method has been widely employed in geotechnical engineering problems by applying the Mohr-Coulomb criterion, which includes the principle of effective stress (Terzaghi, 1923):

$$\tau = c' + (\sigma - u_w)tan\phi' \quad (2.4)$$

in which τ (kPa) is the shear strength, c' (kPa) the effective cohesion, σ (kPa) the total normal stress, u_w (kPa) the pore water pressure, and ϕ' the effective friction angle (degrees).

Equation (2.4) is valid only in fully saturated or dry conditions, where the effective normal stress is equal to the total normal stress minus the pore water pressure. When soils are unsaturated the voids are occupied partly by water and partly by air.

The pore water pressure must always be less than the pore air pressure due to surface tension at the air-water interface. As pore air pressure u_a is assumed to be in equilibrium with atmospheric pressure (i.e. zero gauge pressure), pore water pressure in the unsaturated portion above the water table is negative. The difference between the two quantities $(u_a - u_w)$ is defined as matric suction and is a positive quantity. Thus, to take account for the presence of matric suction in unsaturated soils the Mohr-Coulomb criterion is modified as follows (Fredlund et al., 1978):

$$\tau = c' + (\sigma - u_a)tan\phi' + (u_a - u_w)tan\phi^b \quad (2.5)$$

where u_a is the pore air pressure and ϕ^b is an angle expressing the rate of increase in strength relative to the matric suction. The angle ϕ^b cannot exceed the value of ϕ' and it typically ranges between 7° and 26° (Fredlund and Rahardjo, 1993).

Another term, called apparent cohesion (c_a), have been also introduced and it is given by the following expression:

$$c = c' + c_a = c' + (u_a - u_w)tan\phi^b \quad (2.6)$$

Riverbanks are for most part of the year in unsaturated conditions, and both the shear strength of the material and the conditions of seepage are strictly controlled by the distribution of matric suction. The apparent cohesion due to matric suction can represent a substantial component of the total shear strength, allowing the bank to remain stable even if it stands at steep angle (Casagli et al., 1999; Rinaldi et al., 2004).

Much research has been carried out in this field (see Table 2-1) since the first attempt by Culmann in 1866 to deal mathematically with the slope stability problem (Yu et al., 1998). Efforts have been made in order to take account for more realistic bank geometries and presence of tension cracks (Osman and Thorne, 1988), as well as for positive pore water pressures and hydrostatic confining pressures (Simon et al., 1991; Darby and Thorne, 1996).

Rinaldi and Casagli (1999), Casagli et al. (1999) and Simon et al. (2000) included the effects of negative pore water pressures in the unsaturated part of the bank. Moreover, the influence of riparian vegetation has been analyzed by Abernethy and Rutherfurd (1998, 2000, 2001), Simon and Collison (2002), Rutherfurd and Grove (2004), Pollen et al. (2004), Van de Wiel and Darby (2004), Pollen and Simon (2005) and Pollen (2006).

Chiang et al. (2010) included the effect of groundwater table fluctuation and the interaction between river stage and groundwater table by combining stability analysis with groundwater flow computation.

Recently, more complex analyses have been utilized for river bank studies (Abernethy and Rutherfurd, 2000; Dapporto et al., 2001, 2003; Simon et al., 2002; Rinaldi et al., 2004) by using various LEM solutions extended to rotational slides (i.e., Bishop, Fellenius, Jambu, Morgestern, GLE) in order to overcome many of the previous limitations. These analyses provide the following advantages: (1) definition of rotational or composite slide surfaces and generic bank geometries; (2) selection of either the Mohr–Coulomb or Fredlund et al. (1978) failure criterion depending on whether the soil conditions are saturated or unsaturated, respectively; (3) definition of a generic pore water pressure distribution and confining pressures exerted by the flow; (4) the possibility to perform several analyses for a large number of different sliding surface types and positions, which provides more confidence in identifying the most critical failure surface (Rinaldi and Darby, 2008).

The impacts of vegetation on river bank processes are complex and most of them are difficult to quantify. They can be divided into mechanical and hydrological effects, some are positive in terms of their impact on bank stability and others are negative. Thus, the change in stability induced by vegetation is highly contingent on site-specific factors.

Analisi	Mechanism of failure and bank geometry	New capabilities (compared to previous methods)	Main limitations	Typical Applications	Main references
'Culmann'	Planar failure, uniform bank slope	Simple to use	Simplified geometry (no tension crack); failure surface passing from the bank toe; only "dry" conditions	Massive silt or clay, incised rivers of the southeastern – midwestern U.S.	Thorne et al. (1981); Thorne (1982)
Thorne and Tovey	Cantilever failure	First method specific for cantilever failure	Data required (cantilever block geometry, tensile strength) not easily available	Composite banks	Thorne and Tovey (1981); Thorne (1982)
Osman and Thorne (OandT)	Planar failure with tension crack; bank profile taking into account basal erosion and relic tension crack	More realistic geometry including effects of basal erosion	Failure surface passing from the bank toe; only "dry" conditions	Homogeneous cohesive banks	Osman and Thorne (1988)
Simon et al.	Planar failure, uniform bank slope	Failure surface not necessarily passing from the bank toe; positive pore pressures are incorporated by a pore pressure ratio; confining pressures are taken into account	Simplified bank geometry (no tension crack);	Homogeneous cohesive banks	Simon et al. (1991)
Darby and Thorne	Planar failure with vertical tension crack, OandT geometry	Failure surface not necessarily passing from the bank toe; positive pore pressures and confining pressures are incorporated	Unsaturated conditions are not considered	Homogeneous cohesive banks	Darby and Thorne (1996b)
Rinaldi and Casagli	Planar failure with vertical tension crack, uniform bank slope	Negative pore water pressures (further than positive and confining pressures) are taken into account	Simplified bank geometry (no basal erosion and relic tension crack); based on the assumption that water table during drawdown remains at the level of the peak river stage	River banks formed in partially saturated soils; rivers with relatively rapid drawdown	Rinaldi and Casagli (1999)
Casagli et al.	Planar failure with vertical tension crack, OandT geometry	More realistic geometry	Homogeneous material; Relation river stage – water table needs to be specified	Homogeneous cohesive river banks formed in partially saturated soils	Casagli et al. (1999), Rinaldi and Casagli (1999)
Simon et al.	Planar failure with vertical tension crack, OandT geometry	Layered bank materials	Relation river stage – water table needs to be specified	Layered cohesive river banks formed in partially saturated soils	Simon et al. (2000)
ARS bank stability model	Planar (wedge-type) failure	Incorporates soil reinforcement and surcharge due to vegetation	Simplified bank geometry	Vegetated river banks	Simon and Collison (2002)
Various software packages(SEEP/W e SLOPE/W)	Slides (planar, rotational, composite); generic bank geometry	Negative pore water and confining pressures are taken into account; generic bank geometry and failure surfaces; possible to account for main vegetative mechanical effects	Generally more data-demanding; requires expertise	When pore water pressure changes at the intra-event scale need to be accounted; rotational or other non planar failure surfaces and generic bank geometry	Dapporto et al. (2001, 2003); Rinaldi et al. (2004)

Table 2-1 Summary of methods of stability analysis applied to river banks (Rinaldi and Darby, 2008).

The first mechanical effect of vegetation is the impact of vegetative surcharge. This can be either beneficial (increase in normal stress and therefore in the frictional component of soil shear strength) or detrimental (increasing the downslope component of gravitational force), depending on the position of the tree on the bank, the slope of the shear surface, and the friction angle of the soil (Gray, 1978; Selby, 1982). However, the most important mechanical effect of vegetation is the increase in soil strength induced by the presence of the root system. Plant roots have high tensile strength but weak compressive strength, whereas soil has high compressive strength but low tensile strength, so that they form a strong composite material (Pollen, 2006). The impact of roots on soil strength can be represented by adding an apparent root cohesion term, in Fredlund et al. (1978) criterion. Abernethy and Rutherfurd (2001) made measures of tensile strength of individual roots in the laboratory. To take account for the added effect of the attractive forces between the root fibers and the soil matrix, the authors developed a field method for measuring the load required to pull a root out of a bank face. Pollen and Simon (2005) measured values of root strength for a variety of species using the root-puller method. These values were then included in the RipRoot model for use with bank stability assessment (Pollen and Simon, 2008).

In terms of the hydrological effects, Simon and Collison (2002), Pollen and Simon (2005), and Pollen (2007) have indicated that vegetation can have both advantageous and disadvantageous impacts on stability, as well as on the mechanical one. One of the positive effects is the removal of soil water from the root zone, contributing to the persistence of negative pore-water pressures in the bank. Negative effects of vegetation include the increased load on the bank and the potential for preferential flow (infiltration), along old root channels.

2.2.4 Interaction between processes

The three main processes described in the previous sections are interconnected and frequently riverbank retreat is the product of their combination. In fact, subaerial processes weaken the surface of the bank prior to fluvial erosion, thus increasing the efficacy of the latter. Fluvial erosion, in turn, is linked to mass failure processes through the concept of basal endpoint control (Carson and Kirkby, 1972; Thorne, 1982). According to this model, the local bank retreat depends on the status of the sediment build up at the bank toe. Thorne (1982) defined three possible conditions: impeded removal, unimpeded removal and excess basal capacity. In the first case,

bank processes or sediment inputs from upstream supply material at a higher rate than it is removed by the flow downstream resulting in basal accumulation and reduction of the bank slope. The second case represents the status of dynamic equilibrium since supplied and removed material are balanced. Finally, excess basal capacity refers to the condition where the rate of sediment removal from the basal region exceeds the rate at which sediment is supplied to the toe, resulting in toe erosion and increasing bank height and slope.

Notwithstanding the undoubted importance of the combined action of different processes, most of the studies focus on a single set of processes. This represents an important limitation because dynamic interactions and feedbacks between processes may lead to outcomes that are not predictable a priori (Rinaldi and Darby, 2008). Only relatively few attempts have been made to couple effects of interacting bank erosion mechanisms (e.g., Simon et al., 2003, 2006; Dapporto and Rinaldi, 2003; Darby et al., 2007). Rinaldi et al. (2008a) followed the approach developed by Darby et al. (2007) where fluvial erosion, finite element seepage and limit equilibrium stability analyses are fully coupled and made further progress by using more advanced hydrodynamic model, namely a version of DELFT3D that employs a 2D depth-averaged hydrodynamic numerical model.

2.3 Spatial and temporal scales in riverbank processes

"It is the purpose of this discussion to demonstrate the importance of both time and space to the study of geomorphic systems." (Schumm and Lichty, 1965)

There are various levels of analyzing riverbank retreat processes, and these views may afford different perspectives of the bank dynamics. The selection of the proper scale depends primarily on the purpose of the study. The features of a river system have been described in a spatial hierarchy (Frissell et al., 1986) ranging from the whole catchment network (Brierley and Murn, 1997; Abernethey and Rutherfurd, 1998; Lawler et al., 1999), through river reaches (e.g. Pizzutto, 1984; Odgaard, 1987; Gurnell, 1997) to a single 'bank' (Figure 2-4). Examples of analyses at the riverbank scale are the stability analysis of Osman and Thorne 1988, the coupled fluvial erosion and stability analyses by Simon et al. (2003, 2006), Dapporto and Rinaldi (2003), Darby et al. (2007), Rinaldi et al. (2008a) or Luppi et al. (2009). Often it results useful to apply a nested hierarchical approach as proposed by Brierley and Fryirs (2005) in their research on *River Styles Framework.*

The parameters which account for bank retreat analyses may vary, depending on the specific spatial scale (Table 2-2). As a first approximation, lateral instability distribution at the network scale may be related to some interactions between stream energy (or power) and resistance afforded by the boundaries. Therefore it is necessary to distinguish between different degrees of lateral confinement. According to Brierley and Fryirs (2005) a river channel may be defined *confined* when the percentage of channel abuting valley margin is higher than 90%, *partly confined* for percentages ranging between 10-90%, and *unconfined* for values lower than 10%. In confined settings channels adjustments are restricted by the valley walls which also increase the flow resistance. In partly confined channels some degree of lateral migration and floodplain development is possible, while unconfined channels are free to migrate. The latter condition is generally typical of lower reaches.

Downstream change in bank erosion process dominance (Lawler, 1992) and predictions of channel instability can be determined through logistic regression analysis by combining the basic hydraulic data, such as discharge, together with sediment characteristics (mean diameter of sediments) and channel slope (Bladsoe and Watson, 2001; Piégay et al, 2005).

At the reach scale, examples of factors that may influence riverbank processes include velocity distributions and secondary currents, as well as bedload, channel width, presence of bars and large woody debris.

Focusing at the riverbank scale, detailed characterizations of soil properties and near-bank shear stresses are required. Moreover, measures of pore water pressure should be accounted for, because it plays an important role in the bank stability.

Couper (2004) provided an exhaustive review aiming to identify the time and spatial scales to be used in bank erosion research.

The author found a positive relationship between the time and the spatial scale used by a number of researchers, such that smaller spatial scales tend to be studied in combination with shorter temporal scales.

At a spatially and temporally large scale, riverbank processes are seen as part of long-term channel change and bank erosion plays a role in landscape development.

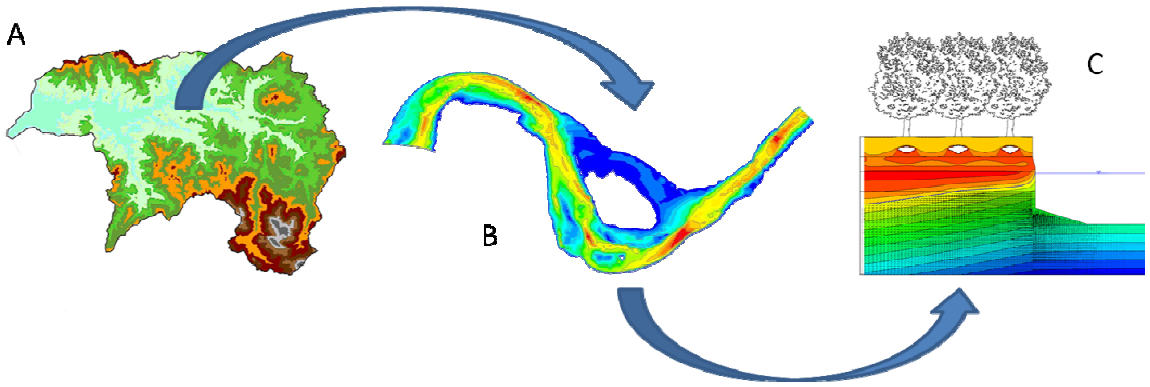

Figure 2-4 Spatial scales for riverbank retreat analyses: (A) Catchment scale, (B) Reach scale and (C) Riverbank scale.

Scale	*Dominant factors*
Network	Slope (S), Discharge (Q), Stream energy or power ($\Omega = \gamma QS$), Boundary resistance.
Reach	Bank composition, Shear stress (τ), Channel curvature, Channel width (w), Bedload, Bars
Riverbank	Near-bank shear stress (τ), Pore water pressures, Bank material properties, Hydrograph

Table 2-2 Dominant parameters for different spatial scales.

Reach scale is mostly studied at shorter time scales ranging from months to few year, while riverbank scale is often studied at the scale of flow event (Rinaldi et al., 2008; Luppi et al., 2009).

Most research methods are not suitable for both broad and local analyses. As a proper model is required depending on the selected spatial (temporal) scale, data necessary for the application of the model may vary. Thus, in order to capture the continuous variations that river displays along its length, extensive and rapid field survey approach foregoes high-precision locally to enable data collection at a large number of sites (e.g. Fonstad and Marcus, 2003). On the other side, methods available to explore the riverbank erosion at the reach or site scale require locally-intense field surveys generating high resolution data.

Techniques are nowadays available for high resolution measuring over broad extents, especially in large rivers. One example is represented by extensive surveys from boats equipped with precision instruments such as sonar or acoustic Doppler velocimeters (Parsons et al., 2005). Nevertheless, their use is generally limited due

to the high costs and logistical complexity, especially when dealing with high gradient streams (Fonstad and Marcus, 2010).

Remote sensing provides a continuous high-resolution and basin extent survey technique at relatively low costs: aerial imagery and LiDAR (Light Detection And Ranging or Laser Radar). These technologies can be used to map rivers using approaches ranging from visual interpretations of the main features, to quantitative data extraction, such as measuring substrate size based on textural filtering. Disadvantages include data validation issues, factors that hinder image interpretation (e.g. trees and shadows), and limitations related to image resolution (Marcus and Fonstad, 2008; Fonstad and Marcus, 2010).

2.3.1 Spatial variability of processes along the river

Channel migration has been studied in considerable detail along many channel reaches around the world, and reviews are reported by Hooke (1980), Lawler (1993) and Millar (2000). Despite extensive international studies on this topic at the reach scale, there have been few attempts to predict rates of bank erosion at the catchments scale using spatial modelling. This is because bank erosion is the result of a range of complex natural processes that depend on in-channel hydraulic conditions and physical characteristics of the banks. Both of them are highly variable within a single river, as well as between rivers (Piégay et al., 2005). Moreover at larger scales (e.g. > 1 km reach) it is difficult to differentiate between mechanisms that cause the migration.

The Downstream Hydraulic Geometry (DHG), developed by Leopold and Maddock (1953), is perhaps the most widely used conceptual framework to describe variations in river form at the catchment scale. According to the DHG, as discharge increases linearly with drainage area in the downstream direction, channel morphology increases proportionately to accommodate the discharge. Because discharge changes linearly with drainage area, and because the area increases as a power function in the downstream direction, DHG states that the channel variables vary as a power function of discharge in the downstream direction. The concept of stream power is founded on the DHG model. The term “stream power” was initially introduced by Bagnold (1966) and it has been used extensively in the literature to quantify sediment transport (Bagnold, 1966, 1977), to describe patterns of bank instability (Lawler, 1992; Abernethy and Rutherfurd, 1998), and to explain bedrock channel incision (Whipple et al., 2000), channel pattern (Chang, 1979; Knighton

and Nanson, 1993) and riparian habitat development (Abernethy and Rutherfurd, 1998; Bendix, 1999; Bendix and Hupp, 2000).

The term "stream power" can be defined as the "rate of energy supply at the channel bed which is available for overcoming friction and transporting sediments" (McEwen, 1994). Lawler (1992) recognized that little was known about the downstream change in the hydraulic properties of rivers and presented a model for the spatial distribution of total stream power. This model is now part of a larger-scale conceptual bank erosion model called DOCPROBE (DOwnstream Changes in the PROcesses of Bank Erosion), developed by Lawler (1992, 1995). Since fluid density and gravitational acceleration can be assumed constant in the longitudinal direction, the stream power can be defined as a function of the discharge and the slope. It is suggested (Lawler, 1992) that downstream change in discharge is best represented as a power function in terms of channel length, L (m):

$$Q = kL^m \tag{2.7}$$

where k and m are both dimensionless constants. Lawler (1992, after Rana et al., 1973) found that slope is best modelled as a negative exponential function of the channel length:

$$S = (S_0 e^{-rL}) \tag{2.8}$$

where S_0 is the slope at the upstream section and r is a coefficient of slope reduction that can be estimated through a non linear regression. Discharge and slope are then combined to produce a generalized catchment-scale downstream change model for total stream power, Ω:

$$\Omega = \rho g Q S = \rho g \cdot (kL^m) \cdot (S_0 e^{-rL}) \tag{2.9}$$

where ρ is fluid density (1000 kgm^{-3}) and g is the gravitational acceleration.

Equation (2.9) predicts that stream power should present a peak at some intermediate location in the basin (Figure 2-5). To exactly predict the position of the peak, Equation (2.9) has to be differentiated (Barker et al.2009).

Further researches (Abernethy and Rutherfurd ,1998; Knighton, 1999 and Reinfelds et al., 2004) confirmed the presence of the stream power peak in the likely middle part of the river catchment.

Based on the stream power, Lawler (1992) introduced a conceptual model of changing bank process dominance in a hypothetical drainage basin (Figure 2-6).

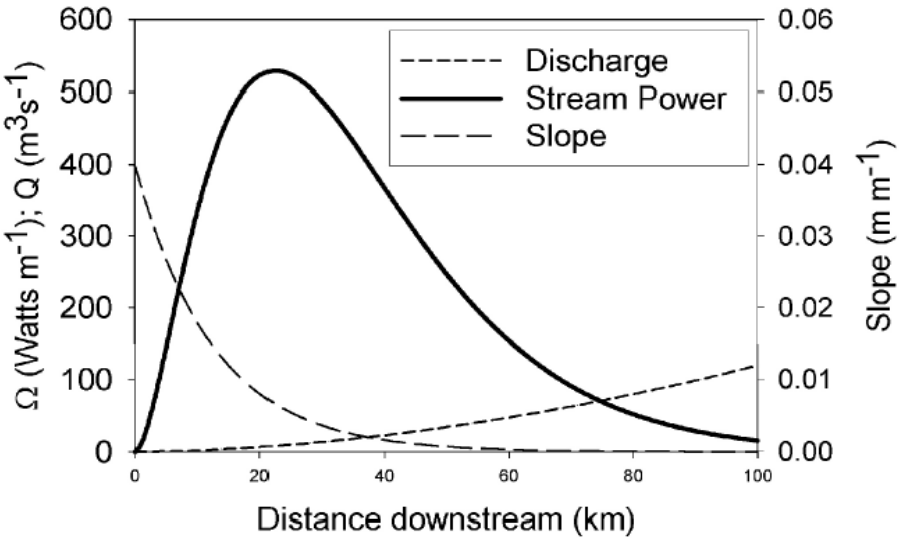

Figure 2-5 Conceptual stream power model proposed by Lawler (1992, 1995).

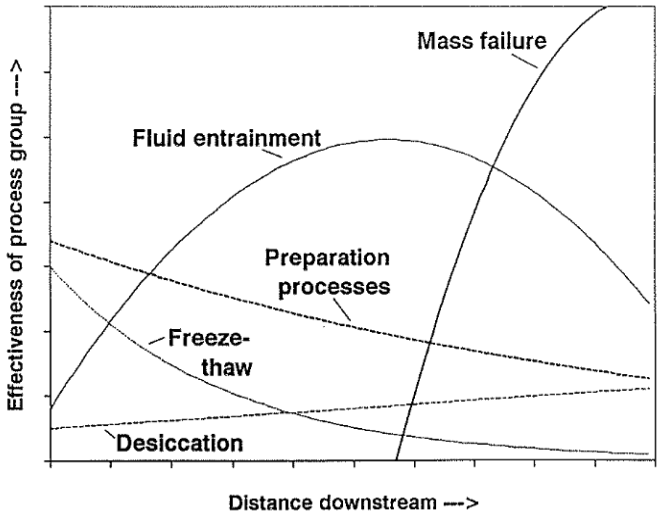

Figure 2-6 Conceptual model of downstream change in bank erosion process groups (Lawler, 1995).

According to the model, in upstream reaches, preparation processes are most effective, because stream power and bank heights are too low for significant fluid entrainment and mass failure, respectively. In middle reaches, where stream power is high, fluid entrainment dominates. At further downstream, bank heights and material properties exceed critical values and mass failure processes prevail.

As well as the total stream power, the specific stream power, $\omega = (\gamma QS)/w$, where w is the channel width, represents an important indicator of the erosive power of the flow. In fact, unit stream power provides more insight to available energy than stream power because it considers the distribution of stream power per unit channel

width. Wider streams produce lower unit stream power values compared to narrow channels because energy is assumed to be distributed over a larger area.

Some empirical methods have been proposed to predict the location of instability along the river. Among the others, Ferguson (1987) and Knighton (1998) found an empirical relationship between channel width and the square root of dominant discharge:

$$w = \alpha Q^{0.5} \tag{2.10}$$

where α is an empirically derived constant.

For the Bellinger River (Australia), Warner (1992) and Cohen (2003) found exponents of 0.72 and 0.59 in relationships between catchment area and channel width.

Bleadsoe and Watson (2001) employed a logistic regression where the dependent variable is the probability that the river is mobile (0 is immobile, 1 is fully mobile) while the channel slope (S), the channel superficial grain size (D_{50}) and the bankfull discharge are independent variables, forming a channel 'Mobility Index', MI, as follows:

$$MI = S\sqrt{\frac{Q}{D_{50}}} \tag{2.11}$$

When tested on 30 rivers in south-eastern France, Bledsoe and Watson (2001) model failed. Thus, Piégay et al. (2005) proposed another model in which the mobility index, here called 'Erosion Index' (EI), is defined as follow:

$$EI = \frac{1}{log\left(\frac{D_{50} \cdot \left(Q_2/A\right)}{S}\right) + 10} \tag{2.12}$$

where Q_2 is the specific discharge with a return period of 2 years, D_{50} is the median grain size of the bed surface and S is the channel slope.

With the increasing availability of geographic information systems (GIS) and digital elevation models (DEM), detailed spatial analysis is now feasible. GIS analyses on high resolution DEM obtained using LiDAR turn out particularly useful when measures of discharge are difficult. These tools allow analyses of the stream power

at the mid-sized catchment scale (e.g. Reinsfelds et al., 2004), as well as at the continental scale (Finlayson et al., 2002 and Finlayson and Montgomery, 2003).

Recently, Fonstad and Marcus (2010) used basin-extent, high resolution observations of fluvial forms to evaluate the ability of different frameworks to characterize system behaviour across a multitude of scales ranging from 100m to the entire basin. They found that, although DHG captures the central tendency of width downstream variations, however, the magnitude of reach-scale and local variability generally far exceeds the DHG predicted trends. The authors suggested that inadequate field measures (often widely scattered cross-sectional measurements), on which DHG equations are based, may be a possible explanation of their underestimated predictions.

Another conceptual framework explored in the fluvial geomorphology field at the catchment extent (Fonstad and Marcus, 2003, 2010; Coulthard and Van de Weil, 2007), is the Self-organized Criticality (SOC). The model is based on the idea that a diffusive system organizes itself to a minimally stable state where the interior elements of the system are interconnected. If a stability threshold is crossed, the movement of mass and energy will be transmitted to neighbouring areas. The self-organized systems have important properties: (1) the magnitude and frequency of the cascade events obey a precise power law; (2) small cascades involving small areas happen frequently, while large cascades operating over large areas are rare; (3) the power law is maintained through both time and space (Fonstad and Marcus, 2010).

Fonstad and Marcus (2003; 2010) explored the SOC model stating that rivers are open dynamic energy dispersive systems and described the relationship between riverbank failure sizes and frequencies through a power law. The authors also suggested a theoretical model to explain how river banks may organize themselves into a critical state: one failure deposits sediment within the channel that (may) then lead to another failure downstream. Thus, the SOC behaviour indicates that local failures are unpredictable leading to relevant implication for river managers (Fonstad and Marcus, 2003, 2010).

2.3.2 Spatial scale linkage

Literature review in fluvial geomorphology highlighted the importance of defining the spatial domain in riverbank retreat analyses. The definition of spatial domain is

recognized to be the starting point to select a proper model and therefore, to take account for those parameters which play the dominant role in shaping channel morphology. Nevertheless, Thorne and Abt (1993) suggested that a 'proper handling of the bank retreat problem depends on the identification of the actual cause of bank erosion, which may be associated with local scour, general scour, lateral instability or system-wide degradation'. Therefore, the exclusive observation at the specific scale of interest may be seen as a limitation, in that it may restrict the view of the researcher and significantly influence the resulting perception of erosion. If a wider perception of the whole fluvial system can be gathered through analyses at the catchment scale, analyses at smaller scales, such as reach and bank scale, may offer an insight into processes variability and their mutual interactions. In general terms, the larger the scale of analysis, the greater the level of generality of form and processes involved. Large-scale attributes are delineated using large-scale characteristics, such as the valley slope, and necessarily include a great deal of variation in small-scale (Brierley and Fryirs, 2005).

Despite of the awareness of the need for linkages between different spatial scales is recognized when facing riverbank retreat study, few attempts have been made to address this gap. Even if the concept of hierarchy within fluvial geomorphology is not novel (Schumm and Lichty, 1965), the idea of nested hierarchy has been only used in study of river habitat and fluvial ecology (Frissel et al., 1986). According to the hierarchical theory, a system is referred as nested hierarchical when each level contains the level below it. Thus, each level represents a constraint on the behaviour within the next lower level.

According to the needs emphasized by literature review, the present study has been organized in three main parts. Each of them deals with a specific spatial scale, namely: catchment, reach and riverbank scale. Schumm and Lichty (1965) recognized that a given parameter may exert a different influence on the system structure and function at different spatial and temporal intervals. Based on this consideration, the framework here presented was thought with the aim of identifying parameters which play the dominant role in riverbank processes at each spatial scale. Once the parameters responsible for channel migration are defined, this structure allows to investigate the potential of transferring observations and results obtained from analyses at one spatial scale to another one. The formulation of explicit linkages between different spatial scales, expressed through mathematical and numerical models, may provide important insight in the

comprehension of riverbank retreat processes. Coupling different spatial scales through an integrated approach could help to answer questions such as ‘which mechanisms are responsible for channel migration? where and when do they occur within the catchment scale? how do different processes relate each other?’.

PART I: LATERAL INSTABILITY AT THE CATCHMENT SCALE

The analyses carried out at the catchment scale aimed (1) to identify the variability of bank processes occurring along the entire length of the river and (2) to determine the dominant mechanisms of retreat. Different predicting models were also undertaken in order to pinpoint causes and factors which control the occurrence of instabilities and evaluate their potential ability to predict the spatial distribution of bank retreat in a fluvial system. Several studies used statistical analyses to define relationships between measured lateral movement rates and hydraulic, sediment, and other channel-form variables. Fluvial form and behaviour vary as a function of position among the numerous variables within a landscape. Hooke (1980) tried to find a relation between bank retreat and the catchment area, but data show a great spread. Nanson and Hickin (1986), MacDonald (1991), and Lawler et al. (1999) found that lateral migration rates increase with flow energy in meandering rivers. Brice (1982) and Nanson and Hickin (1986) also noted a relation between channel width and lateral migration.

At the river scale it is possible to apply a geomorphologic approach which includes: (1) characterization of the riverbanks in the present conditions (2) analysis of past channel changes and present trends of channel adjustment (3) application of the models for prediction spatial distribution of lateral instabilities.

3. Riverbank erosion processes along the Cecina River

3.1 The catchment

The Cecina River is located in the Central Tuscany (Italy) (Figure 3-1). The river has a total length of 79 km and its catchment area is about 905 km^2. The middle and lower portion of the watershed is dominated by hilly slopes constituted by erodible fluvio-lacustrine and marine sediments. The basin falls within a temperate climatic zone with a dry season and is characterized by a high variability in flow discharges and flashy floods. The mean annual precipitation is about 944 mm. The alluvial portion of the Cecina River has been classified in a series of relatively homogeneous reaches and sub-reaches. A first division in four main segments (CA, CB, CC, and CD) reflects the major structural controls (direction and confinement of the alluvial valley), while a second further division in sub-units (CA1, CA2, …, CD2) is mainly based on channel morphology, resulting in a total of 10 sub-reaches (Figure 3-1).

The upstream segment CA is characterized by a narrow alluvial valley; nevertheless the channel is mobile and presents relatively fine sediments. Wandering and meandering processes are observed at the segment CB. CC presents a transitional morphology and may be described as sinuous with alternate bars; meandering processes are also found. Moving downstream toward the segment CD, the numbers of bars decreases and the river is characterized by single channel morphology.

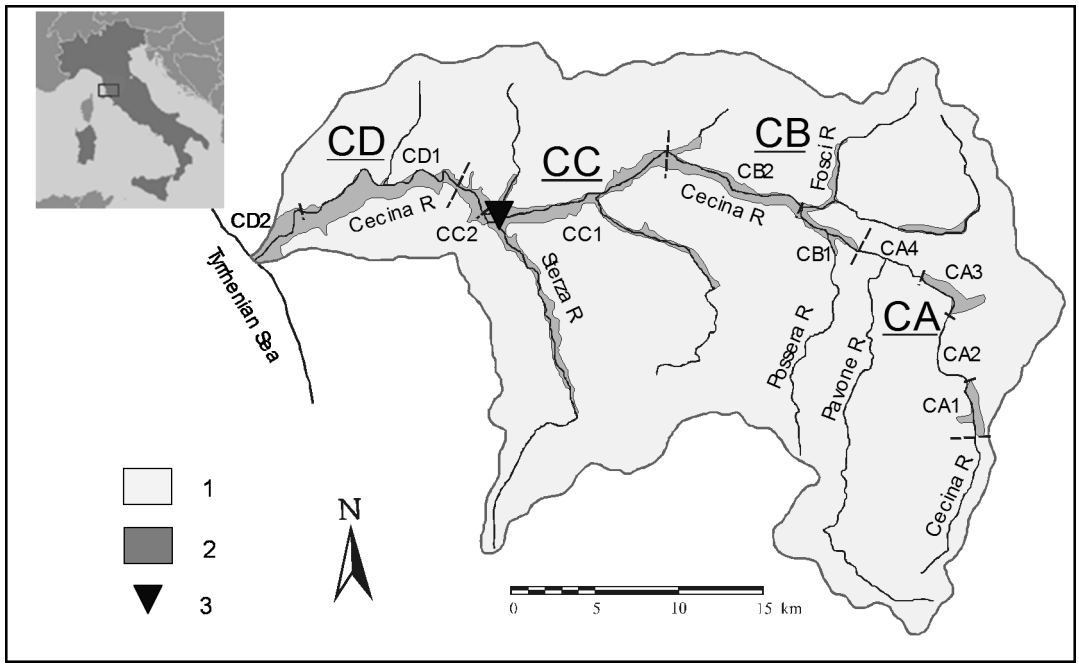

Figure 3-1 Cecina catchment and its division into reaches and sub-reaches.

Analyses carried out along 40 km reach length provided slopes ranging between 0.2-0.5% and a mean diameter of sediments between 13-43 mm (Surian et al., 2009).

3.1.1 Medium-term adjustments

The present configuration reflects the channel adjustments that occurred over the last decades. In fact, the Cecina River, as well as the main alluvial rivers of northern and central Italy, was affected by drastic changes during the 20th century (Rinaldi, 2003; Surian et al., 2009).

Human disturbances appear to be mainly responsible for these changes: the main phase of vertical change occurred during the period 1945–80, in concomitance with the phase of maximum sediment mining activity at the regional scale.

The second dominant type of alteration consists of a narrowing of the active channel (Rinaldi, 2003, Surian et al., 2009; Teruggi and Rinaldi, 2009). Temporal trends of the active channel width and sinuosity index (Table 3-1 and Figure 3-2) were obtained (the semi-confined reach CA and the partially artificial sub-reach CD2 were not included in this analysis) through GIS analyses based on a series of available aerial photos (Surian et al., 2009).

The results show a progressive reduction of channel width through time (Figure 3-2), with three stages of channel narrowing and incision.

Cecina bedlevel lowering has been generally moderate (1–3 m) during about the past 100 yr, in comparison with other study cases explored by Surian et al. (2009).

Field evidences suggested the authors that the current dominant situation is a bed stability or, in some cases, a limited aggradations.

Reach	Width change (1880s-1950s) (%)∗	Width change (1950s-1990s) (%)∗	Width change (1994-2004) (%)∗	Width change (1994-2004) (%)◊
Upper	-35	-16	-23	-50
Middle	-50	n.c.	-13	-27
Lower	-39	-34	-9	-31

(%)∗- calculated referring to the original width in the early nineteenth century or in the 1880s.

(%)◊- calculated referring to the width at the beginning of the 3rd phase of adjustment

Table 3-1 Width changes from the 19th century (Surian et al, 2009).

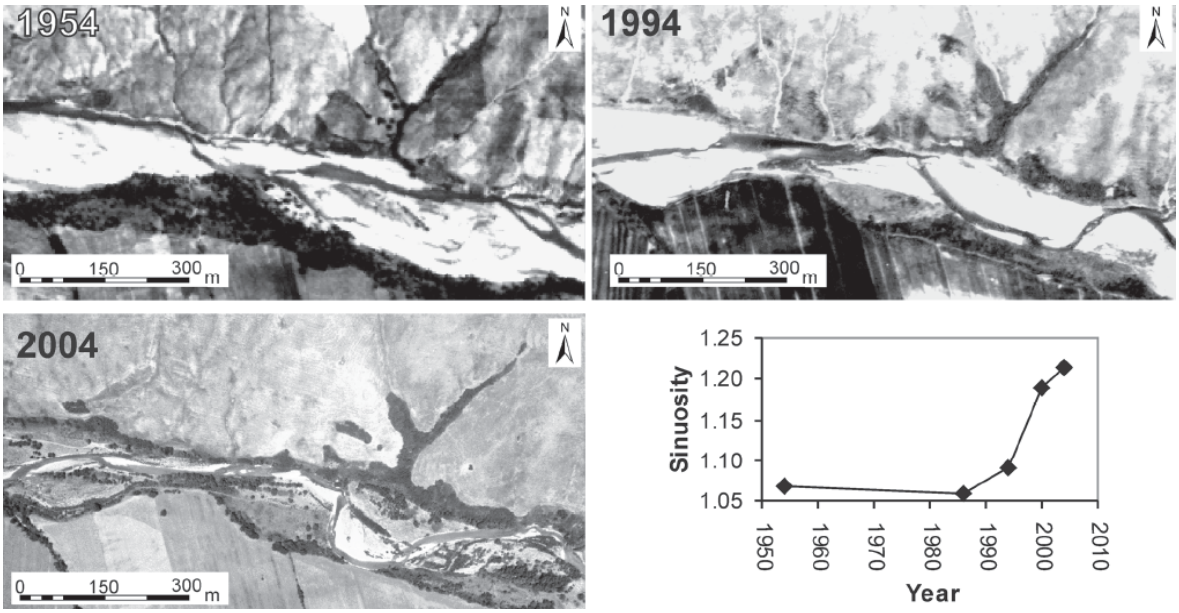

Figure 3-2 Channel adjustment in the Cecina River (Surian et al., 2009).

The dominant channel morphology of the Cecina in the 1950s can be described as wandering (locally braided), while in the following decades a significant narrowing occurred, with a change in morphology to a sinuous, single-thread channel with alternate bars.

Finally, Surian et al. (2009) observed a significant increase in sinuosity, associated with channel narrowing, particularly during the last two decades.

A detailed GIS analysis of channel changes, carried out by using a two-temporal series of aerial photos (Teruggi and Rinaldi, 2009), provided the historical evolution of the river during the last decade (Figure 3-3).

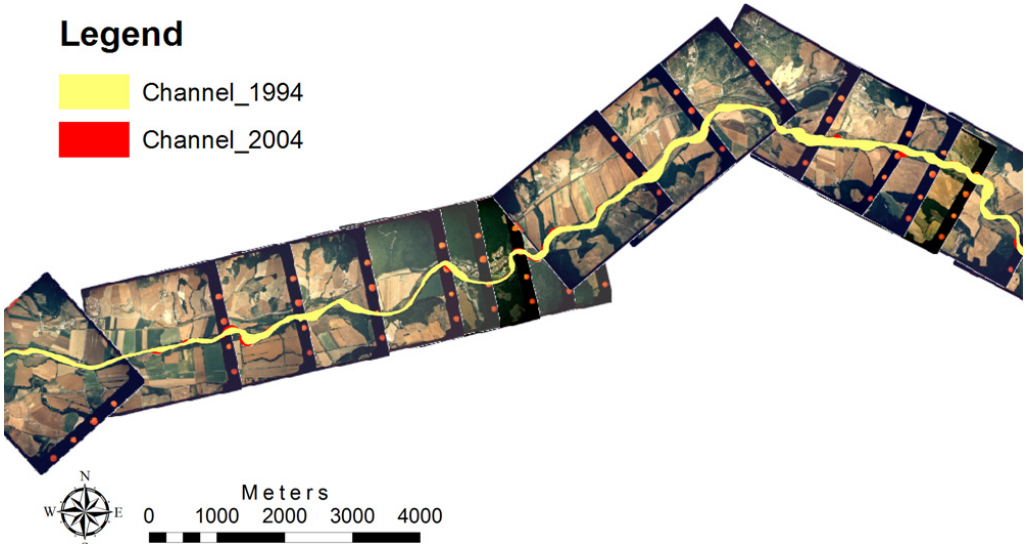

Figure 3-3 Overlay of channel 1994 and 2004 on aerial photos at segment CC of 2004 trough ArcMap 9.0.

Specifically, by means of these analyses the rates of riverbank retreat along the entire length of the Cecina were measured. Figure 3-4 shows the rate of retreat occurred between the years 1994 and 2004, excluding the first semi-confined reach (CA), where bank retreat is prevented by the presence of hillslopes.

In the alluvial part of the Cecina, the maximum rates of bank retreat show a decreasing trend downstream, except in the local point at the sub-reach CC. At this site the measured rate of riverbank retreat corresponds to 3.8 m/year.

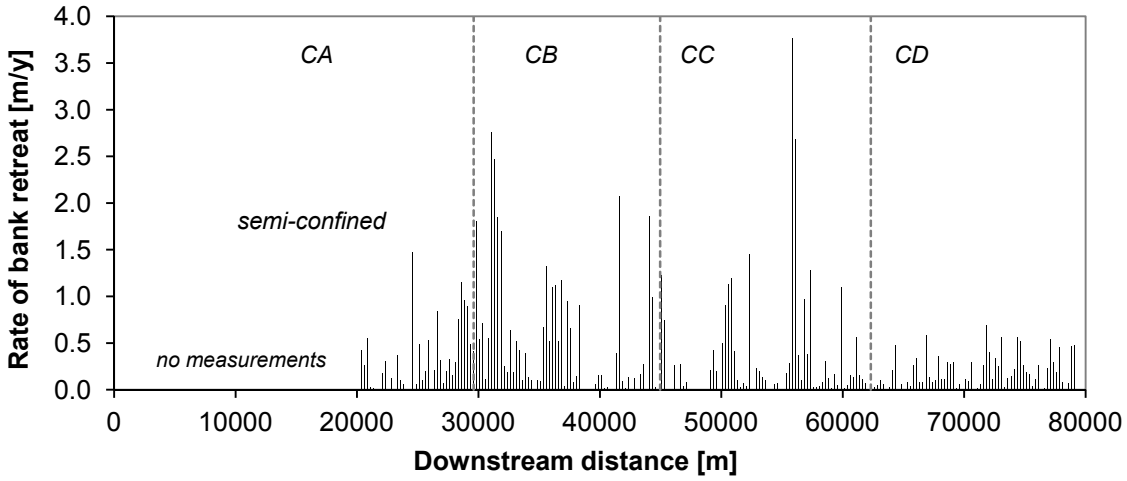

Figure 3-4 Riverbank retreat occurred along the Cecina R. between 1994-2004.

3.2 Riverbanks and processes along the Cecina River

Field surveys along the entire length of the Cecina River were carried out with particular focus on the characterization of banks. Gravel bars were also sampled through the pebbles count method, which provided median sediment size (D_{50}) ranging between 13 and 43 mm. These values, as expected, tend to decrease downstream, as shown in Figure 3-5.

Riverbanks along the Cecina were surveyed (see locations of sites in Figure 3-6) by using Thorne geomorphologic sheets (1998) and forms specifically developed for gravel banks surveys. In addition, samples of material from banks were collected for grain size distribution analyses.

Data collected during the survey of 51 riverbanks were analyzed (a) to investigate the possible relationships between height and bank slope taking account for the composition of different layers (Figure 3-7), and (b) to identify dominant processes occurring on the banks. Data plotted in Figure 3-7 show a great dispersion, although coarse gravel layers, characterized by weak cohesion, usually do not exceed 2 m height.

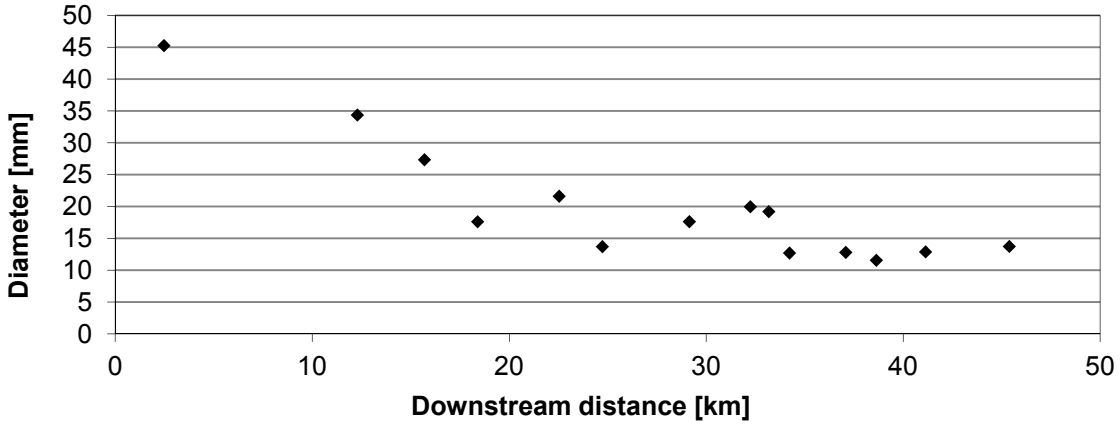

Figure 3-5 Median sediment size (D_{50}) of bars along the Cecina River.

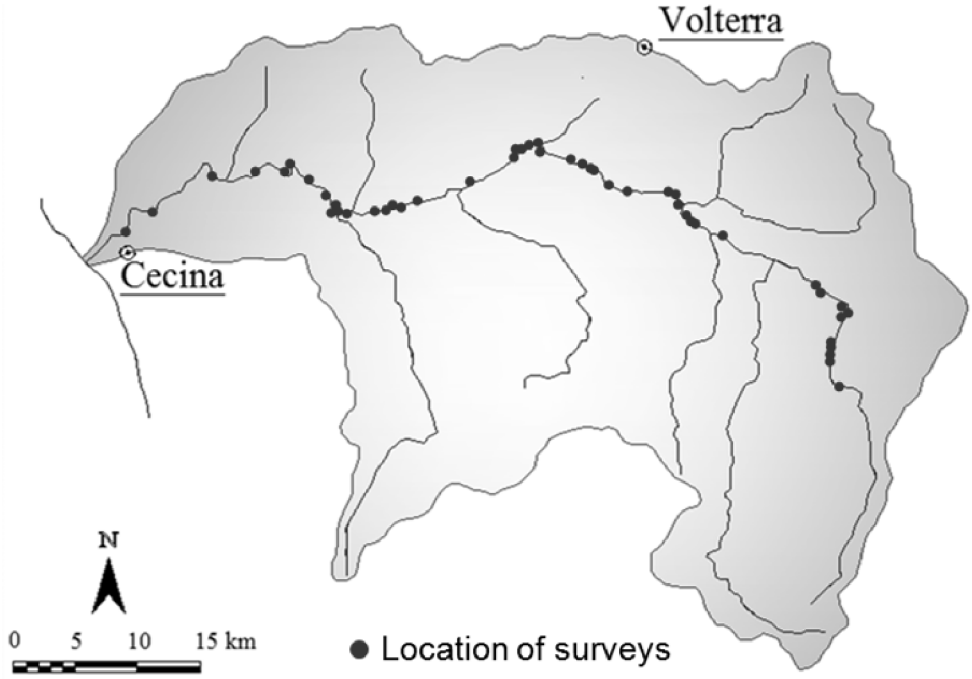

Figure 3-6 Cecina River and locations of surveyed banks and bars.

Taking into account for the presence of the different layers, riverbanks can be divided into cohesive, non-cohesive and composite. All of these types of banks can be found along the Cecina (Figure 3-8). In particular, composite banks are the most frequent starting from the middle-upstream part of the river, non-cohesive banks are observed in the upstream, while those few completely cohesive are located downstream (Figure 3-9).

Thorne's stream reconnaissance field sheets were employed to analyze systematically processes involving banks at the selected sites (Figure 3-10). These processes were divided in two main classes: mass failure and fluvial erosion. For each class, further subdivisions were made in order to identify qualitatively which are the dominant processes (divided into the subclasses) responsible for the retreat

of the three types of riverbank (Figure 3-11a and Figure 3-12a). Results suggest that composite banks are affected by the greatest variety of both fluvial and mass failure processes.

Cohesive banks are also prone to a range of processes. Nevertheless, concerning the mass failures, there is dominance in soil failures and shallow slides, while parallel flow is the most frequent process of fluvial erosion. On the opposite, debris flow and parallel flow affect non-cohesive banks for the most cases.

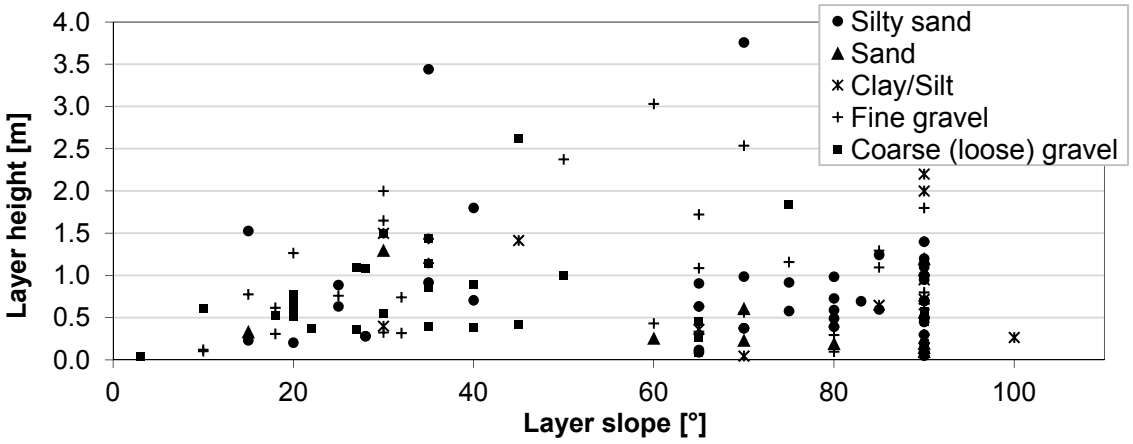

Figure 3-7 Relationship between bank height and slope for layer composed of different soils.

Figure 3-8 A: Non-cohesive bank (reach CA); B: Cohesive bank (reach CC); C: Composite bank (reach CC).

It is interesting to note that the occurrence of rotational slip has been found on these types of banks.

The downstream distribution of processes (Figure 3-11b and Figure 3-12b) directly reflects the spatial distribution of bank types; thus, for example, debris flows develop upstream where non-cohesive banks are present.

Some grain size analyses were carried out with the aim to describe the spatial distribution of the sediments, and looking for its relation with instabilities. Results, divided into non-cohesive and cohesive sediment, are shown in Figure 3-13 and Figure 3-14, respectively.

In Figure 3-15, the trend of the median diameter (D_{50}) of sediments composing the toe of the banks shows a tendency to decrease downstream.

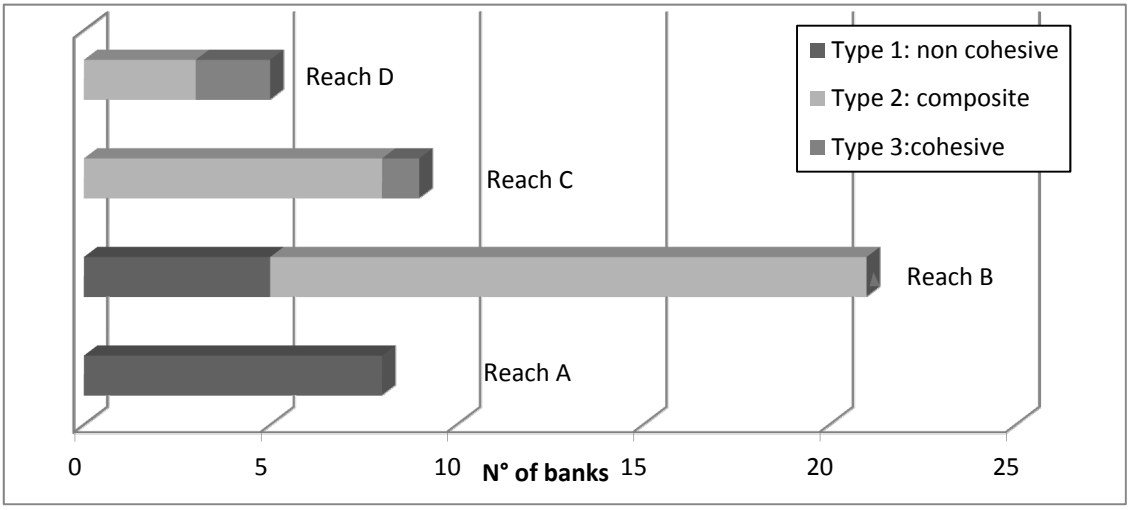

Figure 3-9 Distribution of different type of banks along the Cecina River.

Figure 3-10 Some processes observed along the Cecina River. A: Slab failure on cohesive bank; B: Rotational failure on gravel bank; C: Sapping at the interface of different layers on a composite bank.

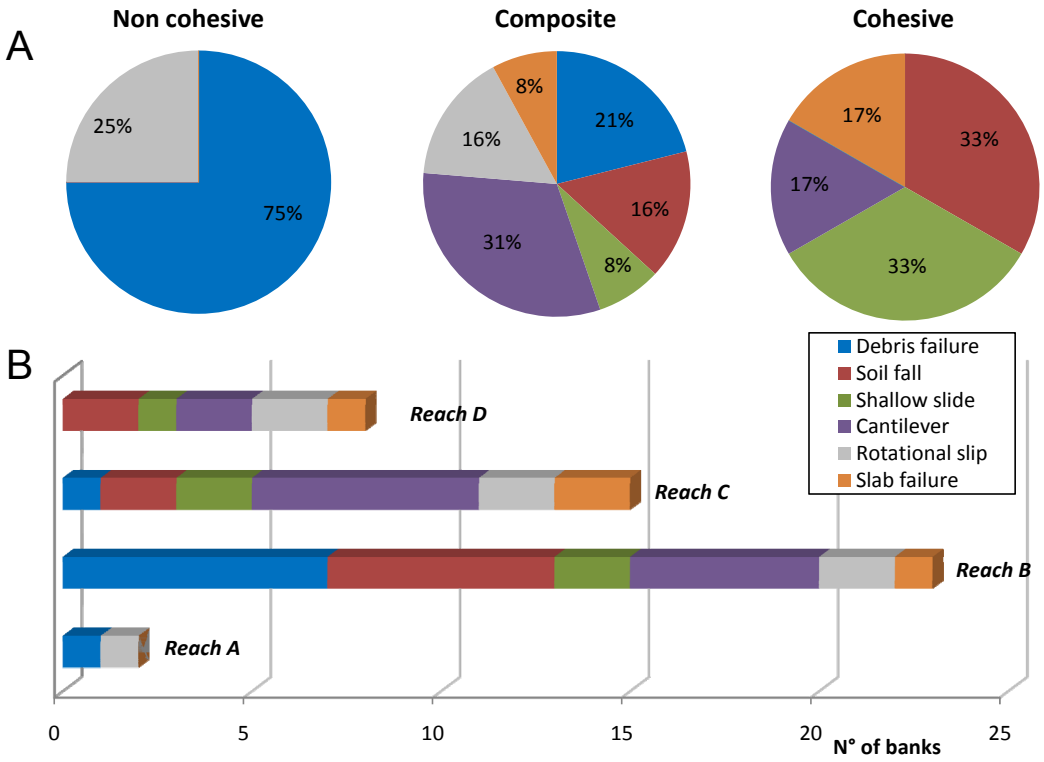

Figure 3-11 Mass failure processes at different type of banks (A) and different reaches (B).

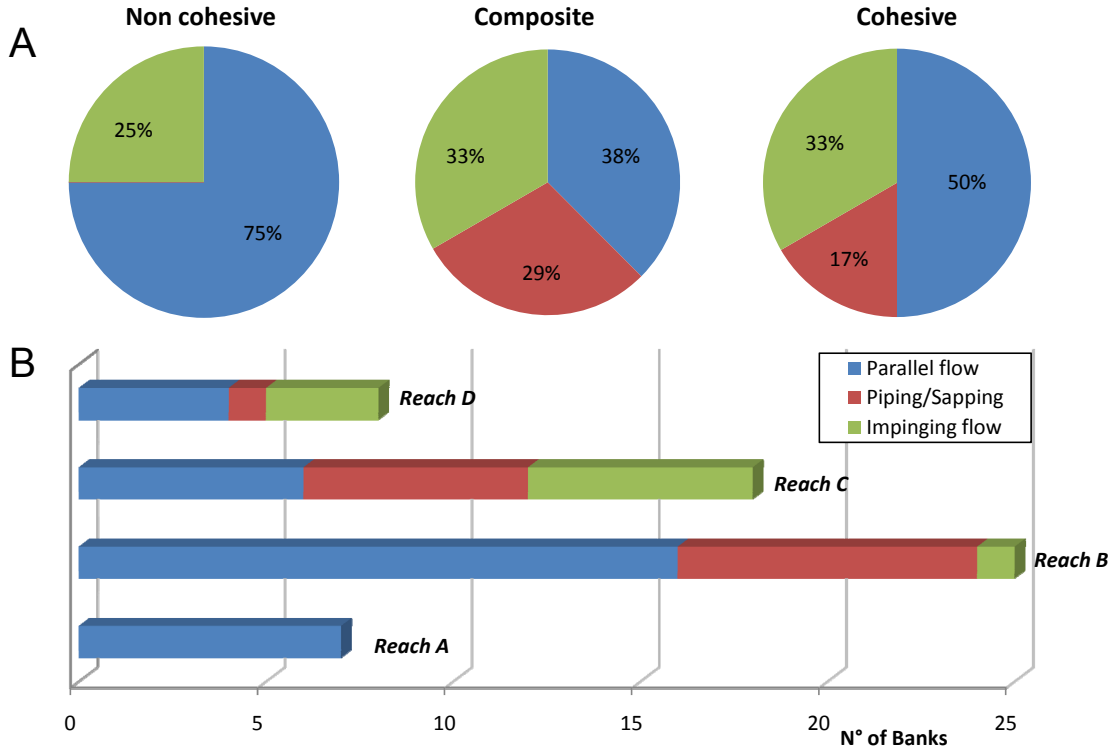

Figure 3-12 Fluvial erosion processes at different type of banks (A) and different reaches (B).

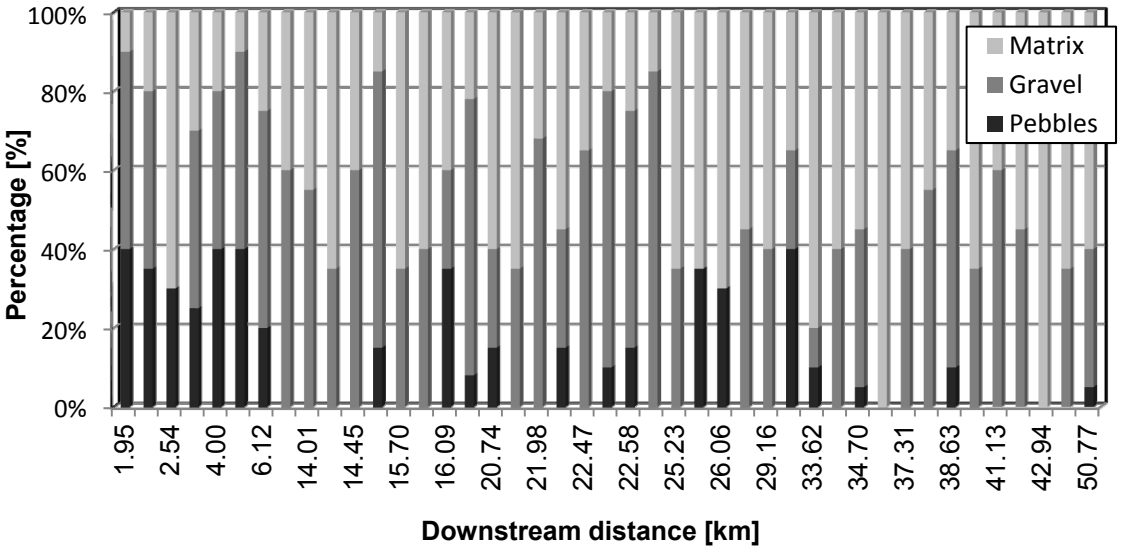

Figure 3-13 Distribution of non-cohesive bank sediments.

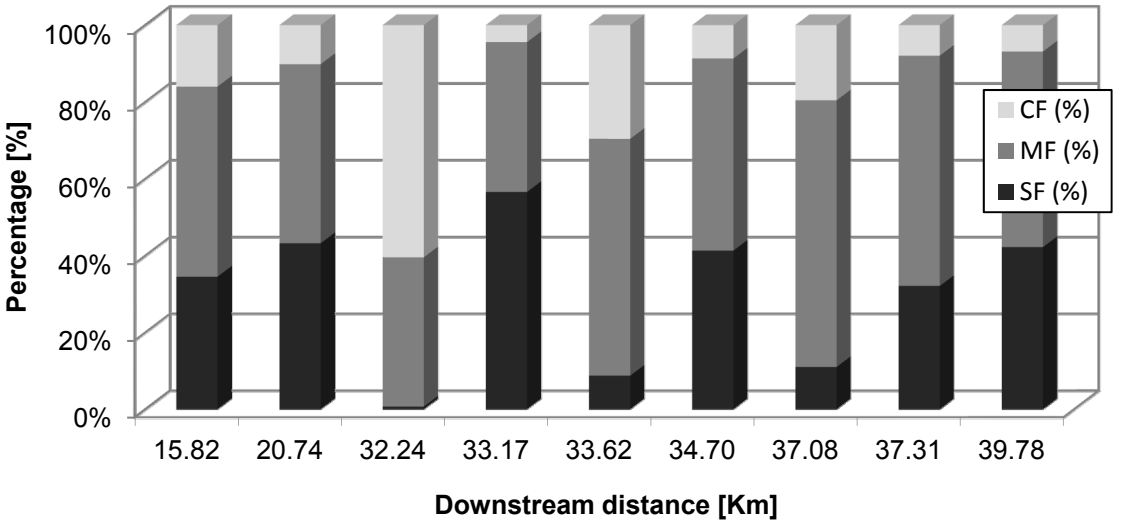

Figure 3-14 Downstream distribution of cohesive sediments. CF, MF and SF are the percentages of clay, silt and sand, respectively.

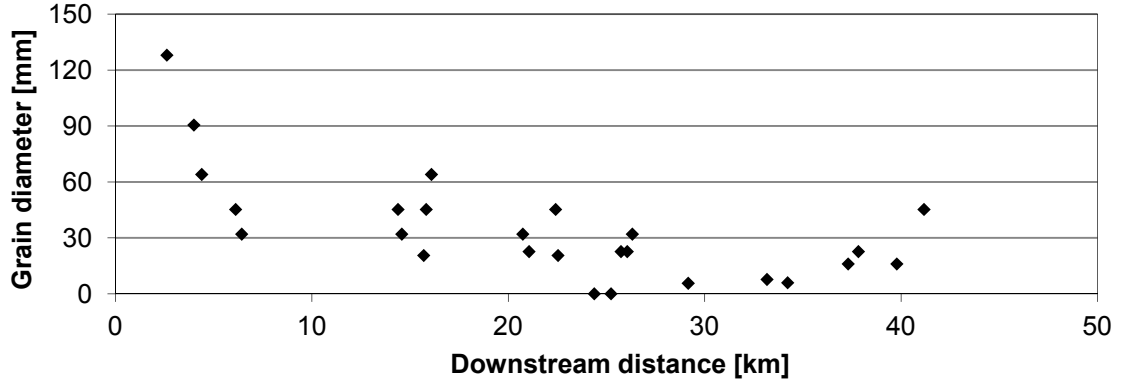

Figure 3-15 Grain size distribution (D_{50}) of sediments at the bank toe.

3.3 Application of models at the catchment scale

Different models, described in Section 2.3.1, were employed at the catchment scale, based on data obtained through field surveys and data available from station gauges located along the river. Specifically, the conceptual model of changing bank processes (Lawler, 1992), the DOCPROBE (Lawler, 1992) and two lateral indexes (Bledsoe and Watson, 2001 and Piégay et al., 2005) were applied with the aim to investigate factors which control the instabilities observed along the Cecina River.

Results were compared with riverbanks retreat distribution derived by GIS analysis on aerial photos.

3.3.1 Conceptual model of changing bank process

Data derived by field surveys and grain size analyses were compared with the conceptual model of changing bank process dominance at the basin scale from Lawler (1992). The model is based on the downstream sorting in grain size distribution, i.e., for instance, mass failures mostly occur downstream where, generally, cohesive banks are dominant.

In the case of Cecina River, the downstream distribution of sediments is not able to justify the conceptual model. In fact, although the percentage of cohesive sediments increases downstream, nonetheless, the spatial variability of non-cohesive sediments is large (Figure 3-16).

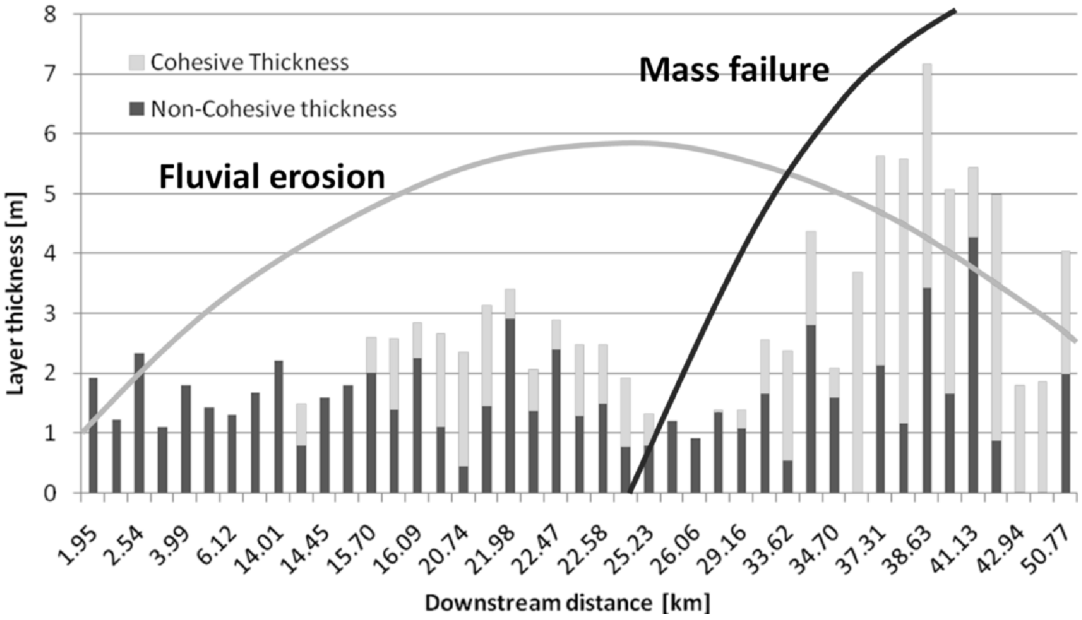

Figure 3-16 Overlay of downstream trend of layer thickness along Cecina River and conceptual model from Lawler (1992).

Because of the small dimension of Cecina catchment, cohesive banks are quite rare, and this could explain why Lawler model cannot describe the reality observed along the river.

3.3.2 DOCPROBE model

The DOCPROBE conceptual bank erosion model (Lawler, 1992), described in Section 2.3 was applied with the aim to explore if the stream power might explain the distribution of lateral instability along the Cecina River. Therefore, the spatial distribution of the total (gross) stream power Ω (Eq.2.9) and the unit stream power $\omega=\Omega/w$ was reconstructed, based on available data, as following described.

The specific weight of the fluid $\gamma=\rho g$ was assumed constant and equal to 9810 N/m^3.

Values of the discharge with a return period of 2 years (Q_2) were obtained every 250 m as a power function in terms of channel length (Eq.2.8). This regression was based on values estimated in previous analyses (Rinaldi, 2003).

Table 3-2 provides the location of the station gauges and values of Q_2 derived from Rinaldi (2003), while in Figure 3-17 results of the discharge distribution along the catchment are shown.

The slope of the channel (S) was obtained, every 250 m, as a negative exponential function of the length (Eq.2.9) using measures of slope carried out on maps and on 142 cross sections provided by Provincia di Pisa.

The sections cover a total length of 27.5 km (from km 30.160 to km 57.6 upstream distances) around 200 m spatially distributed between the reaches CB and CC. These data were integrated with values of slope at the segment CA obtained through measures on topographic maps. Thus, given the initial slope and the coefficient of slope reduction in downstream direction, values of the slope were estimated every 250 m through the regression (Figure 3-17).

A [m^2]	Downstream Distance [m]	Q_2 [m^3/sec]
254.1	32447.96	165.2
397.5	37547.12	258.5
495	50323.19	311.4
634	57660	339.9
825	61729.18	427.9

Table 3-2 Station gages locations and values of discharge Q_2.

Values of the channel width *w* were derived from GIS analyses on aerial photos and fitted with a second order polynomial every 250 m. This fitting method has been selected because it provided the highest correlation coefficient; moreover it is able to represent the narrowing occurring downstream the reach CC. The downstream decreasing of width depends on the development of different channel morphologies (e.g. sinuous with a decreasing number of alternate bars), together with higher degree of urbanization. However measures of channel width are highly scattered (Figure 3-18). Consequently the correlation is still low.

The trends of the total and unit stream power are shown in Figure 3-19 together with measured riverbank retreat occurred between 1994 and 2004. The total stream power, calculated through the regressions of discharge and slope, presents a maximum in the final part of sub-reach CA (km 25.750), where the river is still semi-confined, whereas downstream, along the sub-reaches where the river is mobile, shows a decreasing trend.

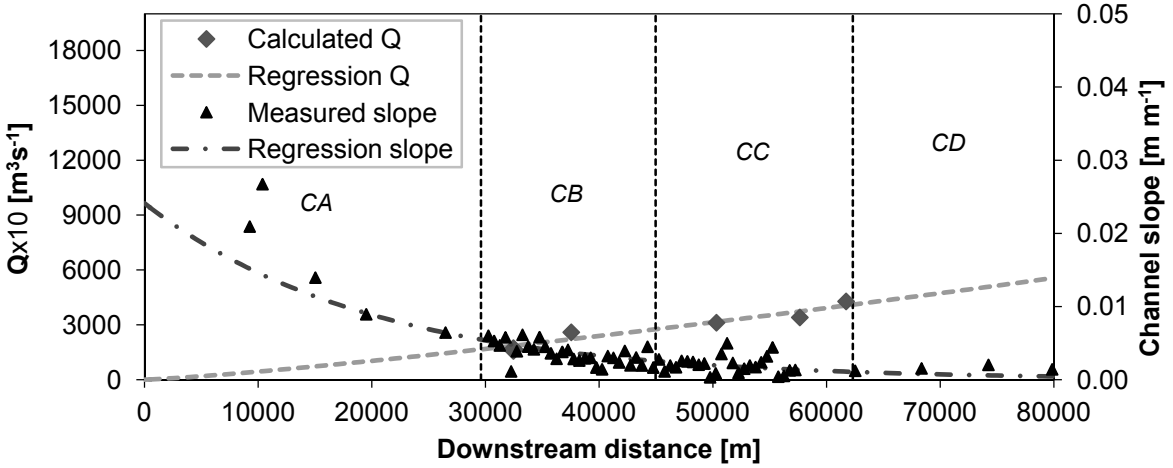

Figure 3-17 Slope and discharge regressions obtained from measured data.

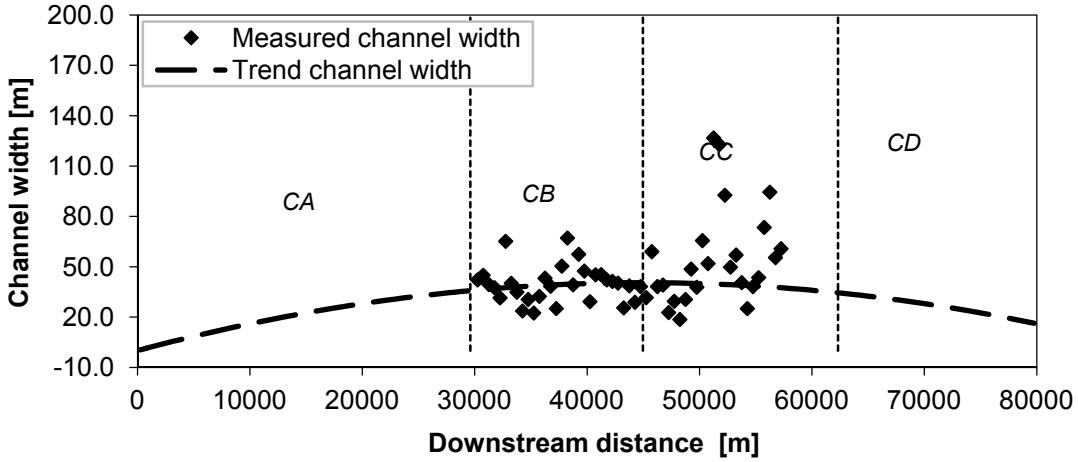

Figure 3-18 Measured and fitted channel width.

The tendency in downstream energy reduction (after the semi-confined reach) and the increasing cohesive bank sediments can partly explain the downstream distribution of bank retreat (slight trend of decreasing rates of retreat).

The peak of retreat occurred within the sub-reach CC is particularly high compared to the other values, and it is not predicted by the stream power. The value of the correlation coefficients R calculated by means of measured values of Ω and ω plotted against values of retreat measured at the same downstream distances (Figure 3-20), confirmed the same qualitative observations.

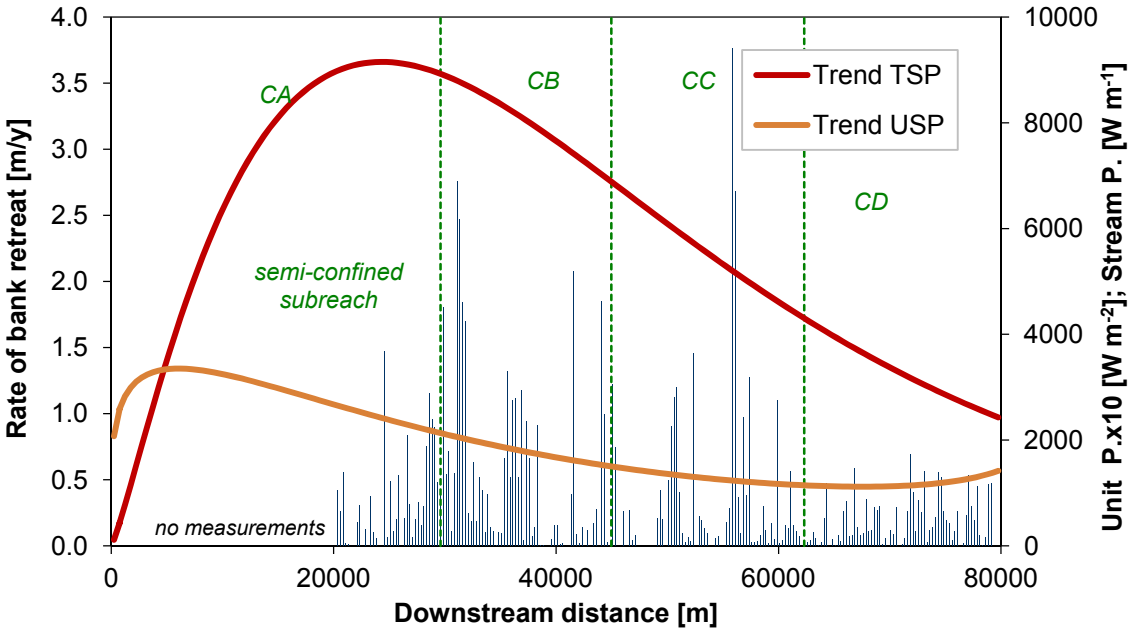

Figure 3-19 Comparison between measured riverbank retreat and trend of total stream power (SP) and unit stream power (USP).

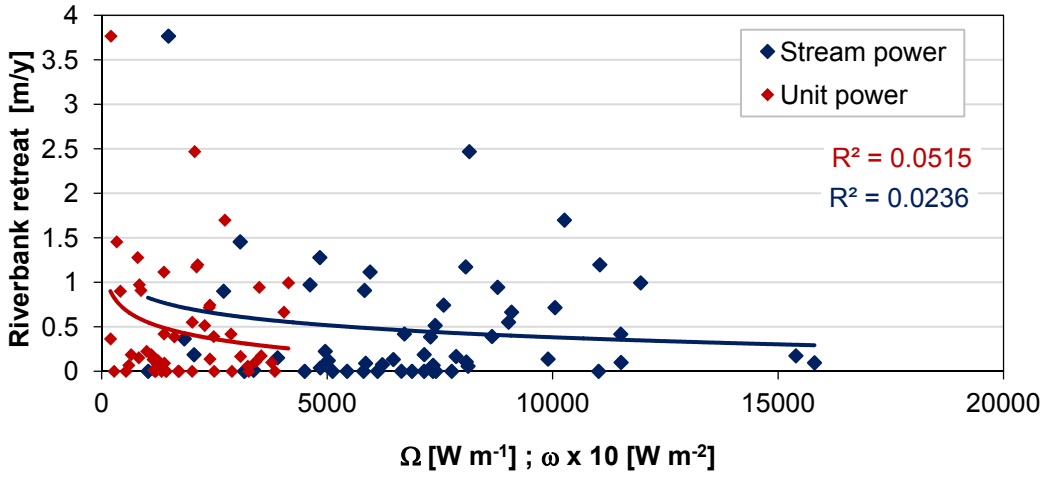

Figure 3-20 Stream and unit power plotted against the riverbank retreat.

The trend of the total stream power better represents the tendency of riverbank retreat than the unit stream power (Figure 3-19). However, due to the high variability of the rates of retreat, qualitative observations show that there is very low correlation between the total stream power and the unit stream power with measure data of retreat. A modest control on the distribution of peaks rate of erosion downstream was found qualitatively. This suggests that the stream power might lightly control the maximum values of retreat, but the high variability is the product of local factors (e.g. presence of bends, bars and vegetation or bank material) which are not accounted by the model.

3.3.3 Lateral indexes

Two empirical indexes based on logistic regression models to predict lateral instability (see description in Section 2.3), namely the Mobility Index (*MI*) by Bledsoe and Watson (2001) and the Erosion Index (*EI*) proposed by Piégay et al. (2005), were undertaken aiming to investigate factors controlling the occurrence of lateral instabilities along the Cecina.

Data required to calculate the indexes (Eq.2.12 and Eq.2.13) were obtained as following: (1) values of the discharge and slope are those employed in the stream power analyses and obtained through the linear regression; (2) values of the median sediment diameters were measured with grain size distribution analyses on samples collected during the surveys; (3) values of the catchment area at the selected sites were estimated through a linear regression, fitting known data with a cubic polynomial function (Figure 3-21).

Comparison between results of the lateral indexes and measured bank retreat (Figure 3-22) suggests that both the Mobility Index and the Erosion Index are not able to predict instabilities for the case study. In fact, notwithstanding the general trends decrease downstream as a consequence of the prevailing effect of slope reduction, the correlation, only based on qualitative observations, is very weak due to the great data dispersion.

The values of correlation coefficients between both lateral indexes and values of retreat measured at the same location (Figure 3-23) definitely prove that the models do not fit with the case of Cecina River.

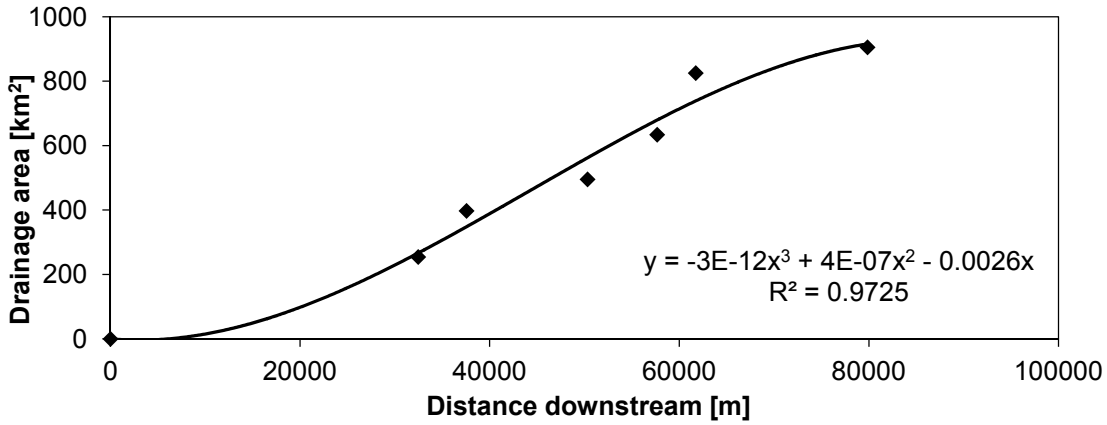

Figure 3-21 Linear regression of catchment area.

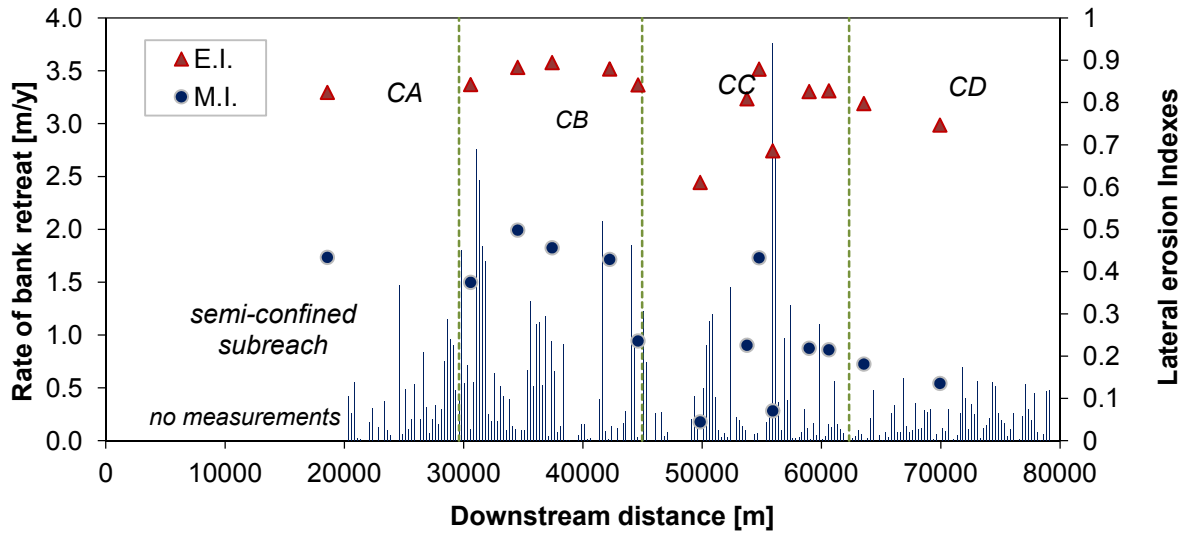

Figure 3-22 Measured river bank retreat with Erosion Index (E.I.) and Mobility Index (M.I.) along Cecina River.

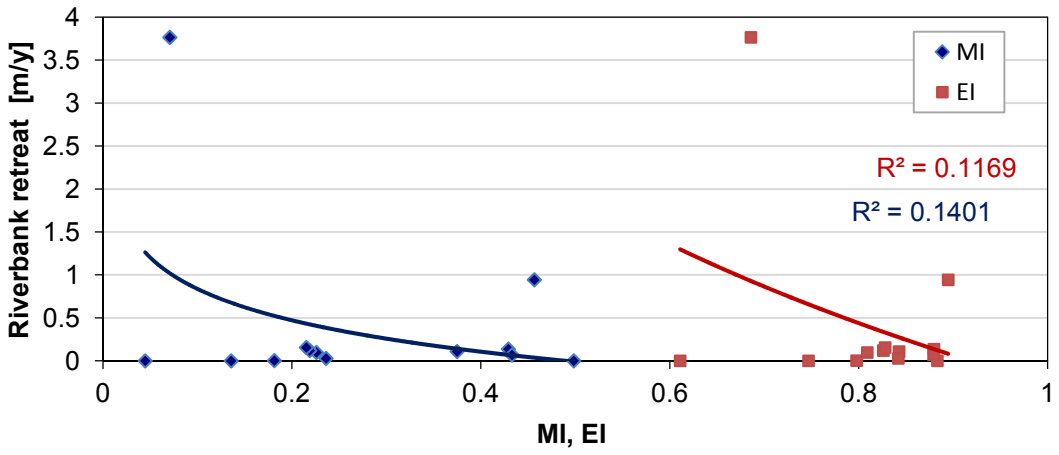

Figure 3-23 M.I and E.I. plotted against the riverbank retreat.

3.4 Conclusions

Cecina riverbanks are mostly composite, having slopes and heights highly variable and percentage of coarse gravels decreasing downstream, as well as the median diameter of sediments. Mass failures and fluvial erosion processes are distributed for the entire length of the river.

Apparently, there is no relation between mass failures and bank geometry, whereas the relation between processes and composition is more evident: non-cohesive bank are prone to debris and rotational failures, composite banks are mostly subject to cantilever, while in cohesive banks shallows slides prevail.

The application of different models at the case study highlighted how prediction of spatial distribution of lateral instability at the catchment scale is still extremely challenging, depending on complex interactions between stream energy and bank characteristics.

In the case of Cecina River, the tendency in downstream energy reduction (after the semi-confined reach) and the increasing cohesive bank sediments partly explain the downstream distribution of bank retreat (slight trend of decreasing rates of retreat). However, local channel conditions (presence of bars, curvature, etc.), that are not taken into account into the predictive models, are probably key factors to explain most of the local lateral instability.

The absence of consideration of bank strength may also explain why the tested models failed to provide accurate predictions.

Moreover, it is possible that lateral indexes do not fit the case of the Cecina River due to the small dimension of the river itself. In fact, the above mentioned models have been developed and tested on wider catchments areas.

Finally, channel evolution and present trends of adjustments are also important and need to be accounted to better understand present distribution of lateral instability: in the case of Cecina River, the tendency towards a meandering channel form may explain part of the spatial distribution and local lateral instabilities.

In conclusion, these models represent an important tool for river management issues due to their straightforwardness. Nevertheless, in order to better understand processes and triggering causes liable to the peaks of riverbank retreat, specific models have to be employed at the reach scale, depending on the channel morphology.

PART II: MODELLING RIVERBANK RETREAT AT THE REACH SCALE

In recent years many progresses have been made in understanding and modelling bank erosion processes, but an accurate quantification of shear stresses exerted by the flow on the bank area, and consequently of the fluvial erosion rate, continues to be a challenging issue. The objective of the present research is to test different methods to estimate the rate of riverbank retreat in the perspective of definition of risk due to fluvial erosion. The first step of the research consisted in data collection, which included field surveys along a study reach of the Cecina River. Different hydraulic models have been selected in order to calculate the flow parameters involved in the quantification of erosion rates, with an attempt to test new methods for the estimation of near-bank shear stresses, and subsequently to link them to bank erosion models. Specifically, a method recently developed by Kean and Smith (2006a,b) to determine the form drag exerted on small-scale topographic bank features, and thus to quantify the near-bank flow field, was employed. Results of the analyses were used to calibrate the erodibility parameter. Moreover they represented a base for a new framework to characterize risk due to fluvial erosion. Finally, an example of coupling fluvial erosion and bank stability is provided by applying the Bank Stability and Toe Erosion Model (BSTEM) on the eroded profiles obtained from the fluvial erosion analysis.

4. Models

This chapter provides a theoretical description of the models employed for the analysis of riverbank retreat at the reach scale. Specifically, two hydraulic models (HEC-RAS and River2D) and two near-bank shear stress models, i.e., a distribution from literature (Simons and Senturk, 1977) and the analytical model proposed by Kean and Smith (2006a,b), have been selected in order to obtain the parameters required by the fluvial erosion model based on the excess shear stress (Partheniades, 1965, Arulanandan et al., 1980). Moreover the BSTEM model has been employed for bank stability analysis.

4.1 Fluvial erosion model

In the present study, the rate of riverbank erosion has been quantified using the excess shear stress approach of Partheniades (1965) and Arulanandan et al. (1980). Following this approach, the fluvial erosion rate is related to the excess shear stress through a simple power relation of the following form:

$$\varepsilon = k_d(\tau - \tau_c)^a \tag{4.1}$$

where ε (m s^{-1}) is the fluvial erosion rate per unit time and unit bank area, τ (Pa) is the boundary shear stress applied by the flow, k_d (m^3 (Ns)$^{-1}$) and τ_c (Pa) are erodibility parameters (erodibility coefficient, k_d, and critical shear stress, τ_c) and a (dimensionless) is an empirically derived exponent, generally assumed equal to 1.0.

Rinaldi and Darby (2008) underlined that, although excess shear stress model is widely accepted and used in a range of geomorphological applications (e.g., Arulanandan et al., 1980; Govers, 1991; Howard, 1994), no formal validation has been yet undertaken. Thus some uncertainty remains over the value of the exponent a (which is commonly assumed to take a value close to 1 for most studies involving cohesive sediments).

In the present research, hydraulic conditions at the selected reach along the Cecina River were modelled using a combination of one and two-dimensional hydraulic models. Thus, the results of these analyses have been coupled with two near-bank shear stress models, namely the Simons and Senturk (1977) distribution and the analytical model developed by Kean and Smith (2006a). These models, together with the erodibility parameters, provided data required to estimate the rate of fluvial erosion through the excess shear stress formulation.

4.2 Hydrodynamic models

The hydrodynamic modelling included the use of two different numerical simulations: one and two-dimensional depth averaged finite element hydrodynamic model, HEC-RAS 4.0 and River2D, respectively. The one-dimensional model was used to provide the boundary conditions required by River2D. Both models have been applied to steady flow analyses.

A 3D-model would be able to better describe velocities and shear stress at the boundary, taking into account the secondary flows developing at the bend which is located at the selected reach; nevertheless, a 2D-model has been employed as a compromise between an accurate description of the hydrodynamics and a method suitable for practical issues.

4.2.1 1D model: HEC-RAS

Developed by the U.S. Army Corps of Engineers (USACE), HEC-RAS (*Hydrologic Engineering Centers River Analysis System*) is one of the most popular one-dimensional model to perform steady and unsteady flow calculations (HEC, 2002). The model supports water surface profile calculations for subcritical, supercritical, or mixed flows; it can also handle the presence of bridges, culverts and variable roughness.

In the HEC-RAS steady state simulation, water surface profiles are computed by adopting the standard step method to solve the energy equation (4.2). From one section to the next one, the standard step method applies conservation of energy using the energy equation to calculate water-surface elevations and energy grade lines along the reach. For the purpose of the standard step, the energy equation is written as follows:

$$Z_2 + Y_2 + \frac{a_2 \bar{V}_2^2}{2g} = Z_1 + Y_1 + \frac{a_1 \bar{V}_1^2}{2g} + h_e \qquad (4.2)$$

where:

Y_1, Y_2 = water depth at x-sections

Z_{12}, Z_2 = elevations of the main channel inverts

$\bar{V}_1, \bar{V}_2$= averaged velocities

a_1, a_2 = velocity weighting coefficients

g = gravitational acceleration

h_e = total energy head loss between adjacent cross section

Total energy loss between adjacent cross sections is defined as:

$$h_e = L\bar{S}_f + C\left|\frac{\alpha_2 \bar{V}_2^2}{2g} - \frac{\alpha_1 \bar{V}_1^2}{2g}\right| \tag{4.3}$$

where L is discharge weighted reach length, $\bar{S}_f$ is representative friction slope between two cross sections, and C is an expansion or contraction loss coefficient. The representative friction slope and the distance weighted reach length are defined in Equation 4.4 and 4.5, respectively.

$$\bar{S}_f = \left(\frac{Q_1 + Q_2}{K_1 + K_2}\right)^2 \tag{4.4}$$

$$L = \frac{L_{lob}\bar{Q}_{lob} + L_{ch}\bar{Q}_{ch} + L_{rob}\bar{Q}_{rob}}{\bar{Q}_{lob} + \bar{Q}_{ch} + \bar{Q}_{rob}} \tag{4.5}$$

where K is the conveyance, L_{lob}, L_{ch} and L_{rob} are the cross-section reach lengths for flow in the left over-bank, main channel, and right over-bank, respectively, and $\bar{Q}_{lob}$, $\bar{Q}_{ch}$, and $\bar{Q}_{rob}$ are the arithmetic average of the flows between sections in the left over-bank, main channel, and right over-bank, respectively.

To determine the total conveyance and the velocity coefficient for a cross-section, HEC-RAS subdivides the flow in the main channel from that in the over-banks. Conveyance is calculated for each subdivision using the following equations:

$$Q = KS_f^{1/2} \tag{4.6}$$

$$K = \frac{1.486}{n}AR^{2/3} \tag{4.7}$$

where n is the Manning's roughness coefficient, A and R are the flow area and the hydraulic radius for each subdivision, respectively. The total conveyance for each subdivision is calculated as the sum of the conveyances from the left over bank, main channel, and right over bank. The flow in the main channel is subdivided only when the Manning's roughness coefficient changes within the channel area. The composite main channel Manning's roughness coefficient is defined as follows:

$$n_c = \left[\frac{\sum_{i=1}^{N}(P_i n_i^{1.5})}{P}\right]^{2/3} \quad (4.8)$$

where n_c is the composite or equivalent coefficient of roughness, P is the wetted perimeter of the entire main channel, P_i is the wetted perimeter of the subdivision i, and n_i is the coefficient of roughness for the subdivision i.

Limitations in the HEC-RAS steady flow simulation include the assumptions that the flow is steady, gradually varied, one-dimensional, and the river channels have small slopes.

For situations when the flow is rapidly varied, the momentum equation is used to solve the water surface profiles. These situations include hydraulics of bridges, river confluences, and mixed flow regimes such as hydraulic jumps.

Additional specifications on the hydraulics applied by HEC-RAS can be found in the HEC-RAS Hydraulic Reference Manual (U.S.A.C.E., 2002).

Input parameters required by HEC-RAS include topographic data in the form of cross-sections, Manning's roughness values across each cross-section, and flow data including flow rates and flow change locations. In addition, boundary conditions must be established at the downstream cross section for a subcritical flow profile and at the upstream cross section for a supercritical flow profile. Both upstream and downstream boundary conditions are required for mixed flow regime computations.

The model allows four boundary condition options: water-surface elevation, critical depth, normal depth and rating curve.

Critical depth is defined as the flow depth when $Fr = 1$. Normal depth is defined as the depth corresponding to uniform flow (Chow, 1959). Normal depth is calculated after the user enters the bed slope downstream of the studied reach. The bed slope is equal to the energy slope for normal depth and, therefore, is used in the flow resistance equation to calculate normal depth.

4.2.2 2D model: River2D

River2D is an implicit finite-element, two-dimensional and depth-averaged hydrodynamic model, based on a conservative Petrov-Galerkin upwinding formulation (Ghanem et al., 1995; Hicks and Steffler, 1992). This model was developed at the University of Alberta (Steffler and Blackburn, 2002) specifically for gravel-bed rivers, and the software is of public domain. River2D has been

employed (a) to predict habitat changes resulting from flow alterations and channel morphology (Lacey e Millar, 2004); (b) to assess the flow rates required to facilitate passage by fish species (Reinfelds et al., 2010); (c) in rehabilitation and restoration programs (Wu and Mao, 2007; Boavida et al., 2009; Lee et al., 2010); (d) to explore the potential effects of floodplain woodland on flood flows (Thomas and Nisbet, 2006); and (e) to predict hydraulics with a partial or total ice cover (Katopodis and Ghamry, 2007).

River2D solves the basic mass conservation and momentum conservation equations at two components (x and y). Outputs from the model are two velocity components (in x and y directions) and the depth at each node. The model is able to handle subcritical, supercritical and transcritical flows.

River2D includes the following sub-modules:

- R2D_Bed to aid in the development of the bed file from field data;
- R2D_Mesh to generate the input computational triangular mesh;
- R2D_Ice intended for defining and editing ice topography files (ice cover of water surface) for the use in the River2D program (not used for this task);
- River2D to perform the hydrodynamic computation; in this module, it is possible to set the parameters for ichthyofauna, e.g. weighted usable area (WUA) (not used for this task).

The ice module models the flow under a floating ice cover with known geometry while the fish habitat module is based on the Weighted Usable Area (WUA) concept used in the PHABSIM family of fish habitat models (Steffler and Blackburn, 2002). WUA is calculated according to flow conditions (velocity, depth and channel substrate) that fish species prefer.

As well as most of 2D models, hydrodynamic computations in River2D are based on the 2D vertically averaged St. Venant equations. These equations represent the principles of conservation of mass and conservation of momentum, both in x and y directions (Equations 4.9, 4.10 and 4.11, respectively).

$$\frac{\partial H}{\partial t}+\frac{\partial q_x}{\partial x}+\frac{\partial q_y}{\partial y}=0 \tag{4.9}$$

$$\frac{\partial q_x}{\partial t}+\frac{\partial}{\partial x}\left(Uq_x\right)+\frac{\partial}{\partial y}\left(Vq_x\right)+\frac{g}{2}\frac{\partial}{\partial x}H^2=gH\left(S_{0x}-S_{fx}\right)+\frac{1}{\rho}\left(\frac{\partial}{\partial x}\left(H\tau_{xx}\right)\right)+\frac{1}{\rho}\left(\frac{\partial}{\partial x}\left(H\tau_{xy}\right)\right) \tag{4.10}$$

$$\frac{\partial q_y}{\partial t}+\frac{\partial}{\partial x}\left(Uq_y\right)+\frac{\partial}{\partial y}\left(Vq_y\right)+\frac{g}{2}\frac{\partial}{\partial y}H^2=gH\left(S_{0y}-S_{fy}\right)+\frac{1}{\rho}\left(\frac{\partial}{\partial x}\left(H\tau_{yx}\right)\right)+\frac{1}{\rho}\left(\frac{\partial}{\partial x}\left(H\tau_{yy}\right)\right) \quad (4.11)$$

where H is the water depth, U and V are the vertically averaged velocities in x and y directions, respectively, and q_x and q_y are the discharge intensities related to the velocity components through the following:

$$q_x = HU \quad \text{and} \quad q_y = HV \quad (4.12)$$

S_{ox}, S_{oy} are the bed slopes; S_{fx}, S_{fy} are the friction slopes; τ_{xx}, τ_{xy}, τ_{yx}, τ_{yy} are the components of turbulent stress tensor (depth averaged transverse shear stresses); g is the gravitational acceleration and ρ is the water density.

The basic assumptions in the equations are:

1. The pressure distribution is hydrostatic thus limiting the accuracy in areas of steep slopes and rapid changes in bed slopes.

2. The horizontal velocities are constant with depth, and so information on secondary flows and circulation are not available

3. Coriolis and wind forces are assumed negligible.

The friction slope terms depend on the bed shear stresses which are assumed to be related to the magnitude and direction of the depth averaged velocity. Equation (4.13) represents the bed resistance model and describes the friction slope in the x direction:

$$S_{fx}=\frac{\tau_{bx}}{\rho gH}=\frac{\sqrt{U^2+V^2}}{gHC_S^2}U \quad (4.13)$$

where τ_{bx} is the bed shear stress in the x direction and C_s is a non-dimensional Chezy coefficient. This coefficient, in turn, is related to the effective roughness height, k_s, of the boundary, and the depth of flow through the Equation (4.14):

$$C_S = 5.75\log_{10}\left(12\frac{H}{k_s}\right) \quad (4.14)$$

A closure turbulence scheme is required in order to estimate the transverse shear stresses which are caused by turbulent flow interactions. Transverse shear stresses represent four additional unknown terms in the 2D St. Venant equations. In River2D, depth-averaged transverse turbulent shear stresses are modelled with a Boussinesq approximation which allows an estimation of the eddy viscosity

coefficient (ν_t) through flow parameters, as described, for example, in the following equation:

$$\tau_{xy} = \nu_t \left(\frac{\partial U}{\partial y} + \frac{\partial V}{\partial x} \right) \tag{4.15}$$

The eddy viscosity coefficient is assumed to be composed of three components: a constant, a bed shear generated term, and a transverse shear generated term as follows:

$$\nu_t = \varepsilon_1 + \varepsilon_2 \frac{H\sqrt{U^2 + V^2}}{C_s} + \varepsilon_3^2 H^2 \sqrt{2\frac{\partial U}{\partial x} + \left(\frac{\partial U}{\partial y} + \frac{\partial V}{\partial x} \right)^2 + 2\frac{\partial V}{\partial y}} \tag{4.16}$$

where ε_1, ε_2 and ε_3 are user definable coefficients and they can be used as a secondary calibration parameters.

Concerning common difficulties (due to the fact that depth is unknown a priori) for two dimensional models in treating areas with shallow (or no water) depth, River2D handles those situations by changing the surface flow equations to groundwater flow equations in these areas.

Additional specification on the hydraulics and on the solver applied by the model can be found in the River2D - User Manual (Steffler and Blackburn, 2002).

As input data, River2D hydrodynamic model requires channel bed topography, roughness and transverse eddy viscosity distributions, boundary conditions and initial flow conditions.

Survey data are used to create a digital elevation model (DEM) which provides the bed topography input data in the form of x, y and z coordinates for River2D. In addition to the bed topography data, the input file also requires the roughness k_s to be defined at every node. A bed topography module is included in River2D to graphically edit and refine the input file. The computational discretization, i.e. the finite element mesh, can be created from the bed topography file using the mesh generation program, R2D_Mesh (Steffler, 2000; Ghanem et al., 1995). The computational boundaries, including inflow and outflow sections, are graphically defined at this stage. The modelled domain is then filled with nodes at a spacing specified by the user before the mesh generation utility is used to perform a triangulation. Only triangular elements are included in the mesh as these elements are considered the simplest possible in two dimensions and result in the minimum

execution time for a given number of nodes (Steffler, 2000). In regions of high interest or where flow variations are large, more closely spaced nodes can be used to minimize errors. Once a satisfactory mesh has been created and boundary conditions specified, River2D simulations can proceed to solve the depths and velocities at all the computational nodes within the modelled domain.

Boundary conditions typically take the form of a specified total discharge at the inflow and fixed water surface elevations or rating curves at the outflow.

Initial conditions, represented by the inflow depth, are also important because they can significantly reduce the total run time and in some cases make the difference between a stable and unstable runs. In locations where the depth of flow becomes very shallow or where there is no water over a part of the modelled area, River2D utilizes groundwater flow equations.

A limitation of River2D is that it only computes the hydrodynamics for a fixed bed. This limitation has been recently overcome with the inclusion of an application of a river morphology allowing for bed elevation changes simulations Kwan (2009).

4.3 Near bank shear stress distribution models

4.3.1 Distribution from literature

In channel bed the force acting in the direction of the flow and resulting from the pull of the water on the wetted area is known as tractive, or shear and drag force. The idea of tractive force is believed to have been firstly introduced in literature by Du Boys in 1879. However, the principle of balancing this force with the channel resistance in a uniform flow was stated by Brahms early in 1754 (Chow, 1959).

In a uniform flow the average value of the shear force per unit wetted area is equal to $\gamma_w RS$, where γ_w is the unit weight of water, R is the hydraulic radius and S is the slope. In wide open channel the hydraulic radius can be approximated to the depth of the flow.

The shear force is not uniformly distributed along the wetted perimeter. Based on empirical data sets obtained from laboratory flumes, distributions of shear stress along the channel cross section were proposed (Leutheusser, 1963; Kartha and Leutheusser, 1972; Simons and Senturk, 1977; Knight et al., 1984). Although the application of these distributions is very simple, they should be employed with

awareness since they are not able to reproduce the effects of natural irregularities of the banks.

Simons and Senturk (1977) distribution (after Chow, 1959) is suitable for trapezoidal and sufficiently wide channel, i.e., when the ratio between the width and the depth of the channel is larger than three. As shown in Figure 4-1, according to this distribution the highest value of shear stress acting on the bank corresponds to 75% of the average shear stress of the cross section.

Simons and Senturk distribution was coupled with the 1D hydraulic model. In addition, the effect of the presence of the bend on the near-bank shear stresses was taken into account through the diagram from the Soil Conservation Service (1977) which expresses the ratio between the boundary shear stress on the outer bank and the averaged shear stress on the cross section as a function of the ratio between the radius of curvature and the channel width (Figure 4-2).

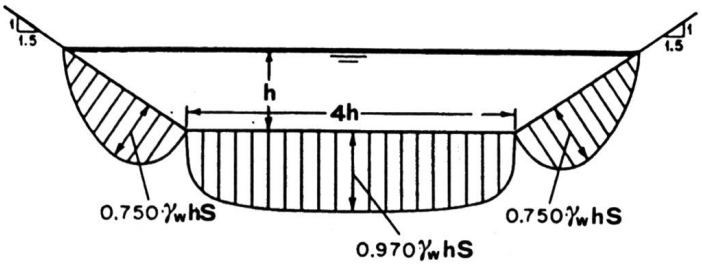

Figure 4-1 Shear stress distribution on cross-section according to Simons and Senturk.

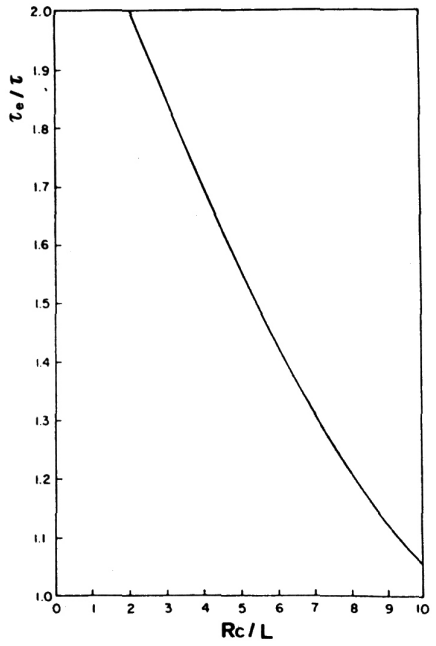

Figure 4-2 Soil Conservation Service diagram. τ_e: shear stress on outer bank; τ: averaged shear stress on cross section; *Rc*: radius of curvature; *L*: channel width.

4.3.2 River2D computation model

A second method employed to estimate the shear stress was represented by the hydrodynamic modelling. Specifically, results directly computed by River2D were used in the following analyses. For each node of the mesh the model calculate the non-dimensional Chezy coefficient. This coefficient is related to the effective roughness height, k_s, of the boundary and the depth of flow, H, through:

$$C_S = 5.75 \log_{10}\left(12\frac{H}{k_s}\right) \tag{4.17}$$

The shear stresses are assumed to be related to the magnitude and direction of the depth-averaged velocity U, through the Chezy parameter, such as:

$$\tau = \rho\frac{|U|^2}{C_S^2} \tag{4.18}$$

4.3.3 Near-bank shear stress model from Kean and Smith

Near-bank flow in natural streams and rivers is deeply affected by the presence of irregularities along the bank profiles (Thorne and Furbish, 1995; Kean and Smith, 2006a). The roughness elements of riverbank commonly include stems, roots of woody vegetation, as well as topographic undulations produced by the erosion and the slumping of bank material.

Kean and Smith model (2006a,b) is based on field and laboratory measurements, and provide an estimation of the shear stress field near riverbank, taking account for the presence of small-scale topographic features. Based on survey data on small stream in midwest and western United States, the authors approximated the roughness elements as Gaussian-shaped features defined in terms of three parameters: a protrusion height H, a streamwise length scale σ, and a spacing between crests, λ.

The model has been recently applied by Darby et al. (2010) to the Lower Mekong River, in combination with a novel field measurement technique which provides values of the critical shear stress for cohesive soils (CSM), aiming to improve the parameterization of the excess shear stress model (Eq.4.1).

Following the approach of Smith and McLean (1977), Kean and Smith method is able to partition the drag on bank roughness elements into form and skin components, as follows:

$$\tau = \tau_{SF} + \tau_D \tag{4.19}$$

where τ is the total shear stress on the boundary of the channel, τ_{SF} is the skin drag component and τ_D the form drag component induced by the pressure differential between front and back of large scale topographic elements which protrude into the flow; such pressure differential produces a force (or drag) on the element surfaces.

Partitioning makes this model a potentially significant advance in riverbank retreat analyses. In fact, although the total stress comprises two components, i.e. the skin drag component and the form drag component, only the former is exerted directly onto the sediment grains, whereas the latter is relevant in the context of bank erosion. It is assumed that the form drag component is dissipated by the macro topography, thereby reducing the total stress available for geomorphic work.

The form drag on an individual roughness element embedded in a series of identical elements is determined using the drag coefficient of the individual element and a reference velocity that includes the effects of further upstream roughness elements. In addition to calculating the drag on each element, the model determines the spatially averaged total stress, skin friction stress and roughness height of the boundary. The effects of bank roughness on patterns of velocity and boundary shear stress are determined by combining the form drag model with a channel flow model (Kean and Smith, 2006a). Specifically, the form drag (F) on an individual roughness element is defined as (Kean and Smith, 2006a):

$$F = \frac{1}{2}\rho C_D H B u_{ref}^2 \tag{4.20}$$

where ρ is the density of water, H is the protrusion height of the element, B is the length of the element normal to the flow direction, u_{ref} is a reference velocity and C_D is the drag coefficient of the element. The reference velocity is defined by Kean and Smith as the average of the square of the velocity that would be present at the location of a roughness element if that element was removed from the flow.

For high Reynolds number flows, such as occurred in rivers and in flows of interest in this study, C_D is a function of the shape of the object and it is nearly independent of the Reynolds and Froude numbers. The product of the element's drag coefficient and the height provides some indication about the relative effects that these bumps

will have on the flow. This product scales the drag on the element, as well as the velocity deficit of its wake, which, in turn, affects the drag on elements located downstream (Kean and Smith, 2006b).

For each topographic element embedded in a sequence of regularly spaced elements, the reference velocity is controlled by the wake of the upstream element. In addition, u_{ref} is affected by a growing internal boundary layer on the wall that begins at the reattachment point (R) of the separation zone on the upstream form (Figure 4-3). Thus, u_{ref} is affected by three interdependent regions, namely, the internal boundary layer region, the wake region, and the outer boundary layer. The velocity field within each region must be determined in order to calculate u_{ref}. Following Smith and McLean (1977) and McLean and Smith (1986) approach, Kean and Smith (2006a) describe the velocity field in each region separately and join them together using matching conditions in order to determine u_{ref}.

Since for most of the internal boundary layers, the velocity is turbulent, it can be described by the law of the wall, which is given by the following equation (Kean and Smith, 2006a):

$$u = \frac{u_{*IBL}}{k} ln \frac{z}{z_{0SF}} \tag{4.21}$$

where κ is von Karman's constant, z is the distance away from the boundary, z_{oSF} is the local roughness height of the boundary without topographic roughness elements, and u^*_{IBL} is the shear velocity within the internal boundary layer ($=\sqrt{\tau_{SF}/\rho}$).

The thickness of layer is estimated using the approach suggested by Miyake (1965), and the slope of the internal boundary layer height is given by:

$$\frac{d\delta}{dx} = \frac{\gamma u_*}{u} \tag{4.22}$$

where δ is the boundary layer height, u is velocity at the top of the boundary layer, and γ is a constant of order 1.

Similarly, the flow in the outer region follows the law of the wall:

$$u = \frac{u_{*T}}{k} ln \frac{z}{z_{0T}} \tag{4.23}$$

where $u_{*T} = \sqrt{\tau_T/\rho}$ and z_{0T} is the roughness height due to both skin friction and form drag.

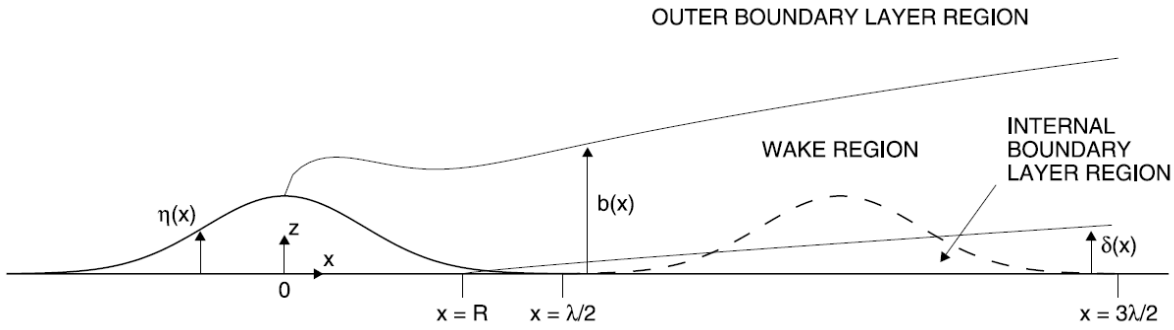

Figure 4-3 Plan view geometry of the topographic roughness elements, along with the internal boundary layer, wake, and outer regions of the flow (flow direction is left to right). The dashed line of the downstream element denotes that it is removed from the flow, with the u^2_{ref} for this element being the average squared velocity over this area. The unit 'cell' from $\lambda/2$ to $3\lambda/2$ is the length over which the stresses are averaged (Kean and Smith, 2006a).

The wake region between the outer and the internal layer is modeled using Schlichting's (1979) far-field wake solution:

$$u = u_b \left[1 - g(x) f\left(\frac{z-\eta}{b}\right)\right] \tag{4.24}$$

where $g(x)$ and $f\left(\frac{z-\eta}{b}\right)$ are defined as follows (Kean and Smith 2006a):

$$g(x) = A_2 \left(\frac{x + x_0}{C_D H}\right)^{1/2} \tag{4.25}$$

$$f\left(\frac{z-\eta}{b}\right) = \left[1 - \left(\frac{z-\eta}{b}\right)^{3/2}\right]^2 \tag{4.26}$$

where x is the distance downstream from the centre of the element producing the wake, z is the distance away from the reference level of the roughness elements, $z = \eta$ is the surface of the boundary, u_b is the velocity at the top of the wake, and x_0 is the virtual origin equal to zero (Kean and Smith, 2006a). The wake thickness, b, is given by:

$$b = 2A_1 C_D H \left(\frac{x + x_0}{C_D H}\right)^{1/2} \tag{4.27}$$

in which A_1 and A_2 are constants set equal to $\sqrt{10\beta}$ and $\sqrt{20/(18\beta)}$, respectively, with β an empirically-determined constant that sets the value of the eddy viscosity within the wake. It has to be specified that, in previous expressions, C_D, H, and b are correlated to the element producing the wake and not to the element for which the reference velocity has to be calculated. Kean and Smith (2006a) calculate the

constant β using results from the flume experiments carried out by Hopson (1999) as follows:

$$\beta = 0.226\left[1 - exp\left(-0.353\frac{\lambda}{H}\right)\right] \tag{4.28}$$

Further details on the velocities matching conditions between the outer and the wake layer, and between the wake and the internal layer, can be found in Kean and Smith (2006a).

Equations (4.21), (4.22) and (4.24), together with the corresponding velocity matching conditions, fully specify the velocity field, *u(x, z)*, that would be present if the roughness element was removed from the flow. Once this field has been defined, the reference velocity required to compute the form is expressed as follows:

$$u_{ref}^2 = \frac{1}{A}\int_A u^2\,(x,z)dA \tag{4.29}$$

where A is the plan view area of the roughness element, which for a Gaussian shape equals to: $\sqrt{2\pi}H\sigma\mathrm{erf}\,(3/\sqrt{2})$.

The total boundary shear stress or the velocity in the outer region may then be specified to obtain a solution. In the context of fluvial erosion, often the total stress on the bank is not known a priori. Therefore, in this situation it is easier to close the problem by specifying a velocity at a level in the outer region of flow.

Using (4.21), and recalling that the bank topographic roughness elements are assumed to be Gaussian shaped, the drag stress is calculated using:

$$\tau_D = \frac{1}{2}\rho C_D\frac{H}{\lambda}u_{ref}^2 \tag{4.30}$$

if the average skin friction stress is expressed in terms of the shear velocity in the internal boundary layer, the total stress on the boundary can be written as follows:

$$\tau = \rho u_*^2 = \rho\langle u_{*IBL}\rangle^2 + \frac{1}{2}\rho C_D\frac{H}{\lambda}u_{ref}^2 \tag{4.31}$$

Kean and Smith (2006a) estimate the drag coefficient using an empirical function derived from the experimental data of Hopson (1999):

$$C_D = 1.79exp\left(-0.77\frac{\sigma}{H}\right) \tag{4.32}$$

To solve Eq.4.32, initial guesses of the total roughness height and shear velocity in the outer flow are made that match the specified outer velocity. Once specified, u_{ref} can be determined via the velocity matching conditions and using Eq.4.29. These values can then be used to obtain improved estimates of u_{*T} and z_{oT} through Eq.4.31 and 4.23.The procedure is iteratively repeated until the solution converges.

4.4 The bank stability model BSTEM

The Bank Stability and Toe Erosion Model is a physically-based model, which represents one of the few attempts to investigate bank-erosion dynamics combining fluvial erosion, pore water pressure changes and mass bank stability into an integrated modelling approach. The model allows to take into account the fluvial erosion processes and the presence of vegetation. However, in the present research BSTEM has been only employed for bank stability analysis on the eroded bank profile obtained through the fluvial erosion model described in section 4.1. This choice was dictated by the impossibility to use as input data the values of the shear stress at the boundary obtained by applying the different models described in section 4.3. Thus the present section only provides a description regarding the bank stability approach.

The first deterministic bank-stability model was developed at the USDA-ARS National Sedimentation Laboratory (Simon et al., 1999) in the late 1990's. The present model (Version 4.2) combines three limit equilibrium-method models that calculate the Factor of Safety (*FS*) for cantilever and planar failure modes. Simulated methods are horizontal layers (Simon et al., 2000), vertical slices with tension crack (Morgenstern and Price, 1965) and cantilever failures (Thorne and Tovey, 1981).

The model is able to account for the strength of 5 different soil layers, the effect of pore- water pressures on both the saturated and unsaturated parts of the failure plane, and the confining pressure from streamflow.

The input data required for bank stability analyses are the bank geometry, the water stage, the material properties of the soil layers and the value of the pore water pressure.

BSTEM allows the user to insert own data describing the different soils, otherwise, when unknown, it is possible to apply values of effective cohesion, effective angle of internal friction, saturated unit weight and angle ϕ^b provided by the model.

When the values of pore water pressure are not measured by the user, hydrostatic conditions are assumed below the water table and a linear interpolation provide the matric suction distribution above the water table.

Moreover, the user is allowed to: (1) vary the shear surface angle to find the lowest *FS* value, (2) use values measured in the field, or (3) let the model to search for the combination of the failure plane emergence elevation and the shear surface angle that minimizes the factor of safety.

The description of the three methods employed by BSTEM in the next subsections follows the 'Tech Background' of the model.

Streambank stability algorithms:

1. Horizontal Layers:

The Horizontal Layer method is a development of the wedge failure type developed by Simon and Curini (1998) and Simon et al. (2000), which in turn is a refinement of the models developed by Osman and Thorne (1988) and Simon et al. (1991). The model is based on the Limit Equilibrium method in which the Mohr-Coulomb failure criterion (Eq.2.5) is applied for the saturated portion of soils, while the Fredlund et al. (1978) criterion (Eq.2.6) is used for the unsaturated portion above the water table. Besides positive and negative pore water pressure, the model incorporates layered soils, changes in soil unit weight based on moisture content, and external confining pressure from streamflow (Simon and Pollen, 2006). The model allows to divide the bank profile into up to five layers, describing different soils composing the bank.

The Factor of Safety (*FS*) is given by the equation:

$$FS = \frac{\sum_{i=1}^{I}(c_i' L_i + (u_a - u_w)_i L_i tan\phi_i^b)}{\sum_{i=1}^{I}(W_i\, sin\alpha - P_i \sin(\beta - \alpha))} + \\ + \frac{\sum_{i=1}^{I}([W_i cos\alpha - u_{ai} L_i + P_i \cos(\beta - \alpha)] tan\phi_i')}{\sum_{i=1}^{I}(W_i\, sin\alpha - P_i \sin(\beta - \alpha))} \tag{4.33}$$

where c_i' is the effective cohesion of *i*th layer (kPa), L_i is the length of the failure plane incorporated within the *i*th layer (m), W_i *is* weight of the *i*th layer (kN), U_i is the hydrostatic-uplift force on the saturated portion of the failure surface (kN/m), P_i is the hydrostatic-confining force due to external water level (kN/m), α the failure-

plane angle (degrees from horizontal), β is the bank angle (degrees from horizontal), and I is the number of layers.

2. Vertical Slices:

The vertical slice method is an adaptation of the method employed in the CONCEPTS model (Langendoen, 2000).

The model is based on the Limit Equilibrium analysis. In addition to the forces incorporated in the Horizontal Layer method, the Vertical Slice method evaluates normal and shear forces active in segments of the failure block. The confining force due to the water in the channel is modelled by extending the slip surface vertically through the water and applying a horizontal hydrostatic force on the vertical portion of the slip surface. For the computations, the bank is divided into vertical slices (Figure 4-4). The number of the J slices is equal to the number of layers. In order to obtain a better accuracy of the Factor of Safety, each slide is then divided into three sub-slices. The forces acting on each slide j are (Figure 4-4):

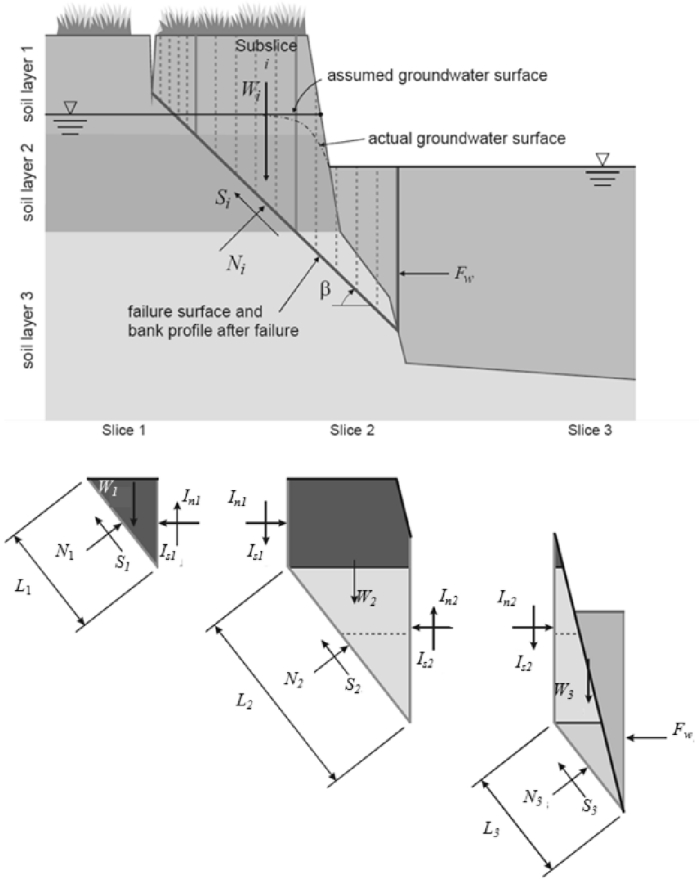

Figure 4-4 Mass wasting along a planar slip surface and forces acting on each slide (modified from Langendoen, 2000).

1. the weight of the slice W_j;
2. the normal force on the base of the slice N_j;
3. the shear force mobilized at the base of the slice $S_j = (u_a - u_w)_j L_j$;
4. the horizontal interslice normal forces, I_{nj} and I_{nj-1};
5. the vertical interslice shear forces, I_{sj} and I_{sj-1};
6. the confining force due to the water in the channel F_w.

The Factor of Safety is calculated through an iterative process, comprising the following steps: (1) vertical forces acting on a slice are summed to determine the normal force acting at the base of a slice, *Nj*; (2) horizontal forces acting on a slice are summed to determine the interslice normal force, In *j*; (3) the interslice shear force, $I_{s\ j}$ is computed from $I_{n\ j}$ using the method of Morgenstern and Price (1965); and (4) horizontal forces are summed over all slices to obtain *FS*. At the first iteration, the interslice normal and shear forces are neglected and the normal force, N_j, is equal to $W_j cos\alpha$.

The interslice normal forces are then determined from:

$$I_{n_j} = I_{n\ j-1} - \left(c'_j L_j + (u_a - u_w)_j L_j tan\phi^b_j - u_{aj} L_j tan\phi'_j\right)\frac{cos\alpha}{FS} + \\ + N_j\left(sin\alpha - \frac{cos\beta tan\phi'_j}{FS}\right) \tag{4.34}$$

and, in turn, the interslice shear forces are determined from:

$$I_{s_j} = 0.4 I_{n_j} sin\left(\frac{\pi L_j}{\sum L_j}\right) \tag{4.35}$$

After the first iteration, the normal force, N_j is:

$$\frac{W_j + I_{s_{j-1}} - I_{s_j} - sin\alpha\left(\frac{c'_j L_j + (u_a - u_w)_j L_j tan\phi^b_j - u_{aj} L_j tan\phi'_j}{FS}\right)}{cos\alpha + \frac{tan\phi'_j sin\alpha}{FS}} \tag{4.36}$$

This completes the second iteration. Often, the calculated interslice normal forces are negative (tension) near the top of the failure block. Since soil is unable to withstand large tensile stresses, a tension crack is assumed to form at the last interslice boundary with tension. Factor of Safety is determined by the balance of forces in horizontal and vertical directions for each sub-slice and in the horizontal direction for the entire failure block. *FS* is given by:

$$FS = \frac{cos\alpha \sum_{j=1}^{J}\left(c'_j L_j + (u_a - u_w)_j L_j tan\phi_j^b + \left[N_j - u_{aj} L_j\right] tan\phi'_j\right)}{sin\alpha \sum_{j=1}^{J}\left(N_j\right) - P_j} \quad (4.37)$$

The model then repeatedly iterates through equations from (4.34) to (4.37) until the value of *FS* converges.

3. Cantilever shear failures:

The cantilever shear failure algorithm results from inserting β = 90° into Equation (4.33). Thus the Factor of Safety is given by the ratio between the shear strength of the soil and the weight of the cantilever. If the bank is submerged then the weight of the layers affected by the water are reduced to their submerged weight. By this method, the vertical hydrostatic confining force is included in the calculation. *FS* is given by:

$$FS = \frac{\sum_{i=1}^{I}\left(c'_i L_i + (u_a - u_w)_j L_j tan\phi_i^b - u_{ai} L_i tan\phi'_i\right)}{\sum_{i=1}^{I}(W_i - P_i)} \quad (4.38)$$

Compared with the finite element model SLOPE/W (GEO-SLOPE International Ltd) employed in previous researches (Rinaldi et al., 2008, Luppi et al., 2009) for bank stability analyses, BSTEM presents some limitations. For instance, contrarily to SLOPE/W, BSTEM is not able to predict rotational slip and the limited number of coordinates which are allowed to describe the bank geometry may results inadequate to characterize complex profiles. Moreover Rinaldi et al. (2008a) and Luppi et al. (2009) combined the bank stability model with a finite element seepage analysis carried out through the model SEEP/W (GEO-SLOPE International Ltd) to take into account the changes in the pore water pressure distributions occurring during a flow event. Conversely, in the present study, given the lack of measured pore water pressure data, hydrostatic conditions have been assumed to describe both positive and negative pore water pressures. However, this method better fits with the general aim of testing less complex models in order to evaluate their potential for practical purposes. In fact, the fully coupled procedure proposed in the previous studies is not automated. Thus, it requires the user to manually deform the bank profile adapting the finite element mesh to the new bank geometry at the end of each time step. Therefore the process is very long and poorly practically usable.

5. Data collection

5.1 Selected reach

Accordingly to the subdivision at the catchment scale, described in Section 3.1, the studied reach is located within the segment CC near Guardistallo (Pisa) and comprises a channel length of about 1150 m. This reach was selected as reference study case due to several reasons, including the presence of eroding banks with highest rates of retreat in the last decade, and the absence of bank protections. In this area, the Cecina River develops a meandering pattern with alternate bar features and actively eroding banks along the outer side of the bends. Surrounding area is widely cultivated (typically wheat) with the presence of sparse structures and infrastructures.

Moving from the inner side of the bends, different depositional features produce a gentle slope (Figure 5-1). Specifically: (1) the terrace, whose presence points out the bed lowering processes occurred in the last century; (2) the floodplain mostly vegetated by poplars; (3) the high bar typified by bushy vegetation; (4) the point bar, typical feature which develops on the inner side of a meander bend, mainly composed of coarse gravels; and (4) the active channel composed of gravels and cobbles (D_{50} ranging between 13.7 and 45.3 mm, Rinaldi et al., 2008b) and characterized by riffles and pools sequences. Erosion takes place at the outer bank resulting as a steep scarp, due to the absence of transitional features.

Eroding banks along the outer bends of the meander experience a range of retreat mechanisms, but mass failures and fluvial erosion play a key role in channel migration.

Significant channel adjustments (i.e. incision and narrowing) occurred along this reach (Figure 5-2) during the last decades, as a result of a combination of human disturbances (Rinaldi, 2003; Rinaldi et al., 2008b, Surian et al, 2009).

The historical map from the IGM (Istituto Geografico Militare) documents a mean channel width of about 189 m in 1883. The mean width measured on the aerial photo of 1954 is around 66 m. In the period 1883-1954 when narrowing occurred, the average being nearly 70%.

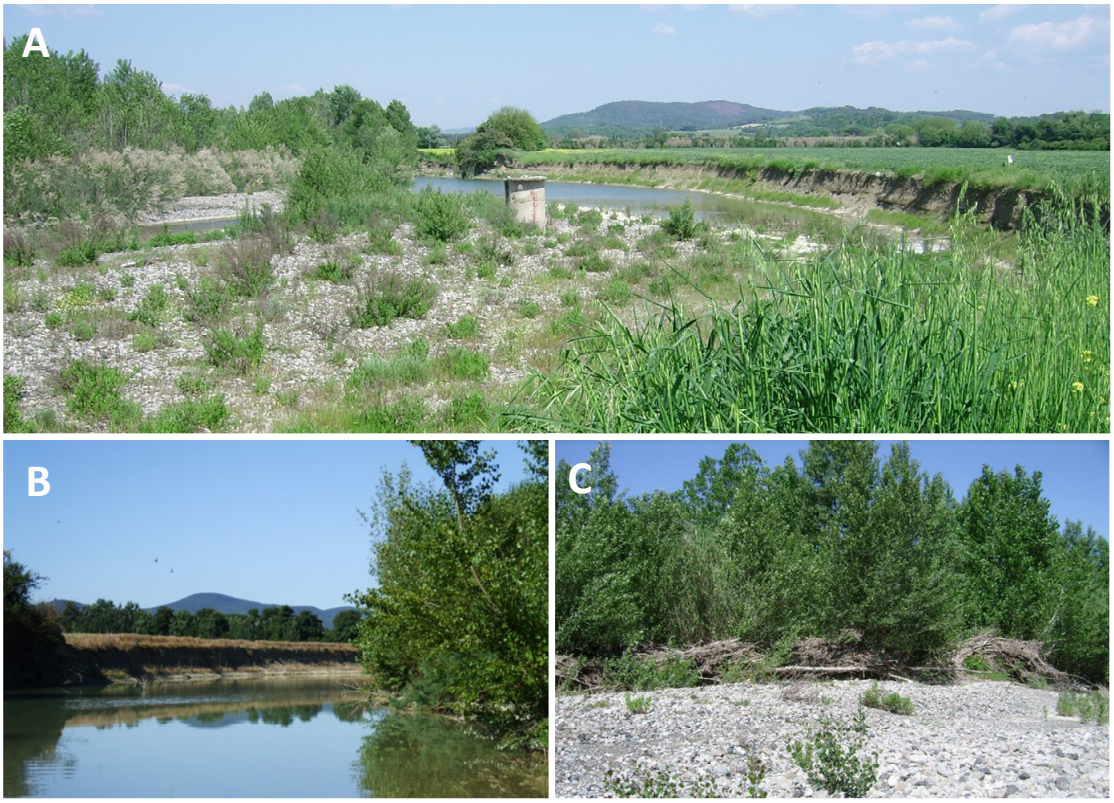

Figure 5-1 A: Upstream bend showing presence of terrace and point bar; B: Upstream bend and low water channel; C: High bar typified by gravels and pebbles and floodplain vegetated with poplars.

Together with the width change, the reach experienced channel morphology changes. Historical map of 1883 shows a braided morphology. Sinuosity increased during the next years (Figure 5-2, Figure 5-3) and consequently longitudinal bar changed into point bars.

Figure 5-3 was obtained through GIS analyses on multi-temporal series of high resolution aerial photos. It shows the development and the evolution of the meander during the last 50 years, starting from 1986. The rates of retreat at the outer bank range from 2.7 to 3.8 m/year over the period 1994-2004. However, the average width in 2004 is around 71 m, hence the channel can be considered in a state of dynamic equilibrium.

The sinuosity index, defined as the length of the stream divided by the length of the valley, was calculated through GIS analyses on high resolution aerial photos of 2006, providing a value equal to 1.5.

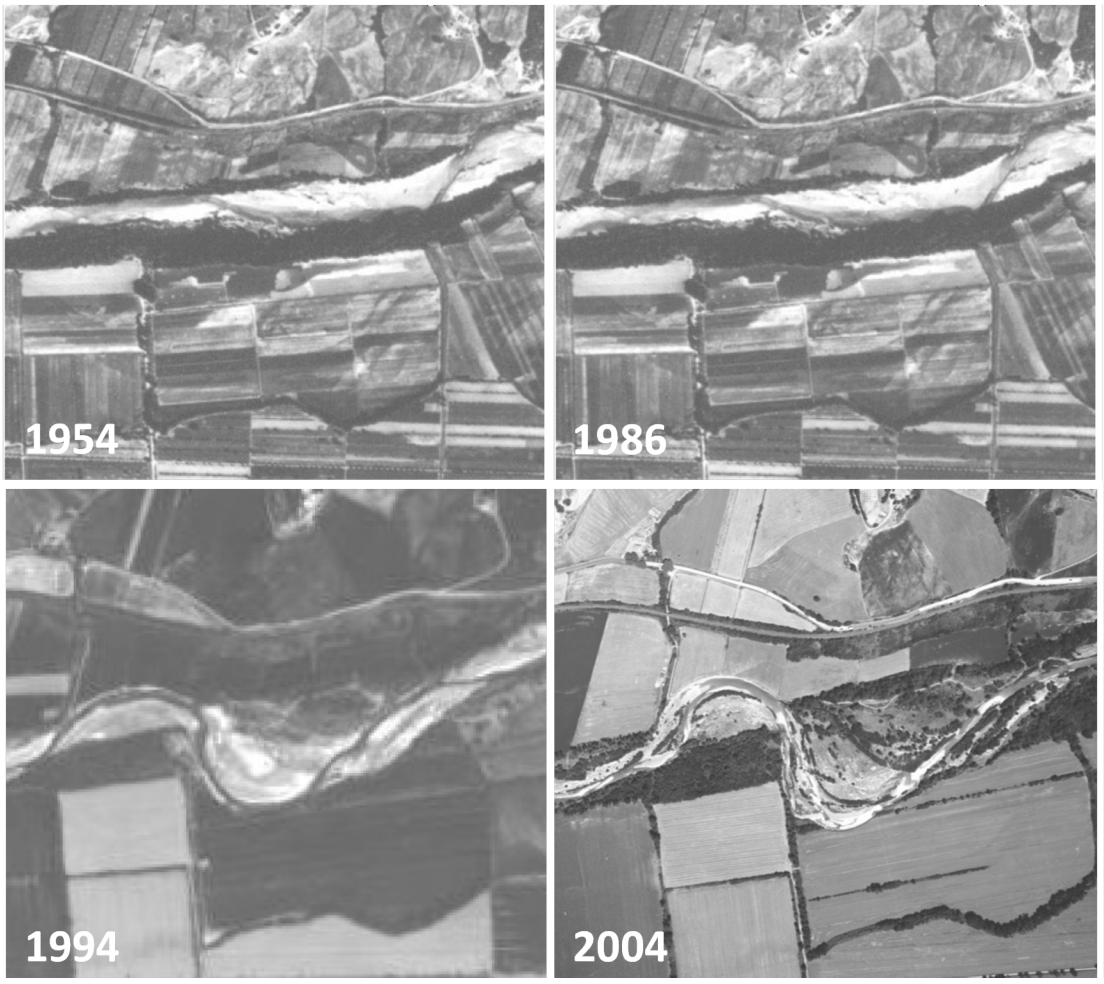

Figure 5-2 Channel evolution at the study reach through aerial photos of 1954, 1986, 1994 and 2004.

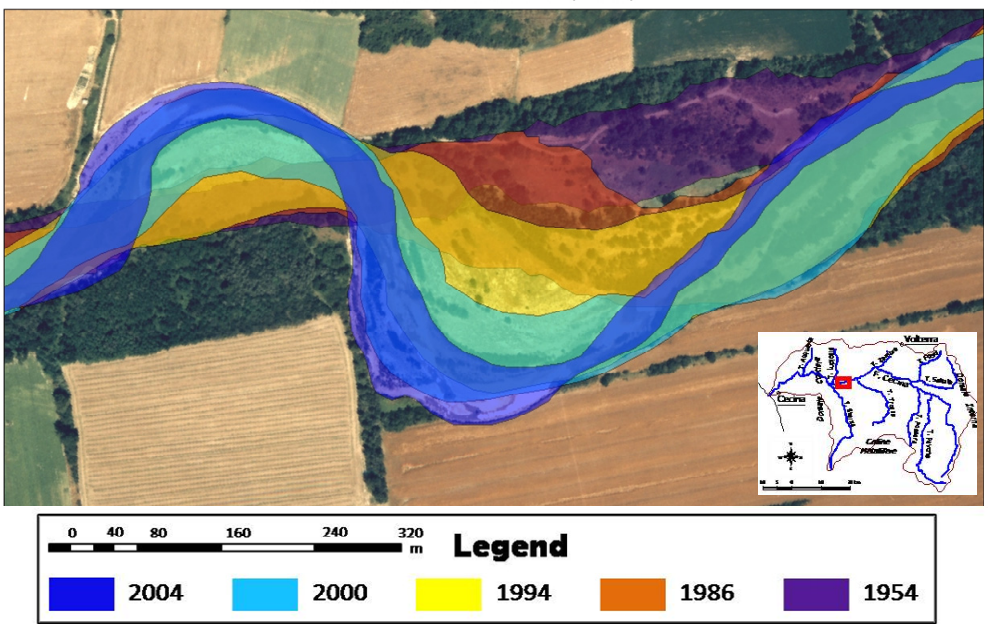

Figure 5-3 Development of the meander over the last 50 years.

5.2 Field survey

Field surveys provided data required by the models described in Section 4. They included (a) topographic surveys, (b) grain size analyses of bank materials, (c) measures of the critical shear stress for cohesive materials, and (d) measures of the small scale bank roughness at representative sites of two eroding banks.

5.2.1 Topographic survey

Obtaining an accurate representation of the bed topography is one of the most time consuming aspects of two-dimensional hydrodynamic modelling (Steffler and Blackburn, 2002), as simple cross-section surveys are generally not adequate.

In order to build the bed topography of River2D, a widespread topographic survey (Figure 5-4B) was carried out on July 2007 by means of the differential GPS Leica1200. Moreover, 19 cross sections from Ponte di Monterufoli to the study site (Figure 5-4A) for a total length of 2.5 km (with an average distance between cross sections of about 200 m) were surveyed and employed in one-dimensional modelling.

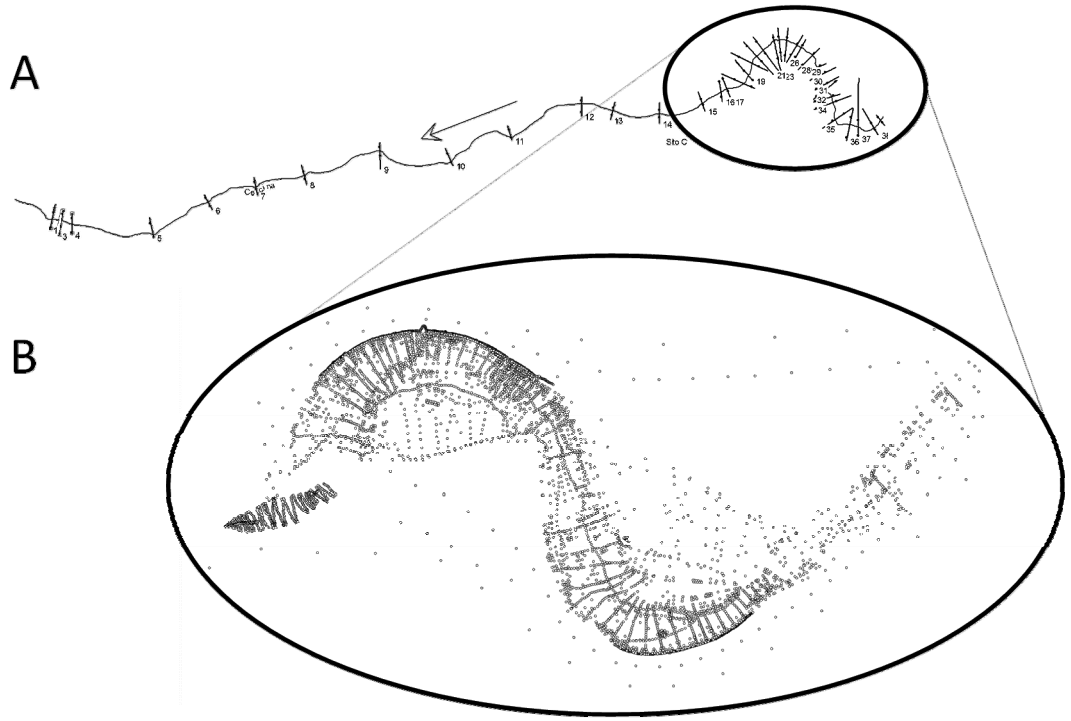

Figure 5-4 (A) Plan view of the 19 x-sections and (B) Topographic survey at the study reach.

5.2.2 Characterization of bank materials

Within the study reach, the eroding banks height ranges between 2.0 to 2.35 m and between 2.8 to 3.9 m upstream and downstream, respectively.

The stratigraphy was characterized by grain size analyses of samples collected from the exposed part of the banks at different location. The grain size distributions are summarized in Table 5-1.

Although bank materials are quite variable in their composition and thickness, the general stratigraphy, from the base to the top, can be described as follows: (1) coarse gravel and cobble at the bank toe with thickness varying between 70 and 200 cm; (2) a layer of in situ packed and slightly cemented gravel (thickness ranging from 17 to 55 cm); (3) well sorted sand with a thickness ranging from 23 to 50 cm; and (4) a massive sandy silt (with a thickness of 90–150 cm). Not all of these layers are always present at the same time on the banks, as Figure 5-5 shows. For simplicity, during the following analyses, riverbanks were considered as being composite. They are schematically described having a median diameter equal to that composing the dominant layer of cohesive and non-cohesive sediments.

Measures of the erodibility parameters were obtained by means of the CSM (Cohesive Strength Meter) which is a portable instrument for the in situ measurements of the critical shear stress of cohesive sediments. It was originally designed by Paterson (1989) and has become widely used to determine the relative stability of estuarine and intertidal sites (e.g. Tolhurst et al., 2000; de Deckere et al., 2001; Defew et al., 2002; Friend et al., 2003; Tolhurst et al., 2003; Watts et al., 2003). Recently the CSM was applied in fluvial geomorphology issues to characterize the cohesive material which composes the riverbank (Darby et al 2010).

The CSM makes use of the vertical jet technique, which is not new: in the past the Jet Test device was already used to measure the erodibility parameters of cohesive materials (Hanson, 1990; Hanson and Simon, 2001; Dapporto, 2001). Previous studies (e.g. Rinaldi et al., 2008a; Luppi et al., 2009; Constantine et al, 2009) applied results from Jet Tests to predict fluvial erosion. Similarly to the submerged jet test (Hanson and Simon, 2001), CSM employs pulses of vertical water jet pumped to the sediment with gradually increasing force. The eroding water jet is driven by air pressure supplied by a diving cylinder. The force, length and timing between pulses are controlled by an onboard microprocessor (Figure 5-6).

	Layer 1 D (mm)	Layer 2 D (mm)	Layer 3 D (mm)	Layer 4 D (mm)
D_{10}	0.1	0.7	0.034	0.032
D_{16}	0.2	1	0.036	0.033
D_{25}	0.6	1.8	0.039	0.034
D_{35}	2.6	3.6	0.042	0.036
D_{40}	4.6	4.4	0.045	0.036
D_{50}	10.9	6.7	0.061	0.038
D_{75}	39.9	14.5	0.094	0.042
D_{84}	50.7	18.8	0.114	0.043
D_{90}	58.4	22.2	0.136	0.044
Mean	6.3	6.9	0.091	0.058
Stand.Dev.	3.6	1.94	0.840	0.550
Skewness	0.68	0.79	-1.077	-4.060
Kurtosis	2.09	3.02	4.359	19.450
% Gravel	67.45	78.24	0.000	0.000
% Sand	23.67	21.76	60.200	9.200
% Silt	8.87	0	39.800	90.800
% Clay	0	0	0.000	0.000

Layer 1: Coarse gravel and cobbles with sandy matric.

Layer 2: Fine gravel with sandy matric

Layer 3: Sand

Layer 4: Sandy silt

Table 5-1 Results of different grain size analyses for soils composing the banks.

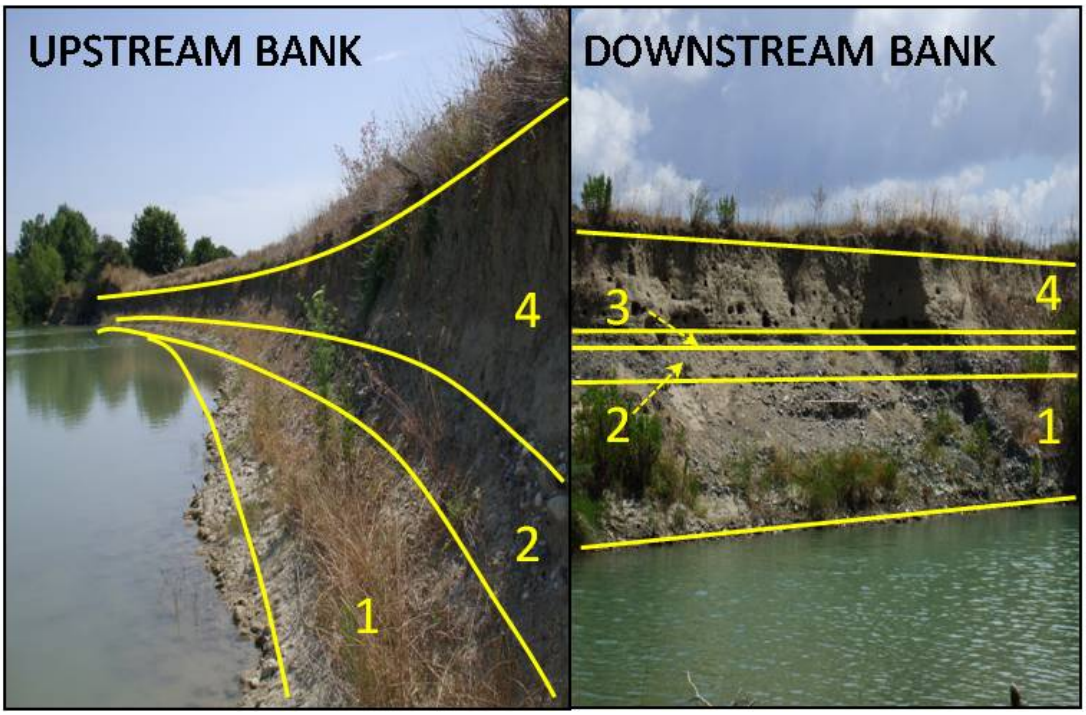

Figure 5-5 Upstream and downstream banks. Boundaries between the different layers of the banks are marked by lines. Numbers in the photos represent different materials: (1) Coarse gravel/ cobbles and sand; (2) Fine gravel and sand; (3) Sand; (4) Sandy silt.

Sediment resuspended within the test chamber is recorded as a change in light transmission across the chamber at a height of 1 cm above the bed. These data are logged for each jet pulse (Vardy et al., 2007).

Compared to the conventional Jet Test by Hanson and Simon (2001), the CSM presents relevant advantages due to its compact dimensions and capacity of measuring relatively small-scale spatial and temporal variations in sediment stability in a short time (about 5 minutes each test). However, unlike submerged Jet Test, CSM provides only measures of the critical shear stress.

The erodibility parameter (k_d), which is necessary to estimate the rate of riverbank retreat, accordingly to Partheniades model (1965), cannot be measured. CSM tests were carried out at the upstream (left) bank on the sandy silt layer and at the downstream (right) bank on the sandy layer (see location in Figure 5-7).

The values of the shear stress (Table 5-2), obtained as the average of three tests for each layer, are quite low if compared to values of the critical shear stress reported in literature for similar soils (Hanson and Simon, 2001). High values of the shear stress exerted by the flow should result in a higher value of riverbank retreat if compared to the observed ones.

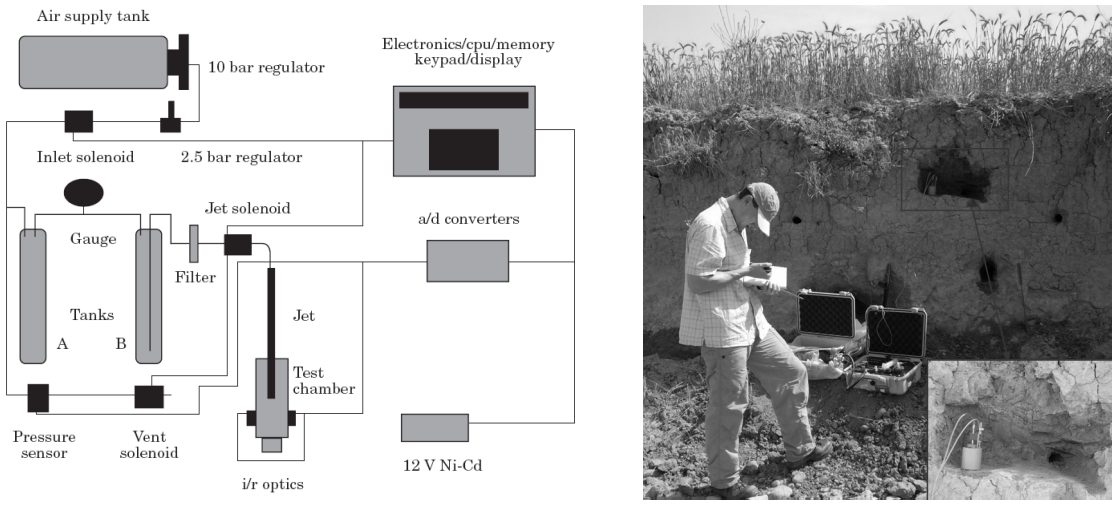

Figure 5-6 Left side: schematic of the Cohesive Strength Meter (Tolhurst et al 1999); Right side: measure of the critical shear stress on Cecina riverbanks.

Layer	τ_c [N/m^2]
Sandy silt	1.25
Sand	1.58

Table 5-2 Value of critical shear stress for two different layers obtained by the CSM test

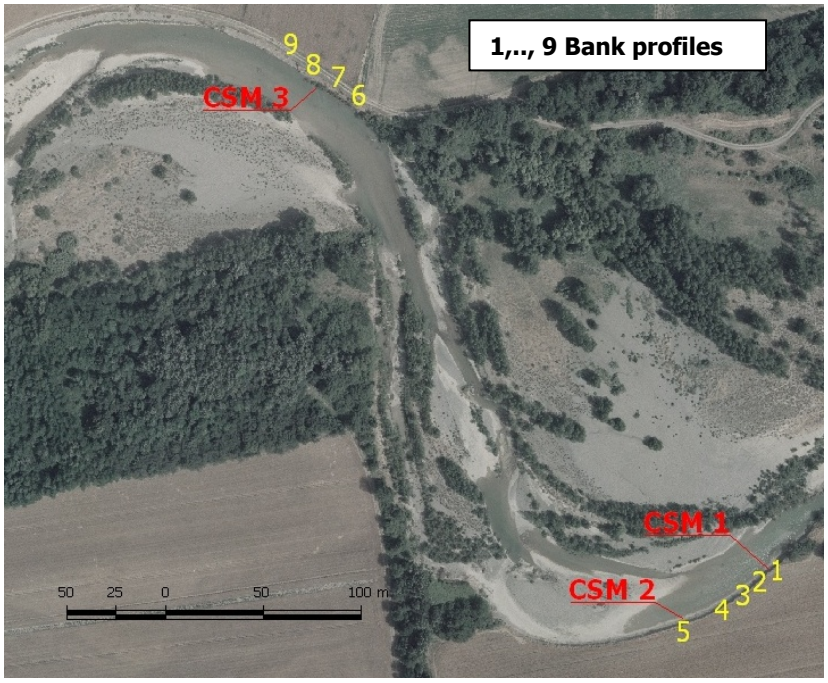

Figure 5-7 Location of CSM measurements (CSM 1-3) and bank profiles (1-9).

5.2.3 Measurement of bank roughness

The application of the near-bank shear stress model from Kean and Smith (2006a,b) requires the characterization of the small-scale topographic features. For this purpose, three surveys (Table 5-3) were made on eroded banks where the presence of riparian vegetation was limited. Specifically, on the eroded bank located at the upstream bend, a first measure was carried out along the cohesive portion (layer 4), and a second one at the gravel level (layer 1). The third survey was carried out along the eroded bank situated at the downstream bend on the fine gravel level (layer 2).

Following the method proposed by Kean and Smith (2006a), a series of the straight edges were placed along the banks (Figure 5-8) and measurements of the distances from them to the bank were made at 5 cm intervals to get a profile of the amplitude and the spacing of the topographic irregularities (Figure 5-9).

Location / Layer	Survey length
Upstream Bank/ sandy silt layer	33 meter
Upstream Bank/ fine gravel layer	9 meter
Downstream Bank/ gravel layer	20 meter

Table 5-3 Straight edges length along the banks at two representative layers.

Figure 5-8 Measure of bank roughness.

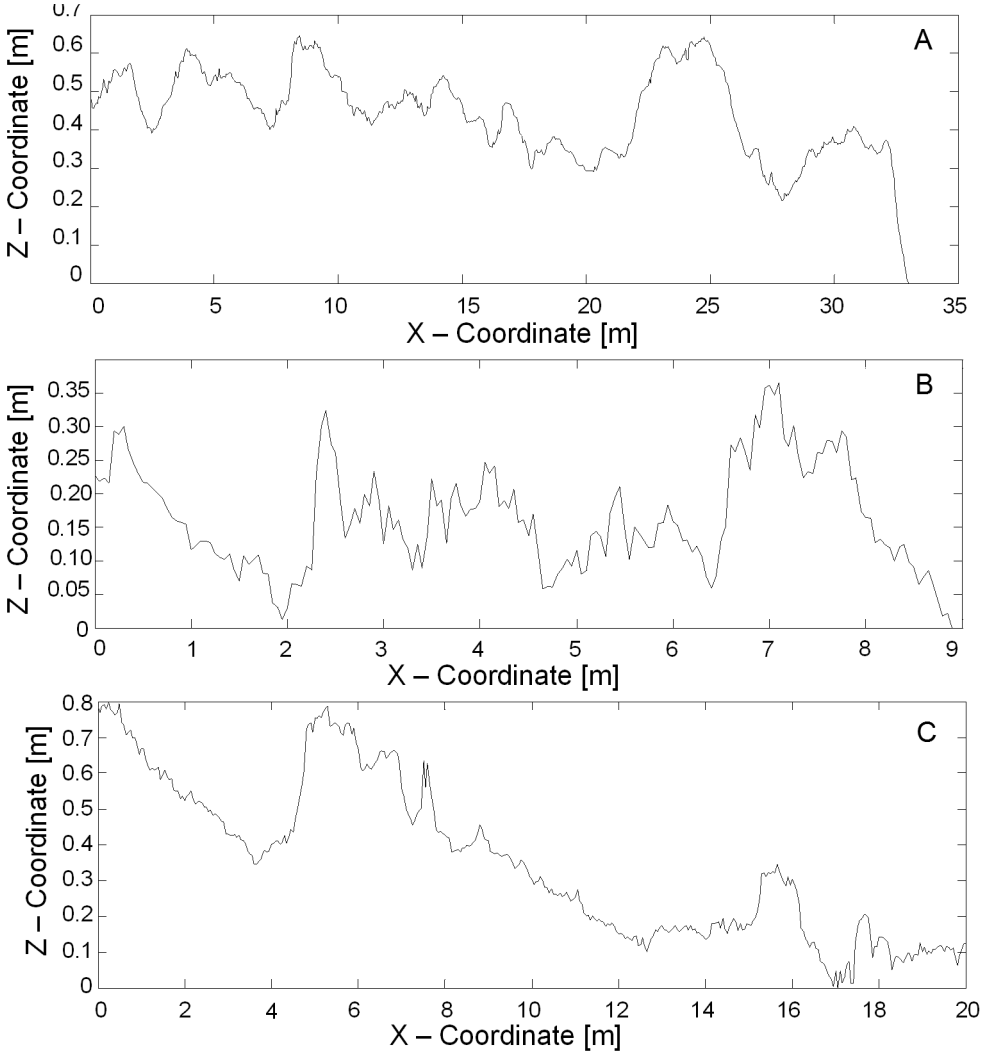

Figure 5-9 Bank profile roughness. A: cohesive layer of the upstream riverbank, B: gravel layer of the upstream riverbank, and C: gravel layer for the downstream riverbank.

5.3 GIS-based analyses

GIS based analyses were carried out aiming to: (1) convert the topographic survey into input geometric data for 1D hydraulic modelling; (2) evaluate the rate of channel migration along the bends.

For the first purpose, the ArcGIS extension HEC-GeoRAS (version 4.2.92), produced by the Hydrologic Engineering Center, was employed. HEC-GeoRAS is a set of procedures, tools, and utilities for processing geospatial data in ArcGIS and allowing the preparation of geometric data for import into HEC-RAS. This interface was employed to extrapolate cross sections at the study reach, because here only a scattered survey was available. Data acquired by the GPS were processed through ArcView 9.2 (Enviromental Systems Research Institute) to create a Digital Terrain Model (DTM) of the river system in the ArcInfo TIN format. Afterward, the procedure essentially involved the use of GeoRAS drawing tools to create a series of line themes pertinent to developing geometric data for HEC-RAS. These themes included stream centerline, flow path centerlines (left, center and right), left and right channel banks and stream cross section lines.

5.3.1 Measurements of riverbank retreat

The rate of channel migration at the reach was measured through GIS analyses on aerial photos, according to a technique well established in the literature (Nanson and Hickin, 1986; Petts, 1989; Gurnell, 1997; Wellmeyer et al., 2005). In this study, the rates of channel retreat, evaluated between 1994 and 2004, were employed to calibrate the erodibility parameters (see Section 6.4) which, in turn, were used in the fluvial erosion modelling.

Depending on the year, the scale of aerial photos approximately ranges between 1:7000 and 1:31000 (Table 5-4) and, consequently, the resolution of the images varies.

Measurements of the bank retreat by means of GIS tools are inevitably affected by errors. Besides the error due to the resolution of the photo, the error of the georeferencing process was taken into account. The rectified aerial photos have been georeferenced using the specific ArcGis 9.2 tool; the second order transformation has been selected to fit polynomial equations to the data, allowing points to be shifted in a non-uniform manner.

Year	Source	Scale	Color & Resolution	Pixel Dimension
1994	Regione Toscana	1:31000	b/w	1 pixel=80 cm
2000	Terra Italy	1:40000	Color	1 pixel=100 cm
2004	Provincia di Pisa	1:7000	Color, 1200dpi	1 pixel=20 cm

Table 5-4 Aerial photos employed for measuring riverbank retreat.

Frame-Time [year]	Upstream bank retreat [m]	Downstream bank retreat [m]
1994-2000	11 ± 2.1	12.5 ± 2.1
2000-2004	19.5 ± 1.5	1 ± 1.5
1994-2004	30.5 ± 1.3	13.5 ± 1.3

Table 5-5 Rate of bank retreat at the representative bank occurred in different periods.

Georeferencing has been considered acceptable when the total residual error (RMS) was less than 30 cm. The analysis showed that the rates of riverbank retreat ranged from 2.7 to 3.8 m/year over the period 1994-2004. The values of total retreat measured at two representative banks, located at the upstream and downstream bends, in combination with their total error, are reported in Table 5-5.

The total error was evaluated by adding in the same direction the pixel dimensions and the error of the georeferencing process (30 cm). This provided the maximum value of objective and measurable error. Subjective errors, such as those due to difficulties in recognizing the edge of banks caused by the presence of vegetation, cannot be objectively estimated. However, along the eroded banks high vegetation is almost absent.

5.4 Time series of discharge

The main flow gauging station for the catchment (Ponte di Monterufoli; drainage area of 634 km^2) provided the river stage and the flow discharge data. The study reach is located approximately 2.5 km upstream. The complete historical set of hourly aggregated discharges which occurred between 30/03/1994 and 28/06/2004 (Figure 5-10) was utilized together with the GIS analyses to calibrate the erodibility parameters (Section 6.4).

The values of hourly aggregated discharges which were available in the years between 1934 and 2007, for a total of 25 years (recordings are not available for all the consecutive years), were collected and used to obtain the flow duration curve.

The latter, represented in Figure 5-11, was employed for the definition of the risk due to fluvial erosion (Section 6.6).

The values of the return periods were taken from previous study (Scozzafava, 2008) using the annual maximum peak discharges for a series of 49 years.

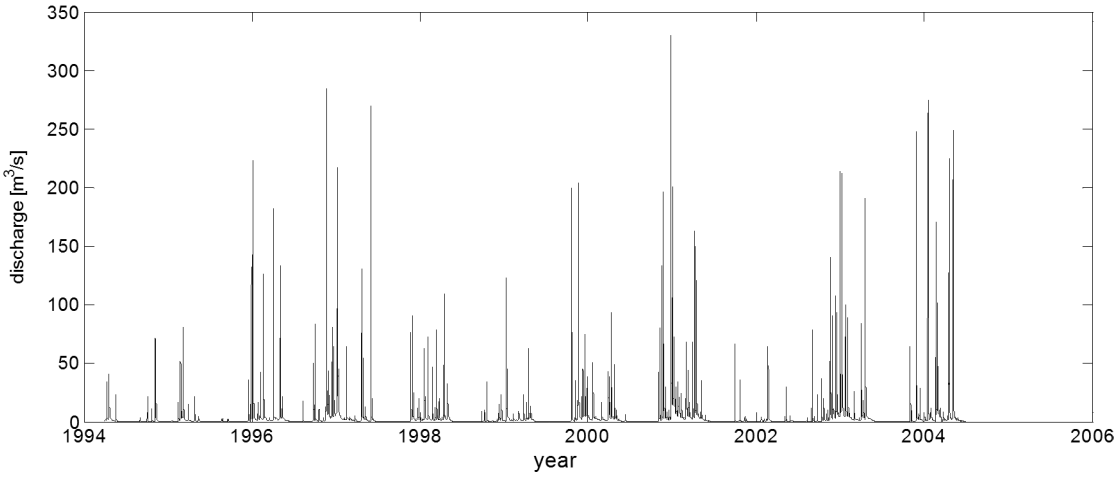

Figure 5-10 Flow events occurred between 1994 and 2004.

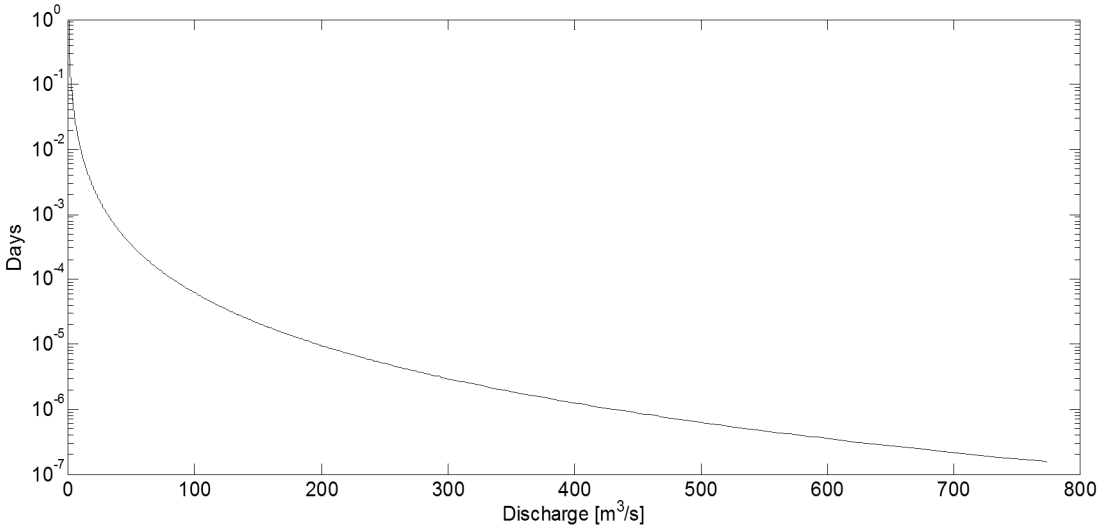

Figure 5-11 Flow duration curve.

6. Applications and results

Different combinations of models were tested to evaluate their applicability in the perspective of definition of fluvial erosion hazard. The research was carried out according to the following steps (Figure 6-1): (1) data collection; (2) hydrodynamic modelling; (3) numerical implementation of the Kean and Smith (2006a,b) model; (4) analysis of near-bank shear stress obtained by applying different models and calibration of the erodibility parameters; (5) coupling the effects of different processes responsible for bank retreat by applying the BSTEM model for bank stability analyses on eroded profiles; (6) definition of risk due to fluvial erosion by means of the excess shear stress model (Partheniades, 1965).

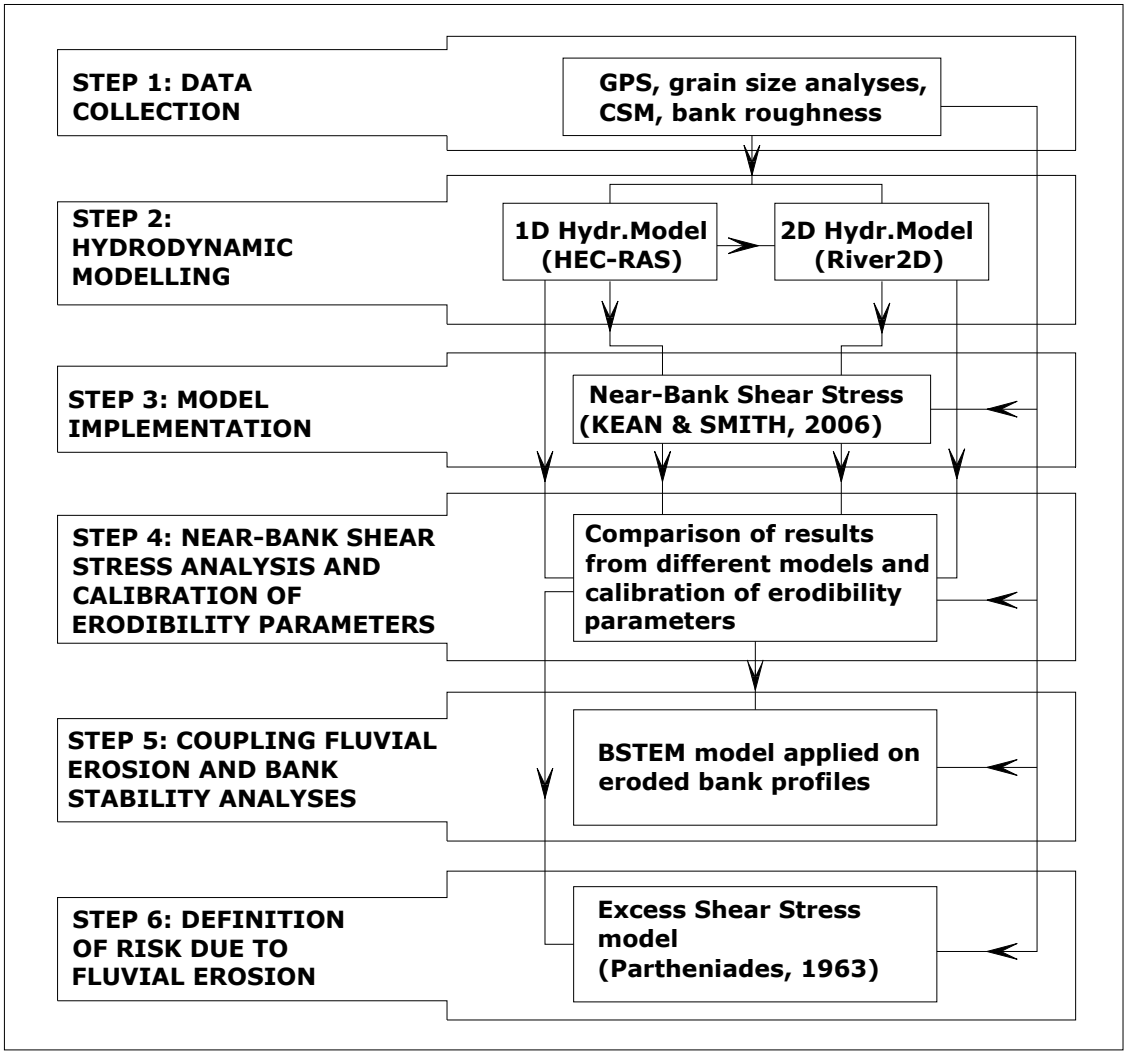

Figure 6-1 Flow chart describing the analyses carried out at the scale of the reach.

6.1 Setup of hydrodynamic models

One-dimensional and the two-dimensional hydraulic modelling were carried out based on topographic surveys and hydrological data.

HEC-RAS was performed with a double purpose: (a) to provide the boundary conditions required by River2D; and (b) to test the potential of coupling 1D model with Kean and Smith's near-bank shear stress model.

Since no gauges to measure the water stage were available at the reach study, it was not possible to calibrate the models with measured data. Thus, it was only possible to optimize the values of roughness (n or k_s, depending on the model) in order to obtain close values of water stage provided by the two models at the same cross sections. Although the unavoidable absence of calibration with measured data undoubtedly represents a lack in the present study, it is necessary to remark that this study aims to develop a methodology to estimate the near-bank shear stress in the perspective of definition of hazard due to fluvial erosion. In fact, the aims of the present study are: (a) to investigate the capability of the selected models to be employed in the risk context, and (b) to analyze relative differences between values and trends of the shear stress provided by the different models for the same water stages.

Bed topography and roughness

The bed topography in both models was acquired during field survey carried out by means of a differential GPS. The HEC-RAS cross sections were obtained through the HEC-GeoRAS tool (Section 5.3) except for the two sections crossing the banks of interest for retreat analyses. In these cases, in order to better compare results of the two models, the sections were extracted from the DTM provided by River2D and inserted manually in the HEC-RAS geometry. Cross sections were then supplemented by interpolating every 10 m, between those surveyed, aiming to avoid that the program ended up defaulting to critical depth, as it may happen when sections are spaced too far apart.

In River2D, topography was saved in a text file with a '*.bed' extension. Within the file, each line contains a unique identity number, the coordinates of one topographic point (x, y, z) and the effective roughness height, k_s. R2D_Bed module provided the digital terrain model based on the Triangulated Irregular Network (TIN) methodology. Breaklines were included at the crest and the toe of the banks to capture the abrupt change in gradient. By means of high resolution orthophotos, the

study area was divided into 4 different zones characterized by the presence of: channel/bars, high bars, herbaceous or bushy vegetation, and trees (Figure 6-2, Table 6-1). For each of these areas, the effective roughness heights were defined. In the case of channel and bars, k_s was defined through the average D_{90} of sediments. This was obtained by means of grain size distributions of channel and bars, collected at different sites along the reach study. In the vegetated areas, values of k_s were based on tables in the literature.

HEC-RAS requires the roughness to be defined through the Manning's n coefficient, allowing the user to subdivide each cross section with different values. The values of the Manning coefficient were set taking account for the same criteria applied in the case of the effective roughness height. The 'Roughness converter' tool available in R2D_bed was employed to verify the consistency of the parameters applied in the two models.

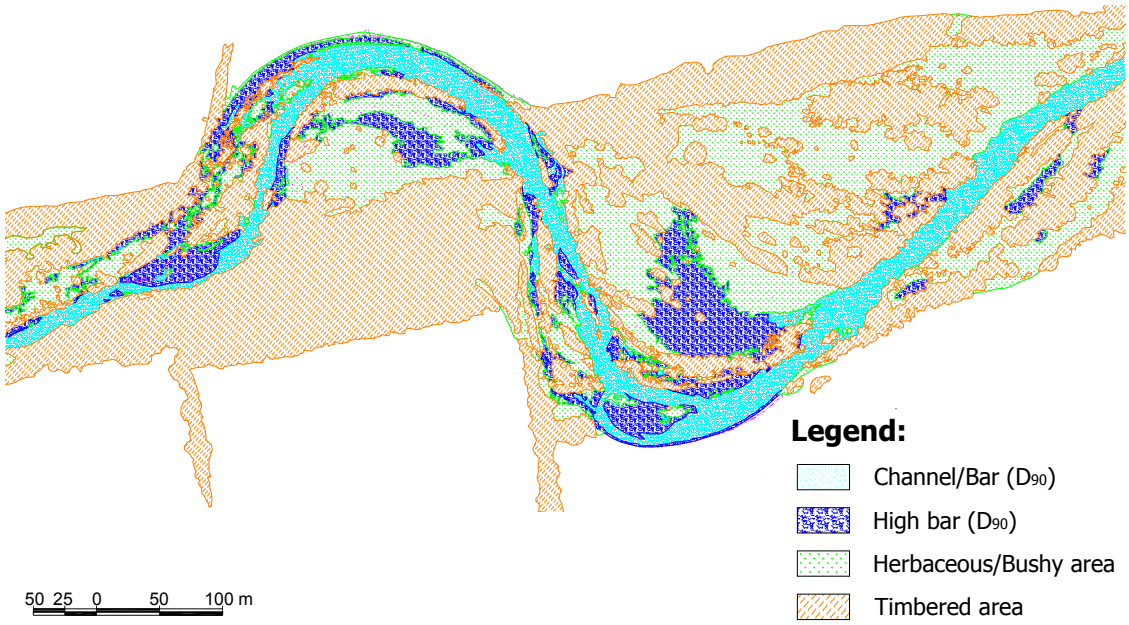

Figure 6-2 Subdivision of the reach into different roughness areas.

Zones	k_s [m]
1 – Channel/ Bar (D_{90})	0.01
2 – High bar (D_{90})	0.06
3 – Herbaceous/ Bushy area	0.35
4 – Area with trees	1.00

Table 6-1 Effective roughness height, k_s for different areas.

Computational mesh

Once the geometry was completed, a computational mesh was created through R2D_Mesh with different resolution depending on the distance from the eroded banks (between 0.5 and 10 m, Figure 6-3). This allowed to find a compromise between obtaining a detailed mesh in the areas of interest and reducing the computational time. R2D_Mesh uses a procedure by which the computational mesh is generated as an overlay on the bed topography. When the computational mesh is generated, values for nodal elevation and roughness height are interpolated from the bed topography.

The initial mesh was smoothed and refined to give a mesh quality index > 0.15, as suggested by Koopaei et al. (2003).

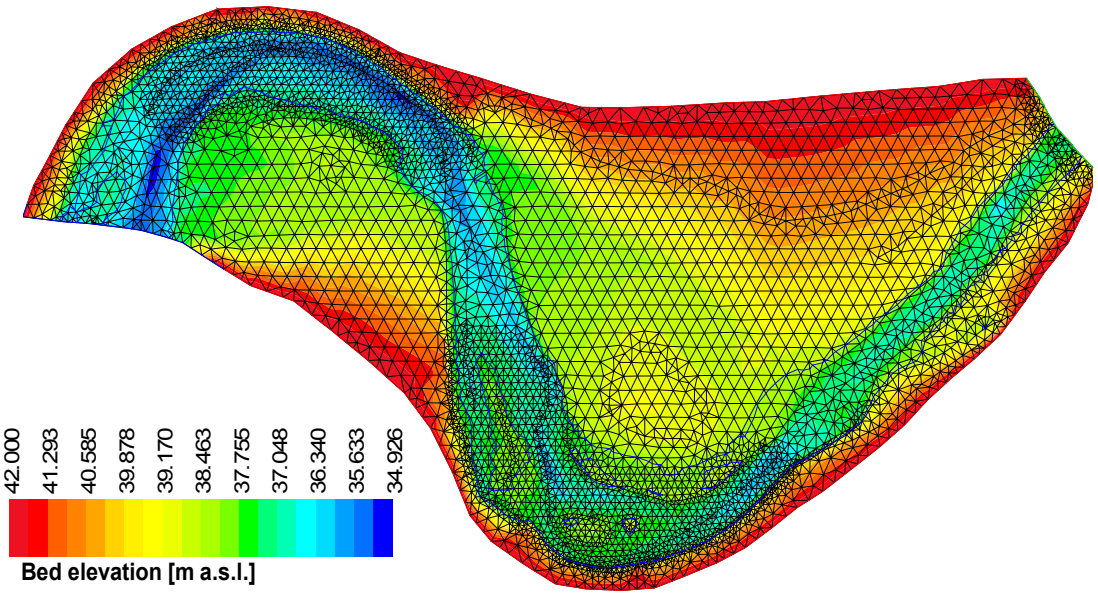

Figure 6-3 Computational mesh at the reach study.

Boundary conditions and flow discharges

Boundary conditions are necessary to establish the starting water surface which allows the models to begin the calculations. Regarding HEC-RAS, upstream and downstream boundary conditions were entered, allowing mixed flow regime runs. At the upstream end, a normal depth, approximated with the upstream slope of the channel (0.0018), was set, whereas, at the downstream end, a critical depth condition was selected, due to the presence of a transverse structure utilized as a riverbed protection under Monterufoli Bridge.

In River2D boundary conditions are represented by a specified total discharge at the inflow section, and fixed water surface elevations at outflow section. To minimize the effect of boundary condition uncertainties the ends were located some distance from areas of interest. Values of water stage were set for each run at the inflow section as the initial guess in the iterative solution procedure. A good guess is important to significantly reduce the total run time and it may make the difference between a stable and an unstable runs. The values of water stages, both at the inflow and outflow sections, were obtained through the 1D modelling. HEC-RAS and River2D were performed in steady flow conditions with discharges ranging from 5 m^3/s to 671.2 m^3/s, the latter corresponding to a return period of 15 years. The relationship between discharges and return periods (Table 6-2 Discharges and return period (R.P.) based on the annual peak instantaneous dischargesTable 6-2 and Figure 6-4) was developed in previous researches (Scozzafava, 2008) at the present reach study, based on the annual peak instantaneous discharges occurred in the period 1935-2000.

River2D was not able to model very low discharges, as the maximum flow resistance that can be generated by the model is limited. The lowest value of discharge simulated by the model corresponded to 15 m^3/s. Figure 6-5, shows results of HEC-RAS modelling, while Figure 6-6, Figure 6-7 and Figure 6-8 represent the flow field computed by River2D for three different discharges, which are 45 m^3/s, 302 m^3/s and 630.4 m^3/s, respectively.

It is interesting to notice in Figure 6-6, Figure 6-7 and Figure 6-8 that as the discharge increases the core of the high velocity fluid shifts away from the banks. Similar findings are reported by Rinaldi et al. (2008a), although this study was carried out at a different reach along the Cecina River, and a different hydrodynamic model (DELFT3D) was applied. This behaviour may have important implications in riverbank retreat, as described in the next Sections.

R.P [years]	Discharge [m^3/s]	R.P [years]	Discharge [m^3/s]	R.P [years]	Discharge [m^3/s]
1	148.7	5	472.9	11	614.7
2	302.3	7	533.2	12	630.4
2.5	345.9	8	557.2	13	645.1
3	380.1	9	578.4	14	658.6
4	432.7	10	597.4	15	671.2

Table 6-2 Discharges and return period (R.P.) based on the annual peak instantaneous discharges

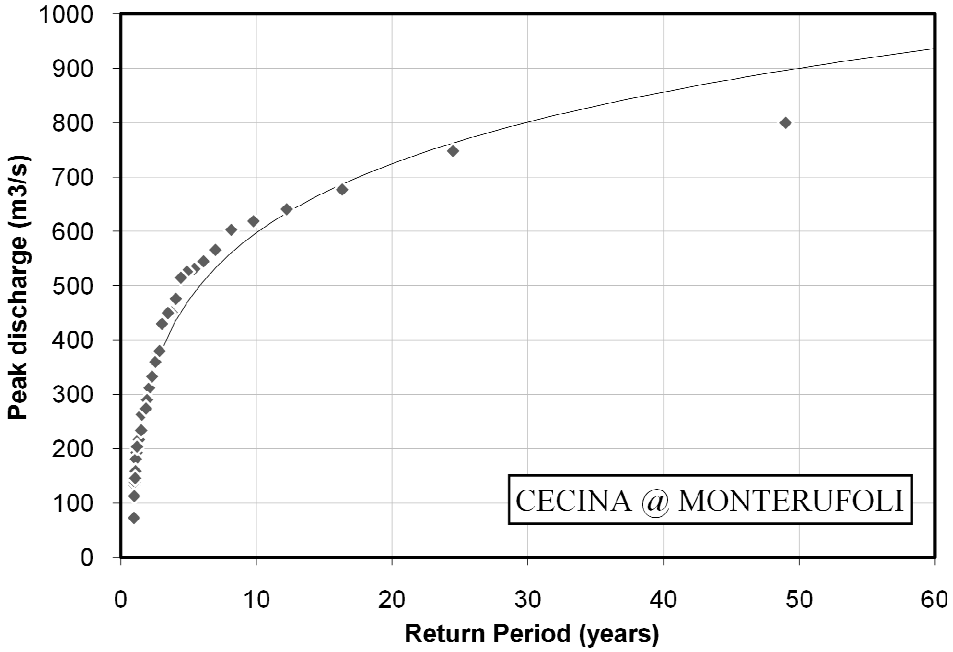

Figure 6-4 Log-normal distribution of annual peak instantaneous discharge. In the table: R.P.= return period, Q=discharge.

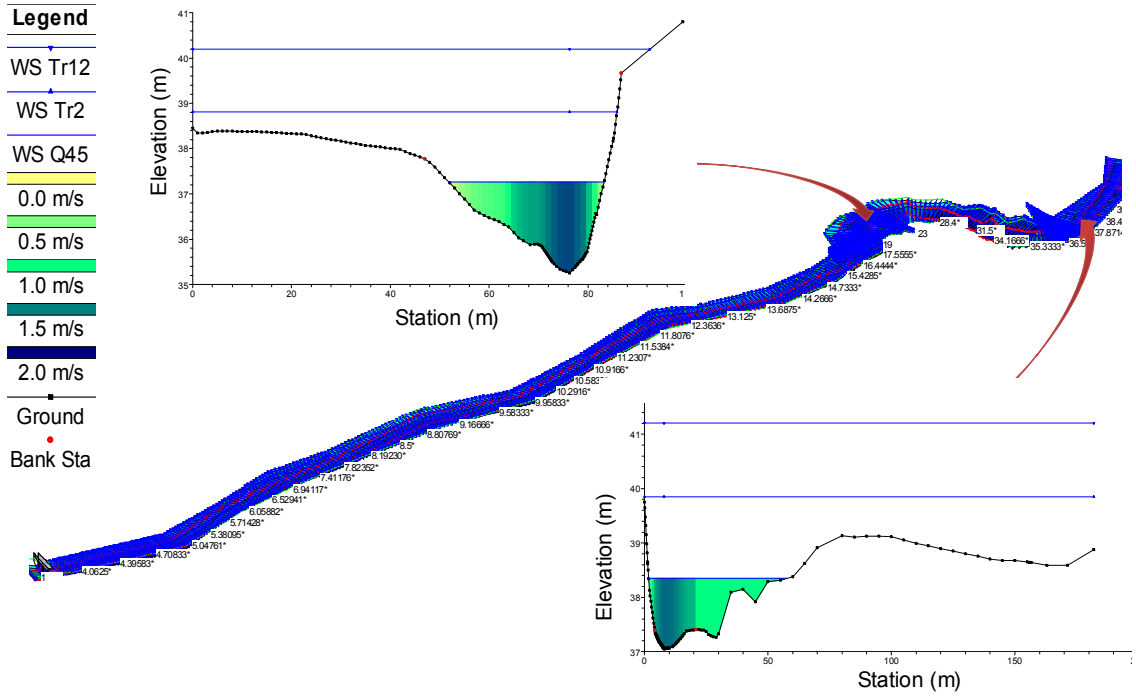

Figure 6-5 Results of HEC-RAS simulations at the left and right banks for discharge equal to 45m^3/s.

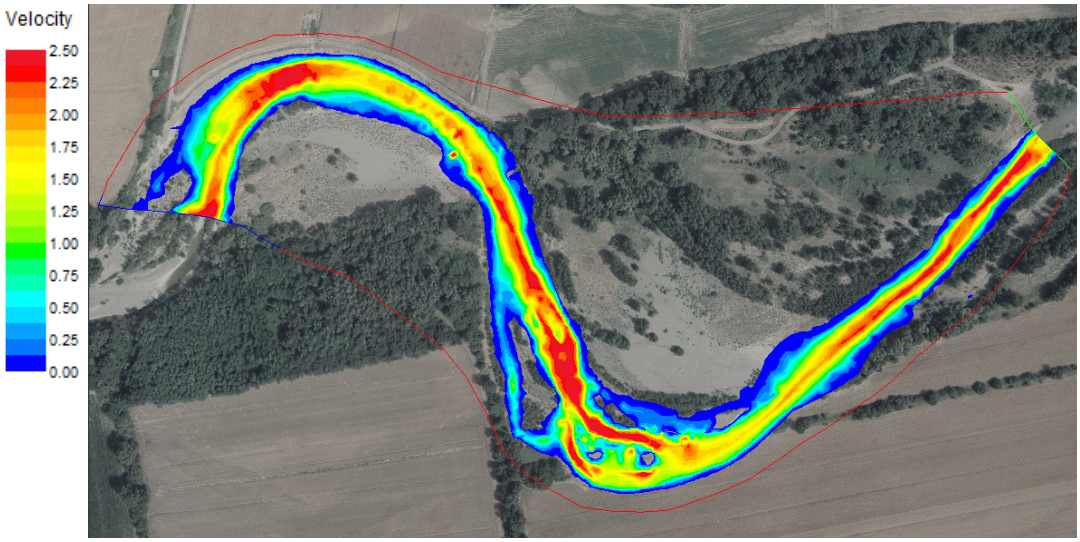

Figure 6-6 Velocity pattern for a discharge equal to 45 m^3/s.

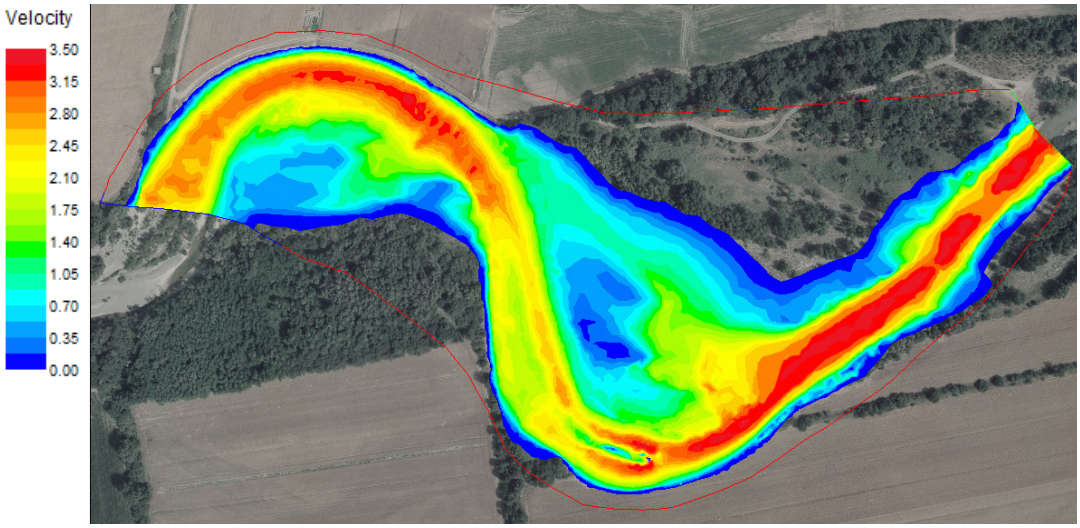

Figure 6-7 Velocity pattern for a discharge equal to 302.3 m^3/s (2 years return period).

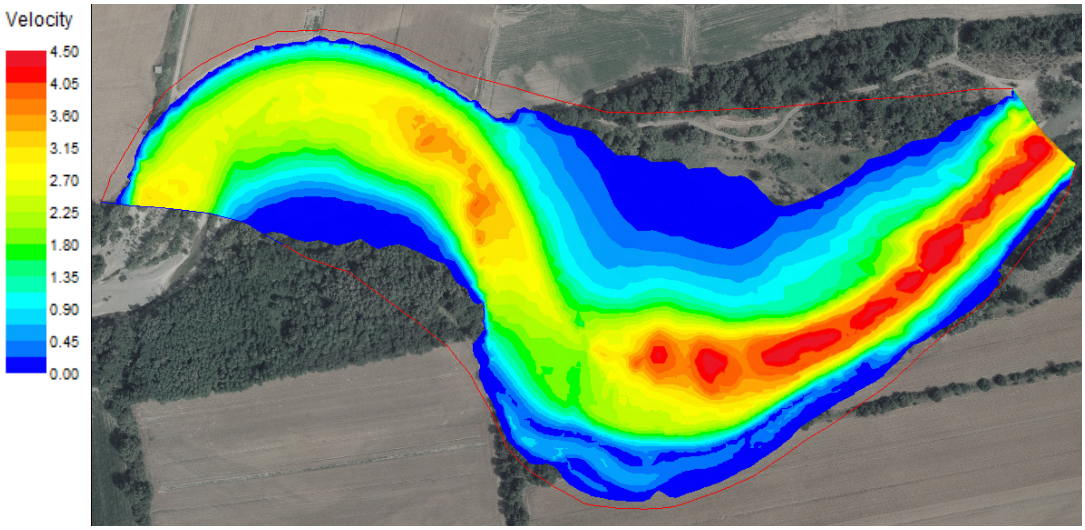

Figure 6-8 Velocity pattern for a discharge equal to 630.4 m^3/s (12 years return period).

6.2 Parameterisation of bank roughness

Field measurements of bank roughness (Section 5.2.3) were post-processed following the Kean and Smith (2005) approach. One set of bank topography post-processing is shown in Figure 6-9.

The long-wavelength variations, marked with green line in Figure 6-9A, roughly correspond to the shape of the channel and do not contribute substantially to flow resistance. Subtracting the amplitude of the long-wavelength oscillations from the series, topographic bank features that dominate the roughness at this location (Figure 6-9B) are found. The positions of the individual roughness elements along the bank were then identified manually, prior by fitting each of the individual 'bumps' with Gaussian curves (Figure 6-9C). Figure 6-9 clearly demonstrates the irregular shape of the natural topographic bank features. Kean and Smith (2006b) found that the topography of irregular surfaces can be transformed into an equivalently rough surface of regularly-spaced, identical elements using the approximation:

$$H_{reg} = H_{88}$$
$$\sigma_{reg} = \sigma_{88} \quad (6.1)$$
$$\lambda_{reg} = 6H_{88}$$

where H_{88} and σ_{88} indicate the 88th percentile of the irregular bank roughness protrusion height and streamwise length scale, respectively.

Following Kean and Smith (2005) approach, z_{0SF} was approximated by taking a tenth of the standard deviation of the residuals by analogy to the relation $z_0 = 0.1D_{84}$ often used for granular surfaces (Whiting and Dietrich, 1989), where D_{84} is the 84th percentile of the size distribution of the nominal diameter. Details of bumps geometries and skin roughness used in subsequent computations are summarised in Table 6-3.

The topographic features of the eroded bank of the Cecina River are essentially two-dimensional in shape as shown in the little change of the profiles with elevation above the bed. Therefore, the Gaussian parameters evaluated at the straight edge elevation were considered being representative of the entire height related to the same material. Potential advantages to avoid this simplification are represented by the application of terrestrial laser scanning, as employed by Darby et al. (2010).

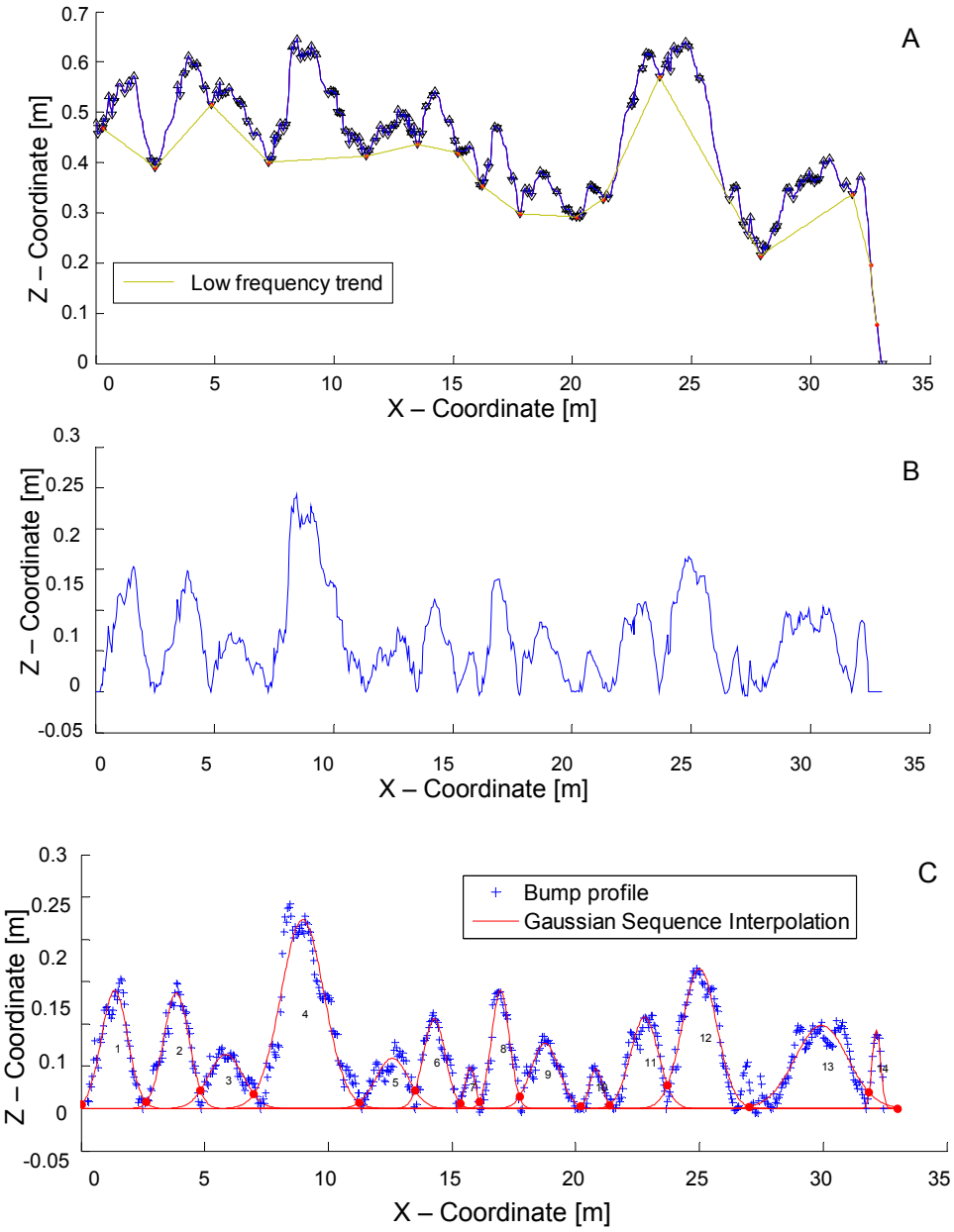

Figure 6-9 Cohesive layer of the upstream bank. A: Original bank profile with low frequency, B: Bank profile with low frequency removed, and C: Gaussian fitting on detrended profile.

	Upstream cohesive layer	Upstream granular layer	Downstream granular layer
zo_{SF} [m]	0.000004	0.0051	0.0018
H_{reg} [m]	0.1621	0.2581	0.1992
σ_{reg} [m]	0.9915	0.9664	1.008
λ_{reg} [m]	6H	6H	6H

Table 6-3 Bank roughness parameters employed in this study.

The topographic features of the eroded bank of the Cecina River are essentially two-dimensional in shape as shown in the little change of the profiles with elevation above the bed. Therefore, the Gaussian parameters evaluated at the straight edge elevation were considered being representative of the entire height related to the same material. Potential advantages to avoid this simplification are represented by the application of terrestrial laser scanning, as employed by Darby et al. (2010).

Practical difficulties due to the height of the bank did not allow measurements of bank roughness on cohesive layer at the downstream bank. Therefore, the characteristic Gaussian-shape parameters determined at the cohesive layer of the upstream bank (Table 6-4) were used to describe both the upstream and downstream cohesive thickness.

Regarding the hydraulic input data required by the model of Kean and Smith (2006a,b), both HEC-RAS and River2D provided the velocity in the outer region.

Due to the relatively low dimensions of the protrusions, at a distance of 1.5 m from the bank profile, velocities were considered not being affected by the presence of the bank roughness. Thus, the outer velocity was evaluated at this distance.

H [m]	σ [m]	λ [m]	C_D [-]	$C_D \cdot H$ [m]
0.13548	0.51685	2.6183	0.094867	0.012853
0.13671	0.51049	2.2142	0.10096	0.013803
0.063952	0.69399	2.1483	0.000421	2.69E-05
0.22314	0.87105	4.2547	0.088601	0.01977
0.059456	0.65545	2.2687	0.000368	2.19E-05
0.10592	0.43893	1.8261	0.073638	0.0078
0.04878	0.19898	0.77264	0.077405	0.003776
0.14073	0.36528	1.6355	0.2426	0.034142
0.078964	0.55427	2.533	0.008046	0.000635
0.0435	0.21382	1.1031	0.040651	0.001768
0.10063	0.50085	2.304	0.03876	0.0039
0.16525	0.68836	3.3374	0.072418	0.011967
0.098287	1.0651	4.8203	0.000426	4.18E-05
0.11338	0.18277	1.1638	0.51736	0.05866

Table 6-4 Characteristic parameters Gaussian shaped at cohesive upstream bank.

Although one-dimensional models provide cross-sectional average velocities, HEC-RAS allows to subdivide the cross sections into slices. Once a water surface elevation is computed, the program divides the cross section into the user defined flow distribution slices, and then calculates the area, the wetted perimeter, and the hydraulic depth (area over top width) for each slice. Using the originally computed energy slope, the cross section Manning's *n* values, the area and wetted perimeter for each slice, and applying Manning's equation, the program computes the conveyance and percentage of discharge for each slice.

The average velocity is estimated by dividing the obtained discharge by the area of each of the user defined slices. The results of the flow distribution computations should be used cautiously. In fact, although the results of the flow distribution are more reliable than those of the standard three subdivisions (left overbank, main channel, and right overbank) provided by the model, the values are still based on average estimates of one-dimensional results.

In the present study cross sections were subdivided into the maximum number of cells (45) obtainable between the main channel and the left or right bank for the upstream or downstream bank, respectively (Figure 6-10). This subdivision provided a better definition of the velocity distribution through cross sections.

As described in the previous sections, both HEC-RAS and River2D are not able to compute the velocity in the vertical direction. In order to obtain the velocities at different elevations (the same elevation for each point describing the bank profile), the logarithmic law for turbulent flow was applied. Specifically, the logarithmic profile was calculated by means of interpolation starting with the average velocity provided by the models.

Looking at Figure 6-11 and considering that 1.5 m is the appropriate distance of the point (x_i, z_i), Kean and Smith model requires the value of the velocity in$(x_{i+1.5}, z_i)$. Therefore, the logarithmic profile was calculated along the vertical line, which is 1.5 m away fromx_i, with the origin at the point $(x_{i+1.5}, z_j)$.

The log-law was used on the results of both one and two-dimensional models. In the first case, given that HEC-RAS can only provide averaged velocities for each slice, the logarithmic profile was applied on the vertical line passing through the centre of the slice. This procedure was carried out for each simulated discharge and for each point describing the bank profile.

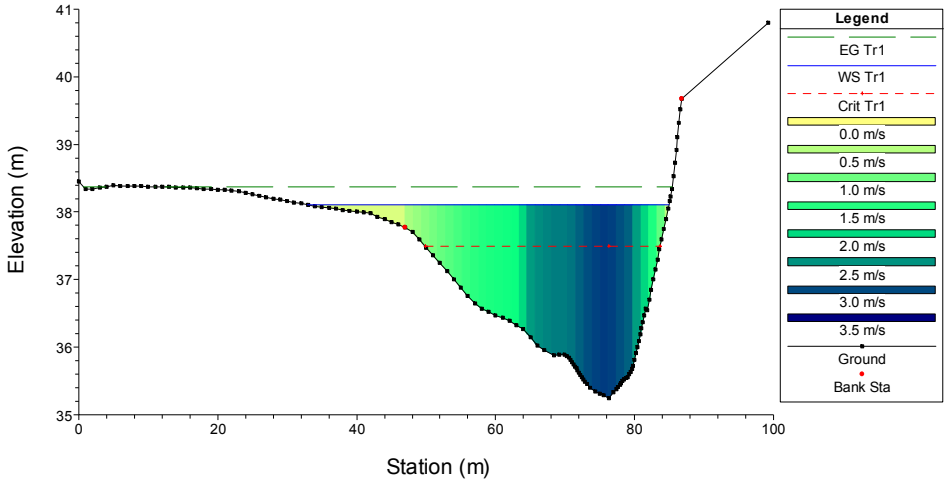

Figure 6-10 Flow distribution output for the downstream bank.

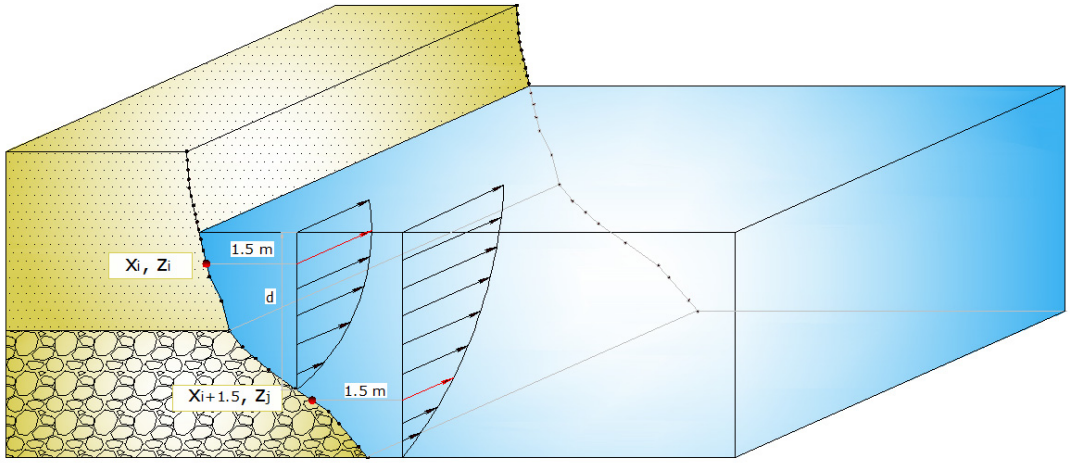

Figure 6-11 Sketch representing the procedure to estimate the outer velocity.

6.3 Results of near-bank shear stress

The values of near-bank shear stress obtained by applying different methods were compared with each other (Table 6-5). This comparison involved two banks located at the upstream (M1) and downstream (V1) bends of the meander, where bank roughness was surveyed. Table 6-5 summarizes models and couplings of models used to estimate the near-bank shear stress.

Figure 6-12 shows the plots of the boundary shear stresses obtained for each point describing the bank (black line) and for a range of discharges. In these graphs, more vivid colours correspond to the highest discharges. For example, the most intense red and blue lines are related to the values of near-bank shear stress and water stage, respectively, which coincide with the 15-years return period discharge.

ID	Hydraulic Model	Near-bank shear stress model
SS HR	HEC-RAS	Simons and Senturk (1977)
KS HR	HEC-RAS	Kean and Smith
R2D R2D	River2D	--
KS R2D	River2D	Kean and Smith

Table 6-5 Different models coupled for near-bank shear stress analysis.

Tested methods provided higher values of near-bank shear stress at the downstream bank. For the aims of the present study, it is worth to emphasize that shear stresses obtained from the River2D model (i.e. R2D R2D M1; R2D R2D V1; KS R2D M1; and KS R2D V1), are significantly lower compared to those provided by 1D model, particularly at the downstream bank. These results are more consistent with measures of the critical shear stress provided by CSM and with field observations. In fact, downstream bank appears quite stable.

In addition, the combination of HEC-RAS with Kean and Smith model (KS HR M1 and KS HR V1, in Figure 6-12) provided some discontinuities in the boundary shear stress distribution, which occurred in correspondence with variations of Gaussian parameter or outer velocity (Nardi and Rinaldi, 2010).

These irregularities may be due to limitations of the 1D hydraulic model. In fact, although HEC-RAS splits the cross section in vertical slices and computes the average velocity for each of them, nevertheless, these values are not continuous and such discontinuities are reflected in the shear stress profiles.

In Figure 6-13, the average shear stresses along the bank profiles are plotted against the discharges. These graphs better highlight the differences between results provided by different models.

According to the 1D model, the shear stress on the bank increases with the discharge - in the case of application of Simons and Senturk distribution - or it reaches an asymptotic value when Kean and Smith model was employed. This behaviour is presumably due to limits of the one-dimension modelling: in fact, bed shear stresses increase with the discharge and although HEC-RAS flow option distribution was applied, computations are still based on average estimates of 1D model.

These results confirm the inadequacy of one-dimensional modelling to describe riverbank erosion, especially when bank are located along a meander.

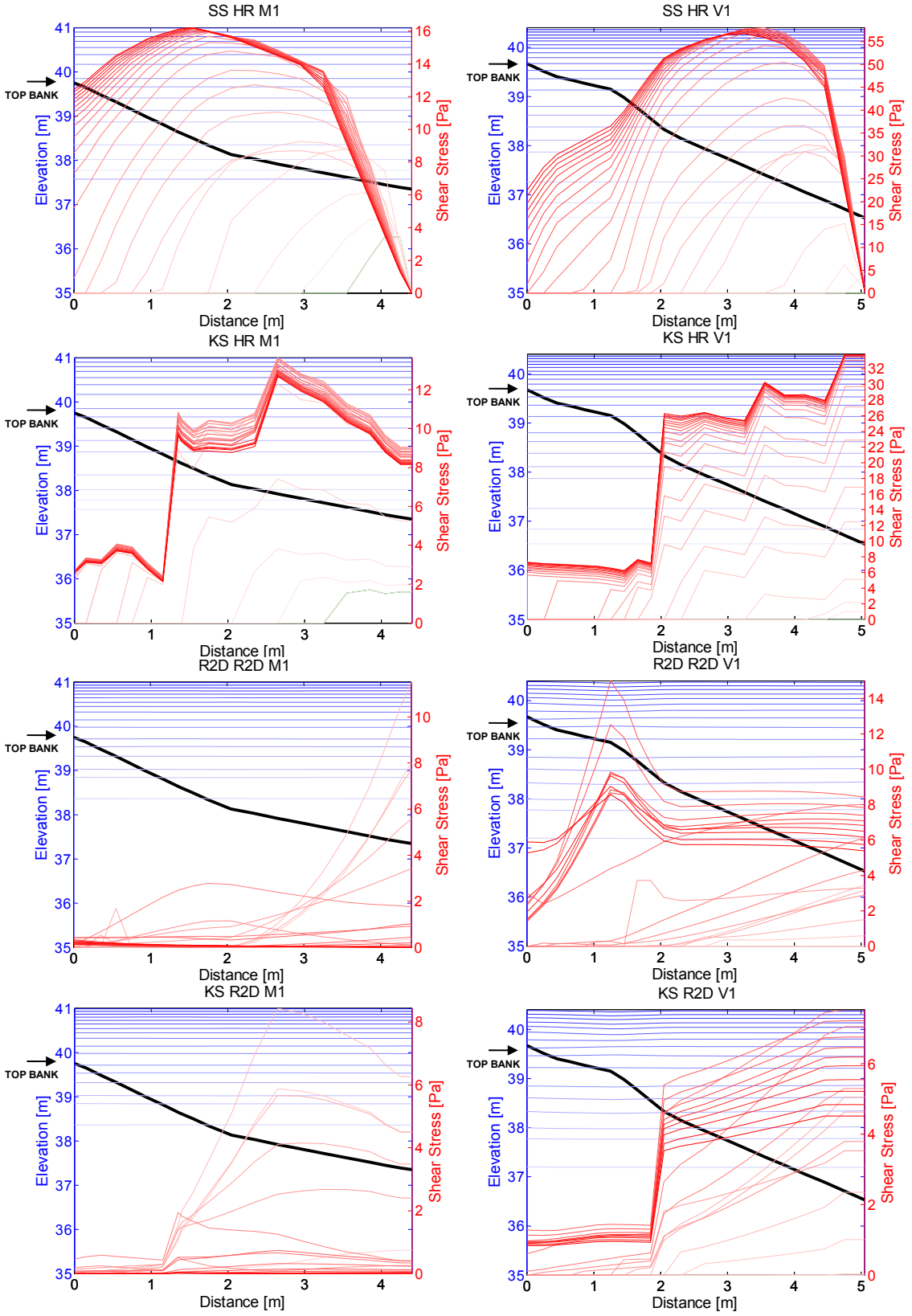

Figure 6-12 Values of near bank shear stress (in red) and water surface elevation (in blue) obtained by applying different methods on the upstream (M1) and downstream (V1) bank for increasing discharges.

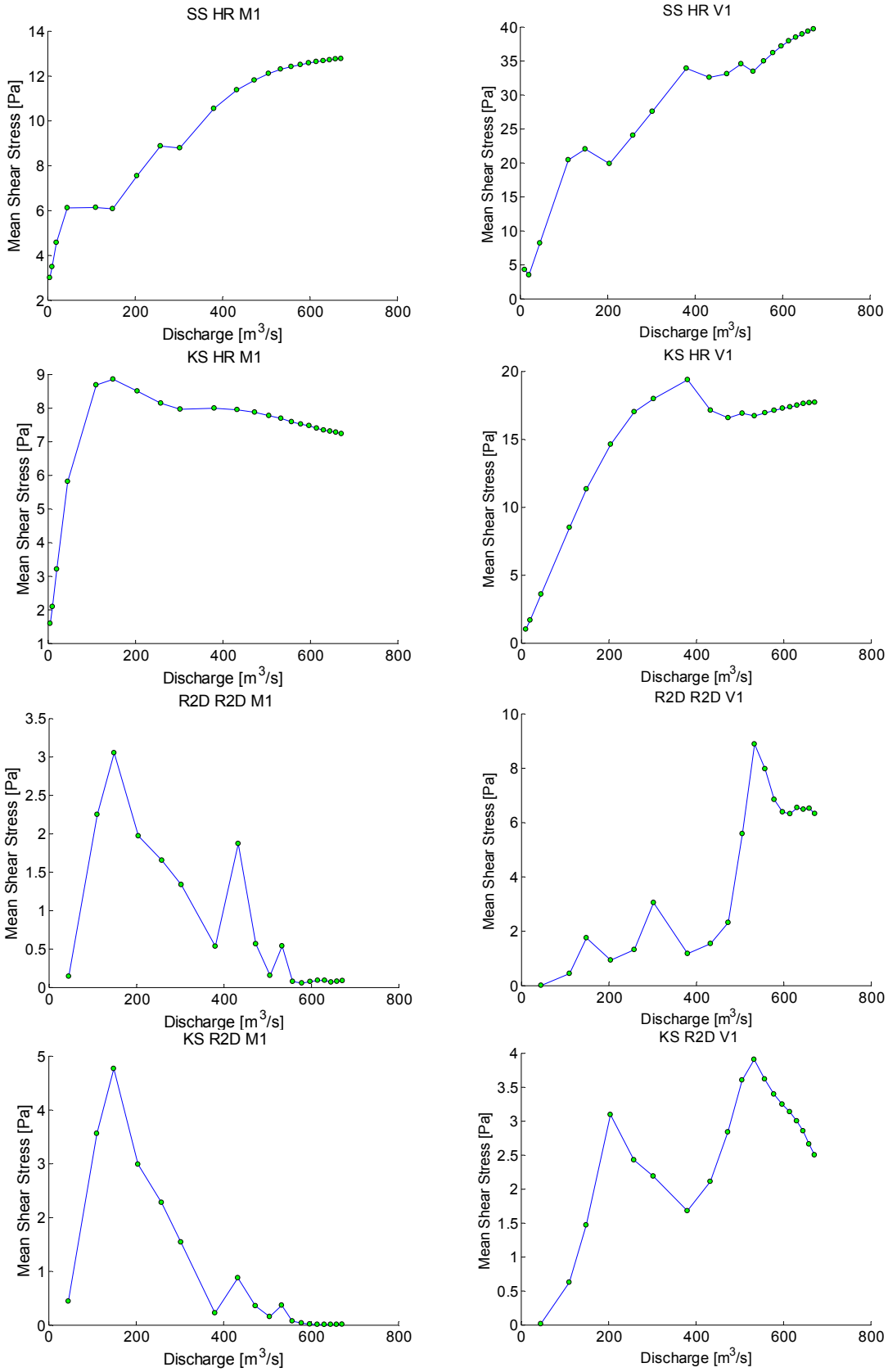

Figure 6-13 Mean values of near bank shear stress obtained by applying different methods on the upstream (M1) and downstream (V1) bank for increasing discharges.

Moreover, it should be noticed that, in cases SS HR M1 and SS HR V1, the value of the shear stress equal to zero at the toe of the bank is due to the exclusive application of near-bank shear stress distribution as represented by Simons and Senturk in Figure 4.1.

Concerning the values of boundary shear stress estimated by River2D different considerations can be made for the upstream and downstream bank. At the upstream bank the shear stress reaches a maximum in correspondence to a discharge of 147 m^3/s, and then it decreases for further increases in the discharge. In fact, the presence of the bends likely induces a shift of the main flow along a chute channel in the central part of the cross section during high flows (see Figure 6-6, Figure 6-7 and Figure 6-8), thereby causing a reduction in near-bank shear stresses. Similar findings have been reported by Rinaldi et al. (2008a), although that study was carried out at a different reach of the Cecina River, and a different hydrodynamic model (DELFT3D) was employed.

Regarding bank shear stresses exerted on the downstream bank it is noticed that values increase with the discharge. This is in agreement with field observations. In fact, currently, downstream bank appears stable, confirming that flow discharges required to promote erosion are higher than those occurred from January 2008 to October 2010. The latter, in turn, did not reach the bankfull discharge. Moreover negative trend of shear stresses could be due to the activation of secondary channels and the increase of flooded areas.

6.4 Calibration of erodibility parameters

The estimate of fluvial erosion rate through the excess shear stress equation (Eq.4.1) requires the knowledge of the erodibility parameters τ_c and k_d.

Various studies have been addressed on the significant spatial and temporal variability in soil erodibility. Hanson and Cook (2004) and Wynn (2004) have focused on the spatial variability, while Wynn et al. (2008) stressed on the temporal changes of the parameters due to subaerial processes, mainly freeze-thaw cycling and soil desiccation. By means of monthly in-situ measures using a multiangle, submerged jet test device, the authors found that k_d was 2.9 and 2.1 times higher during the winter than in the spring/fall, respectively. These observations explained the failure of the first attempt of simulating riverbank retreat at a multiyear temporal scale, by assuming values of the erodibility parameters from literature. In fact,

although the sediments were very similar in terms of grain size distribution, previous studies (Rinaldi et al, 2008; Luppi et al, 2009) estimated these values via calibration on the time scale of a single flow event.

At the reach study, banks are composite presenting a gravel toe. Due to the application of the modelling at a multiyear temporal scale, not all the processes responsible for bank retreat were taken into account. The retreat at the bank toe was extended to the entire bank height. This assumption is justified by field evidences showing subvertical bank profiles induced by failure of cantilevered blocks which are characterized by confined thickness. This explains why fluvial erosion at the bank toe may be recognized as the dominant process which controls the overall long-term retreat. Therefore, for the specific aims of this study, the issue is represented by the fluvial erosion of gravel at the basal layer. The mean values of critical shear stress for the gravel, and the erodibility coefficient for both non-cohesive and cohesive soils were determined via calibration. Calibration was based on measures of the retreat occurred in about 10 years, by means of GIS analysis on high resolution aerial photos. GIS analyses together with measures of discharges recorded at the nearest downstream station gage, Ponte di Monterufoli, supplied data required by the calibration.

The calibration procedure was performed by selecting the parameters which provided equivalent values for the measured riverbank retreat. In details, the total amount of lateral retreat due to erosion was subdivided in 2 periods: 1994-2000 and 2000-2004 due to the date of available aerial photos. The flow events occurred during these periods were discretized in steps corresponding to the values of discharge used in the hydraulic modelling (Figure 6-14). Afterward, the total duration of each discharge was calculated and utilized to compute the fluvial erosion rate across the total period. For each value of near-bank shear stress (obtained for the selected banks by applying different combinations of models), and for each period (1994-2000, 2000-2004 and the total period 1994-2004), the calibration of the parameters was accomplished by applying the Nelder-Mead algorithm. The main limitation of this analysis is represented by the use of the topographic data collected in 2006. In fact, the shear stresses occurring in the recent channel geometry may differ from those that were responsible for the riverbank retreat in the years 1994-2004.

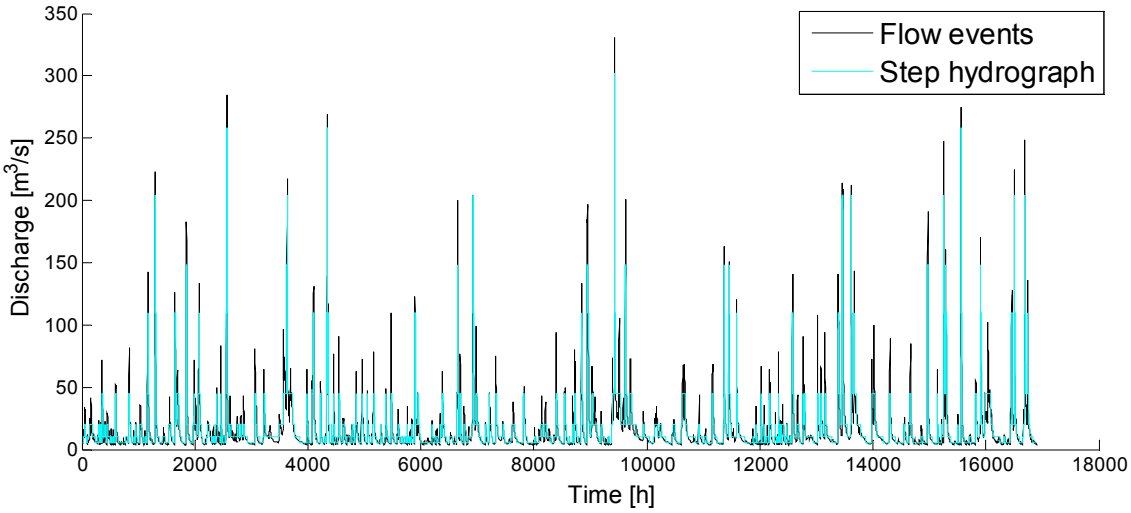

Figure 6-14 Flow event occurred between 1994 and 2004 and correspondent step hydrograph. Discharge lower than the simulated ones (5 m^3/s) have been removed.

This method provided the values of the unknown parameters which minimized the error between the measured data and the retreat values estimated through Partheniades formulation. The minimization of the error for each case was obtained following a multi-start approach. Each minimization was initialized with a range of 'reasonable' (according to the values in the literature) first guess of both the critical shear stress for gravel material (τ_{c_g}) and the erodibility parameters for both cohesive (k_{d_c}) and gravel (k_{d_g}) sediments.

The most part of minimization led to small final errors. Therefore, the following criteria were adopted in order to select a unique optimal triplet of values among the several ones provided by the research algorithm for each case.

- Error (difference between simulated and measured retreat) < 2m
- Value of critical shear stress for gravel, similar to the value provided by Millar and Quick (1993)
- $10^{-9} < k_{d\_c} < 10^{-6}$, $10^{-6} < k_{d\_g} < 10^{-4}$ and $k_{d\_c} < k_{d\_g}$

The first criterion was chosen as a consequence of the resolution of the aerial photos (Table 5-5). In regards to the second criterion, the Millar and Quick (1993) formula (Eq. 2.4) was selected since it has been specifically developed for partly packed and cemented sediments. Using as input data values reported in Table 6-6 it provided 5.68 N/m^2 and 4.26 N/m^2 at the upstream and downstream bank, respectively. The last criterion was defined considering the values reported in literature (Hanson and Simon, 2001).

	β [°]	ϕ^* [°]	D_{50} [m]
Upstream bank	35	70	0.0109
Downstream bank	33	70	0.0067

Table 6-6 Parameter of the upstream and downstream banks used in the Millar and Quick formula. β = bank angle from horizontal; ϕ^*= equivalent friction angle of material.

1994-2004

X_Sect	Hydr.Mod	Shear Strss Mod.	τ_{c_g}	k_{d_c}	k_{d_g}	Error
M1	HR	SS	5.61	5.07E-07	1.07E-06	8.63E-08
M1	HR	KS	5.59	5.24E-07	1.38E-06	9.03E-05
M1	R2D	R2D	5.67	2.42E-07	6.85E-06	8.01E-05
M1	R2D	KS	5.65	4.04E-07	2.75E-05	2.30E-06
V1	HR	SS	***	***	***	***
V1	HR	KS	4.39	2.89E-08	6.47E-07	5.99E-07
V1	R2D	R2D	***	***	***	***
V1	R2D	KS	4.09	2.58E-07	7.06E-05	1.19E-04

1994-2000

X-sect	Hydr.Mod	Shear Strss Mod.	τ_{c_g}	k_{d_c}	k_{d_g}	Error
M1	HR	SS	5.56	7.25E-07	1.15E-06	2.22E-06
M1	HR	KS	5.41	6.70E-07	1.54E-06	1.10E-04
M1	R2D	R2D	5.64	1.41E-07	9.42E-06	1.22E-07
M1	R2D	KS	5.62	1.02E-08	4.59E-05	1.72E-06
V1	HR	SS	4.96	6.79E-08	3.54E-07	7.33E-05
V1	HR	KS	4.57	2.93E-07	2.26E-06	1.18E-05
V1	R2D	R2D	2.72	7.22E-07	2.58E-04	3.97E-05
V1	R2D	KS	4.23	5.04E-07	2.93E-04	6.10E-05

2000-2004

X-sect	Hydr.Mod	Shear Strss Mod.	τ_{c_g}	k_{d_c}	k_{d_g}	Error
M1	HR	SS	5.74	4.05E-08	1.09E-06	1.42E-04
M1	HR	KS	5.72	9.71E-07	1.33E-06	4.80E-08
M1	R2D	R2D	5.68	7.55E-07	5.92E-06	7.90E-05
M1	R2D	KS	5.64	3.02E-07	2.17E-05	5.48E-05
V1	HR	SS	29.14	2.89E-07	3.53E-07	9.30E-06
V1	HR	KS	8.02	7.37E-08	1.27E-07	9.15E-06
V1	R2D	R2D	4.50	1.13E-07	3.73E-06	1
V1	R2D	KS	4.28	4.28E-07	9.03E-06	4.90E-10

Table 6-7 Erodibility parameters (τ_{c_g} [N/m^2] is the critical shear stress for gravel, k_{d_c} and k_{d_g} are the erodibility coefficient [m^3/N·s] for cohesive and gravel, respectively) obtained by mean of the calibration. In the cases marked with the symbol * it was not possible to find the triplet within the range of acceptable errors.**

Since different combinations of models provided important differences in the estimation of near-bank shear stresses, it was impossible to find a unique triplet of erodibility parameters producing rate of retreat with acceptable errors at the same time for all of the cases. The erodibility parameters determined via calibration are reported in Table 6-7 for all combinations of models.

Due to the intermittent behaviour of the retreat, especially at the downstream bank (see Table 5-5), it was not always possible to find a triplet of values for which the calibrated parameters were both within an acceptable error and in the range of the values reported in the literature, at the same time. This only happened in two combinations of models for the downstream bank: by combining the Kean and Smith and the one-dimensional models, and by computing the value of boundary shear stress through the 2D-modelling. For all other cases, we found a small discrepancy between the simulated retreat values and those measured with erodibility parameters. The results of the calibration highlight differences between the models employed: the erodibility parameter for gravel (k_{d_g}) is higher in case of the two-dimensional model to balance the lower shear stresses computed with the River2D model (or with River2D combined with Kean and Smith model).

6.5 Coupling fluvial erosion and bank stability analyses

Fluvial erosion analysis carried out through the excess shear stress formula was coupled with bank stability analysis in order to better understand the interactions between different bank processes at the scale of the flow event. The analyses were not undertaken for the entire period of 10 years, but only for two flow events selected as representative. The bank stability was performed through the BSTEM model. As mentioned in Section 4.4, the model that includes also the computation of fluvial erosion rates, was here used only for bank stability analyses given that it does not allow the user to specify the own shear stress data.

Deformation of the bank profile to account for fluvial erosion or mass failures during the flow event was achieved by using the same procedure described in detail by Darby et al. (2007) and applied in further studies (e.g. Rinaldi et al., 2008a). However, in the present study, less complex models were employed aiming to explore the predicting ability of simple tools in the perspective of their application for practical issues. Due to the limitations of the 1D modelling, an example of application was carried out on the results derived by Kean and Smith model coupled

with River2D. The bank stability analysis was performed on profiles resulting from fluvial erosion occurred at the upstream bank during two flow events selected within the period 2000-2004 (Figure 6-15A and B).

For the purpose of simulating fluvial erosion and bank stability throughout the flow events, hydrographs were discretized into time steps, corresponding to the discharge values used in River2D modelling.

Bank profiles were described by 23 points, as this is the maximum number of coordinates allowed by BSTEM.

The fluvial erosion for each time step was calculated integrating the excess shear stress formula (Partheniades, 1965; Arulanandan et al., 1980), across time-step interval, as follows:

$$LE = \varepsilon \Delta t = k_d(\tau - \tau_c)^a \Delta t \tag{6.2}$$

where LE (m) is the lateral erosion per unit bank area and Δt (s) is the time-step interval.

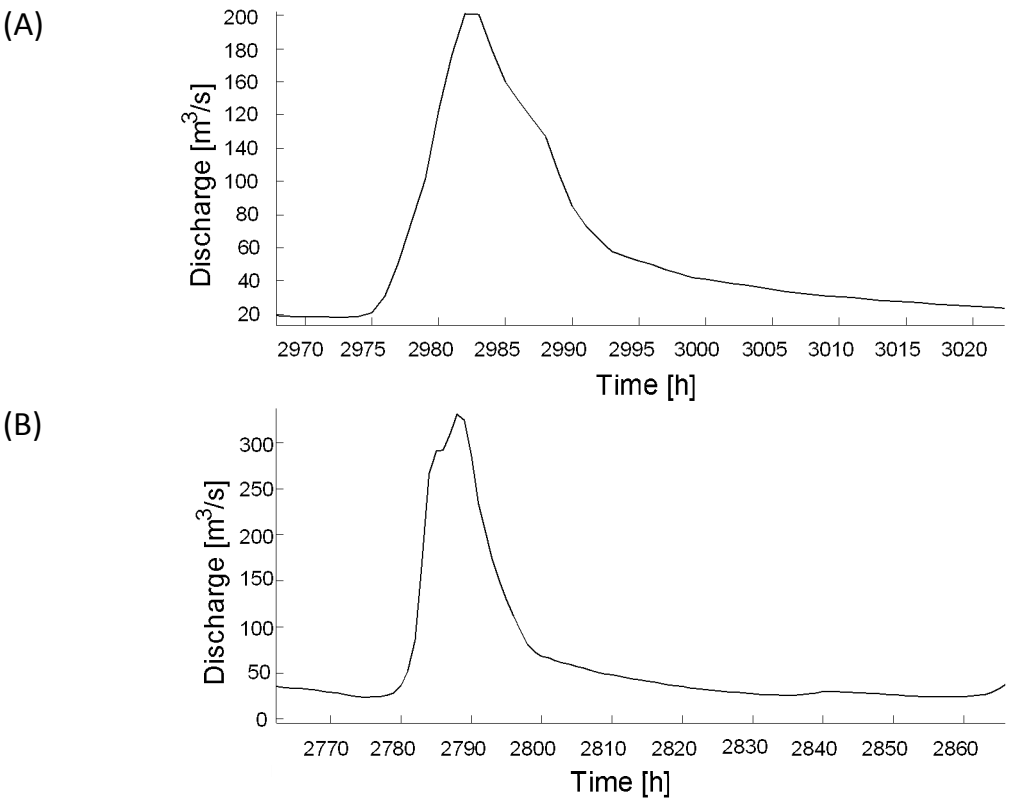

Figure 6-15 Flow events selected for the purpose of simulating fluvial erosion and bank stability. (A) Flow event with 1 year return period , (B) Flow event with 2 years return period.

The calibration of the erodibility parameters for the period 2000-2004 provided the critical shear stress τ_c and the erodibility coefficient k_d (Table 6-8).

Layer	τ_c [Pa]	k_d [m^3 /N s]	ϕ' [°]	c' [kPa]	γ_s [kN/m^3]	ϕ^b [°]
Cohesive	1.25	3.02E-07	35.9	3.9	20.2	25.5
Gravel	5.64	2.17E-05	36	0	20	15

Table 6-8 Parameters used for the fluvial erosion and stability modelling at the upstream bank. τ_c is the critical shear stress; k_d, the erodibility coefficient; ϕ' the effective friction angle; c' the effective cohesion; γ_s the saturated unit weight and ϕ^b the matric suction angle.

Geotechnical parameters for the cohesive layer (ϕ', c', and ϕ^b) derive from previous studies (Rinaldi et al., 2008a, and Luppi et al., 2009) carried out on banks with similar characteristics. Geotechnical parameters for the gravel layer are provided by BSTEM for this type of material (Table 6-8).

Since the pore water pressures were not measurable, a hydrostatic pressure distribution was assumed to define positive (below water table) and negative (above water table) pressures. The water table level was assumed equal to the water stage.

Fluvial erosion and bank stability were coupled according to the flow chart in Figure 6-16.

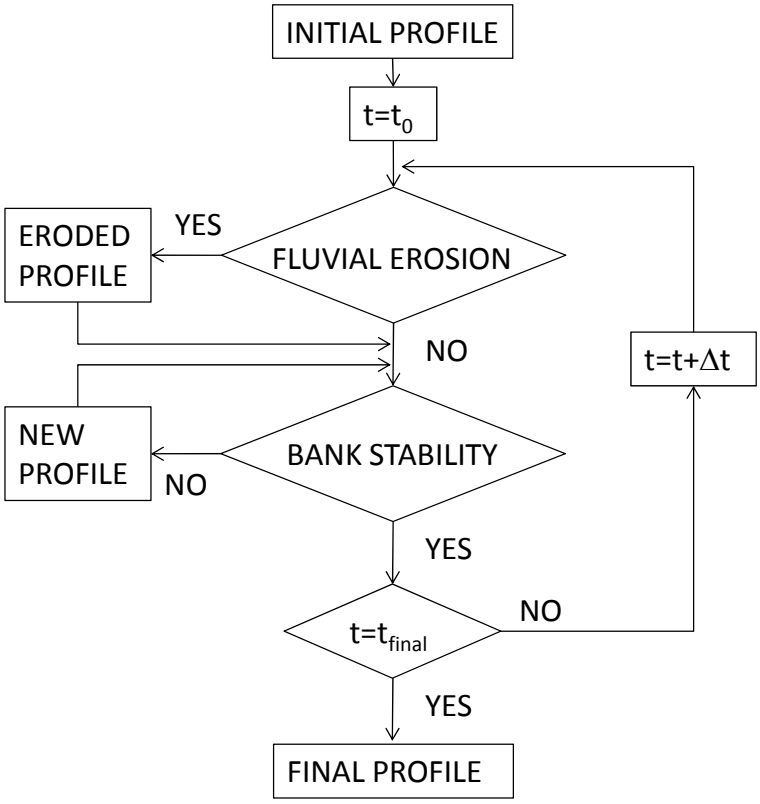

Figure 6-16 Flow chart representing the steps of the procedure for riverbank retreat analyses.

The stability analysis was carried out taking into account the presence of tension cracks with depth of 0.5 m as suggested by field evidences. The results were then compared with those provided by analyses in case of absence of tension cracks. The random walk search algorithm implemented in the BSTEM model was used in order to search for the minimum Factor of Safety, since the failure plane angle was not known a priori. Table 6-9 and Table 6-10 show the values of the Factor of Safety computed by BSTEM model applied on the eroded profile of the upstream bank, whereas Figure 6-17 and Figure 6-18 graphically represent their evolution.

The analysis predicted the occurrence of a planar failure (*FS*=0.9) at the peak of the lower flow event due to the presence of a deep scour at the bank toe. After the failure, the final bank profile, corresponding to Step 4, was again stable with a Factor of Safety equal to 2.21.

1. Initial [Q45]		**4. [Tr1.3 In.Ph.]**		**7. [Tr1.62 Out.Ph.]**		**10. [Q110 Out.Ph]**	
FS T.Crk	3.15	FS T.Crk	3.9	FS T.Crk	4.64	FS T.Crk	2.55
FS no T.Crk	3.8	FS no T.Crk	3.45	FS no T.Crk	3.72	FS no T.Crk	2.58
2. [Q110 In.Ph.]		**5. [Tr1.62 In.Ph.]**		**8. [Tr1.3 Out.Ph.]**		**11. Final [Q45]**	
FS T.Crk	3.05	FS T.Crk	4.69	FS T.Crk	3.88	FS T.Crk	2.44
FS no T.Crk	3.41	FS no T.Crk	3.72	FS no T.Crk	3.45	FS no T.Crk	2.92
3. [Tr1 In.Ph.]		**6. [Tr2 Peak]**		**9. [Tr1 Out.Ph.]**			
FS T.Crk	3.21	FS T.Crk	4.65	FS T.Crk	3.65		
FS no T.Crk	3.34	FS no T.Crk	4.65	FS no T.Crk	3.68		

Table 6-9 Factor of safety computed by BSTEM for each step of the flow event with 2 years return period.

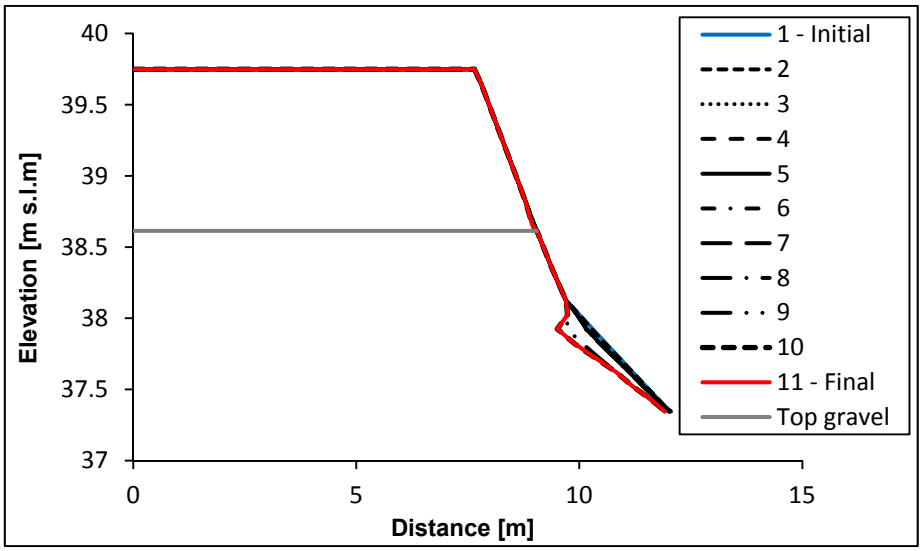

Figure 6-17 Bank profile evolution for 2 years return period flow event.

1. Initial [Q45]		3. [Tr1 peak]		5. [Q110 Out.Ph.]	
FS T.Crk	3.15	FS T.Crk	0.9	FS T.Crk	1.89
FS no T.Crk	3.8	FS no T.Crk	1.1	FS no T.Crk	1.91
2. [Q110 In.Ph.]		**4. [Tr1 Post failure]**		**6. Final [Q45 Out.Ph.]**	
FS T.Crk	3.05	FS T.Crk	2.21	FS T.Crk	1.86
FS no T.Crk	3.41	FS no T.Crk	1.97	FS no T.Crk	2.16

Table 6-10 Factor of safety computed by BSTEM for each step of the flow event with 1 year return period.

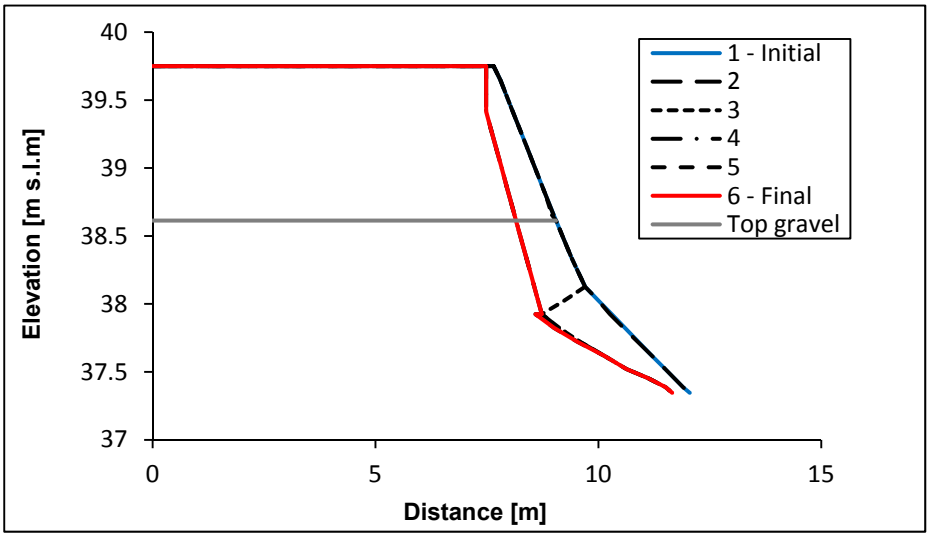

Figure 6-18 Bank profile evolution for 1 year return period flow event.

On the contrary, the final bank profile following the flow event with a return period of 2 years was achieved through the entire fluvial erosion process. In fact, in the second case fluvial erosion was less severe and the scour at the toe of the bank was not deep enough to trigger the failure. These analyses emphasize how the most effective discharges, in terms of fluvial erosion, are those having frequent recurrence which take place for prolonged periods.

It also underline how coupling fluvial erosion and mass failure using straightforward models, which enable medium term analyses, results in dominant fluvial erosion process. The main limitation in this procedure is due to the utilization of the near-bank shear stresses obtained by the hydrodynamic models which employs the initial geometry. In fact, the occurrence of fluvial erosion or mass failure leads to a new bank profile that in turn, may change the shear stress distribution. Therefore, hydraulic computations based on the updated geometry would be desirable to estimate the new values of near-bank shear stresses. In the present study this simplification is justified by the rough dimension of the

computational mesh, whose order of magnitude is equal to the rate of fluvial erosion. Consequently, River2D was not sensitive to such bank profile deformations.

Moreover, the initial distance of the outer velocity (z_{out}=1.5 m), required by Kean and Smith model, increased with the evolution of the eroded profile. This entails a reduction in the velocity and in the estimation of the shear stress as a consequence of a wider cross section. This assumption was made in order to take account for a rate of retreat higher than the rate of accretion of the bar in the internal bend of a meander (Crosato, 2008).

6.6 Framework for a characterization of risk due to fluvial erosion

As conclusion of the analyses at the reach scale, it was explored the possibility to employ the methods, heretofore presented, in order to develop a framework for risk assessment. The estimation of the near-bank shear stress along the Cecina River showed that the amount of retreat was not always proportional to the discharge. These considerations led to the development of a novel algorithm for characterizing the risk due to fluvial erosion, as summarized in the following steps:

1. Computation of the river flow-duration curve;
2. Estimation of the near-bank shear stress for each value of the discharge;
3. Application of the fluvial erosion model for each value of the near-bank shear stress;
4. Computation of the loss duration curve.

The result of the algorithm is represented in the co-axial graphs of Figure 6-19 where each step of the procedure corresponds to a quadrant reading clockwise.

For the study case, the flow-duration curve was obtained from hourly time series of discharge flows occurred in the years 1974-2007. The analysis of near-bank shear stresses, combined with values of the erodibility parameters determined via calibration for the period 1994-2004, provided, for increasing discharges, values of the excess shear stress which is responsible for the fluvial erosion, defined as:

$$\tau_{exc} = max(\tau - \tau_c, 0) \quad (6.3)$$

where τ is the shear stress along the bank profile, and τ_c is the critical shear stress.

The computed values of the near-bank shear stress were interpolated through a spline every 5 m^3/s, in order to increase the number of values and to obtain more readable graphs.

In the third step, the loss (here expressed in €/m·days) was defined through the rate of retreat and the economical value of the eroded land (in this case the land use was agricultural) as follows:

$$Loss = L = Riverbank\ retreat[m] \cdot Price\ of\ land \left[\frac{€}{m^2}\right] \tag{6.4}$$

The line in the third quadrant was obtained by applying the excess shear stress linear formulation from the equation (2.1), and multiplying it for the price of the land in order to obtain directly the retreat loss. Thus, the slope of the line is the product of k_d and the price of the land.

The graph in the fourth quadrant represents the *local loss duration curve,* defined, in analogy to the flow duration curve, through an exceedance probability curve, which expresses the probability that a certain level of loss is surpassed in a specific time period. Hence, a characterization of the mean hydrological year in terms of loss was defined.

The local loss duration curve was obtained by searching for the near-bank shear stresses corresponding to the discharges in the second quadrant (every 5 m^3/s). In this way the historical series of the excess shear stress, necessary to build the duration curve, were found.

The value of risk was evaluated by integrating the local loss as follows:

$$R = \int_0^{1\ year} Ldt \tag{6.5}$$

Since the erodibility parameters were determined via calibration for each combination of hydrodynamic and near-bank shear stress models, the resulting values of the risk are very similar.

The value of risk estimated in these analyses might result quite low when erosion removes lands under cultivation of wheat as the valley of the Cecina River. The resulting value of risk may increase considerably when fluvial erosion occurs on lands tilled with precious cultivations or, even more, when structures or infrastructures are present (see Section 2.1). More interesting are the different distributions on the mean hydrological year.

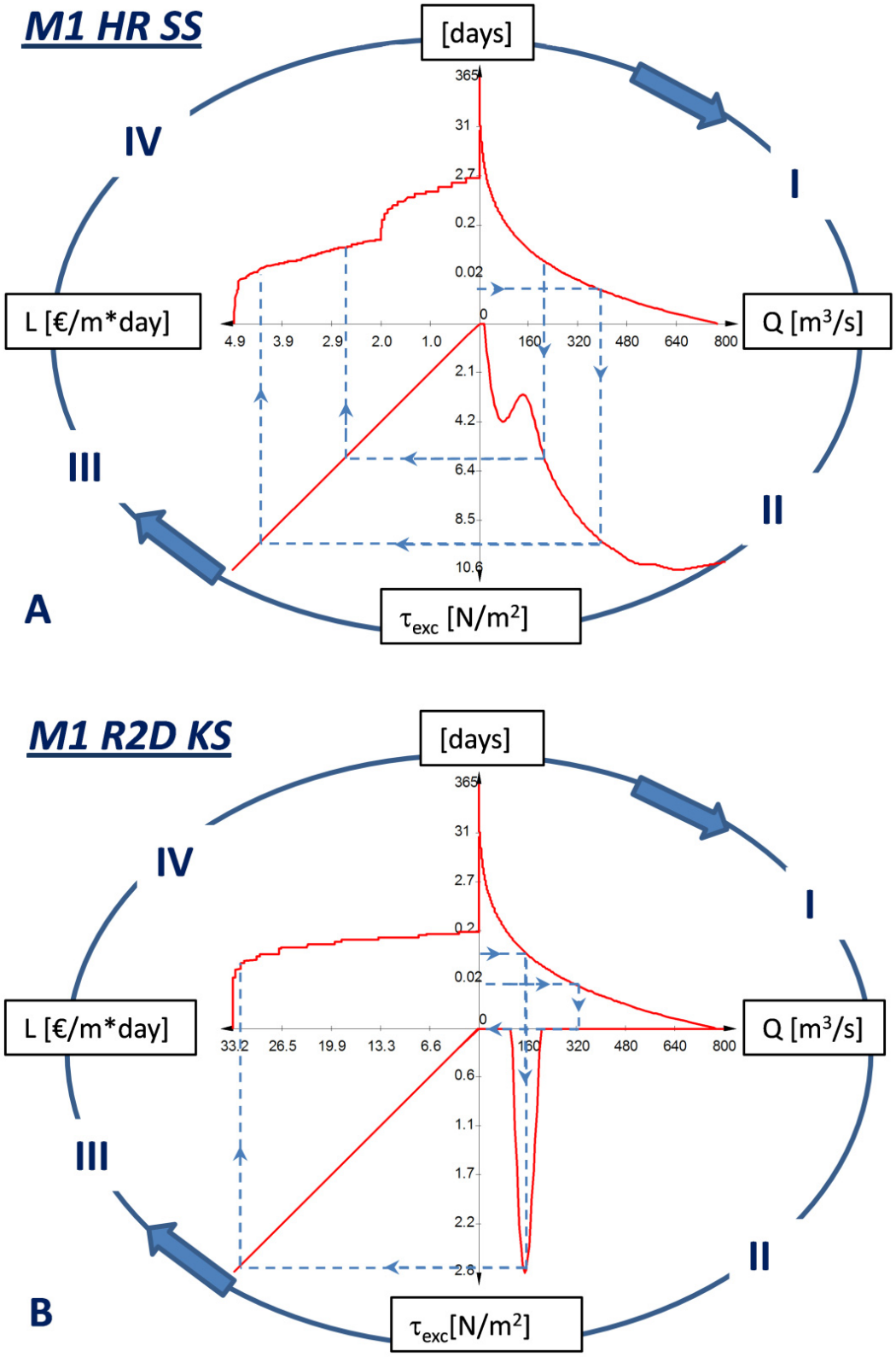

Figure 6-19 Representation of the risk throughout a co-axial graph for 2 different coupling models applied at the upstream bank: (A) HEC-RAS and Simons and Senturk and (B) River2D and Kean and Smith model.

Figure 6-19 shows two scenarios obtained by applying two different combinations of model. The examples reported here were selected to highlight the differences resulting from the models. M1-HR-SS represents the combination of the most simplified models HEC-RAS and Simons and Senturk shear stress distribution, whereas M1-R2D-KS is the combination of the most complex models applied in the present study, namely River2D and Kean and Smith models. For instance, it is observed, for the M1-HR-SS and M1-R2D-KS cases, that the non-monotonic relationships between the discharge flow and the effective shear stress are differently affecting the shape of the loss duration curve. This co-axial graph may be used as a nomogram to yield the expected loss corresponding to a discharge flow value with a known occurrence frequency in the mean hydrological year. In Figure 6-19 examples of such paths are shown.

It is important to note that the characterization of the risk in the present study is only statistical: the framework cannot predict when the loss occurs.

It is also necessary to highlight that these analyses were carried out taking account only for the fluvial erosion, although mass failures represent an important process responsible for the channel migration. This choice was supported by the results of coupling fluvial erosion and bank stability analyses which pinpointed the dominance of fluvial erosion process. Finally, the presence of structures such as bridges, near-river roads, etc, was not taken into account to provide a “continuous” relation between the retreat and the loss.

6.7 Summary and conclusions

The values of the near-bank shear stresses exerted by the flow on two banks were computed through steady flow analyses combined with shear stress models for a range of discharges. Different combinations of models supplied different results both in quantitative terms and in their trends. While the 1D model computed values of shear stress increasing with the discharge, results provided by River2D highlight that fluvial erosion mainly occurs during flow events with formative discharges. These results are in agreement with those found by previous studies (Rinaldi et al., 2008a) and may be explained by the presence of the bend which steers the core of the high velocity fluid away from the bank during high flow discharges. As a result of the specific planform configuration, bank erosion occurs during particular phases of the hydrograph, whereas it is ineffective at higher peak discharges.

The output of the hydraulic and shear stress modes have been utilized, together with the fluvial erosion model, flow data and measured retreat, for the calibration of the unknown erodibility parameter. The results of the calibration highlight differences between the models employed: the erodibility parameter for gravel (k_{d_g}) is higher in case of the two-dimensional model to balance the lower shear stresses computed with the River2D model (or with River2D combined with Kean and Smith model). Thus, it was not possible to find a unique triplet of erodibility parameters producing rate of retreat with acceptable errors at the same time for all cases. Excluding two cases, small discrepancies between the simulated and the measured values of retreat with erodibility parameters were found for each model.

Since the erodibility parameters obtained via calibration were not validated, it was not possible to define which of them are correct by far. The analyses only underline that, by applying different models, much carefulness is required in order to avoid over or underestimation of riverbank retreat.

The erodibility parameters obtained via calibration were applied in the excess shear stress formulation (Partheniades, 1965, Arulandan et al., 1980). The analyses of fluvial erosion were coupled with the stability analyses through the BSTEM model, providing a factor of safety for planar failure and cantilever. Compared to models applied in previous studies for bank stability analyses (e.g the SLOPE model employed by Rinaldi et al., 2008a), BSTEM represents a less complex alternative and a solution for practical purposes.

Coupling bank erosion and mass failure resulted in dominant fluvial erosion process. Nevertheless, it is necessary to underline that bank stability models at the state of the art have been developed for cohesive banks. Therefore they might reveal not always adequate to describe processes occurring on composite banks.

The analysis here proposed allowed the assessment of risk due to bank erosion for a specific cross section of the channel. Due to results of coupling different processes, mass failures were not taken into account. The presence of structures and infrastructure was not considered as well.

Notwithstanding uncertainties on values of the near-bank shear stress exist, due to the impossibility to make direct measurements of the velocities, the goal of this analysis is represented by the development of a framework to estimate the risk of fluvial erosion in terms of economical loss due to loss of lands. This model may be

employed to build site specific co-axial graphs by applying appropriate erodibility parameters.

The analyses carried out in the present study may represent a starting point for further developments for mapping risks of fluvial erosion in terms of monetary loss. This, in turn, may constitute a suitable tool in river corridor managing.

PART III: EXPERIMENTAL INVESTIGATION ON MASS FAILURES AT THE BANK SCALE

Bank failure is a key process in meandering channels and its quantification is a challenging issue for advances in interpretation and prediction of the altimetric and planimetric evolution of river meanders.

The majority of studies dealing with modelling bank failures are focused on fine-grained (sand, silt, and clay), cohesive banks. The retreat of these banks, often occurring along sandy rivers and tidal channels, has been mainly related to instability and mass wasting processes (e.g. Darby and Thorne, 1996; Rinaldi and Casagli, 1999; Simon et al., 2000; Rinaldi et al., 2004; Rinaldi and Darby, 2008), and assessed using algorithms originally developed in the geotechnical field.

Riverbanks totally or partially composed of relatively coarse, granular sediment (gravel or cobble mixed with sand) are common along meandering channels with relatively coarse bed material. Other transitional gravel-bed channel morphologies (e.g. sinuous with alternate bars or wandering) where bank retreat is a key process in meander initiation and development are also common. However, these types of banks have received less attention compared to fine-grained, cohesive banks. As a consequence, models of coarse-grained bank stability are limited, and with the tendency to oversimplify the complex nature and behaviour of such banks.

Along composite banks, the failures occurring within the upper, cohesive layer are strongly related to the processes occurring within the basal layer of coarse material

(e.g. Rinaldi et al., 2008; Luppi et al., 2009). Field evidence suggests that the processes acting on coarse sediment at the bank toe are extremely variable with combinations of fluvial entrainment and a variety of small-scale mass failures. In fact, mixtures of granular sediment (gravel, cobble) with fine interstitial matrix (predominantly sand) often exhibit an intermediate behaviour between loose and partially cohesive sediment.

Morphodynamic models of river planform evolution traditionally consider fluvial entrainment and erosion as the most important, if not the exclusive, mechanism for bank retreat. In many models bank retreat is evaluated through over-simplified schematizations based, for instance, on the knowledge of the near bank flow velocity and some erodibility coefficient (e.g. Ikeda et al., 1981; Lancaster and Bras, 2002; Seminara, 2006; Frascati and Lanzoni, 2009).

Increasing efforts was recently made to include the erosion of granular layers at the bank toe in morphodynamic and regime models. The most common geotechnical model for coarse material is that of infinite slope failure, that corresponds to the assumption of an ultimate stable angle equal to the angle of repose (see for instance Nagata et al., 2000; Eaton et al., 2004; Eaton, 2006; Chen and Duan, 2006, 2008; Dulal et al., 2009). This model can reproduce the geometry of the wedge of loose sediment often accumulated at the bank toe, but it is not suitable for explaining near-vertical faces of coarse sediment, with angles much higher than the angle of repose, often observed in nature. To explain such geometries, different models and additional factors need to be considered, including effects of apparent cohesion acting in the matrix of fine sediment, packing, partial cementation of the material, and vegetation.

The aim of this research is to investigate the basic processes controlling the stability of relatively coarse, granular bank sediments, by carrying out a series of laboratory physical experiments.

Physical experiments have been rarely adopted in the past for riverbank processes, given difficulties in scale reproduction, with particular reference to scaling sediment sizes. Only more recently there has been an increasing employment of laboratory experiments including investigations of bank failures. For example, various works have been carried out to investigate dam-break flow and associated downstream sand bank failures (Spinewine et al., 2002; Spinewine and Zech, 2007; Soares-Frazao et al., 2007; Zech et al., 2008). Other works have carried out experiments on

small scale banks composed of fine-grained, sandy sediments, with specific focus on the occurrence of seepage erosion processes due to seepage flow gradients and related mass failures (Howard and McLane, 1988; Fox et al., 2006, 2007; Wilson et al., 2007; Lindow et al., 2009).

This research, started from an experimental setup similar to that used in these latter works, but with the intent to extend the observations to coarser sediment and associated basic processes. The Cecina River (Tuscany, Central Italy) was used as a reference study case. The bank reconstructed in the laboratory was intended to mimic a coarse-grained layer of the basal portion of a typical bank profile of this river. The experiments focussed on processes related to gravity (mass failures) and to the interaction between water and sediment. Flow entrainment was not modelled for technical limitations of the experimental setup. In spite of this limitation, it allowed for the exploration of how the stability of a coarse bank is affected by processes associated to bank geometry and pore water pressure changes, independently of flow.

The specific objectives of this study is summarised as follows: (1) investigation of dominant processes acting on banks composed of loose or slightly cemented sediment; (2) identification of different mechanisms of failure in the reproduced banks; (3) understanding initiation of the investigated processes and factors controlling stability, with emphasis on the role of apparent cohesion and cementation in maintaining bank stability; (4) investigation of the importance of initial instability conditions related to bank geometry or transient changes in bank stability due to the action of water. The overall findings may be instrumental to the development of more realistic algorithms of coarse-grained bank retreat for incorporation into hydro-morphodynamic models of river planimetric and bed evolution.

7. Experimental setup and description of physical modelling

At the bank scale the research was carried out through physical modelling aiming to investigate processes occurring on gravel banks. The characteristics of bank models were defined on the basis of a series of observations and grain size analyses carried out on basal layers of composite riverbanks along the Cecina River (Tuscany, Central Italy). The bank reconstructed in the laboratory was not intended to scale an entire bank of the Cecina River, but rather to mimic a single layer of the basal portion.

7.1 Experimental apparatus

The physical modelling consisted of 4 main tests based on results and analyses of 22 preliminary tests. The main experiments were carried out in a static tank designed for the specific purpose of this research.

The tank is 1 m wide, 3 m long, and 1 m deep, having a steel structure, zinc platted bottom, and glass walls to allow observations and video monitoring during the experiments (Figure 7-1). The front side has a zinc platted door. A smaller reservoir is included on the back of the tank to maintain a given water head during the experiments, with a porous plate separating the reservoir from the main body of the tank ("lysimeter" modality, according to the experimental setup developed by Fox et al., 2006).

This experimental layout was designed to reproduce the effects of: (1) movement of water from the river into the bank (Figure 7-2A) and vice versa, and consequent changes in pore water pressures; (2) lateral confining water pressures; (3) possible seepage induced erosion by groundwater gradients towards the river, in case of imposing a water head higher than the river stage in the reservoir back of the bank (Figure 7-2B, this option was not used in the experiments described here).

The effect of fluvial entrainment due to the boundary shear stresses along the bank is not reproduced.

The experimental apparatus includes the monitoring instruments to measure parameters which play an important role in the bank stability: the water stage, the positive and negative pore water pressures and the water content.

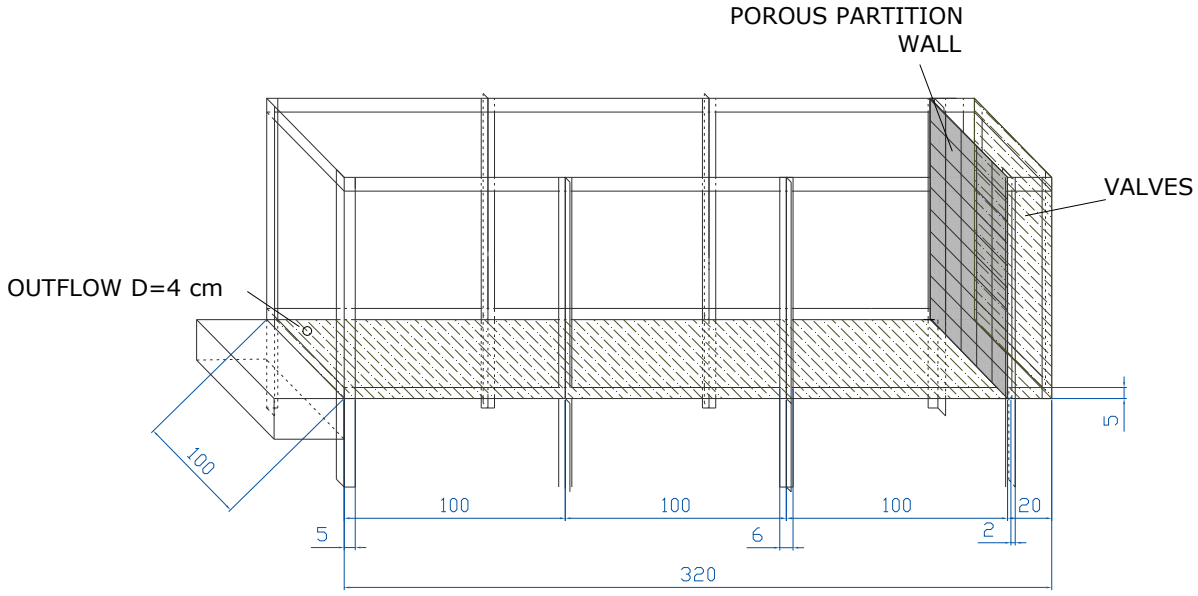

Figure 7-1 Sketch of the experimental apparatus.

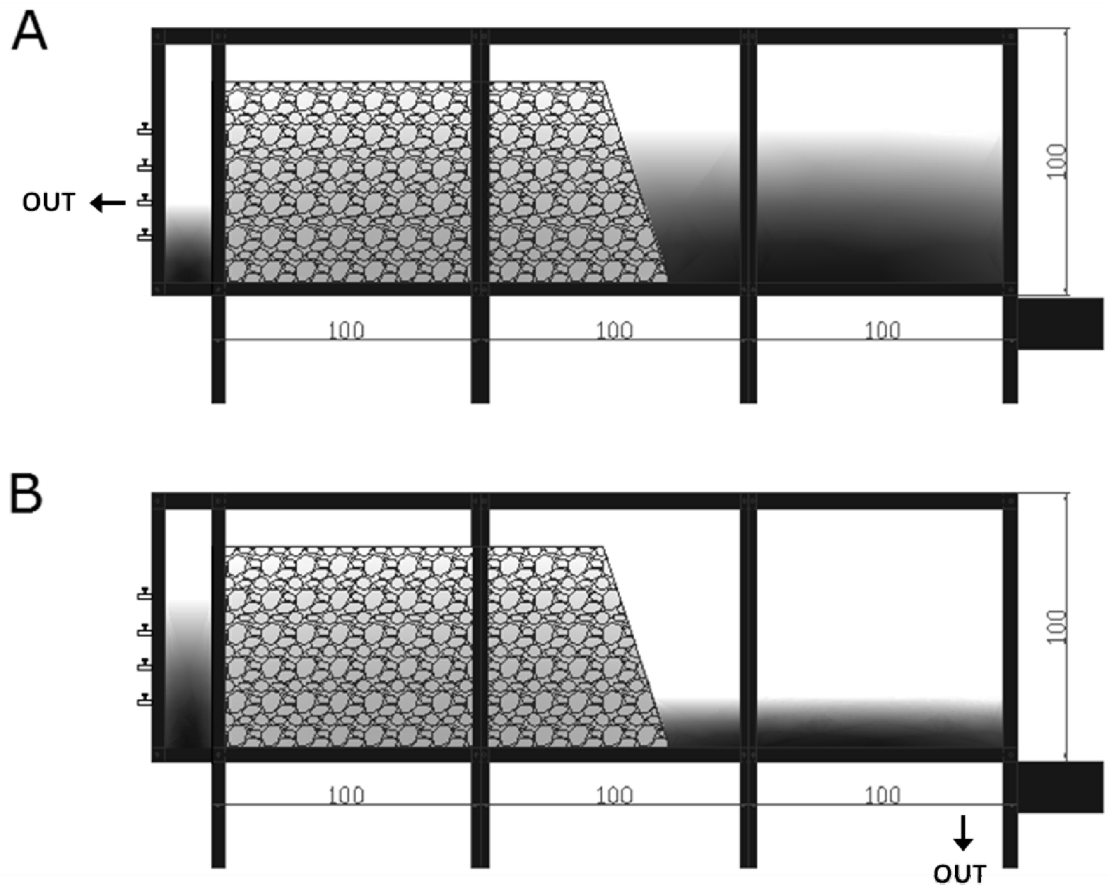

Figure 7-2 A: Normal modality with the direction of the water is from the river to the bank; B: Lysimeter modality, the water flows from the bank to the river.

The water stage was measured by ultrasonic distance sensors 943-F/T4V from Honeywell Sensing and Control, allowing a repeatability of ±2 mm. The detection of the sensor ranges between 300 and 3000 mm, while its beam angle is 8°. The sensor works with an ultrasonic transducer used for both transmitting and receiving. With each cycle, ultrasonic pulses are transmitted. The pulses are then reflected back from the target, and received by the sensor. By means of the temperature compensated measurement of the elapsed time of the acoustic signal, the target distance is determined. The instrument was calibrated measuring the output of the sensor in mV at known distances from the water table. Therefore, it was possible to define a linear relation between the output (mV) and the distance (cm).

The TDR (*Time Domain Reflectometry*) ThetaProbe ML2x from Delta T Device Ltd. measured the volumetric soil water content by determination of the apparent dielectric constant. Volumetric soil water content (θ_v) is a dimensionless parameter, defined as the ratio between the volume of water present in the soil and the total volume of the sample. The sensor was calibrated through the comparison with specimens having known water content by mean of double weighing before and after the soil drying for 12 hours at a temperature of 105°.

The pore water pressure inside the bank at different positions was measured by tensiometers T4e from UMS, Umwelt Monitoring Sisteme. Tensiometers allow for positive and negative pressure measure (the range varies from -85 kPa up to 100 kPa), thus they were employed both in saturated or unsaturated conditions.

Soil water and tensiometer water have contact through the porous ceramic as a wetted porous ceramic creates an ideal pore/water interface. The soil water tension is directly conducted to the pressure transducer which offers a continuous signal. The atmospheric reference pressure is provided through a membrane on the cable.

The datalogger DL2e produced by Delta-T Device Ltd. was used to read and to storage the measures acquired by sensors.

7.2 Characterization of the material

Grain size of the basal gravel layers along Cecina riverbanks are quite variable in their composition, and the sediment size of layers composed by finer gravel and sand was as reference. Gravel, sand and silty sand were mixed varying their percentages in order to identify, throughout the preliminary tests (Section 7.3), a

desirable composition. The characteristics of the three different sediments are described in Table 7-1.

The sediment mixture for the main tests inside the bank was composed of about 60% of gravel, and 40% of sand (the amount of silt and clay was negligible). Sediment mixture was also the same, but during the last two tests (EXP3 and EXP4) a small quantity of cement (1 %) was added.

Experimental research on naturally cemented sediment is rare due to extreme difficulties in acquiring undisturbed samples (Haeri et al., 2005). Because recreating natural conditions of cementation is not possible in laboratory, an artificially cemented mixture was used to simulate the different behaviour (related to the increased shear strength) due to possible precipitation of various agents (salts) from circulating interstitial water in natural riverbanks.

Proctor compaction tests were carried out to determine the maximum practically-achievable density of soil used for the main tests. The procedure consisted of compacting the soil (or aggregate) to be tested into a standard mould using a standardized compactive energy at several different levels of moisture content. The maximum dry density was found 19.6 kN/m^3 with an optimum moisture content equal to 8.5%.

Constant-head permeability tests were also carried out to measure the permeability coefficient of the mixture composing the main banks. During the tests, a confined sediment sample was subject to a constant head that was maintained by replenished column of water.

The volume flux of water through the sample was measured allowing the permeability to be determined, given the fluid properties.

Non-back-pressured (i.e. fluid flows out of the sample to atmospheric pressure) tests were selected because they are best suited for sediments with high permeability as in the case of material used for experiments. The tests provided an averaged value equal to $3.64 \cdot 10^{-6}$ m/s with 1.53 10^{-7} m/s standard deviation.

	Gravel [mm]	Sand [mm]	Silty sand [mm]
D_{10}	2.83	0.10	0.04
D_{50}	5.88	0.34	0.08
D_{90}	9.32	1.55	0.26

Table 7-1 Grain size diameters for the different soils.

7.3 Preliminary tests

A series of preliminary experiments were carried out on small boxes aimed to test the behaviour, in terms of processes and stability, of different sediment mixtures, hydrographs, and bank geometries (Table 7-2). The boxes were constructed of wood, with a rectangular base of 45 x 50 cm and a height of 40 cm, and a frontal wooden panel with an assigned slope angle which was removed at the start of the test. During the tests, the boxes were placed in the tank, and subject to given hydrographs with a peak water stage of 25 cm.

A first group of preliminary tests aimed to (1) define the initial geometry; (2) test which possible sediment mixture (relatively higher or lower percentage of sand) appeared to be more suitable to reproduce the desired mass failures, avoiding excessive stability or instability; and (3) identify how to obtain a good compaction of the material. For the last purpose both dynamic and static (by means of the application of loads) modalities were tested.

ID	Geometry	Sed. Mixture [%]	Ligands [%]	Compaction	Tests [#]
T1	H=22 cm, β= 70°	75 G – 25 S	-	S	1
T2	H=22 cm, β= 70°	60 G – 40 S	-	S	1
T3,T5	H=30 cm, β= 75°	75 G – 25 S	-	D	2
T4	H=30 cm, β= 75°	54G – 37 S	9 Silt	D	1
T6	H=30 cm, β= 75°	60 G – 40 S	-	D	1
T7, T8	H=30 cm, β= 75°	60G – 40 S		S-L	2
T9, T10, T11, T12	H=30 cm, β= 90°	60 G – 40 S		S-L	4
T13	H=30 cm, β= 90°	60 G – 39.5 S	0.5 C	S-L	1
T14, T15, T16	H=30 cm, β= 90°	59.5 G – 39.5 S	1 C	S-L	3
T17, T18, T19	H=30 cm, β= 90°	59G – 39.5S	1.5 C	S-L	3
T20	H=30 cm, β= 90°	59.5 G – 39.5 S	1 B	S-L	1
T21	H=30 cm, β= 90°	58.5 G – 38.5 S	3 B	S-L	1
T22	H=30 cm, β= 90°	57.5 G – 37.5 S	5 B	S-L	1
				TOTAL	22

Table 7-2 Bank geometries and sediment mixtures used during the preliminary tests. H: bank height; β: bank slope; G: gravel; S: sand; C: cement: B: bentonite. Compaction is static (S), dynamic (D), or static layer by layer (S-L).

A second group of preliminary tests was carried out after the first main test. The purpose of these tests was mainly to investigate different percentages of cement and bentonite in order to identify which quantity would better mimic the light

cementation that in natural bank is due to the minerals precipitation from pore water fluid circulation, avoiding, as well as in the first tests, excessive stability or instability.

During each preliminary test, the banks were subject to hydrographs shaped as shown in Figure 7-3. Measures of water content were collected before and after each test, together with measures of changes in the thickness of each layer, before and after consolidation. The small dimension of the models, did not allow to introduce tensiometers with a shaft 20 cm long. Therefore, values of pore water pressure during the preliminary tests are not available.

The results of these tests were used in later analyses for classification of different failure mechanisms and observations on instability conditions, as some mechanisms were more frequently observed in these tests than during the main experiments.

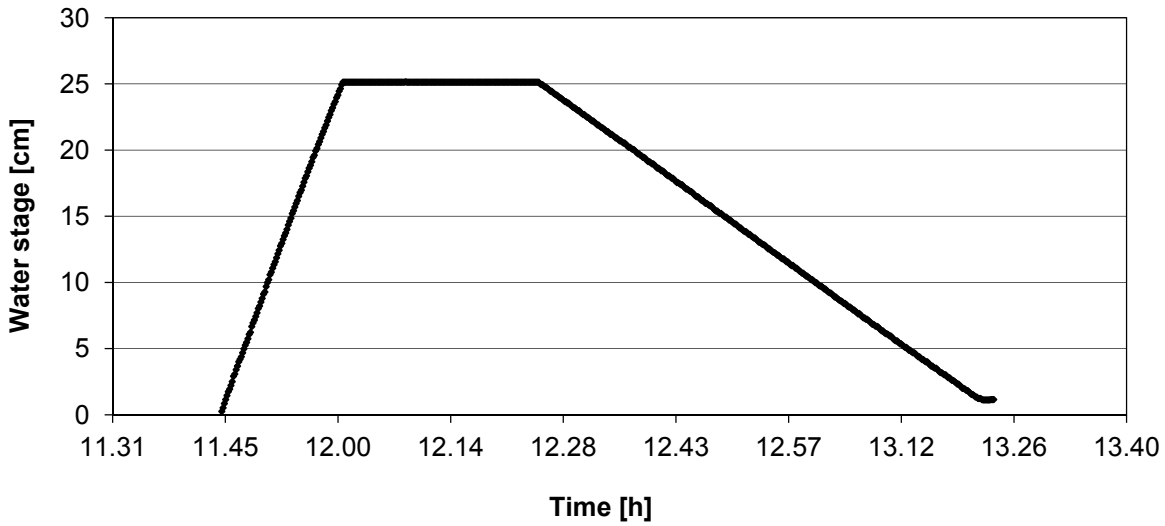

Figure 7-3 Typical hydrograph applied during the preliminary tests.

7.3.1 Preliminary tests – Group I: T1»T8

The first group of preliminary tests was performed in order to identify the physical characteristics (i.e. geometry and sediment mixture) and the procedure to construct the bank for the main tests. For this purpose, a range of sediments mixture was tested varying the percentage of gravel and sand. Different bank slopes and percentages of water content were also investigated. The compaction was carried out, both in static and dynamic way and its efficiency evaluated through the displacement of the material subject to the load. The preliminary tests suggested that the best method to build the bank was by creating a series of layers, each layer

subject to a static compaction by means of application of loads with a weight decreasing from the bottom to the top of the bank model. In fact, though the dynamic procedure provided higher values of compaction (see Table 7-3), the option of such compaction by using a mechanical earth compactor was excluded due to the following reasons: (1) to avoid the formation of interstitial over-pressures; (2) because static compaction better reproduce the conditions that normally occur in nature due to lithostatic loads; and (3) to avoid damages to the tank.

Although the characteristics of the first models were highly variable, the type of failures observed during the tests was very similar. Common succession of processes (Figure 7-4) included a first phase of erosion due to loss of matric suction, with creation of a basal scour (Figure 7-4B), development of tension cracks and a subsequent series of cantilever failures, initially tensile and then shear (e.g. T4, T5) or beam (e.g. T6, T8) failures. Tension cracks developed mostly on banks composed of higher percentages of finer sediments (T2, T4, T6, T7, and T8). Water stage corresponding to the first failure varied for each test within the range of 4-20 cm (Figure 7-5). No failures occurred during the drawdown phase of the hydrograph. This may be due to the presence of failed material at the toe of the bank, acting as a protection and preventing the occurrence of new failures during the outflow phase. The failed material settled down with slope angle ranging between 25-30°, while the upper part of the bank reached a nearly vertical configuration (Figure 7-4C).

Observation of this process was possible during the tests because the initial bank face remained stable after the panel removal, so that water entered directly in contact with an intact, near-vertical bank. A similar evolution was observed only during EXP3 of the main experiments.

ID Test	Slope [°]	Sed. Mixture [%]	Compaction	Water content [%]	ΔV [%]
T1	70	75 G - 25 S	S	10	-
T2	70	60 G - 40 S	S	10	-
T3,T5	75	75 G - 25 S	D	7	$10^{(*)}$
T4	75	54 G - 37 S - 9 Silt	D	7	13
T6	75	60 G - 40 S	D	8	13
T7, T8	75	60 G - 40 S	S-L	8	$9^{(*)}$

Table 7-3 Characteristics of bank of first group preliminary tests. (*):mean value.

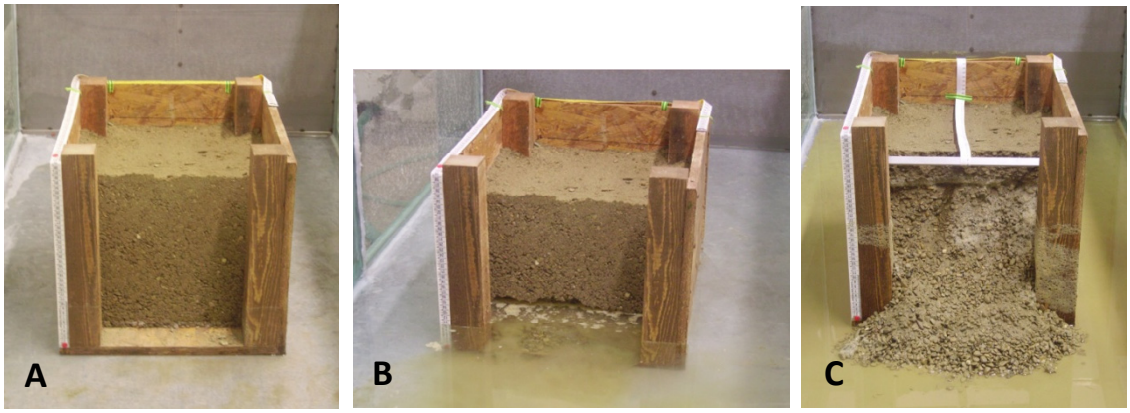

Figure 7-4 Bank evolution of T4. A: initial profile; B: scour at the bank toe; and C: final profile.

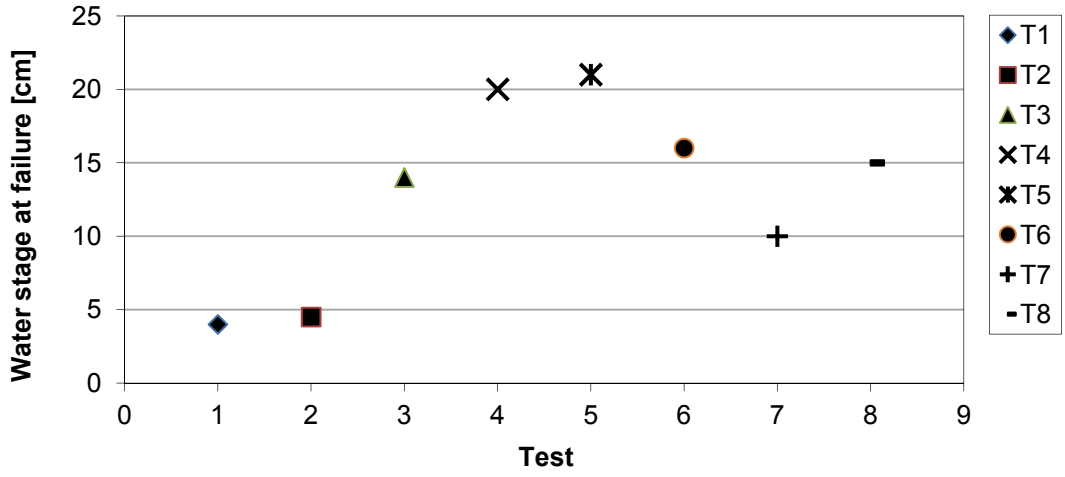

Figure 7-5 Water stage corresponding to main failures occurred during the first group of preliminary tests.

7.3.2 Preliminary tests – Group II: T9»T22

The second group of preliminary tests was carried out after the first main test (EXP1). The specific purpose of these models was to test different percentages of cement and bentonite in order to mimic the light cementation that in natural bank is due to the minerals precipitation from pore water fluid circulation. Therefore, the relative percentages of sand and gravel (60% gravel and 40% sand) and the procedure to compact the material (static load applied on each layer) were no more varied. The load profile applied to consolidate preliminary banks of the second group is described in Table 7-4. The experience of EXP1 showed practical difficulties to apply the load along the slope boundary (see Section 7.4) thus, vertical profiles were created afterwards.

Specific load for each layer [kN/m2]			
	I Compaction (24h)	II Compaction (24h)	III Compaction (24h)
Bottom layer	3.9	5.5	5.1
Middle layer		3.9	3.5
Upper layer			2.0
	mean	**mean**	**mean**
	3.9	**4.7**	**3.5**

Table 7-4 Mean static load applied during each compaction of layer composing the preliminary models (except the first 6 tests).

Different percentages of cement or bentonite in vertical bank, caused the evolution of different profiles, as described in the next sub-sections.

T9, T10, T11, T12: Bank composed by gravel (60%) and sand (40%)

The mean values of models made with gravel and sand are summarized in Table 7-5.

ID	Water content [%]	Slope [°]	Sediment mixture [%]	Displacement [cm]
T9	7.9	90	60 G - 40 S	3.5
T10	8.3	90	60 G - 40 S	3.8
T11	7.6	90	60 G - 40 S	4.4
T12	7.8	90	60 G - 40 S	3.8

Table 7-5 Mean parameters measured on model made of gravel and sand.

The development of these banks from the initial to the final profile can be summarized in the following steps:

1. A mass failure occurred during the removal of the frontal wood panel, causing the retreat at the edge of the bank ranging between 5 and 10 cm. The loose material at the toe of the bank was removed before the start of the test, and the tests started with an initial profile with a slope of nearly 80° (Figure 7-6A);
2. As the water stage rose, tension cracks developed at the top of the bank (Figure 7-6B);
3. When the water stage reached a level comprised between 4 and 6 cm a rotational failure occurred, causing nearly 15 cm retreat (Figure 7-6C);
4. New tension cracks occurred and they were followed by smaller failures involving the upper part of the banks;

5. No failure was observed during the drawdown phase of the hydrograph;
6. The final profile is characterized by a plane surface with a slope around 35° (Figure 7-6D).

Conversely to what observed during the first group of preliminary tests, the underscour at the bank toe did not develop and rotational failures took place instead of cantilevers.

One of the 4 preliminary models was tested after 1 year exposure time. Although the material was the same, it behaved differently compared with the previous tests. In fact, no failure occurred when the front panel was removed.

During the inflow phase of the hydrograph a scour at the toe of the bank developed, causing a cantilever failure when the water level was 10 cm. The sequence scour-cantilever was recorded during the second part of the inflow phase. The final profile was flat with 35° slope and a total retreat of 25 cm.

Figure 7-6 Preliminary tests. Evolution of bank composed with gravel and sand. A: Beginning of test after the first failure (the loose material at the toe of the bank was removed); B: development of tension cracks; C: rotational failure; D: final profile.

T13: Bank composed by gravel, sand and cement (0.5%)

The mean values of the model made with gravel, sand and 0.5% of cement are summarized in Table 7-6.

ID	Water content [%]	Slope [°]	Sediment mixture [%]	Displacement [cm]
T13	7.3	90	60 G – 39.5 S – 0.5 C	2.4

Table 7-6 Mean parameters measured during construction of T13.

This mixture was tested once, since it was clear that the percentage of cement was too low to guarantee a sufficient degree of stability. In fact, although the bank was more stable during the removal of the frontal panel, a scour at the toe of the bank occurred as the water touched the bank, and tension cracks developed with low water stages. A failure occurred when the water reached 12 cm, causing a 5 cm retreat at the edge of the bank. Smaller failures occurred on the upper part of the bank followed by a second one involving the entire bank. The final profile, globally retreated of about 20 cm, is very similar to that reached by banks without cement.

T14 » T19: Bank composed by gravel, sand and cement (1% or 1.5%)

The mean values of models made with gravel, sand and 1% or 1.5 % of cement are summarized in Table 7-7 and Table 7-8, respectively.

ID	Water content [%]	Slope [°]	Sediment mixture [%]	Displacement [cm]
T14	7.6	90	59.5 G – 39.5 S – 1% C	2.5
T15	7.3	90	59.5 G – 39.5 S – 1% C	2.2
T16	7.6	90	59.5 G – 39.5 S – 1% C	3.0

Table 7-7 Mean parameters measured during construction of T14-T16.

ID	Water content [%]	Slope [°]	Sediment mixture [%]	Displacement [cm]
T17	6.9	90	59 G – 39.5 S – 1.5% C	1.8
T18	7.4	90	59 G – 39.5 S – 1.5% C	2.8
T19	7.4	90	59 G – 39.5 S – 1.5% C	2.5

Table 7-8 Mean parameters measured during construction of T17-T19.

Each mixture was tested three times. The evolution of these models was very similar, because no failure and tension cracks occurred during the removal of the front panel (Figure 7-7A) or during the hydrograph.

The detachment of small blocks at the bank toe was the exclusive process observed with high water stages (Figure 7-7B and C). Thus, the initial profile did not change significantly during the tests.

Figure 7-7 Representative sequence for preliminary models composed by gravel, sand and 1% of cement. A: initial profile; B: near the peak of the flow; and C: final profile.

T20, T21, T22: Bank composed by gravel, sand and bentonite

The mean values for each layer composing the models made with gravel, sand and different percentages of bentonite are summarized in Table 7-9.

ID	Water content [%]	Slope [°]	Sediment mixture [%]	Displacement [cm]
T20	7.4	90	59.5 G – 39.5 S – 1% B	2.9
T21	7.5	90	58.5 G – 38.5 S – 3% B	2.6
T22	7.4	90	57.5 G – 37.5 S –5% B	3.3

Table 7-9 Mean parameters measured during construction of T20-T22.

In banks composed of 1% and 3% bentonite a failure occurred before starting the tests when the front panel was removed. Differently to failures occurred in bank without cement, in the case with bentonite the collapse involved exclusively the first 10 centimetres of the upper part of the banks. No failure occurred in this phase when 5% of bentonite was added (Figure 7-8A). A shallow scour at the toe of the bank and thin tension cracks developed with low water stage.

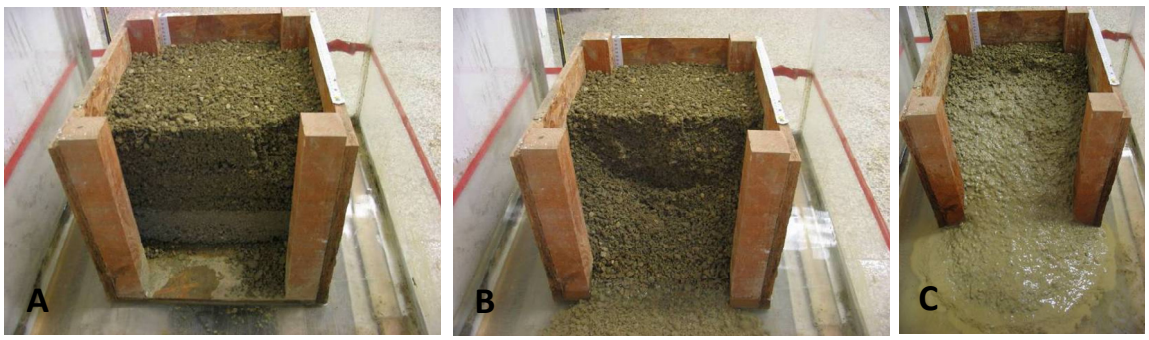

Figure 7-8 Evolution of the bank composed of 5% bentonite. A: Initial profile; B: slab failure for low water level; C: final profile.

Depending on the different mixtures, with water stages ranging from 1 to 3 cm a slab failure occurred, followed by a number of planar failures (Figure 7-8B). The final profile is characterized by a plane surface with a slope that is lower than the angle of the repose for the same loose material (Figure 7-8C).

7.3.3 General considerations on preliminary tests

The preliminary tests enabled to make some first considerations on the effects of geometry and presence of ligands on the bank stability. A dominant factor controlling the stability of banks without cementing agents is the slope. The steepest profile allowing for a stable bank had a slope angle of 75°. Indeed, while removing the wood panel in vertical models, a failure always occurred and the new initial profile settled down at nearly 75° sloping.

Concerning the presence of ligands, low percentages of cement were sufficient to assure an initial stability in vertical banks. The only addition of 0.5% cement (T13) induced to modify the mechanisms of failure. In fact, the presence of cement reduced the quantity and the extent of tension cracks and allowed the underscour developing. The latter, in turn, triggered the failure of the cantilevered portion of the bank. Banks composed of higher percentages of cement (from T14 to T19) were stable during the entire hydrograph. The presence of bentonite produced the same effects of the cement, but higher quantity (5%) was required.

In the light of these first considerations, 1% of cement was added to gravel and sand in the third main experiment. In fact, due to the dimensions of the main tests, this percentage seemed to be sufficient to highlight dissimilarities in the mechanisms of failure, avoiding excessive stability, at the same time.

7.4 Main tests

Further to the preliminary tests four main tests were carried out inside the static tank. Their geometric characteristics and compositions are summarized in Table 7-10.

Following the same procedure defined after the first preliminary tests, the banks were built by creating a series of 10 cm layers, until the banks were 70 cm high. A distributed load (made by steel plates as represented in Figure 7-9A) was applied to the top of each layer, with a weight decreasing from the bottom to the top of the bank model. Thus, sediments were subject to a static load varying from 0.045 to

0.013 kg/cm^2. These values are somewhat similar to the lithostatic loads acting on the basal layer and in nature associated to the presence of an upper cohesive layer. Each layer was left under the assigned load for about 20 hours in order to allow for a sufficient consolidation. Measurements of changes in the thickness of each layer were carried out before and after consolidation.

Sediment mixtures were initially wetted with an initial water content of about 7- 9 % in agreement with the *optimum* of the Proctor test.

During construction of the bank and compaction, a wooden panel was positioned to assign a given slope angle to the bank (see Figure 7-9A).

The panel was removed immediately before starting each experiment. For EXP1, a basal failure occurred immediately after the panel removal (Section 7.5 for details).This unforeseen collapse could be explained in part by a limited compaction of the material along the slope boundary, as in that portion of the bank the application of the load was more difficult, and the portion of sediment directly in contact with the panel was not really subject to vertical overloads. Consequently, the assigned bank slope angle was changed to 90° for second group of preliminary tests, EXP2 and EXP3. After one year EXP4 was carried out on the model used in EXP3.

A failure occurred also at the beginning of EXP2, but not in EXP3 presumably because of the presence of cement in the sediment mixture. The reasons for the occurrence of an initial failure for EXP1 and EXP2 are discussed later.

To measure pore pressure, a series of five tensiometers and one TDR were installed inside the bank (Figure 7-9B), in a vertical position at different distances from the bottom. In particular, three tensiometers were positioned along one lateral side of the bank, and the other two along the rear side. The TDR was placed in the rear corner near the tensiometers (Figure 7-9C). Based on the results of the first experiment, the configuration was optimized by small changes in the position of the tensiometers. For example, tensiometer T1 was located further away from the bank slope in order to avoid disturbance to initial failures (Table 7-11,Table 7-12 and Table 7-13).

Due to the coarse size of the sediments, instruments were installed during the construction of the bank, by inserting them in steel pipes placed vertically into the sediment and removing the pipe after the material had completely covered the length of the sensors.

	Bank Geometry	Sediment mixture
EXP1	H=70 cm, β= 75°	60% G – 40% S
EXP2	H=70 cm, β = 90°	60% G – 40% S
EXP3	H=70 cm, β = 90°	59.5 % G – 39.5 % S – 1% C
EXP4	Final EXP3	59.5 % G – 39.5 % S – 1% C

Table 7-10 Geometry and composition of the main banks.

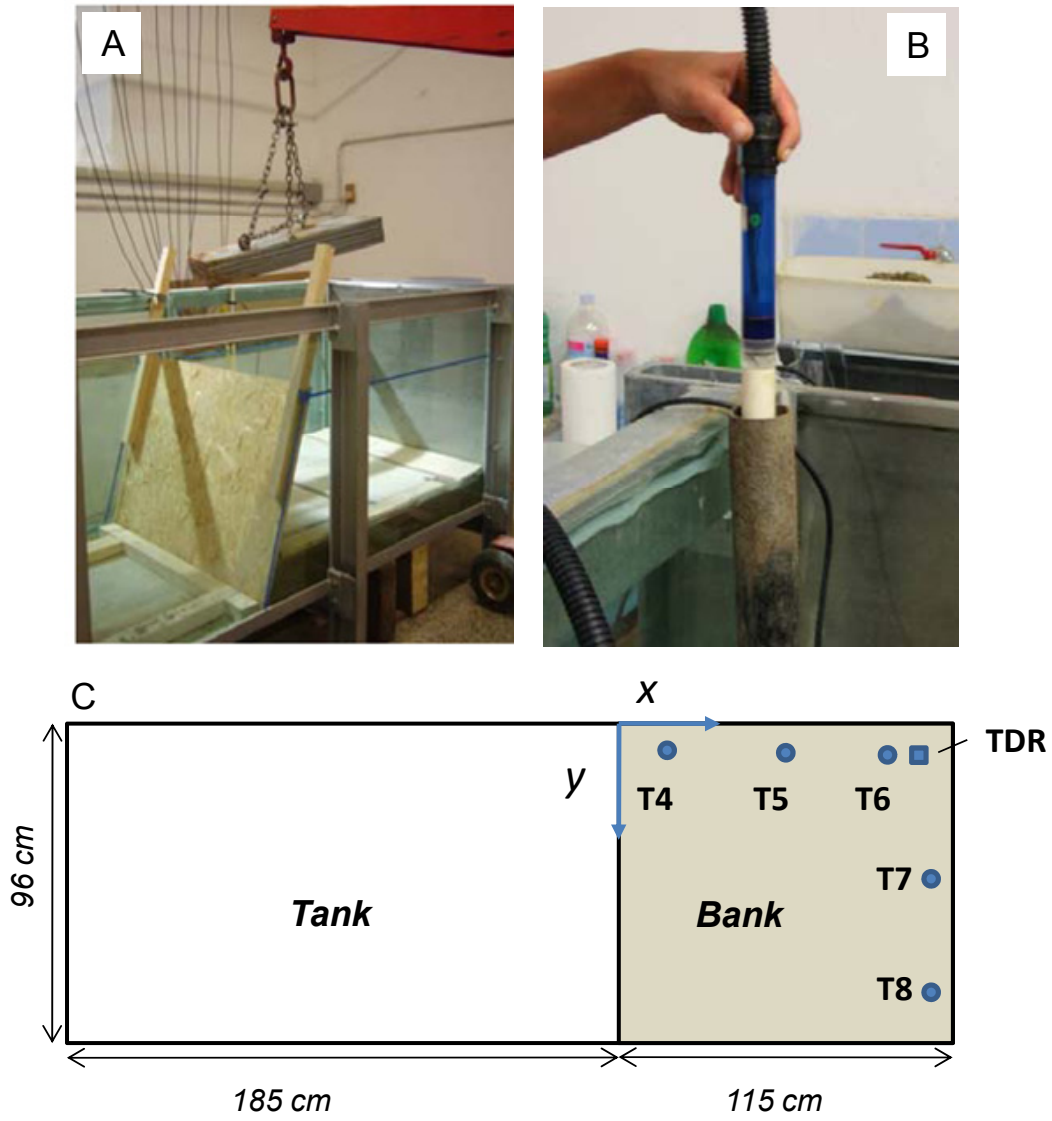

Figure 7-9 Experimental setup. A: loads made by steel plates and setup of the wooden panel during the construction of the bank physical model; B: Insertion of sensors; C: location of monitoring instruments.

Two ultrasonic sensors level were set in order to measure the water stage in the front, and back in the lysimeter, except during EXP1.

Imposed boundary conditions for the three experiments included the hydrograph and the water stage in the lysimeter in the back of the bank. A hydrograph with

similar characteristics for the four experiments and with a shape similar to that observed in a series of monitored flow events occurred on the Cecina River (Luppi et al., 2009) was imposed. The water stage in the front of the bank was measured through the ultrasonic sensor level. During EXP1, a peak of 59.89 cm was reached in 3 hours and 14 minutes, while the descending part of the hydrograph was slightly longer, for a total duration of 6 hours and 40 minutes. The water stage in the lysimeter was maintained constant once the water exceeded 34 cm from the bottom of the bank by opening the lowest valve located behind the lysimeter. This layout was set to simulate a water outflow discharge through the back of the tank, thus avoiding an excessive and unrealistic accumulation of water within the volume of the bank model.

During EXP2, a peak of 59.6 cm was reached in 3 hours and 6 minutes. The total duration of the test was 6 hours. The water stage in the lysimeter was kept constant at 34 cm.

A lower peak of the hydrograph was reached during EXP3. As in the previous experiments, the water stage at the lysimeter was maintained at 34 cm. Due to an excessive outflow discharge from the valve at the back, which was not balanced by the inflow discharge in the tank, in the third experiment it was not possible to obtain water stages higher than 50.3 cm. This stage was reached in 2 hours and 59 minutes. The greater outflow discharge was probably due to a higher conductivity of the sediment with cement. The total duration of this experiment was about 5 hours.

During EXP4 the peak of 58.3 cm was reached in 2 hours and 10 minutes. In this last experiment the decreasing phase of the hydrograph was faster, since during the previous preliminary and main tests, failures were only observed during the inflow phase.

During the experiments a video and periodic photos were made from frontal and lateral positions. Furthermore, additional measurements were carried out. They included: (1) water stage in the lysimeter; (2) water discharge outflowing the valve; (3) bank profiles drawn on transparent sheets placed on one lateral glass of the tank for every mass failure to provide time lines of the bank evolution. Videos recorded from frontal and lateral positions allowed one to verify when bank changes occurred locally on the lateral side or on the entire bank. Since the water was clear during the drawdown phase, no measurements of turbidity were collected.

7.5 Occurrence of failures during the main experiments

During the main experiments, different mechanisms of failure were observed. The occurrence of mass failure at the scale of each hydrograph and resulting modifications from the initial to the final bank profiles, are reported in Figure 7-10.

In this figure, mass failures indicated as large are those involving a significant portion of the bank height and approximately the entire width, while small failures are those occurred on localized portions of the bank profile and/or width.

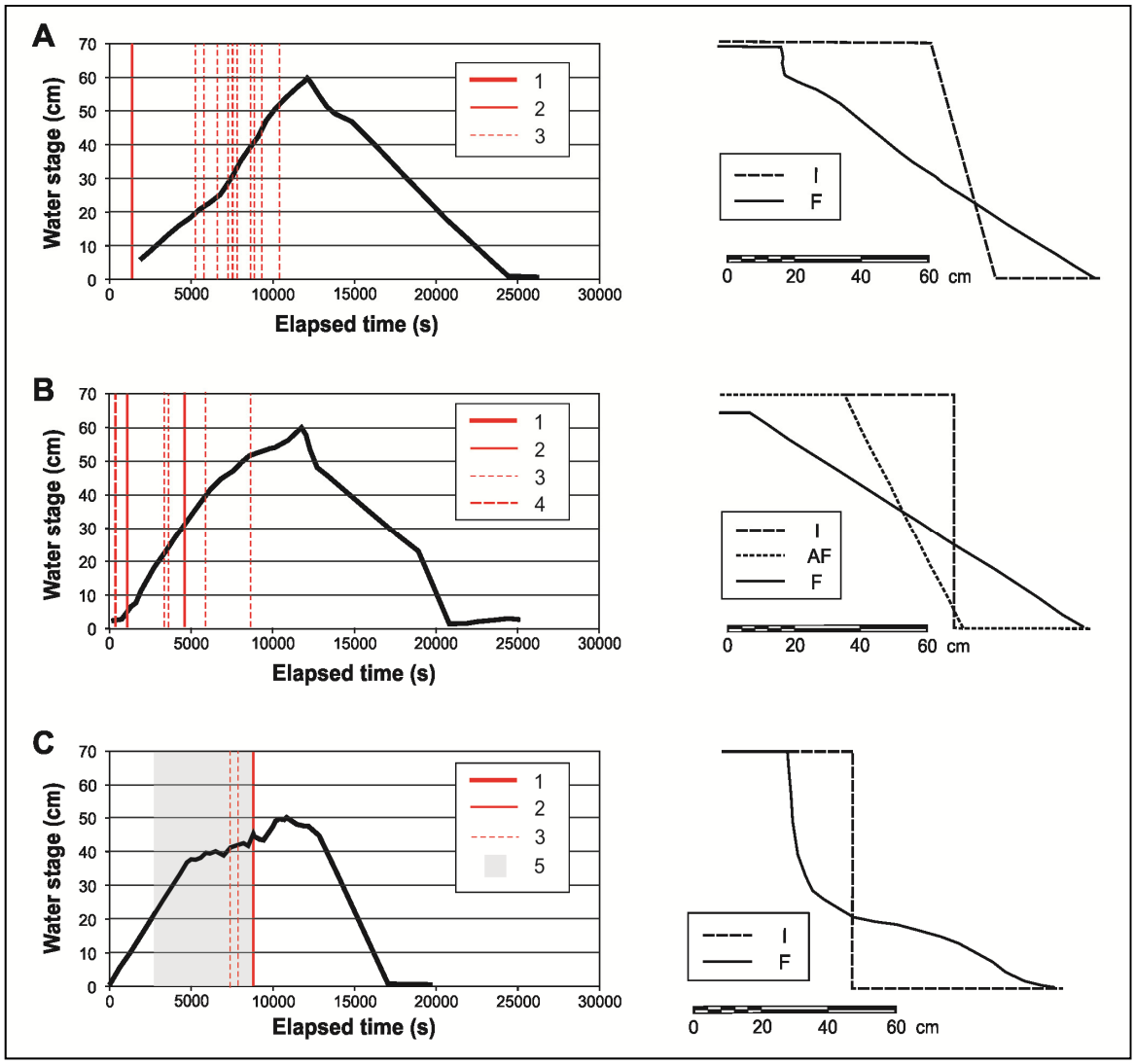

Figure 7-10 Summary of failures and profile evolution during EXP1 (A), EXP2 (B), and EXP3 (C): hydrograph and failures (on the left), and changes in bank profile (on the right). 1: Hydrograph; 2: Failures; 3: Small failures; 4: Initial failure immediately after the panel removal; 5: scour at the bank toe due to seepage erosion; I: Initial profile; F: final profile; AF (in EXP2): new profile after immediate failure.

It is possible to observe that all the mass failures occurred during the rising phase of the hydrographs. However, while in the case of the EXP1 and EXP2 mass failures were distributed along the entire rising part of the hydrograph, in the case of EXP3, as effect of cementation and increased shear strength, the failures occurred exclusively in proximity of the peak of the hydrograph. EXP4 is not represented in the figure, since during the entire experiment, no failures occurred.

The following subsections provide in detail, the description of each bank evolution.

EXP1 (see Figure 7-11). The experiment was preceded by the removal of the wooden panel (1), when a rotational (alcove-type) slide failure immediately occurred involving all the basal portion of the bank, up to about 30 cm from the toe. After about 10 minutes (2), a rapid succession of tensile and beam cantilever failures were observed, involving only the upper part of the right side of the bank. After 18 minutes (elapsed time 28 min) (3), a failure occurred involving the central portion of the bank, while a tension crack, created earlier, became progressively more evident (4). About 34 minutes later (elapsed time 62 min) (5), a cantilever failure occurred on the left margin, followed by a failure in the middle part of the bank (6). Immediately after that another cantilever on the left side was detected. About 62 minutes later (elapsed time 124 min) (7), a large, arcuate failure surface appeared involving the entire width of the bank top, followed by a succession of failures of blocks around 10 cm in width (8). Close to the peak of the simulated event, the profile reached the configuration of a nearly plane surface with a slope angle of about 35°. The bank maintained this geometry during the entire descending hydrograph, until the end of the experiment (9).

Looking at the trend of measured parameters during the test, pore water pressure increased with water stage and water content. Figure 7-12 shows that pore water pressure became positive as the water reached 37 cm at some level of the tensiometers T4, T5 and T6. Figure 7-12 also shows that, when the water stage in front was 37 cm, the material surrounding the TDR (placed at 30 cm from the bottom of the bank and at a distance of 112 cm from the frontal surface, Table 7-11) was close to saturation with the water content equal to 19.6% (Figure 7-13). This value in water content was constant also in the first part of the drawdown phase, until the water stage was 20 cm. The tensiometer T7 initially appeared not to respond to the imposed hydrograph, as values recorded were much lower than the others. However, this discrepancy became smaller with the increase in water stage.

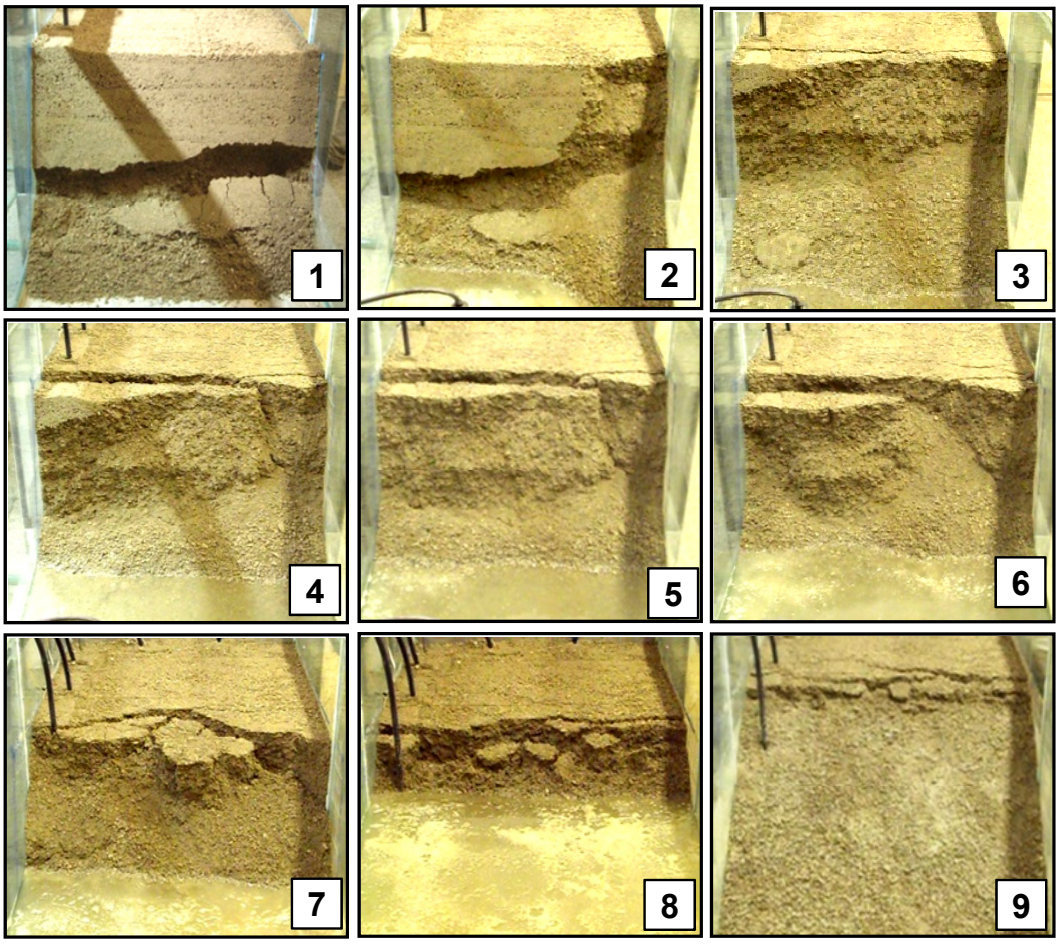

Figure 7-11 Photos of bank profile evolution during EXP1.

	T4	T5	T6	T7	T8	TDR
X [cm]	21.5	61.5	96	112	112	112
Y [cm]	6.7	6.7	6.7	48	90	6.7
Z [cm]	37	37	37	54	64	30

Table 7-11 Position of tensiometers and TDR during EXP1. H = sensor height from the bottom of the bank, d = distance from the edge of the bank.

Tensiometers at 37 cm, located in front of the bank and in the middle (T4 and T5), gave almost the same values, while T6 showed lower values during the first part of the test, to reach similar values to T4 and T5 after about 2 hours from the beginning of the experiment. It is possible that T7 and T6 were disturbed by localized phenomenon such as drier material (water content not constant) or imperfect adherence between the material and the porous cup of the tensiometers.

Tensiometer T8, located at the back of the bank at 64 cm from the bottom, did not reach the saturation. Given that, the peak of the hydrograph was lower (59.9 cm) than the elevation of the tensiometer.

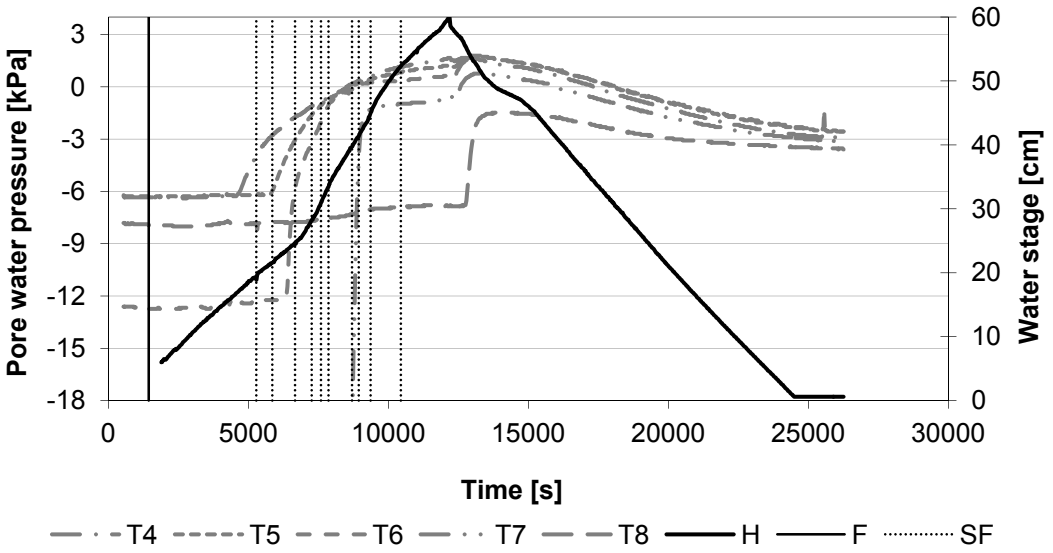

Figure 7-12 Trends of measured parameters and failures in EXP1.T4, T5, T6, T7, T8: pore water pressure measured by the tensiometers; H: Hydrograph; F: Failures; SF: Small failures.

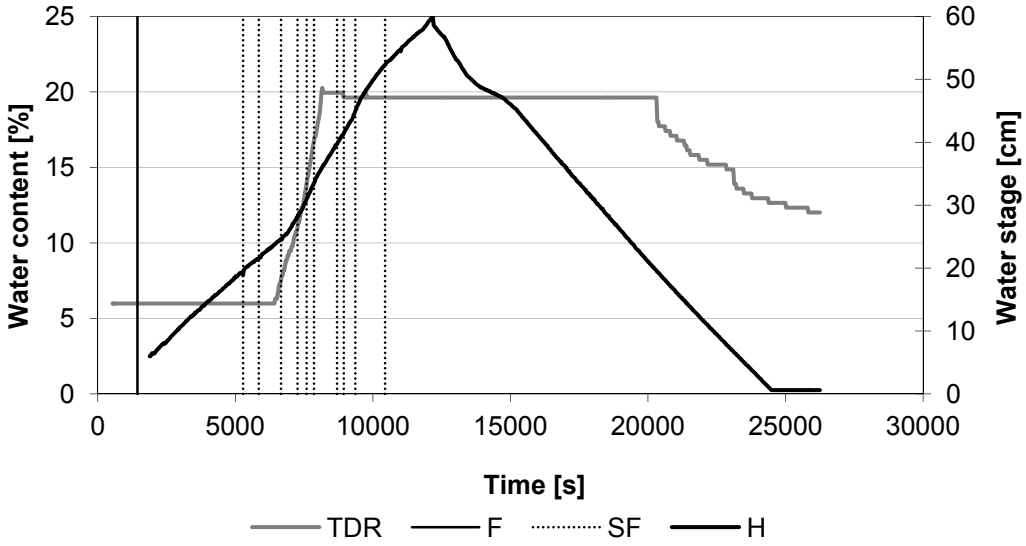

Figure 7-13 Trends of measured parameters and failures in EXP1. F: Failures; SF: Small failures; TDR: water content measured by the TDR.

EXP2 (see Figure 7-14). The initial bank slope was set at 90°, but immediately after the removal of the wooden panel (1), a failure across the whole bank occurred, classified as a granular flow in loose cohesionless material, creating a nearly plane surface. The failed material was removed from the bank toe, and the bank was shaped according to an angle of about 67° to continue the experiment (2). When the water reached 2.5 cm level (3), a large rotational failure occurred involving the

upper and medium portion of the whole bank and causing a retreat ranging between 15 and 20 cm. This can be better described as flow slide, because multiple and temporary concave failure surfaces were observed. After this event, only small failures occurred during the ascending phase of the hydrograph (4, 5), until the profile became a nearly plane surface with a slope angle of about 35° (6), corresponding approximately to the angle of repose for this sediment. Similarly to EXP1, the bank profile did not change during all the descending phase of the hydrograph.

For this experiment, as previously mentioned, a slightly different configuration of the sensors was used (Table 7-12), so interpretation of pore water pressures trends needs to consider this change in depth.

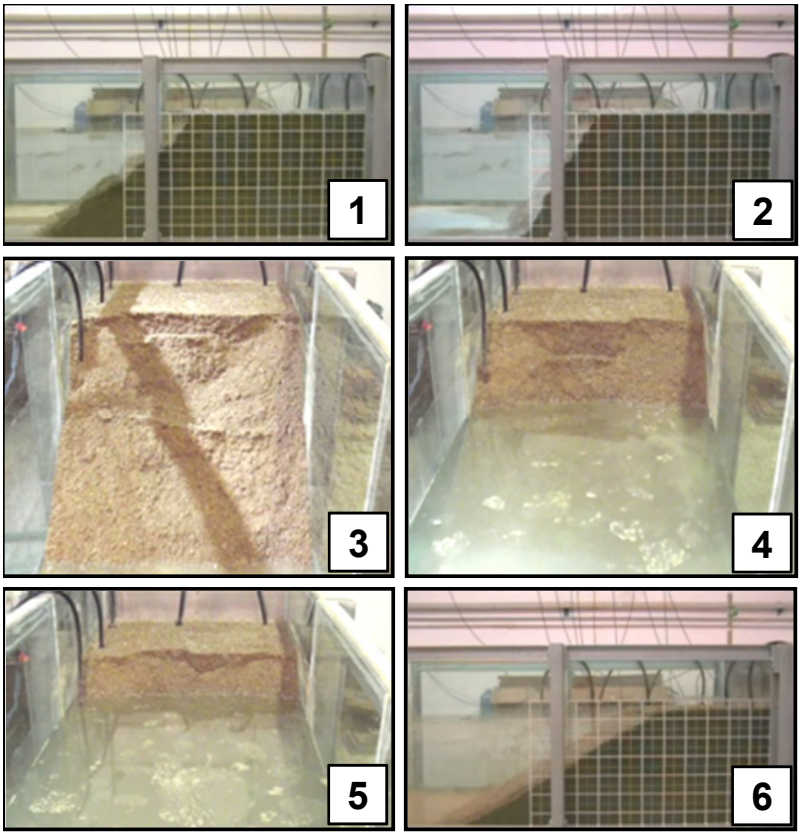

Figure 7-14 Photos of bank profile evolution during EXP2 .

	T4	T5	T6	T7	T8	TDR
X [cm]	35.5	71	101	110	110	110
Y [cm]	6.7	6.7	6.7	48	90	6.7
Z [cm]	27	39	52	39	27	45

Table 7-12 Position of tensiometers and TDR during EXP2. H = sensor height from the bottom of the bank, d = distance from the edge of the bank.

Figure 7-15 shows that T4 was the first tensiometer to reach saturation when the water stage was 32 cm followed by T5 and T7 for water stage from 38 to 40 cm. T8 was located in a lower position than T7 at the beginning of the test and measured higher pressure than T7; however T8 reached saturation later when the water stage was 43.5 cm.

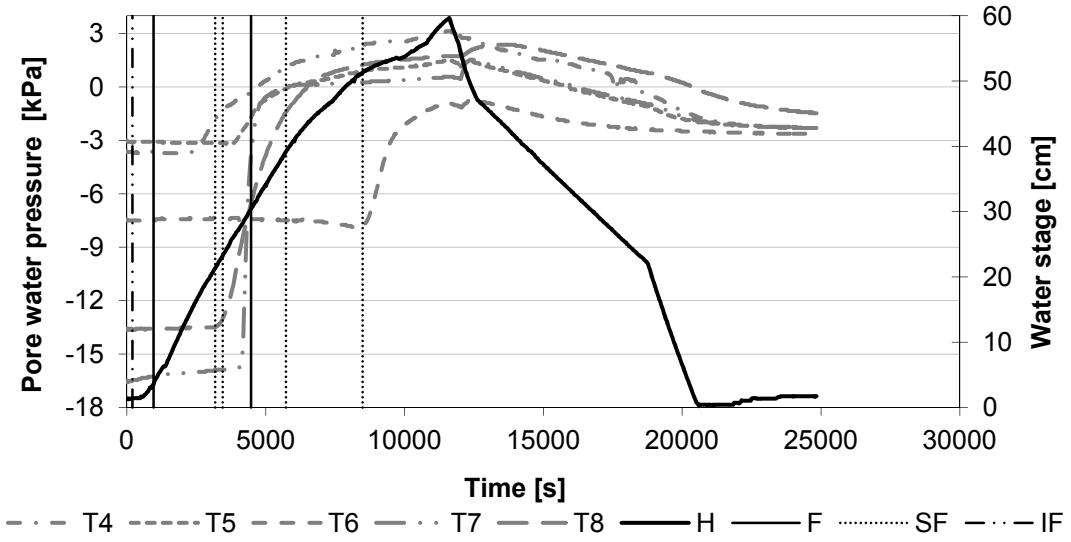

Figure 7-15 Trends of measured parameters and failures in EXP2. T4, T5, T6, T7, T8: pore water pressure measured by the tensiometers; H: Hydrograph; F: Failures; SF: Small failures; IF: Initial failure occurred in EXP2 after the panel removal.

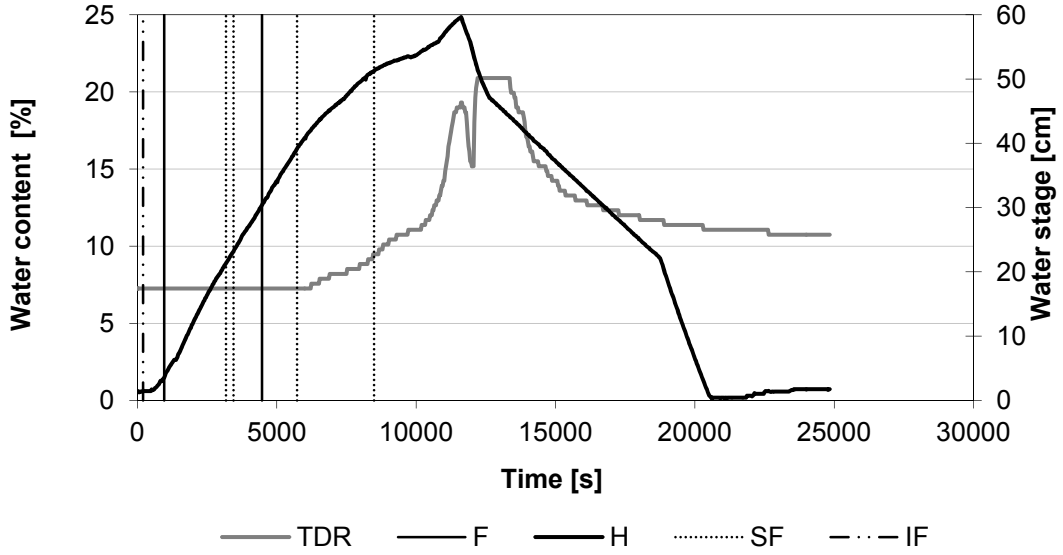

Figure 7-16 Trends of measured parameters and failures in EXP2. F: Failures; SF: Small failures; IF: Initial failure occurred in EXP2 after the panel removal; TDR: water content measured by the TDR.

This occurred because the reaction of T8 was slower than T7. T6 did not reach saturation because it was located in the back of the bank at 52 cm from the bottom, while the valve behind the lysimeter was open at 34 cm.TDR indicates that saturation at around 45 cm from the bottom of the bank, corresponding to the height of the sensor, occurred when the water stage was 51.4 cm. The water content of saturated material for this test was 20.9% (Figure 7-16).

During the descending phase of the hydrograph, parameters decreased to similar final values.

EXP3 (see Figure 7-17). The bank material in this experiment included a small quantity of cement. Consequently, the bank showed a different behaviour from previous experiments.

The initial bank was set at 90° and remained stable after the removal of the wooden panel (1a-1b). After about 40 minutes (2), a scour due to loss of matric suction started to manifest along most of the basal area and became more evident on the right and central part. This process started at the interface of different sub-layer of 10 cm built during the compaction procedure. As time progressed, the scour progressively continued to extend laterally and within the bank. The first manifestation of failure involved a small block on the left margin (3), located 10 cm below the water stage. This failure rapidly progressed upward as a tensile cantilever failure, including an emerged portion, and laterally up to the water stage (4). After 145 minutes and 54 seconds from the beginning, a rapid succession of further tensile failures occurred in various portions, until the cantilivered bank was completely up to the water stage (5). About 5 seconds later (elapsed time 146 min), a rapid succession of three cantilever failures occurred (6, 7). The smaller was a tensile failure and the two larger were beam failures, recreating a nearly vertical bank face.

This became the final bank configuration, as no failures occurred during the descending phase of the hydrograph (8).The final profile showed a basal wedge of failed material at a slope angle of about 20°-25° and some of the failed blocks still recognizable, and an approximately vertical face of about 40 cm. For this experiment the same configuration of the sensors as in EXP2 was used (Table 7-13).

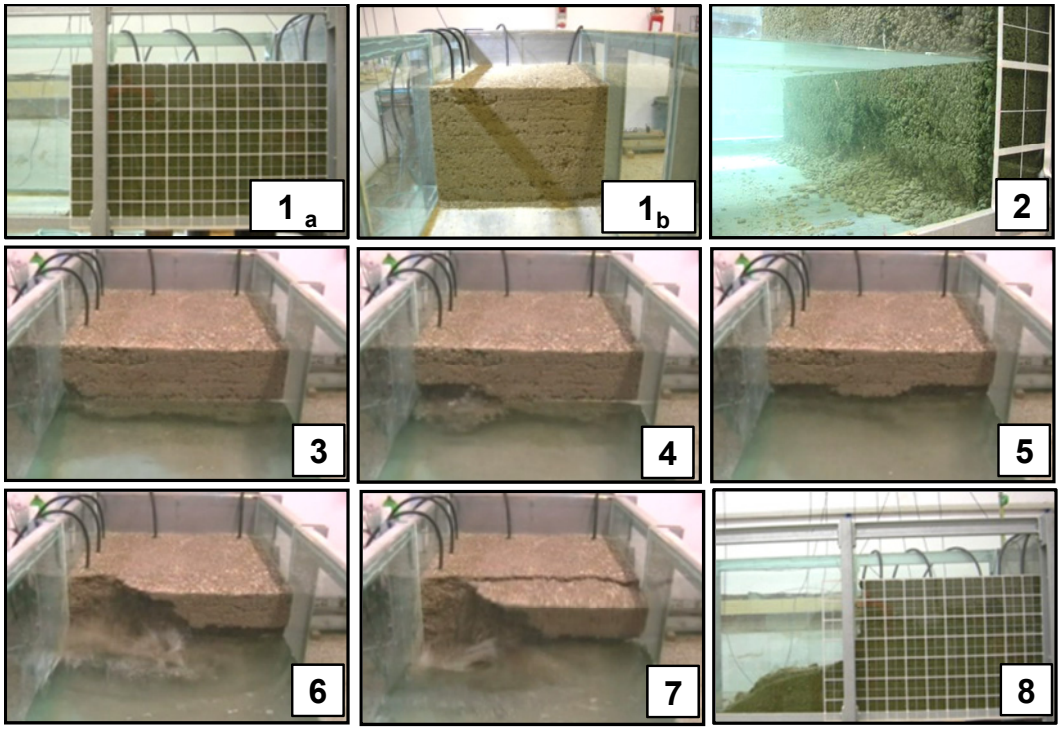

Figure 7-17 Photos of bank profile evolution during EXP3.

	T4	T5	T6	T7	T8	TDR
X [cm]	35.5	71	101	110	110	110
Y [cm]	6.7	6.7	6.7	48	90	6.7
Z [cm]	27	39	52	39	27	45

Table 7-13 Position of tensiometers and TDR during EXP3. H = sensor height from the bottom of the bank, d = distance from the edge of the bank.

As in previous tests, the initial values recorded by the tensiometers are very different: T8 measured the lowest value, followed by T7 and T6, respectively. This could be due to the proximity of these three tensiometers to the porous plate of the lysimeter which dries the material around.

As the water stage increased, between 28.5 and 35 cm, all of the tensiometers, except T6, started to react. Due to its highest position, T6 started to measure increasing values of pore water pressure when water stage was 41.8 cm, but did not reach saturation. In fact, during this experiment the peak of the hydrograph did not exceed 50.3 cm.

The TDR measured the water content of saturated material equal to 19.6% when the water stage was 49.9 cm (Figure 7-19).

Figure 7-18 shows that the increase of the water stage from 36.7 until the peak of the flow event was very slow and not constant. This depended on the unexpected

high value of conductivity of the bank material. In fact, when the water stage exceeded 36.7 cm the inflow discharge was likely the same as the outflow discharge from the valve at the lysimeter. For that reason, further increase in the water stage was slower and the peak stage was lower than the previous experiments.

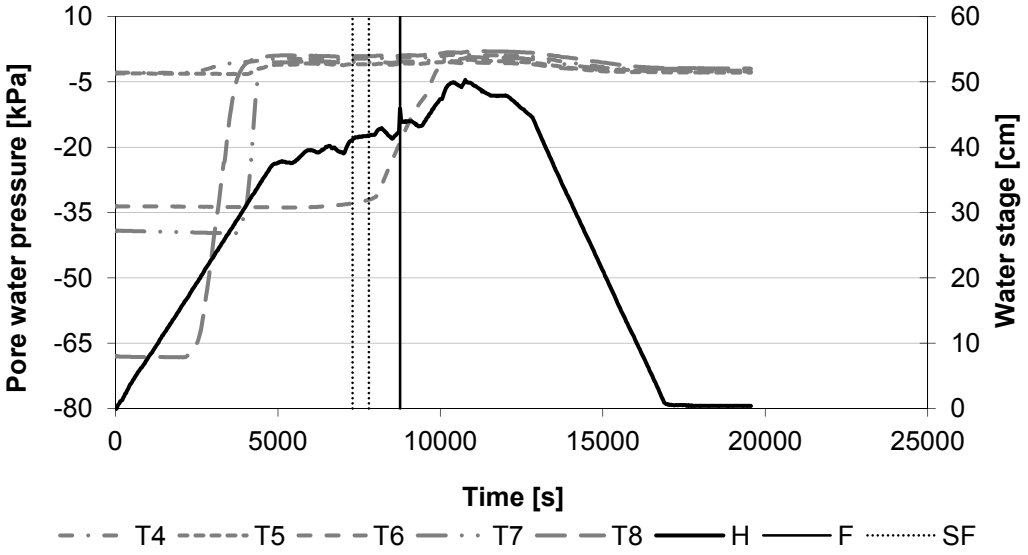

Figure 7-18 Trends of measured parameters and failures in EXP3. T4, T5, T6, T7, T8: pore water pressure measured by the tensiometers; H: Hydrograph; F: Failures.

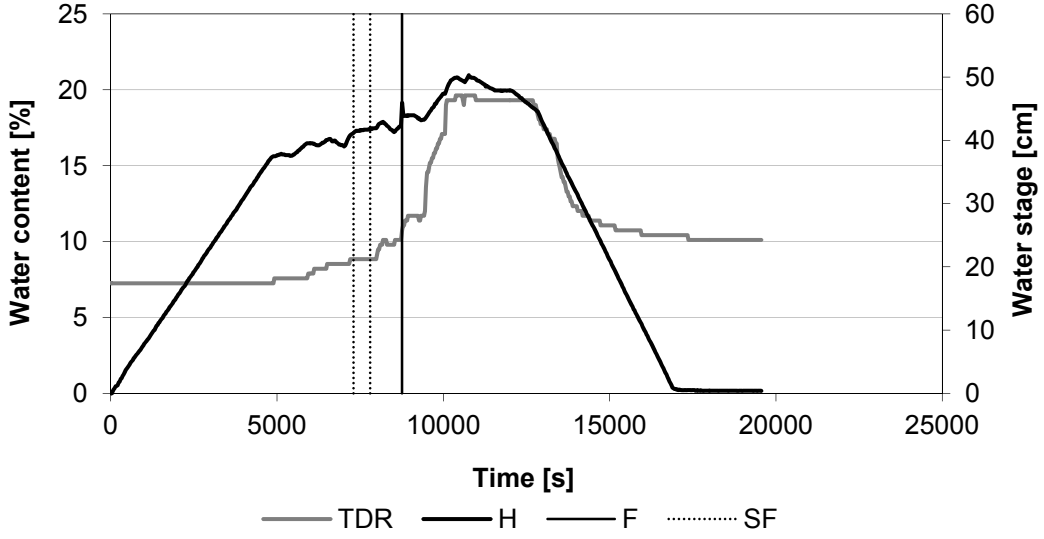

Figure 7-19 Trends of measured parameters and failures in EXP3. F: Failures. TDR: water content measured by the TDR.

Since the bank of this test was built accordingly to the same procedures of the banks for EXP2 and EXP3, the difference in the behaviour in terms of porosity could be explained by the presence of the cement. Specifically, during the bank construction, Portland cement was added to the sediments.

This cement requires a minimum initial setting time of 75 minutes to start hardening through the chemical reaction (hydration) and to develop its compressive strength. Thus, although in such a small percentage (1%) and in short period, the cement was enough to prevent displacement of the material subjected to the load during the construction of the bank. This hypothesis was confirmed by the values of displacement measured during the construction of the banks: while in EXP1 and EXP2 the total displacement was 4.5 and 3.5 cm respectively, during EXP3 it was only 1.2 cm. Therefore, the compaction was less effective, and this, in turn, may explain the higher permeability. To explain the high porosity another hypothesis (needing further investigation) is that the cement allowed particles agglomeration, increasing the mean sizes of sediments and consequently increasing the porosity. The higher permeability is clear by comparing the relation between the water stages in the front and in the lysimeter during EXP2 and EXP3 (Figure 7-20).

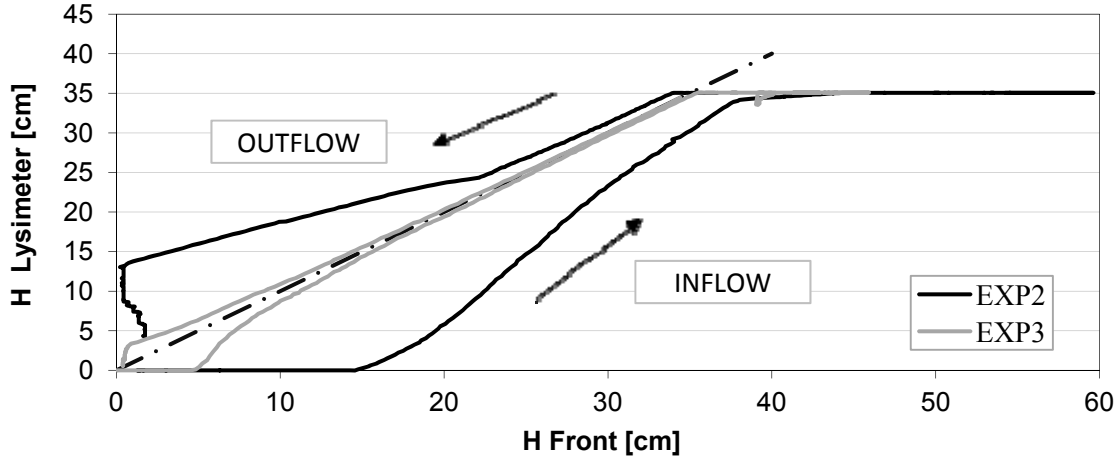

Figure 7-20 Ratio between water stage in front of the bank and water stage inside the lysimeter during EXP2 and EXP3. Red dotted line has unit slop.

EXP4 (see Figure 7-21). The test on the preliminary model subject to the hydrograph after one year (T12) highlighted a different behaviour with respect to the experiments carried out on models made with the same material. Therefore, a second test on model EXP3 was carried out, after about one year. The basal wedge of failed material was removed before the experiment (1).

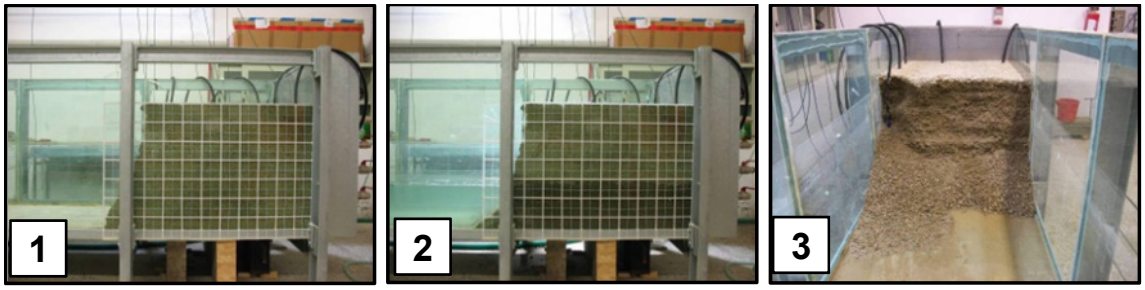

Figure 7-21 Photos of bank profile evolution during EXP4.

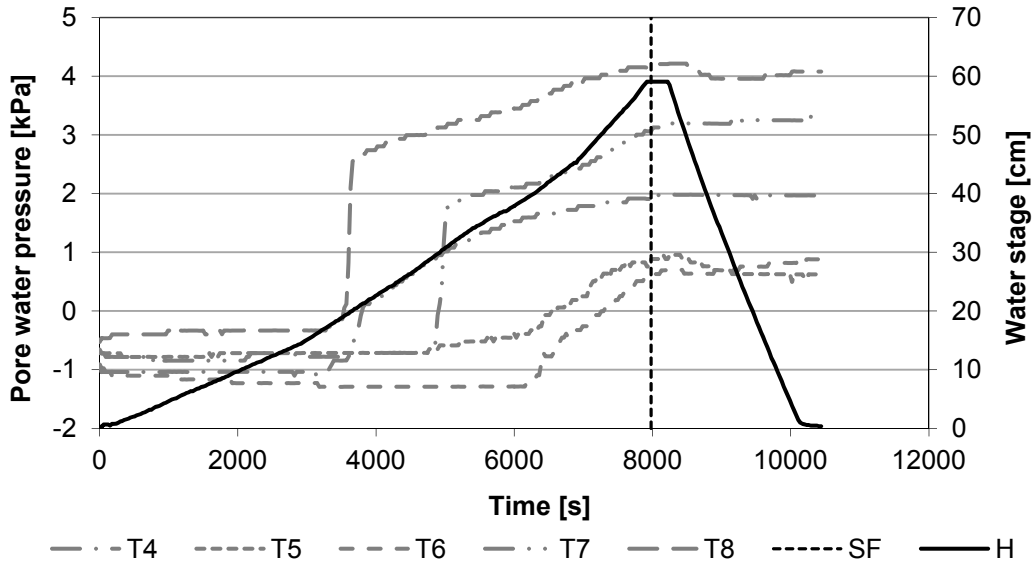

Figure 7-22 Trends of measured parameters and failures in EXP4. T4, T5, T6, T7, T8: pore water pressure measured by the tensiometers; H: Hydrograph; SF: Small failure.

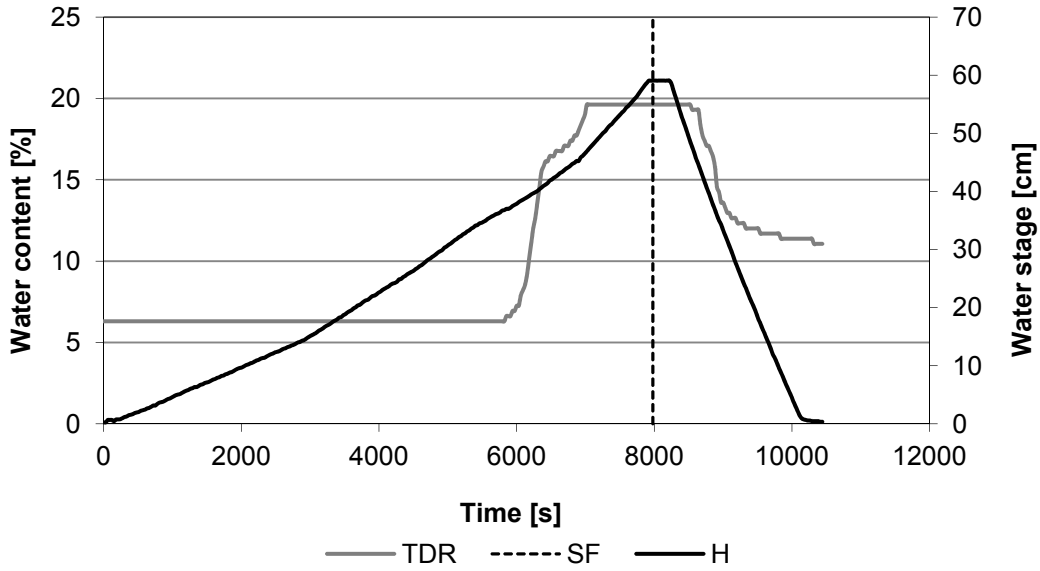

Figure 7-23 Trends of measured parameters and failures in EXP4. SF: small failure; TDR: water content measured by the TDR.

At the beginning of the test the material was dry and the nearly horizontal water table was clearly visible through the lateral wall of the tank (2). When the water level was around 20 cm, a scour was observed developing at the same level of the water stage. When the hydrograph was close to the peak, a small collapse occurred involving the left side of the bank (3). No more failures occurred until the end of the experiment when all the final profile emerged (3), with a basal wedge of failed material at a slope angle of about 38° and an approximately vertical face of about 40 cm.

To avoid problems occurred in EXP3 due to high permeability (Figure 7-24), during EXP4 the water stage was not kept constant at 34 cm, conversely it was free to rise inside the lysimeter. At the beginning of this experiment, tensiometers measured very similar values of pore water pressure (Figure 7-22).

The values of matric suction were unexpectedly lower than values measured at the beginning of the previous tests. T8 and T4 were the first tensiometers to reach the saturation when the water stage was around 20 cm. This level corresponds to the height of the sensors from the bottom of the bank (Table 7-13). The same was for the others sensors, except for T5, which appeared to respond slower, at water level of 43 cm. The TDR measured a water content of the saturated material equal to 19.8 % when the water stage was 45.7 cm (Figure 7-23). At the end of the experiment, contrary to the previous main tests, all the tensiometers still measured positive values of pore water pressure. This could be due to the faster drawdown phase of the hydrograph. In fact, given that no failures occurred during the drawdown phase of previous (preliminary and main) experiments, during EXP4 a faster descending phase of the hydrograph was imposed in order to test if a rapid decrease of water stage could destabilize the bank. Various authors (e.g. Thorne, 1982; Casagli et al., 1999; Dapporto et al., 2001; Rinaldi et al., 2004) observed that bank failures are likely to occur during a rapid drawdown phase, when the pore water pressures are still positive inside the bank and the confining pressure of the river decreases to zero. Nevertheless this process was studied on cohesive portions of riverbanks. With coarse grained material, due to the high permeability, the dissipation of positive pore water pressures is much more rapid, avoiding the flow from the bank towards the river. This may explain why during the experiments no failure occurred also during a rapid drawdown phase of the hydrograph.

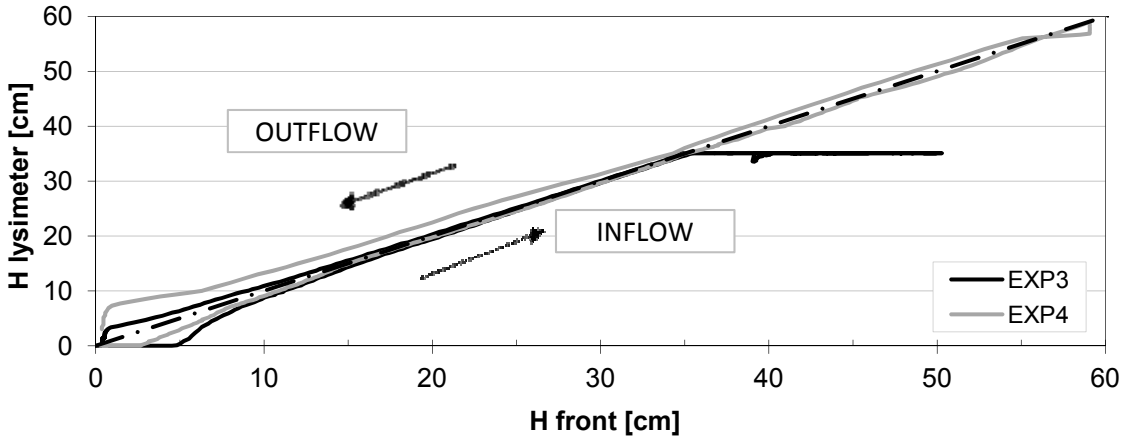

Figure 7-24 Ratio between water stage in front of the bank and water stage inside the lysimeter during EXP3 and EXP4. Red dotted line has unit slop.

8. Interpretation of results and discussion

Data collected during each experiment were processed and analysed in order to classify all mass failures and other processes occurred, searching for a correlation between these processes and measured data.

Moreover measured parameters were required to carry out the bank stability analysis through the Limit Equilibrium Method.

8.1 Types of observed mass failures

For the interpretation of the results, it is useful to define and classify the observed mechanisms of failure that occurred during the three main experiments and the initial tests.

1) Erosion and failures due to loss of matric suction. This process is related to a loosening of the weak links between particles as soon as the pores are saturated by water and the resulting increased weight of aggregates or small blocks due to sediment saturation. The erosion process initially produces a scour at the bank toe (Figure 8-1, case A1), followed by small-scale mass failures, resulting in the collapse of the upper small block or aggregate of particles by tensile failure (Figure 8-1, case A2).

2) Cantilever failures. These are the most frequently observed failures, and are often the consequence and evolution of the previous mechanism, or of basal slide (alcove-shaped) failures (see mechanism 4). All the three types of cantilever failure have been observed: shear, tensile, and beam failures (following Thorne and Tovey, 1981). Shear failures are defined here as failures occurring by shear along a vertical and lateral surface delimiting the cantilever block up to the bank top (Figure 8-1, case B1). Tensile failure is defined as a failure along a horizontal upper surface of the failing block in which the detachment occurs by tensile stress (Figure 8-1, case B2). In some cases, a beam cantilever failure was also observed (Figure 8-1, case B3), with a rotational component (toppling) of the movement.

3) Slab failures. They are classified separate from the cantilever beam failures as they do not occur on cantilevered, undercut blocks, but usually involve relatively small blocks on the bank top detached by deep tension cracks which stand on the top of the debris cone derived from previously failed material (Figure 8-1, case C).

4) Slides. This type of failure, very common along cohesive riverbanks, was observed only in a few occasions during the experiments. We distinguish two modes of slide failures: (1) small-scale slides on the middle and lower portion of the bank with a slight rotational component (Figure 8-1, case D1); (2) rotational failure involving the whole bank, with a slightly concave slip surface emerging on the bank top (or eventually with a short tension crack) (Figure 8-1, case D2). The first type can be actually described as a combination of detachment of material under tensile stress along an arcuate surface and a contemporary slide, resulting in an alcove-shaped surface, similar to what has been frequently observed along steep fine-grained banks (Bradford and Piest, 1977, 1980; Thorne et al., 1981; Dapporto et al., 2001, 2003).

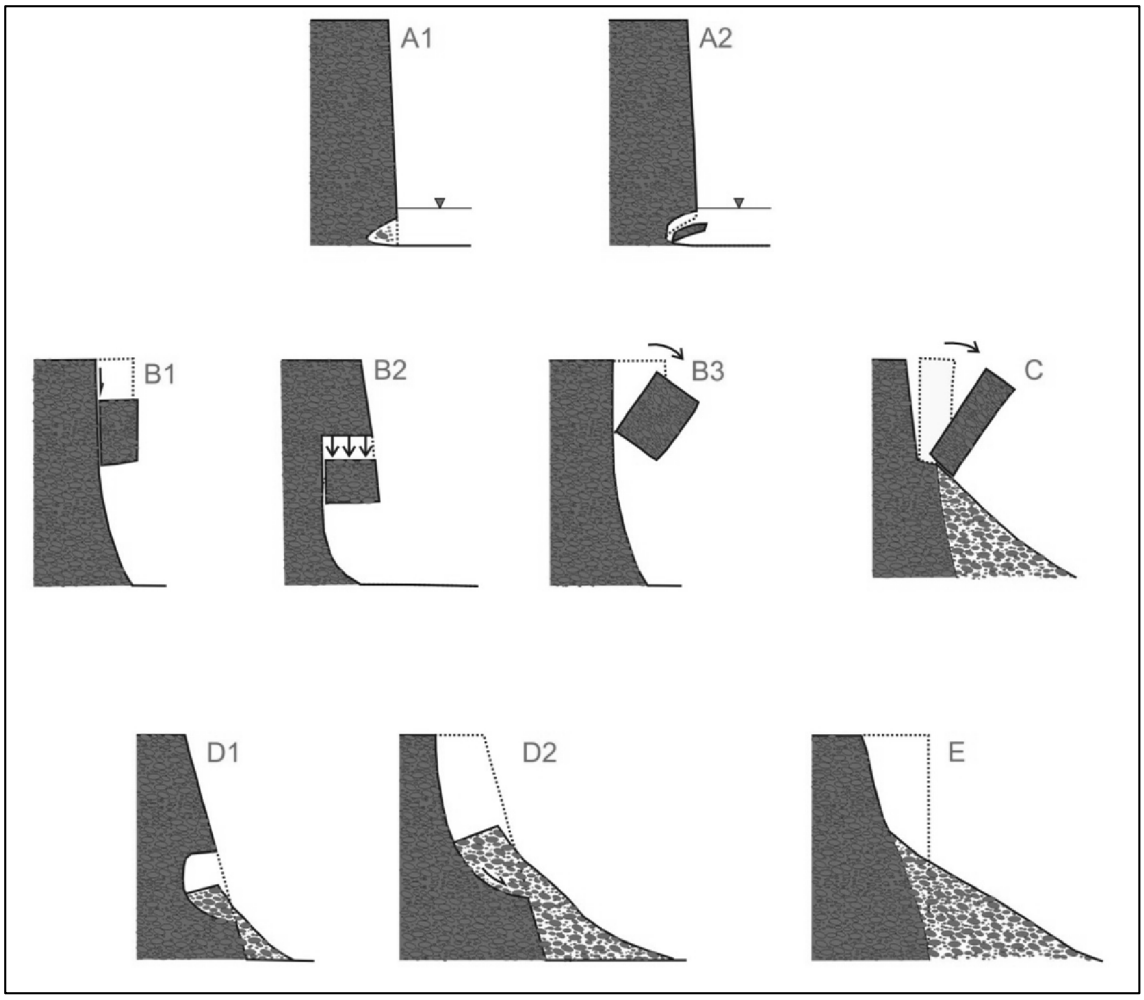

Figure 8-1 Types of processes. A: erosion due to loss of matric suction (A1) and failure (A2); B: cantilever failures (B1: shear failure; B2: tensile failure; B3: beam failure); C: slab failure; D: slides (D1: alcove-type failure; D2: rotational slide); E: dry granular flow.

Although the resulting geometry can be sometimes similar to the failures due to loss of matric suction, it differs from it because it involves larger scale mass movement (rather than "particle-by-particle" erosion). The second type was actually observed only in one occasion, and can be better described as a combination of slide and flow (see next mechanism).

5) Dry granular flow. It consists of an avalanche of granular, loose sediment, creating a fan-shaped debris accumulation close to the angle of repose (Thorne et al., 1996) (Figure 8-1, case E). This was observed in one case as an initial mechanism of failure (EXP2), and in other cases as movement along the existing debris accumulation of failing material originated by other mechanisms.

8.2 Analysis of results

A first general consideration is that we observed a large variety of mechanisms of erosion and failures. Previous research has often underestimated the occurrence of mass failures in gravelly bank layers, and this has important implications in terms of modelling bank erosion in composite banks. For example, Rinaldi et al. (2008a) and Luppi et al. (2009), in their analysis of a composite riverbank of the Cecina River, excluded mass failures from the basal layer of gravel, due to difficulties in assigning reliable shear strength parameters to such material, and allowed deformation of this layer only by fluvial erosion; this now appears to be a gross simplification. Two aspects are discussed in the following part of this section: (1) occurrence of erosion and mass failures due to loss of matric suction; (2) reciprocal role of factors related to initial instability and to changes in water stage.

8.2.1 Erosion and failures due to loss of matric suction

As mentioned previously, erosion due to loss of matric suction occurred during the rising phase of the hydrograph, with scour forming up to the water surface (in loose sediment), or at a level lower than the water surface (in slightly cemented sediment). This was clearly observed during the preliminary tests because, for the most, the initial near-vertical bank face was stable in contact with water, as was the vertical bank-face in EXP3. However, during EXP1 and EXP2, the initial failure immediately after the panel removal caused the failed material to enter into contact with water and cover the basal bank, preventing the direct contact of water with the intact vertical face.

Many studies have focussed on seepage erosion, its quantification and triggering conditions. This process is commonly associated to a seepage outflow, implying that a water table gradient is necessary, and it occurs during the descending phase of the hydrograph, when the water table can be higher than the river stage. The erosion features observed in the experiments of this study are similar to those classified as seepage-induced erosion and associated to a seepage outflow in many studies (Howard and McLane, 1988; Fox et al., 2006, 2007; Wilson et al., 2007; Lindow et al., 2009). However, in the present study these features have been always observed during the rising phase of the hydrograph, with a gradient from the river into the bank. In case of loose sediment, this process can be simply linked to the complete loss of apparent cohesion, due to rapid infilling of the pores within the bank sediment. This causes a disappearance of the weak links among particles, and small-scale breaks and falls occur "particle-by-particle" rather than by mass movements. In this sense, this process can be partly considered as a weakening factor, that is a decrease of the erosion resistance and mechanical stability of the bank material (Thorne et al., 1996), followed by detachment of particles (erosion). When a basal cavity is first created, subsequent falls of small blocks of particle aggregates can also occur. The increasing size of the basal hollow generates a stress-release on the remaining upper portion of the bank, similar to that described for the case of gully head retreat by Collison (2001), inducing the occurrence of cantilever failures.

The same type of process has been also observed in the slightly cemented sediment of EXP3. In this case, the simple loss of apparent cohesion cannot explain the occurrence of erosion, as some effective cohesion exists. The occurrence of erosion was observed to take place at portions of the bank lower than the water stage that is in submerged conditions. Therefore, it can be explained by the occurrence of positive pore water pressures and an increase in weight of bank sediment, notwithstanding a partial stabilizing effect of confining water pressures. In fact, the loss of apparent cohesion and the weight of the upper bank material are not balanced by the hydrostatic force. Another possible explanation is that the erosion process was observed to start at the boundary of two basal sub-layers of 10 cm built during the compaction procedure. This created a discontinuity in the bank sediment, favouring water infiltration and therefore generating higher local pressures. The enlargement of these fissures was probably the triggering process. Although this process was due to the construction of the bank, similar discontinuities can be found in nature at the interface of different layers.

These mechanisms observed in the experiments during the rising phases of the hydrograph have rarely been described before and can represent an important process of basal deformation in gravel layers with low cohesion. Many observations carried out along several composite banks of the Cecina River have revealed the presence of similar features in basal gravel layers, generally attributed to toe fluvial erosion but can also be due to processes similar to those observed in the experiments.

8.2.2 Initial instability versus changes in pore water pressures

Considering all the observed processes and mechanisms of failure during the experiments, two groups of causes can be considered in creating instability conditions: (1) possible initial instability due to the bank geometry and low shear strength values of the material; (2) changes in pore water pressure conditions related to changing water stage in the tank.

The first two experiments (EXP1 and EXP2) showed that the failures were possibly related to unstable geometric conditions (excessive bank height and slope for such type of material), because the same material appeared stable for near-vertical slopes with smaller bank heights during the first group of preliminary tests. This suggests that bank height and slope can play a significant role and that if some critical geometric condition may exist, which is difficult to predict a priori due to uncertainties in shear strength parameters and unknown apparent cohesion.

To allow for a better interpretation of the results and to discuss the reciprocal role and relative importance of geometric factors and pore water pressure conditions, some geotechnical analysis was performed. Specific bank stability analyses for observed failures were not possible due to a number of factors, including the difficulty in clearly identifying the failure surface, the absence of specific models for some of the observed mechanisms, and the uncertainty in the shear strength parameters. Therefore, the use of a more general approach based on the construction of stability charts, where the overall stability of the bank is analysed rather than the stability associated with specific mechanisms was preferred. This type of approach can be applied to predict the likelihood of bank failure for each of the experiments, after defining its initial geometric conditions (slope and height) and shear strength properties. In detail, a series of stability charts (bank height versus slope) were created for each experiment, following the approach used in Rinaldi and Casagli (1999). This entails plotting curves obtained from geotechnical limit equilibrium

analysis, by using the slope stability charts proposed by Hoek and Bray (1981) for circular failures with a tension crack at a critical depth. This mechanism is considered here as representative of the overall bank instability, rather than associated to specific observed failures (although in two experiments, failures with a component of sliding along a rotational surface were actually observed).

The shear strength of bank material was quantified according to the failure criterion for unsaturated soils of Fredlund et al. (1978), expressed (Eq.2.6) as follows:

$\tau = c' + (\sigma - u_a) \tan \phi' + (u_a - u_w) \tan \phi^b$

where τ = shear strength (kPa), c' = effective cohesion (kPa), σ = normal stress (kPa), u_a = pore air pressure (kPa), ϕ' = effective friction angle (º), u_w = pore water pressure (kPa) and ϕ^b = angle (º) expressing the rate of increase in strength relative to the matric suction ($u_a - u_w$).

The previous equation can also be written as:

$\tau = c + (\sigma - u_a) tg\phi'$

where c is the total cohesion, which results from the sum of the effective cohesion c' and the apparent cohesion $c_a = (u_a - u_w) tg\phi^b$ due to the effects of matric suction (following Dapporto et al., 2003; Darby et al., 2007; Rinaldi and Darby, 2008).

To apply the slope stability charts of Hoek and Bray (1981), dry conditions were considered, and the negative pore water pressure effects were incorporated into the total cohesion c.

Determination of shear strength parameters in coarse granular sediment is extremely complex, and it was not possible to directly measure them in this research. Therefore, a series of hypotheses were necessary to define the parameters involved in the analysis, as follows.

(1) For the first two experiments (loose sediment), c'=0, ϕ'=35° were assumed (corresponding to about the observed angle of repose of the sediment), and ϕ^b = 15°, which is similar to values assumed for low pore water pressures in previous riverbank stability analyses (i.e. Rinaldi et al., 2008a).

(2) The pore water pressure measured at the tensiometer T4 (the closest to the bank face) was assumed as the mean value along the whole bank (as a matric suction

profile was not available). Based on this value, the initial apparent cohesion was evaluated.

(3) The unit weight γ (kN/m^3) of bank sediment was calculated as:

$$\gamma = \gamma_d + \rho\, g\, \theta \tag{8.1}$$

where γ_d = 15.2 kN/m^3 is the unit weight of sediment under completely dry conditions, and θ is the volumetric water content (m^3/m^3), the latter being estimated from the measured initial value at TDR.

(4) Regarding the last two experiments (EXP3 and EXP4), an estimation of the effective cohesion *c'* of the sediment with cement was made, based on the observed geometry of a stable cantilever block (before failure) developed during EXP3, and assuming the factor of safety equal to 1 (limit equilibrium), by the following equation:

$$FS = \frac{Lc}{\gamma A} \tag{8.2}$$

where L is the vertical length (m), c is the mean total cohesion (kPa) given by the sum of effective and total cohesion, γ is the mean unit weight (kN/m^3), and A is the cross-sectional area of the cantilever block (m^2). This analysis provided a value of *c'*=2.2 kPa. As the estimation of c' depends on the value of the apparent cohesion, the uncertainty related to the variability of the angle ϕ^b and of the pore water pressures was investigated. This analysis showed that *c'* could vary in the range 1.81÷2.36 kPa, with ϕ^b ranging from 35° to 5° respectively, and in the range 1.84÷2.42 kPa, with $(u_a - u_w)$ varying from the maximum to the minimum value measured during the experiment at the closest tensiometers. This uncertainty can be considered acceptable, as it did not significantly affect the overall results of the following analysis.

The parameters used in the analysis are summarized in the following Table 8-1.

EXP	ϕ' [°]	ϕ^b [°]	γ_d [kN/m^3]	θ [m^3/m^3]	γ [kN/m^3]	c' [kPa]
1	35	15	15.2	0.06	15.8	0
2				0.073	15.9	0
3				0.0725	15.9	2.2
4				0.063	15.1	2.2

Table 8-1 Parameters employed in the stability chart.

For each experiment an upper curve associated with limit equilibrium for the initial conditions was obtained by using these parameters. This curve represents the upper bound of stability when the total cohesion is maximum (beginning of the experiment).

Then, limit equilibrium conditions were estimated in case of a complete loss of apparent cohesion. For EXP1 and EXP2, being c'=0, when c_a=0 and assuming that positive pore pressures have not yet developed, the bank stability does not depend on the bank height, but the bank slope coincides with the friction angle. This is represented by a vertical line with abscissa equal to ϕ'=35°, that can be identified as a lower bound corresponding to an ultimate stable angle of the sediment mixture when the total cohesion is equal to zero. For EXP3 and EXP4 (c'>0), the condition associated with c_a=0 is represented by a second curve, on the left of the upper bound.

In this way, for each experiment the stability chart can be divided in three regions, defined as follows (Figure 8-2 and Figure 8-3):

(1) Unstable conditions: above and on the right of the upper bound, the bank is always unstable, including at the beginning of the experiment (a higher value of apparent cohesion would be needed to maintain a stable bank);

(2) Conditionally stable conditions: they refer to the range of geometries of banks, between the upper and the lower boundary curves, that are stable because of the apparent cohesion, but would be destabilized in case of increasing pore water pressures;

(3) Stable conditions: to the left of the lower bound, the bank is stable even in the case of zero apparent cohesion, and could be destabilized only in case of development of positive pore water pressures.

Although there is uncertainty in the shear strength parameters, the stability charts allow for a better interpretation of the results for each experiment. It can be noted that all the three conditions defined before are represented during the experiments: in EXP1 and EXP3 the bank are initially in conditionally stable conditions, in EXP2 the bank is initially unstable, and in EXP4 the bank is initially stable (Figure 8-2 and Figure 8-3). Therefore the experiments allow for making interesting comparisons among the three situations.

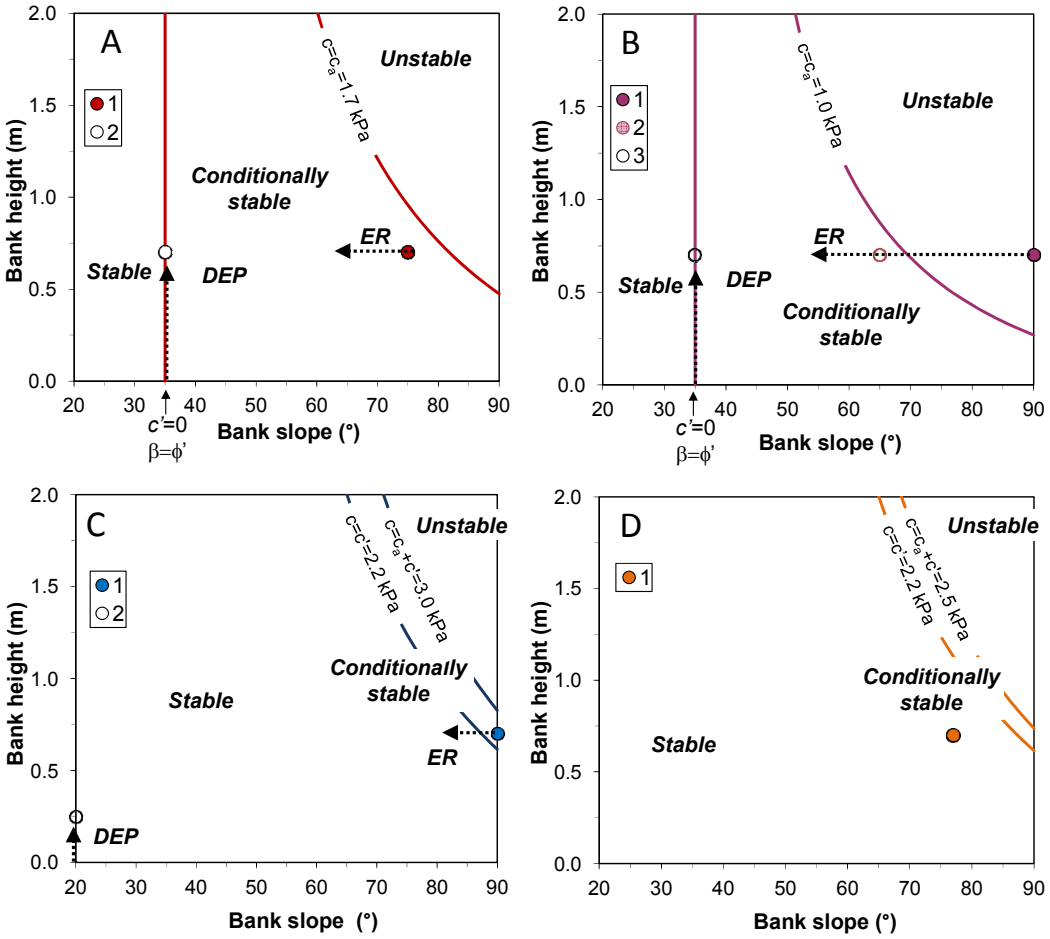

Figure 8-2 Stability charts. A: EXP1. 1: Initial bank geometry (packed bank); 2: final bank geometry (loose bank). B: EXP2. 1: Initial bank geometry (packed bank); 2: new bank geometry (after initial failure); 3: final bank geometry (loose bank). C: EXP3. 1: Initial bank geometry (slightly cemented bank); 2: final bank geometry (loose bank). D: EXP4. 1: Initial and final bank geometry. ER: trajectory of eroding (packed) bank; DEP: trajectory of depositing (loose) basal bank.

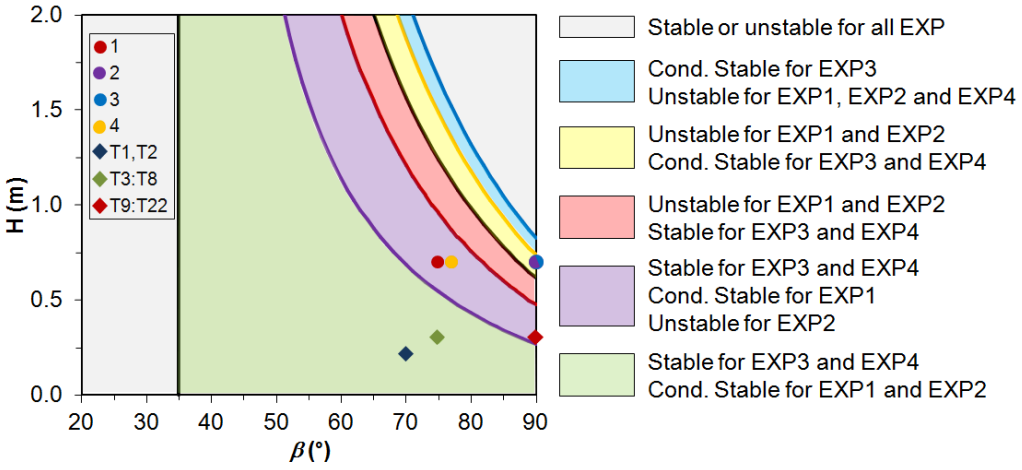

Figure 8-3 Stability charts: summary of all experiments. 1, 2, 3, 4: Initial bank geometry of EXP1, EXP2, EXP3, EXP4, respectively; T1 to T22: initial bank geometry of preliminary test from T1 to T22.

A general conceptual sketch of bank profile evolution interpreted by using this concept is reported in Figure 8-4.

EXP1. The initial bank geometry is in the region of conditionally stable conditions (Figure 8-2A), that means that it should remain stable until the apparent cohesion would decrease. Actually, as observed before, the bank is subject to an initial failure. This is not predicted by the stability chart for a series of reasons, including: (1) it is not a rotational failure involving the whole bank, but occurring on the lower portion of the bank; (2) this failure can be associated to the sudden stress release due to removal of the panel, and to the poor compaction of the sediment in that zone due to the non verticality of the bank. The initial failure in turn generates additional stress release on the upper portion and induces a series of cantilever failures. Subsequent failures are associated to increasing pore water pressures (during this phase the upper bound moves towards the left with decreasing apparent cohesion, decreasing the region of conditional stability). The packed eroding bank moves towards the left of the chart (progressively decreasing the slope), while a new bank of loose sediment is progressively deposited at a slope approximately equal to the angle of repose.

EXP2. In this case the bank starts from unstable conditions (Figure 8-2B). This is due to the increase in bank slope, and lower initial apparent cohesion. In fact, an overall failure immediately occurs after the panel removal. After remodelling the bank, a new failure affects the entire bank, so the profile moves rapidly towards left in the chart (decreasing bank slope), while a loose bank is generated at the angle of repose.

EXP3. In this case, it is evident how the presence of a small percentage of cement changes the stability chart, with a much wider region of stable conditions, and a very narrow region of conditionally stable conditions. Nevertheless, the bank is again in a conditionally stable region (Figure 8-2C). It has been verified that the bank remains in this region even considering the uncertainty of the effective cohesion, e.g. varying *c'* in the range 1.81-2.42 kPa (see section 8.5 and Figure 8-5).

A change in stability conditions can be due to a decrease of apparent cohesion and/or to some modification of bank geometry by other factors. In fact, the bank remains stable until erosion due to loss of matric suction, occurring with positive pore water pressures (submerged conditions), starts to manifest on the bank toe.

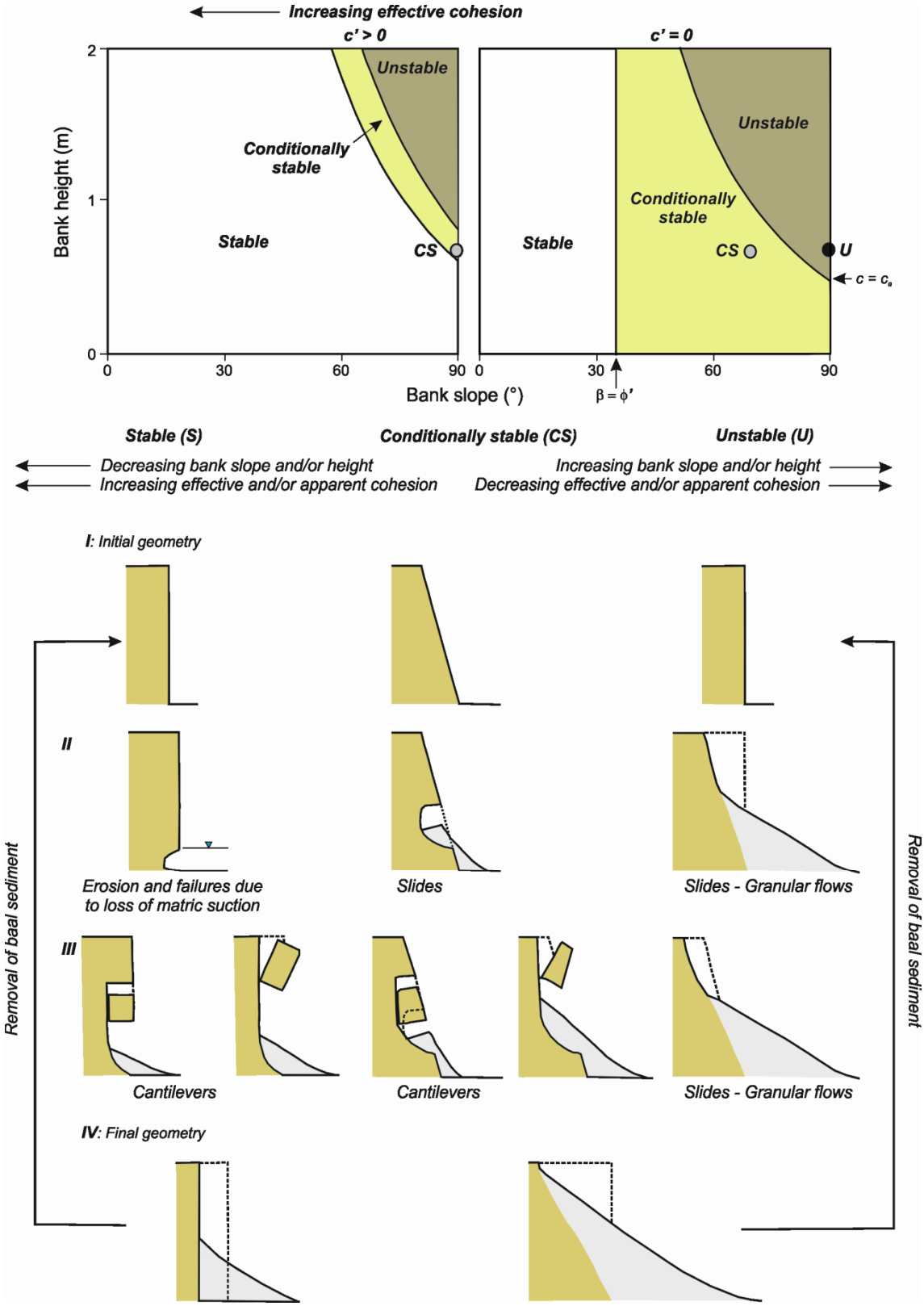

Figure 8-4 Conceptual sketch of bank profile evolution, depending on initial conditions.

At the end, after the occurrence of cantilever failures, the bank geometry of the cohesive portion moves to a slightly lower bank slope, while a new wedge of loose material is formed at the bank toe, but with a height significantly lower than the previous experiments.

EXP4. In this case, the bank is below and on the left of both the bounding limits (Figure 8-2D), meaning that it can maintain a stable configuration. The stability is guaranteed by the combination of two factors: the initial geometry and the presence of cement. This allowed the bank to be stable during all the phases of the experiment.

The bank trajectories shown in the conceptual sketch of Figure 8-4 illustrate the occurrence of different dominant processes, starting from different initial bank conditions (I), although some common points can be recognized.

The second phase of instability (II) is dominated by slides and granular flows, in case of loose sediment, and by erosion due to loss of matric suction, in case of slightly cemented sediment.

The third phase (III) is dominated by the progressive instability of the upper portion by cantilever failures (excluding the unstable banks where cantilevers are unlikely to occur).

The final geometry (IV) is distinct in the two cases: (a) in case of loose sediment, the final geometry is the same, independent from the previous bank profile evolution, and corresponds to a plane slope with angle of about the angle of repose of the material; (b) in case of slightly cemented sediment, the final geometry of the intact sediment is almost identical to the initial one (parallel retreat of a near-vertical bank), but with the addition of a wedge of loose sediment with a slope equal to the angle of repose. To return to the initial geometry, a removal of the sediment accumulated at the base is required (according to the concept of basal endpoint control: Thorne, 1982).

In the case of unstable geometry, a temporary increase in shear strength is also required to see such geometry as stable, and this would be possible by an increase in matric suction (i.e. during a relatively dry period) (see for example Rinaldi and Casagli, 1999; Simon et al., 2000; Rinaldi et al., 2004), but these geometries are rare in nature if the sediment has no effective cohesion. Removal of sediment at the

bank toe can also occur within a flow event (not only during following events): in such a case the result will be to increase the rate of retreat (i.e. Luppi et al., 2009). Actually the cycle of processes can occur more times during a runoff event, if fluvial erosion removes delivered sediments at the bank toe. In such a case the mass failures would not be limited to the ascending phase of the hydrograph but may also occur during the descending phase. Further investigations would be needed to detail this conceptual model with varying bank characteristics and introducing the removal of basal sediment delivered by bank failures. These aspects can be crucial in the prediction and interpretation of the planimetric evolution of straight and meandering rivers (see for instance Kobayashi et al., 2008; Dulal et al., 2009).

8.3 Parameters uncertainties

The stability charts represent a tool to explain processes observed during the experiments. Nevertheless, as mentioned, these analyses are affected by uncertainties due to the difficulties in measuring the shear strength parameters ϕ' and the angle ϕ^b of the bank material employed to construct the bank. Therefore, a series of analyses were undertaken in order to verify if the interpretations were still meaningful for a range of values of shear strength parameters. Specifically, for each experiment two stability charts were created as follows:

(1) Two different curves were created assuming ϕ'equal to 30° and 40°, while the angle ϕ^b was kept constant at 15°.
(2) Two different curves were created assuming ϕ^b equal to 5° and 35°, while the angle ϕ' was kept constant at 35°.

The value ϕ^b=5° was assumed as a minimum value to take account for the presence of apparent cohesion, while ϕ^b=35° is the maximum admissible value. In fact, for definition, the highest value of the angle ϕ^b corresponds to the value of the friction angle ϕ'. Figure 8-5 summarizes the results of these analyses.

For all the experiments, the initial conditions predicted by the stability charts do not change within the values of the shear strength ranging between 30° and 40° (e.g. the initial condition of the bank in EXP1 and EXP3 is conditionally stable within the range, see Figure 8-5 cases A1 and C1). Therefore, this analysis confirmed that ϕ'=35° may be considered a reliable value.

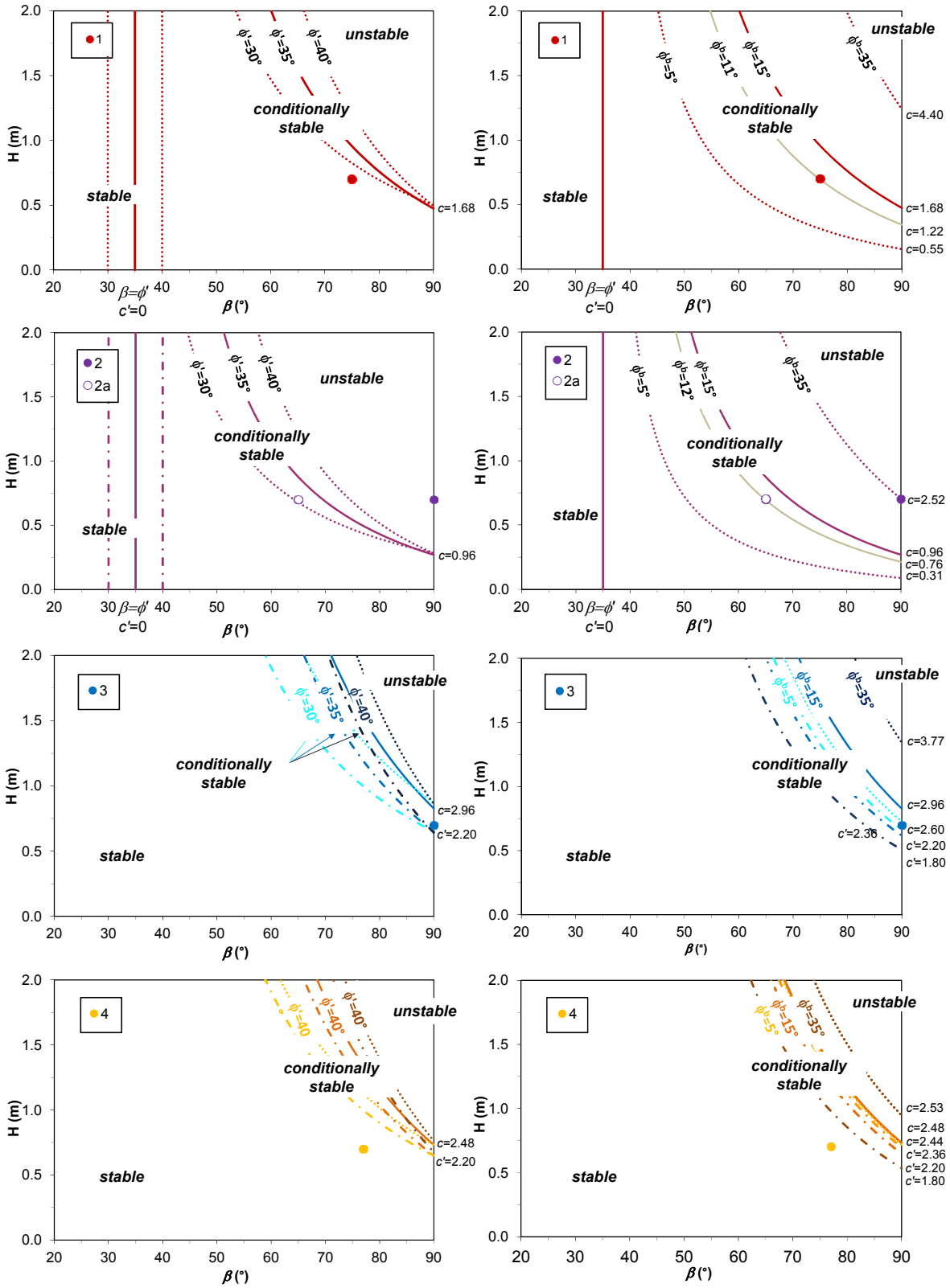

Figure 8-5 Stability chart for a range of ϕ' (30÷40°) and ϕ^b (5÷35°). 1-4 are the initial bank geometries of the experiments EXP1 to EXP4, respectively. c and c' are expressed in KPa.

On the opposite, in the cases EXP1 and EXP2, low values of the angle ϕ^b would lead the initial geometry of the banks to lay within the unstable instead of the conditionally stable region (Figure 8-5 cases A2 and B2).

The search of the curve which divides these regions passing through the initial bank geometry, provided values of ϕ^b equal to 11° and 12° for EXP1 and EXP2, respectively. Considering that failures in these two experiments occurred when the water stage were very low, these values may be considered in agreement with the value assumed in the analyses (ϕ^b=15°). Moreover, similarly to previous researches (e.g. Casagli et al., 1999; Rinaldi et al., 2004) where the apparent cohesion was found to represent a substantial component of the total shear strength in cohesive banks, these analyses highlighted how the apparent cohesion plays a key role also on the stability of coarse grained banks. In fact, the presence of apparent cohesion allowed the banks in EXP1 and EXP2 (at the start of the test, i.e. the position of 2a in Figure 8-2) to be conditionally stable.

Moreover, given that the effective cohesion due to the presence of cement was estimated through the limit equilibrium analysis for the cantilever failure occurred in EXP3, for the cases EXP3 and EXP4 the curves associated with c_a=0 were defined assuming the corresponding values of c' associated with ϕ^b=5° and ϕ^b=35° (Figure 8-5 cases C2 and D2). Finally, Figure 8-5 also shows how the dimension of the conditionally stable region may vary with the value ϕ^b (e.g. it is wider for ϕ^b=35°).

8.4 Conclusions

Riverbanks composed of coarse, granular sediment can have a markedly different erosion mechanism than fine-grained, cohesive banks. Failures in coarse riverbanks tend to occur during the rising phase up to the peak of the hydrograph, mainly due to the disappearance of apparent cohesion. Further failures could be possible during the remaining part of the hydrograph. The rate of retreat would increase in case fluvial entrainment removes failed sediment accumulated at the bank toe.

Erosion and failures due to loss of matric suction are significant processes in this type of banks. A basal scour was often observed during the rising phase, and explained as consequence of disappearance of apparent cohesion in loose sediment. In slightly cemented sediment, additional factors can be the development of positive

pore water pressures, increase in unit weight of sediment, and the infiltration along the boundary of different layers.

Interpretation of the results by using stability charts clearly show, on a quantitative basis, that the processes of instability observed during the experiments are in most cases the results of a superimposition of factors of initial (geometric) instability, and progressive reduction of apparent cohesion during the experiments. Apparent cohesion is sufficient to maintain a stable bank in loose material, but only for low bank height and/or slopes, and unstable conditions can be triggered when bank material becomes saturated. A very limited percentage of cement is able to explain a markedly different behaviour in terms of stability, mechanisms and timing of failure. These results may have relevant implications in terms of modelling of bank stability and planform evolution of river channels.

9. Synopsis

9.1 Summary and conclusions

Riverbank retreat results from a complex combination of fluvial erosion processes and mass failure mechanisms and affects a wide range of physical, ecological and socio-economic issues in the fluvial environment. It represents an important factor in driving planform changes, meander development and channel width adjustments in alluvial rivers.

Although in their natural state, rivers generally migrate freely across their floodplains, with eroding banks representing the norm rather than the exception, bank erosion may also be a significant river management problem given that it may be responsible for: loss of farmlands, damage to structures and infrastructures adjacent to the river channel, and delivery of excessive volumes of sediment to downstream reaches which in turn, may cause turbidity problems. These negative impacts make bank erosion closely related to the risk assessment.

Knowledge of the spatial and temporal trends and dominant processes of channel adjustment is central to plan and implement maintenance or mitigation measures to reduce economic and environmental risk associated with the channel instability.

Despite the undoubted importance of riverbank retreat processes, many aspects of fluvial erosion and instability occurring in gravel-bed rivers are still not well understood.

Although in recent years many progresses have been made in understanding and modelling bank erosion processes, the accurate quantification of the shear stresses exerted by the flow on the bank area, and consequently of the fluvial erosion rate, continues to be a challenging issue.

Further investigations are also needed to provide a better understanding of processes occurring on riverbank totally or partially composed of relatively coarse sediments, which are common in gravel-bed rivers. Traditionally, morphodynamic models of river planform evolution oversimplify their complex behaviour considering fluvial entrainment and erosion as the dominant, if not exclusive, mechanism of retreat for such banks.

The study was organized to provide a general framework of analysis at different spatial scales. It aimed to give a contribution to the knowledge of riverbank

processes addressing particular attention to the near bank shear stress estimation and to the processes involving coarse grained banks.

Different analyses, for each spatial scale, were carried out based on field surveys, numerical and physical modelling, using as a reference study case the Cecina River (Tuscany, Central Italy). A summary of the main results is provided herewith.

Catchment scale:

Summary of the analyses: Analyses at the catchment scale mainly aimed to provide a cognitive frame of the Cecina River. Riverbank processes along the entire length of the river were studied based on field survey data carried out by means of geomorphologic tools. The analyses aimed to identify the variability of bank features (geometry and composition), the dominant mechanisms of retreat and their spatial distribution.

Different methods to predict lateral instabilities were also undertaken in order to pinpoint causes and factors which control the occurrence of different mechanisms of retreat. Results provided by the application of the Stream Power model and the Erosion and Mobility Indexes were compared with values of bank retreat acquired through GIS analyses on aerial photos. Hence, their ability to predict the location of instabilities was evaluated.

Main results:

- Cecina riverbanks are mostly composite, having slopes and heights highly variable and percentage of coarse gravels decreasing downstream.
- Mass failures and fluvial erosion processes are distributed for the entire length of the river.
- Apparently, there is no relation between mass failures and bank geometry, while the relation between processes and composition is more evident: non-cohesive banks are prone to debris and rotational failures, composite banks are mostly subject to cantilever, while in cohesive banks shallows slides prevail. Observation of mass failure processes occurring on non-cohesive banks motivated the laboratory experiments carried out at the bank scale.
- In the case of Cecina River, a tendency in downstream energy reduction and the increasing cohesive bank sediments partly explain the downstream distribution of bank retreat (slight trend of decreasing rates of retreat). However, local channel conditions (presence of bars, curvature, etc.), that are

not taken into account into the predictive models, are probably key factors to explain most of the local lateral instability. The following reasons may explain why tested models failed in providing accurate predictions for the study case: (1) the absence of consideration of bank strength; (2) the small dimension of the Cecina River compared to those catchments employed to develop and test the models; (3) the lack of measured data and the use of input data obtained through regressions.

- In conclusion, although the tested models represent an important tool for river management issues due to their simplicity, further investigations and case studies are needed to better explore these research gaps. At the state of the art, in order to better understand processes and their triggering causes providing the peaks in riverbank retreat, specific models have to be employed at the reach scale, depending on the channel morphology. Therefore results of the analyses carried out at the catchment scale motivated the analyses undertaken at the reach scale.

Reach scale:

Summary of the analyses: Using as reference study case the reach which experienced the highest rate of retreat, different analyses were undertaken with the specific objective of testing methods to estimate the rate of riverbank retreat in the perspective of definition of risk due to fluvial erosion. Based on data collected at the selected reach, the values of the near-bank shear stresses exerted by the flow on two banks were computed through steady flow analyses combined with shear stress models for a range of discharges.

The output of the hydraulic and shear stress modes were utilized, together with the fluvial erosion model, flow data and measured retreat, for the calibration of the unknown erodibility parameter. The erodibility parameter for gravel obtained via calibration employing the two-dimensional model, is higher to balance the lower shear stresses computed with the River2D model (or with River2D combined with Kean and Smith model). Thus, it was not possible to find a unique triplet of erodibility parameters producing rate of retreat with acceptable errors at the same time for all cases. Excluding two cases, small discrepancies between the simulated and the measured values of retreat with erodibility parameters were found for each model.

Nevertheless, since it was not possible to validate the erodibility parameters obtained via calibration, it was not possible to define which of them are correct by far. The analyses only underline that, by applying different models, much carefulness is required in order to avoid over or underestimation of riverbank retreat.

The erodibility parameters were then applied in the excess shear stress formulation (Partheniades, 1965, Arulandan et al., 1980). Fluvial erosion model was coupled with stability analyses to better understand the interactions between different processes. Specifically, BSTEM model was employed to estimate the factor of safety for planar failure and cantilever. Compared to models applied in previous studies for bank stability analyses (e.g. the SLOPE model employed by Rinaldi et al., 2008a), BSTEM represents a less complex alternative and a solution for practical purposes. Two examples of coupling bank stability and fluvial erosion were undertaken by applying BSTEM model on eroded profiles. The latter were obtained through the excess shear stress model by employing the Kean and Smith model based on velocity estimated through River2D. The analyses predicted the occurrence of a planar failure only in the case of flow event with low return period (1 year).

The analysis proposed here allowed the assessment of risk for a specific cross section of the channel. The presence of structures and infrastructures was not taken into account. Notwithstanding uncertainties on values of the near-bank shear stress exist, due to the impossibility to make direct measurements of the velocities, the goal of this analysis is represented by the development of a framework to estimate the risk due to fluvial erosion in terms of economical loss due to loss of lands. This model may be employed to build site specific co-axial graphs by applying appropriate erodibility parameters.

The characterization of risk in this study, solely based on loss of farmland (without structures) due to fluvial erosion process, allowed to obtain a direct relation between the economical loss and the physical process which represents the damage (loss of land). Mass failures which contribute to bank retreat are not directly modelled, but they are implicitly accounted for. In fact, at a time scale of years or decades, as usually risk analyses are studied, the retreat at the toe of the bank may be awarded to the entire height of the

bank. This assumption is justified by field evidences showing subvertical bank profiles induced by failure of cantilevered blocks having confined thickness. This explains why fluvial erosion at the toe of the bank may be recognized as the dominant process which controls the overall retreat in the long-term. While this assumption can be accepted in long-term analyses, in the short-term, commonly associated with smaller spatial scale, it may oversimplify the natural behaviour of non-cohesive banks. In fact, although morphodynamic models traditionally consider fluvial erosion as the dominant (often the exclusive) mechanism of retreat, field evidences carried out along the Cecina River at the catchment scale, suggested that non-cohesive banks are prone to a range of processes. Hence the necessity to better understand mechanisms of retreat affecting such type of banks, which are very common in gravel-bed rivers, motivated the analyses carried out at the bank scale.

Main results:

- Different combinations of models supplied different results both in quantitative terms and in their distribution. Shear stresses values provided by the 2D model are significantly lower compared to those provided by 1D model. The reliability of values obtained through the 2D modelling is supported by the measures of the critical shear stress obtained by means of the CSM and field observations. Conversely, given the critical shear stress, the values of shear stress computed by 1D model are not consistent with the measured rate of retreat. Therefore the analyses highlighted the inadequacy of 1D modelling to describe bank erosion processes, especially when they occur in reaches having high sinuosity.
- Results of the 2D modelling combined with appropriate near-bank shear stress model, highlight that bank erosion is not governed by extreme events. Conversely, discharges responsible for bank erosion can be even lower than bankfull discharges if they occur for prolonged periods. These results are in agreement with those found by previous studies (Rinaldi et al., 2008a) and can be explained with the presence of the bend which steers the core of the high velocity fluid away from the bank during high flow discharges. Therefore, due to the specific planform configuration, fluvial erosion occurs during particular phases of the hydrograph, whereas it is ineffective at higher peak discharges.

- Coupling fluvial erosion and mass failure processes using straightforward models enabled medium term analyses and resulted in dominant fluvial erosion process. In fact, failures were triggered by deep underscour at the bank toe which in turn was formed by fluvial erosion. Note that mass failure models are developed for cohesive banks, being therefore not completely reliable in case of composite banks.

Main contributions of the analyses at the reach scale:

- The coupling of 2D hydraulic model with near-bank shear stress model and bank stability model provided a method which takes account for different processes responsible for bank retreat occurring along gravel-bed rivers. The selection of straightforward models makes this method suitable at the temporal scale of years or decades.
- Development of a method based on numerical modelling which provides an estimation of risk due to fluvial erosion, in monetary terms.

Riverbank scale:

Summary of the analyses: A series of laboratory physical experiments were carried out with the specific aim of investigating the basic processes controlling the stability of relatively coarse, granular bank sediments.

The Cecina River was again used as a reference study case, and the bank reconstructed in the laboratory was intended to mimic a coarse-grained layer of the basal portion of a typical bank profile of this river.

After a series of initial tests, four main experiments were carried out in a glass walled tank, where a bank model was built with bank angles varying from 75° to 90°, bank height of 70 cm, and same sediment mixture (60% gravel, 40% sand), but with the addition of 1% of cement in the third and fourth experiment. During the experiments, the bank was subject to a given hydrograph associated with a static oscillation of the water level and corresponding variations in pore water pressures were measured. Flow entrainment was not modelled for technical limitations of the experimental setup. While this was obviously a limitation, it allowed for the exploration of how the stability of a coarse bank is affected by processes associated to bank geometry and changing pore water pressures, independently of flow. To allow for a better interpretation of results and to discuss the reciprocal role

and relative importance of geometric factors and pore water pressure conditions, some geotechnical analysis was performed. Specific bank stability analyses for observed failures were not possible due to a number of factors, including the difficulty in clearly identifying the failure surface, the absence of specific models for some of the observed mechanisms, and the uncertainty in the shear strength parameters. Therefore, the use of a more general approach based on the construction of stability charts, where the overall stability of the bank is analysed rather than the stability associated with specific mechanisms was preferred. This type of approach can be applied to predict the likelihood of bank failure for each of the experiments, after defining its initial geometric conditions (slope and height) and shear strength properties.

Main results:

- The physical modelling showed marked differences in the behaviour of coarse grained banks compared to that of fine-grained, cohesive banks.
- Failures in coarse riverbanks tend to occur during the rising phase up to the peak of the hydrograph, mainly due to the disappearance of apparent cohesion. Further failures could be possible during the remaining part of the hydrograph, although they were never observed during the experiments. The rate of retreat would increase in case fluvial entrainment removes failed sediment accumulated at the bank toe.
- Erosion and failures due to loss of matric suction are significant processes in this type of banks. A basal scour was often observed during the rising phase and it was explained as consequence of disappearance of apparent cohesion in loose sediment. In slightly cemented sediment, additional factors can be the development of positive pore water pressures, increase in unit weight of sediment, and the infiltration along the boundary of different layers.
- The analyses clearly showed, on a quantitative basis, that the processes of instability observed during the experiments are in most cases the results of a superimposition of factors of initial (geometric) instability and progressive reduction of apparent cohesion during the experiments. Apparent cohesion is sufficient to maintain a stable bank in loose material, but only for low bank height and/or slopes. Unstable conditions can be triggered when bank material becomes saturated.

- A very limited percentage of cement is able to explain a markedly different behaviour in terms of stability, mechanisms and timing of failure.

Main contributions of the analyses at the bank scale:

The experimental methodology here presented represents a novelty at the state art in the geomorphology field. In fact, although recently some physical experiments were undertaken, these few examples were carried out on fine-grained sandy sediments and focused on the seepage processes (Fox et al., 2006, 2007; Wilson et al., 2007; Lindow et al., 2009). No physical models dealing with coarse grained banks (gravel and sand) were found in previous researches. The experiments substantiated the occurrence of a range of mass failure processes, providing an important a contribution in understanding processes occurring in such type of riverbanks.

Links across the scales:

The framework presented in this study allowed to select different methods of analyses depending on the spatial scale of interest and specific aims within each scale. For each scale, an attempt of identifying parameters which play the dominant role in riverbank retreat processes was made. This identification was considered the first step to develop mathematical linkages between different scales. Analyses at the catchment scale did not allow to detect parameters governing channel migration on the Cecina River. However, recent studies (e.g. Barker et al., 2009, Parker et al., 2011) confirm that unit stream power, together with bedload analysis, may explain the development of channel morphology. Therefore, it should not be excluded that unit stream power and bedload, based on more consistent measured data, could be key parameters in riverbank dynamics at the catchment scale and that their inclusion in reach scale analyses could improve comprehension of processes.

At the reach scale, fluvial erosion at the toe of the bank was recognized as the main process which controls the overall retreat in the long-term. Moreover, analyses on the Cecina River pointed out how the presence of curvature makes fluvial erosion to occur only within a certain range of discharge. Therefore, at the risk of grossly oversimplifying the problem, near-bank shear stress and curvature may be considered as the dominant parameters in long-term riverbank retreat processes at the reach scale. Their inclusion in catchment and bank scale analyses could offer further insight into riverbank processes.

At the flow event temporal scale, laboratory experiments highlighted the importance of sediments cohesion and cementation in bank stability and in the type of failure. Therefore it could be advisable to take account for the presence of cement in short-term reach scale analyses.

From a modelling point of view, results underlined difficulties in combining analyses carried out at the catchment scale with those at the reach scale. As a matter of fact, catchment scale models (stream power and lateral indexes) based on empirical formula seem excessively straightforward to be included in analyses at the reach scale. On the other hand, the extension of reach scale analyses to the entire length of the river appears to be not feasible. In fact, the onerous efforts to estimate the near-bank shear stress and to define bank material properties (particularly erodibility parameters) make reach scale modelling not suitable for the catchment scale analyses.

The possibility to mathematically link reach and riverbank scale through an analytical model is more realistic, even if at the state of the art not yet feasible. The next section provides suggestions for further developments in this direction.

9.2 Outlook for further research

Based on the experience achieved in the present study, more efforts would be required in order to better understand processes occurring on banks of gravel-bed rivers. Future developments are suggested hereafter.

Catchment scale

The application of the Stream Power and lateral indexes at the Cecina catchment revealed the inability of these models to predict the location of instabilities along the entire length of the river. Some reasons to explain why the application of these models to the study case was not successful have been already discussed in Section 9.1. However, given that input data employed in the present study mostly derived from regressions, it cannot be excluded that higher accuracy of input data could provide better correlation with measured riverbank retreat. In order to address problems of limited data, the use of new approaches, such as CAFES (Barker et al., 2009), which combines Flood Estimation Handbook systems with high resolution digital elevation model, are suggested.

Finally, the close correlation between bed-load transport rate and the critical stream power per unit bed area, recently explored by Parker et al. (2011), suggests that a reach-based sediment balance approach could be helpful to predict areas of morphological instability within the fluvial system.

Reach scale

Analyses carried out at this spatial scale are founded on fluvial erosion modelling which, in turn, is based on the erodibility parameters, represented by the critical shear stress and the erodibility coefficient. The parameterization of the two latter requires further investigation, because they are affected by a high degree of uncertainty due to their seasonal variability. Therefore more efforts are required in order to obtain repeated in site measure aiming to describe the temporal variability of the erodibility parameters. The uncertainty increases in case of non-cohesive material given that direct measures (like Jet test or CSM) are not available for this material. Thus, some reliable alternative in situ test is needed.

Further progresses are also required to investigate different aspects following described:

- *Applicative developments*: Starting from the proposed framework for the characterization of risk due to fluvial erosion, maps of risk could be achieved by applying the model along a reach of the river. A starting point to trace such maps may be represented by the application of the model to several cross sections closely located each others. Note that maps of risk due to riverbank retreat should be frequently updated, given that lines which define areas affected by different degrees of risk shift according to bank retreat itself.
- *Modelling developments:* In this study the choice of selecting straightforward models is justified by the necessity of modelling riverbank retreat at the temporal scale of years, as commonly required in risk management issues. Further efforts would be desirable in order to make automatic the proposed procedure, with particular reference to the inclusion of near-bank shear stress model and geometry updating. The application of sophisticated morphodynamic models at the state of the art would have been anyway not sufficient to describe processes responsible for channel retreat. In fact channel migration is usually modelled through fluvial erosion processes.

Therefore, further progresses are needed to include a bank stability model. CONCEPT (Langendoen, 2000) represents an exception given that it includes a bank stability model. Nevertheless, its use of one-dimensional hydraulics, as highlighted by the results of the present study, makes the model not appropriate to describe the flow field along meanders, where the highest rates of retreat are measured.

Riverbank scale

At the riverbank scale, based on the results obtained through the physical modelling described in this study, further progresses would be desirable. Future developments can deal with both additional physical modelling and numerical implementation, as following pointed out.

- *Physical modelling*: Further experiments are needed to include the effect of the shear stress. Such experiments could give an important contribution in understanding the effects of the interaction between fluvial erosion and mass failure processes, which are unpredictable a priori.
- *Numerical modelling*: Additional efforts are needed in order to develop a model able to describe processes affecting coarse grained bank which were observed during the experiments. Once developed, the bank model could be included in existing morphodynamic models.

  The inclusion of appropriate mass failures models combined with the fluvial erosion model at the case of Cecina River would significantly modify the dynamic modelling of riverbank retreat. The laboratory experiments carried out with a static tank showed that riverbank retreat may occur also in absence of the shear stresses exerted by the flow. It is possible suppose that fluvial erosion is the dominant process of retreat occurring when the shear stress exerted by the flow exceeds the critical shear stress of bank material. Nevertheless, observations carried out during the physical experiments let us presume that riverbank retreat may also occur when the shear stress is lower than the critical shear stress. In this condition retreat could take place through mass failures caused by potential variations of pore water pressure. Nonetheless the excess of the critical shear stress is required to remove the failed material at the toe of the bank and thus it is necessary for the channel evolution. The combination of mass failures and fluvial erosion processes

could produce not obvious superposition effects. The direct consequence of coupling different processes very likely would lead to different estimations of erodibility parameters, given that in the present study they have been obtained taking account only for fluvial erosion process.

BIBLIOGRAPHY

Abernethy, B., Rutherfurd, I.D., 1998. Where along a river's length will vegetation most effectively stabilize stream banks? Geomorphology 23, 55–75.

Abernethy, B., Rutherfurd, I.D., 2000. The effect of riparian tree roots on the mass-stability of riverbanks. Earth Surf. Process. Landf. 25, 921–937.

Abernethy, B., Rutherfurd, I.D., 2001. The distribution and strength of riparian tree roots in relation to riverbank reinforcement. Hydrol. Process. 15, 63–79.

Amiri-Tokaldany, E., Darby, S.E., Tosswell, P., 2003. Bank stability analysis for predicting land loss and sediment yield. J. Am. Water Resour. Assoc. 39, 897–909.

Arulanandan, K., Gillogley, E., Tully R., 1980. Development of a Quantitative Method to Predict Critical Shear Stress and Rate of Erosion of Natural Undisturbed Cohesive Soils. Report GL-80-5, U.S.Army Engineers, Waterways Experiment Station: Vicksburg, Mississippi.

Awad, M.M., Darwich, T., 2009. Evaluating sea water quality in the coastal zone of north Lebanon using TELEMAC-2D. Lebanese Science Journal, Vol. 10, No. 1.

Bagnold, R.A., 1966. An approach to the sediment transport problem from general physics, USGS Professional Paper, 422-I, Washington, DC.

Bagnold, R.A., 1977. Bed load transport by natural rivers. Water Resources Research 13: 303–312.

Barker, R., Dixon, L., Hooke, J., 1997. Use of terrestrial photogrammetry for monitoring and measuring bank erosion. Earth Surf. Process. Landf. 22, 1217–1227.

Barker, D.M., Lawler, D.M., Knight, D.W., Morris, D.G., Davies, H.N., Stewart E.J., 2009. Longitudinal distributions of river flood power: the combined automated flood, elevation and stream power (CAFES) methodology. Earth Surf. Process. Landforms 34, 280–290.

Bendix, J., 1999. Stream power influence on southern Californian riparian vegetation. Journal of Vegetation Science 10: 243–252.

Bendix, J., Hupp, C.P., 2000. Hydrological and geomorphological impacts on riparian plant communities. Hydrological Processes 14:2977–2990.

Bledsoe, B.P., Watson, C.C., 2001. Logistic analysis of channel pattern thresholds: meandering, braiding, and incising. Geomorphology 38 (2001) 281–300.

Boavida, I., Santos, J., Lourenço, J., Cortes, R.M.V., Ferreira, T., Pinheiro, A., 2009. Using a Two Dimensional Approach To Evaluate Channel Rehabilitation In A Mediterranean Stream (Southern Portugal). Proceedings 4th European Conference on River Restoration, Italy, Venice, S. Servolo Island, 16-21 June, 2008. 749-758.

Bradford, J.M., Piest, R.F., 1977. Gully wall stability in loess-derived alluvium. Soil Science Society of America Journal 41, 115-122.

Bradford, J.M., Piest, R.F., 1980. Erosional development of valley-bottom gullies in the Upper Midwestern United States. In: Coates, D.R., Vitak, J.D. (Eds), Thresholds in Geomorphology, pp. 75-101.

Bravard, J.P., Amoros, C., Pautou, G., 1986. Impact of civil engineering works on the successions of communities in a fluvial system. A methodological and predictive approach applied to a section of the Upper Rhone river, France. Oikos, 47(1), 92±111.

Bravard, J.P., Kondolf, G.M., Piégay, H., 1999. Environmental and societal effects of channel incision and remedial strategies. In: Darby S.E. and Simon A. (Eds), Incised River Channels, John Wiley & Sons Ltd., 303-341.

Brice, J.C., 1982. Stream Channel Stability Assessment, January 1982, Final Report. U.S. Department of Transportation, FHA, Washington, D.C

Brierley, G.J, Murn, C.P., 1997. European impacts on downstream sediment transfer and bank erosion in Cobargo catchment, New South Wales, Australia. Catena 31 119– 36.

Brierley, G.J. & Fryirs, K.A., 2005. Geomorphology and River Management. Applications of the River Styles Framework. Blackwell Publishing, 398 pp.

Buijse, A.D., Coops, H., Startas, M., Jans, L.H., Van Geest, G.J., Grifts, R.E., Ibelings, B.W., Oosterberg, W., Roozen, F.M., 2002. Restoration strategies for river floodplain along large lowland rivers in Europe. Freshwater Biology, 47, pp 889-907.

Bull, L.J., 1997. Magnitude and variation in the contribution of bank erosion to the suspended sediment load of the River Severn, UK. Earth Surf. Process. Landf. 22, 1109–1123.

Carson, M.A., Kirkby, M.J., 1972. Hillslope Form and Process. Cambridge Univ. Press, Cambridge.

Casagli, N., Rinaldi, M., Gargini, A., Curini, A., 1999. Pore water pressure and streambank stability: Results from a monitoring site on the Sieve River, Italy, Earth Surf. Processes Landforms, 24, 1095– 1114.

Cassuli, V., Cattani, E., 1994. Stability, accuracy and efficiency of a semi-implict method for three-dimensional shallow water flow. Computers and Mathematics with Applications 27:99–112.

Chang, H.H., 1979. Minimum stream power and river channel patterns. Journal of Hydrology 41: 303–327.

Chen, D., Duan, J.G., 2006. Modeling width adjustment in meandering channels. J. Hydrology 321, 59–76.

Chen, D., Duan, J.G., 2008. Case study: two-dimensional model simulation of channel migration processes in West Jordan River, Utah. J. Hydraul. Eng. 134, 315-327.

Chiang, S.W., Tsai, T.L., Yang, J.C., 2010. Conjunction effect of stream water level and groundwater flow for riverbank stability analysis. Environ Earth Sci.

Chow, V.T., 1959. Open-channel Hydraulics, McGraw-Hill, New York.

Church, M., 1992. Channel morphology and typology. in Calow, P. and Petts, G. E.: (Eds), The Rivers handbook. Hydrological and Ecological Principles. Blackwell Scienti®c Publications, Oxford. pp. 126±143.

Cohen, T.J., 2003. Late Holocene floodplain processes and post-European channel dynamics in a partly confined valley of New SouthWales Australia. Unpublished PhD Thesis. School of Geosciences, University of Wollongong, NSW, Australia.

Collison, A.J.C., 2001. The cycle of instability: stress release and fissure flow as controls on gully head retreat. Hydrological Processes 15, 3-12.

Constantine, C.R., Dunne, T., Hanson, G.J., 2009. Examining the physical meaning of the bank erosion coefficient used in meander migration modeling. Geomorphology 106 (2009) 242–252.

Costard, F., Dupeyrat, L., Gautier, E., Carey-Gailhardis, E., 2003. Fluvial thermal erosion investigations along a rapidly eroding river bank: Application to the Lena River (central Yakutia), Earth Surf. Processes Landforms, 28, 1349–1359.

Coulthard, T.J., Van de Wiel, M.J., 2007. Quantifying fluvial nonlinearity and finding self-organized criticality? Insights from simulations of river basin evolution. Geomorphology 91(3–4): 216–235.

Couper, P., Maddock, I., 2001. Subaerial River Bank Processes and Interaction with other Bank Erosion Mechanisms on the River Arrow, Warwickshire, UK. Earth Surface Processes and Landforms, 26 (6). pp. 631-646.

Couper, P.R., 2004. Space and time in river bank erosion research: A review: Area, v. 36, no. 4, p. 387–403.

Crosato, A., 1990. Simulation of meandering river processes, Communications on Hydraulic and Geotechnical Engineering. Technical Rep., Civil Engineering Dept., Delft University of Technology, Delft, The Netherlands.

Crosato, A., 2008. Analysis and modelling of river meandering. Ph.D. Thesis Delft University of Technology, IOS Press, Amsterdam, Netherlands, ISBN 978-1-58603-915-8, 251 p.

Dapporto, S., 2001. Non-vertical jet testing of cohesive streambank toe material. School of Geography, University of Nottingham, in collaboration with USDA-ARS National Sedimentation Laboratory, Oxford, Mississippi.

Dapporto, S., Rinaldi, M., Casagli, N., 2001. Mechanisms of failure and pore water pressure conditions: analysis of a riverbank along the Arno River (Central Italy). Engineering Geology 61, 221-242.

Dapporto, S., Rinaldi, M., 2003. Modelling of river bank retreat by combining fluvial erosion, seepage and mass failure. Geophys. Res. Abstracts, EGS-AGU-EUG Joint Assembly, Nice, France, 6–11 April 2003.

Dapporto, S., Rinaldi, M., Casagli, N., Vannocci, P., 2003. Mechanisms of riverbank failure along the Arno River, Central Italy. Earth Surface Processes and Landforms 28, 1303-1323.

Darby, S.E., Thorne, C.R., 1996. Development and testing of river-bank stability analysis. J. Hydraul. Eng. 122 (8), 443–454.

Darby, S.E., Gessler, D., Thorne, C.R., 2000. Technical communication – Computer program for stability analysis of steep, cohesive riverbanks. Earth Surface Processes and Landforms, 25, 175-190.

Darby, S.E, Alabyan, A., van de Wiel, M.J., 2002. Numerical simulation of bank erosion and channel migration for meandering rivers. Water Resources Research 38: 1163.

Darby, S.E., Rinaldi, M., Dapporto, S., 2007. Coupled simulations of fluvial erosion and mass wasting for cohesive riverbanks. J. Geophys. Res., 112.

Darby, S.E., Trieu, H.Q., Carling, P.A., Sarkkula, J., Koponen, J., Kummu, M., Conlan, I., Leyland, J., 2010. A physically based model to predict hydraulic erosion of fine-grained riverbanks: The role of form roughness in limiting erosion. Journal of Geophysical Research, Vol. 115, F04003, 20 pp., 2010.

de Deckere, E.M.G.T., Tolhurst, T.J., de Brouwer, J.F.C., 2001. Destabilisation of cohesive intertidal sediments by infauna. Estuarine, Coastal and Shelf Science 53, 665–669.

Defew, E.C., Tolhurst, T.J., Paterson, D.M., 2002. Site-specific features influence sediment stability of intertidal flats. Hydrology and Earth System Sciences 6 (6), 971–981.

Department of the Army U.S. Army Engineer District, Alaska, 2006. Kenai River Bank Erosion. Technical Report Kenai, Alaska.

Downs, P.W., Simon, A., 2001. Fluvial geomorphological analysis of the recruitment of large woody debris in the Yalobusha river network, Central Mississippi, USA. Geomorphology 37: 65–91.

Downward, S.R., Gurnell, A.M., Brookes, A., 1994. A methodology for quantifying river channel planform change using GIS: variability in stream erosion and sediment transport. In Proceedings of the Canberra Symposium, Canberra, 1994. Olive LJ, Loughran RJ, Kesby JA (eds). International Association of Hydrological Sciences, Publication 224; 449–456.

Duan, J.G., 2005. Analytical approach to calculate rate of bank erosion. Journal of Hydraulic Engineering, 131(11), 980-990.

Dulal, K.P., Kondo, Y., Kimura, I., Shimizu, Y., Parker, G., 2009. Prediction of evolution process in free meandering rivers using 2D numerical model considering slump blocks and inner bank deposition. In: Vionnet, C., García, M.H., Latrubesse, E.M., Perillo, G.M.E. (Eds), River, Coastal and Estuarine Morphodynamics: RCEM 2009, Proceedings RCEM 2009 Symposium, 21-25 September 2009, Santa Fe, Argentina, Taylor & Francis Group, London, 627-634.

Eaton, B.C., Church, M., Millar, R.G., 2004. Rational regime model of alluvial channel morphology and response. Earth Surface Processes and Landforms 29, 511-529.

Eaton, B.C., 2006. Bank stability analysis for regime models of vegetated gravel-bed rivers. Earth Surface Processes and Landforms 31, 1438-1444.

Ferguson, R., 1987. Hydraulic and Sedimentary Controls of Channel Pattern. In: Richards, K. (ed), River Channels. Environment and Process. Basil Blackwell, Oxford, UK, pp. 129-158.

Finlayson, D.P., Montgomery, D.R., Hallet, B., 2002. Spatial coincidence of rapid inferred erosion with young metamorphic massifs in the Himalayas: Geology, v. 30, p. 219–222.

Finlayson, D.P., Montgomery, D.R., 2003. Modelling large-scale fluvial erosion in geographic information systems. Geomorphology 53, 147-164.

Florsheim, J.L., Mount J.F., Chin A., 2008. Bank erosion as a desirable attribute of rivers. Bioscience. 58:519-529.

Fonstad, M.A., Marcus, W.A., 2003. Self-organized criticality in riverbank systems. Annals of the Association of American Geographers 72(4): 320–339.

Fonstad, M.A., Marcus, W.A., 2010. High resolution, basin extent observations and implications for understanding river form and process. Earth Surf. Process. Landforms 35, 680–698.

Fox, G.A., Wilson, G.V., Periketi, R.K., Cullum, R.F., 2006. Sediment transport model for seepage erosion of stream-bank sediment. J. Hydraul. Eng. 11, 603-611.

Fox, G.A., Wilson G.V., Simon A., Langendoen E., Akay O., Fuchs J.W., 2007. Measuring streambank erosion due to groundwater seepage: correlation to bank pore water pressure, precipitation and stream stage. Earth Surface Processes and Landforms 32: 1558–1573.

Frascati, A., Lanzoni, S., 2009. Morphodynamic regime and long-term evolution of meandering rivers. Journal of Geophysical Research, 114, F02002.

Fredlund, D.G., Morgenstern, N.R., Widger, R.A., 1978. The shear strength of unsaturated soils. Can.Geotech.J. 15, 312-321.

Fredlund, D.G., Rahardjo, H., 1993. Soil Mechanics for Unsaturated Soils, John Wiley & Sons, New York, 482 pp.

Friend, P.L., Ciavola, P., Cappucci, S., Santos, R., 2003. Biodependent bed parameters as a proxy tool for sediment stability in mixed habitat intertidal areas. Continental Shelf Research 23, 1899–1917.

Frissell, C.A., Liss, W.J., Warren, C.E., Hurley M.D., 1986. A Hierarchical Framework for Stream Habitat Classification: Viewing Streams in a Watershed Context. Environmental Management 10(2):199-214.

Gatto, L.W., 2000. Soil freeze–thaw-induced changes to a simulated rill: Potential impacts on soil erosion. Geomorphology, 32: 147–160.

Ghanem, A., Steffler, P., Hicks, F., Katopodis, C., 1995. Twodimensional modeling of flow in aquatic habitats. Water Resources Engineering Report No. 95-S1. University of Alberta, Canada.

Goodson, J.M., Gurnell, A.M., Angold, P.G., Morrissey, I.P., 2002. Riparian seed banks along the lower River Dove UK – their structure and ecological implications. Geomorphology 47, 45–60.

Govers, G., 1991. Rill erosion on arable land in central Belgium: Rates, controls and predictability. Catena 18, 133–155.

Gray, D.H., 1978. Role of woody vegetation in reinforcing soils and stabilising slopes. Proc. Symp. Soil Reinforcing and Stabilising Techniques, Sydney, Australia, pp. 253–306.

Grissinger, E.H., 1982. Bank erosion of cohesive materials. In R.D.Hey, J.C.Bathurst & C.R.Thorne (eds), "Gravel-bed Rivers", Wiley, Chichester, 273-287.

Gurnell, A.M., 1997. Channel change on the River Dee meanders 1946–1992, from the analysis of air photographs Regulated Rivers: Research and Management 13 13–26.

Haeri, A.M., Hosseini, S.M., Toll, D.G., Yasrebi, S.S., 2005. The behaviour of an artificially cemented sandy gravel. Geotechnical and Geological Engineering 23, 507-560.

Hanson, G.J., 1990. Surface erodibility of earthen channels at high stresses. Part II - Development of an in situ testing device. Transactions of the American Society of Agricultural Engineers 33(1): 132-137.

Hanson, G.J., Simon, A., 2001. Erodibility of cohesive streambeds in the loess area of the midwestern USA. Hydrological Processes 15: 23-38.

Hanson, G.J., Cook, K.R., 2004. Apparatus, test procedures, and analytical methods to measure soil erodibility in situ. Applied Engineering in Agriculture. 20(4):455-462.

Hasegawa, K., 1989. Universal bank erosion coefficient for meandering rivers. Journal of Hydraulic Engineering, 115, No.6, 744-765.

Hervouet, J.M., Bates, P., 2000. The TELEMAC Modelling System. Hydrological Processes - Special Issue, 14(13): 2207–2208.

Hicks, F.E., Steffler, P. M., 1992. Characteristic dissipative Galerkin scheme for open-channel flow. Journal of Hyd. Res., 118(2), 337-352.

Hoek, E., Bray, J.W., 1981. Rock Slope Engineering, Revised 3rd Edition, Istitution of Mining and Metallurgy, London.

Hooke, J.M., 1980. Magnitude and distribution of rates of river bank erosion. Earth Surface Processes and Landforms, 5, 143-157.

Hopson, T.M., 1999. The form drag of large natural vegetation along the banks of open channels, M. S. thesis, 114pp., Univ of Colo., Boulder.

Howard, A.D., McLane, C.F., 1988. Erosion of cohesionless sediment by groundwater seepage. Water Resources Research 24, 1659-1674.

Howard, A.D., 1994. Badlands. In: Abrahams, A.D. and Parsons, A.J. (Eds), Geomorphology of Desert Environments. Chapman and Hall, London, pp. 213–242.

Hutton, D., Emdad Haque, C., 2003. Patterns of Coping and Adaptation Among Erosion-Induced Displacees in Bangladesh: Implications for Hazard Analysis and Mitigation. Natural Hazards 29: 405–421, 2003.

Ikeda, S., Parker, G., Sawai, K., 1981. Bend theory of river meanders. 1. Linear development, J. Fluid Mech. 112, 363-377.

Kartha, V.C., Leutheusser, H.J., 1972. Distribution of tractive force in open channels. J. Hydraul. Div. ASCE 96, 1469–1483.

Katopodis, C., Ghamry, H. K., 2007. Hydrodynamic and physical assessment of ice-covered conditions for three reaches of the Athabasca River, Alberta, Canada. Can. J. Civ. Eng. 34(6): 717–730 (2007).

Kean, J.W., Smith, J.D., 2004. Flow and boundary shear stress in channels with woody bank vegetation. Riparian Vegetation and Fluvial Geomorphology, Water Scie. Appl. Ser., 8, edited by Bennett, S. J., and Simon, A., 237-252, AGU, Washington, D.C.

Kean, J.W., Smith, J.D., 2005. Generation and verification of theoretical rating curves in the Whitewater River Basin, KS. J. Geophys. Res., 110, F04012.

Kean, J.W., Smith, J.D., 2006a. Form drag in rivers due to small-scale natural topographic features:1. Regular sequences. Journal of Geophysical Reserch, Vol. 111, F04009.

Kean, J.W., Smith, J.D., 2006b. Form drag in rivers due to small-scale natural topographic features: 2. Irregular sequences. Journal of Geophysical Reserch, Vol. 111, F04010.

Kean, J.W., Kuhnle, R.A., Smith, J., Dungan, J., Alonso, C.V., Langendoen, E.J., 2009. Test of a method to calculate near-bank velocity and boundary shear stress. Journal of Hydraulic Engineering, 135(7), pp. 588-601.

Kirkby, M.J., Imeson, A.C, Bergkamp, G., Cammeraat, L.H., 1996. Scaling up processes and models from the field plot to the watershed and regional areas. Journal of Soil and Water Conservation 51 391–6

Knight, D., Demetriou, J.D., Hamed, M.E., 1984. Boundary shear in smooth rectangular channels. J. Hydraul. Eng. 110, 405–422.

Knighton, A.D., Nanson, G.C., 1993. Anastomosis and the continuum of channel form. Earth Surface Processes and Landforms, 18, 613-625.

Knighton, D.A., 1998. Fluvial forms and processes: London, Edward Arnold, 377 p.

Knighton, A.D., 1999. Downstream variation in stream power. Geomorphology 29: 293–306.

Kobayashi, K., Dulal, K.P., Shimizu, Y., 2008. Numerical computation of free meandering process of rivers consider-ing the effect of slump block in outer bank region. In: Altinakar, M.S., Kokpinar, M.A., Aydin, I., Cokgor, S., Kirkgoz, S., (Eds), River Flow 2008 - Proceedings of the International Conference on Fluvial hydraulics. Turkey, Kubaba Congress Department and Travel Services, 1289-1296.

Koopaei, K.B., Ervine, D.A., Pender, G., 2003. Field Measurements and Flow Modeling of Overbank Flows in River Severn, U.K. Journal of Environmental Informatics 1 (1) 28-36 (2003)

Kwan, S., 2009. MASC Thesis: A two dimensional hydrodynamic river morphology and gravel transport model. University of British Columbia, Vancouver.

Lacey, R.W., Millar, J.R.G., 2004. Reach Scale Hydraulic Assessment of Instream Salmonid Habitat Restoration. Journal of the American Water Resources Association (JAWRA) 40(6): 1631-1644.

Lam, N.S-N., Quattrochi, D.A., 1992. On the issues of scale, resolution, and fractal analysis in the mapping sciences. Professional Geographer 44 88–98.

Lancaster, S.T., Bras, R.L., 2002. A simple model of river meandering and its comparison to natural channels. Hydrological Processes, 16, 1-26.

Lane, E.W., 1955. Design of stable channels. Trans. Am. Soc. Civil Eng. 120, 1–34.

Lane, S.N., 1998. Hydraulic modelling in hydrology and geomorphology: a review of high resolution approaches. Hydrological Processes 12:1279–1298.

Langendoen, E., 2000. CONCEPTS-Conservational Channel Evolution and Pollutant Transport System. Research Report No. 16. USDA-ARS National Sedimentation Laboratory. Oxford, MS.

Larsen, E.W., 1995. Mechanics and Modeling of River Meander Migration. Ph.D thesis, University of California at Berkeley, Berkeley, California..

Lawler, D.M., 1992. Process dominance in bank erosion systems. In: Lowland Floodplain Rivers: Geomorphological Perspectives, P. A. Carling and G. E. Petts (eds.), John Wiley, Chichester, UK, 117-143.

Lawler, D.M., 1993. Needle ice processes and sediment mobilization on river bends; the River Ilston, West Glamorgan, UK. Journal of Hydrology 150, 81–114.

Lawler, D.M., 1995. The impact of scale on the processes of channelside sediment supply: a conceptual model. In Effects of Scale on the Interpretation and Management of Sediment and Water Quality, IAHS Publication 226, Osterkamp WR (ed.); 175–184.

Lawler, D.M., Thorne, C.R., Hooke, J.M., 1997. Bank erosion and instability. In: Thorne, C.R., Hey, R.D., and Newson, M.D. (Eds), Applied Fluvial Geomorphology for River Engineering and Management. Wiley, Chichester, 137–172.

Lawler, D.M., Grove, J.R., Couperthwaite, J.S., Leeks, G.J.L., 1999. Downstream change in river bank erosion rates in the Swale-Ouse system, northern England Hydrological Processes 13 977–92.

Lee, J.H., Kil, J.T., Jeong, S., 2010. Evaluation of physical fish habitat quality enhancement designs in urban streams using a 2D hydrodynamic model. Ecological Engineering 36:1251–1259.

Leopold, L.B., Maddock, T.Jr., 1953. The Hydraulic Geometry of Stream Channels and Some Physiographic Implications. USGS Professional Paper 252, 57 pp.

Leutheusser, H.J., 1963. Turbulent flow in rectangular ducts. Proc. Am. Soc. Civil Eng. 89, HY3.

Lindow, N., Fox, G.A., Evans R.O., 2009. Seepage erosion in layered stream bank material. Earth Surf. Process. Landforms 34, 1693–1701.

Luppi, L., Rinaldi, M., Teruggi, L.B., Darby, S.E., Nardi, L., 2009. Monitoring and numerical modelling of riverbank erosion processes: a case study along the Cecina River (Central Italy). Earth Surface Processes and Landforms.

MacDonald, T.E., 1991. Inventory and analysis of stream meander problems in Minnesota. M.S. Thesis, University of Minnesot

Malavoi, J.R., Bravard, J.P., Piégay, H., Hérouin, E., Ramez, P., 1998. Détermination de l'espace de liberté des cours d'eau. Guide technique no. 2, SDAGE RMC, 39 pp.

Marcus, W.A., Fonstad, M.A., 2008. Optical remote mapping of rivers at sub-meter resolutions and watershed extents. Earth Surface Processes and Landforms 33: 4–24.

Marston, R.A., Girel, J., Pautou, G., Piégay, H., Bravard, J.P., Arneson, C., 1995. Channel metamorphosis, floodplain disturbance, and vegetation development: Ain River, France. Geomorphology 13: 121–131.

McEwen, LJ., 1994. Channel planform adjustment and stream power variations on the middle River Coe, West Grampian Highlands, Scotland. Catena 21: 357–374.

McLean, S.R., Smith, J.D., 1986. A model for flow over two-dimensional bed forms, J. Hydraul. Eng., 112, 300-317.

Millar, R.G., Quick, M.C., 1993. Effect of bank stability on geometry of gravel rivers. Journal of Hydraulic Engineering, 119, 12, 1343-1363.

Millar, R.G., 2000. Influence of bank vegetation on alluvial Channel patterns. Water Resour. Res. 36 (4), 1109–1118.

Miller, A.J., 1995. Valley morphology and boundary conditions influencing spatial patterns of flood flow. In: Costa, J.E., Miller, A.J., Potter, K.W., Wilcok, P.R. (Eds.), Natural and Anthropogenic Influences in Fluvial Geomorphology: The Wolman Volume. American Geophysical Monograph, pp. 57–81.

Miyake, M., 1965. Transformation of the atmospheric boundary layer over inhomogeneous surfaces, M.S. thesis, Dep. of Atmos. Sci, Univ. of Wash, Seattle.

Morgenstern, N.R., Price, V.E., 1965. The analysis of the stability of general slip surfaces. Geotechnique, 15, 79-93.

Mosselman, E., 1998. Morphological modelling of rivers with erodible banks. Hydrological Processes 12: 1357–1370.

Nagata, N., Hosoda, T., Muramoto, Y., 2000. Numerical analysis of river channel processes with bank erosion. J. Hydraul. Eng. 126, 243–252.

Nagata, N., Hosoda, T., Muramoto, Y., 2002. Numerical analysis of river channel processes with bank erosion. Journal of Hydraulic Engineering 126: 243–252.

Nanson, G.C., Hickin, E.J., 1986. A statistical analysis of bank erosion and channel migration in western Canada. Geological Society of American Bulletin 97: 497–504.

Nardi, L., Rinaldi, M., 2010. Modelling riverbank retreat by combining reach-scale hydraulic models with bank-scale erosion and stability analyses. In: Dittrich A., Koll K., Aberle J. & Geisenhainer P. (Eds), Proceedings River Flow 2010, Bundesanstalt für Wasserbau, Braunschweig, September 2010, 1285-1291.

Odgaard, A. J., 1987. Streambank erosion along two rivers in Iowa Water Resources Research 23 1225–36.

Odgaard, A.J., 1989. River meander model. I: Development, II Applications Journal of Hydraulic Engineering, 115: 1433-1464.

Olsen, N.R.B., 2002. A three-dimensional numerical model for simulation of sediment movements in water intakes with moving option. User's Manual, Department of Hydraulic and Environmental Engineering The Norwegian University of Science and Technology, Trondheim, Norway.

Olsen, N.R.B., 2003. Three-dimensional CFD modeling of self-forming meandering channel. Journal of Hydraulic Engineering 129: 366–272.

Osman, A.M., Thorne, C.R., 1988. Riverbank stability analysis. I: Theory. Journal of Hydraulic Engineering, 114(2), 134-150.

Papanicolaou, T., Wilson, C., Dermisis, D., 2008. The effects of headcut and knickpoint propagation on bridges in Iowa, Iowa City.

Parsons, D.R., Best, J.L., Orfeo, O., Hardy, R.J., Kostaschuk, R., Lane, S.N., 2005. Morphology and flow fields of three-dimensional dunes, Rio Parana, Argentina: Results from simultaneous multibeam echo sounding and acoustic Doppler current profiling. Journal of Geophysical Research – Earth Surface 110(F4): F04S03.

Partheniades, E., 1965. Erosion and deposition of cohesive soils. Journal of the Hydraulics Division, American Society Civil Engineers 91: 105–139.

Paterson, D.M., 1989. Short-term changes in the erodibility of intertidal cohesive sediments related to the migratory behaviour of epipelic diatoms. Limnology and Oceanography 34, 223–234.

Petts, G.E., 1989. Historical analysis of fluvial hydrosystems. In: Historical Change in Large Alluvial Rivers (ed. by G. E. Petts, H. Moller & A. L. Roux), 1-18. J. Wiley, Chichester, UK.

Piégay, H., Bravard, J.P., Dupont, P., 1994. The French water Law: a new approach for alluvial hydrosystem management, French alpin et perialpin stream exemples). In Annual summer symposium of the American Water Resources Association, Effects of human-induced changes on hydrologic systems. Marston RA, Hasfurther VR (eds). American Water Resources Association: Jackson Hole, WY; 371–383.

Piégay, H., Barge, O., Landon, N., 1996a. Streamway concept applied to river mobility/human use conflict management. In First International Conference on New/Emerging Concepts for Rivers. Proceedings Rivertech 96. International Water Resources Association: Chicago; 681– 688.

Piégay, H., Landon, N., Barge, O., Citterio, A., 1996b. Contribution à la définition d'une méthode de détermination de l'espace de liberté des riviéres. CNRS, Agence de l'Eau RMC, 25 pp.

Piégay, H., Cuaz, M., Javelle, E., Mandier, P., 1997. Bank erosion management based on geomorphological, ecological and economic criteria on the Galaure River, France. Regulated Rivers: Research & Management, 13: 433-448.

Piégay, H., Darby, S.E., Mosselman, E., Surian, N., 2005. A review of techniques available for delimiting the erodible river corridor: a sustainable approach to managing bank erosion. River Research and Applications, 21: 773-789.

Pizzutto, J. E., 1984, Bank erodibility of shallow sandbed streams. Earth Surface Processes and Landforms 9 113–24.

Pliefke, T., Sperbeck, S.T., Urban, M., Peil, U., Budelmann, H., 2007. A Standardized Methodology for Managing Disaster Risk – An Attempt to Remove Ambiguity. 5th International Probabilistic Workshop, Ghent, 2007.

Pollen, N., Simon, A., Collison, A., 2004. Advances in assessing the mechanical and hydrologic effects of riparian vegetation on streambank stability. In: Bennett, S.J. and Simon, A. (Eds), Riparian Vegetation and Fluvial Geomorphology. American Geophysical Union, Washington, DC, pp. 125–140.

Pollen, N., Simon, A., 2005. Estimating the mechanical effects of riparian vegetation on stream bank stability using a fiber bundle model. Water Resour. Res. 41:W07025.

Pollen, N., 2006. Temporal and spatial variability in root reinforcement of streambanks: Accounting for soil shear strength and moisture. Catena 69:197–205.

Pollen-Bankhead, N., Simon, A., 2008. Enhanced Application of Root-Reinforcement Algorithms for Bank-Stability Modeling. Earth Surface Processes and Landforms

Prosser, I.P., Hughes, A.O., Rutherfurd, I.D., 2000. Bank erosion of an incised upland channel by subaerial processes: Tasmania, Australia. Earth Surface Processes and Landforms 25, 1011 –1085.

Rana, S.A., Simons, D.B., Mahmood K., 1973. Analysis of sediment sorting in alluvial channels. Journal of the Hydraulics Division – Proceedings of the American Society of Civil Engineers 99: 1967–1980.

Rathburn, S., Wohl, E.E., 2003. Predicting fine sediment dynamics along a pool–riffle mountain channel. Geomorphology 55, 111–124.

Reinfelds, I., Cohen, T., Batten, P., Brierley, G., 2004. Assessment of downstream trends in channel gradient, total and specific stream power: a GIS approach. Geomorphology 60: 403–416.

Reinfelds, I., Lincoln-Smith, M., Haeusler, T., Ryan, D., Growns, I., 2010. Hydraulic assessment of environmental flow regimes to facilitate fish passage through natural riffles: Shoalhaven River below Tallowa dam, New South Wales, Australia. River Research And Applications 26: 589–604.

Reneau, S.L., Drakos, P.G., Katzman, D., et al., 2004. Geomorphic controls on contaminant distribution along an ephemeral stream. Earth Surf. Process. Landf. 29, 1209–1223.

Rinaldi, M., Casagli, N., 1999. Stability of streambanks formed in partially saturated soils and effects of negative pore water pressures: The Sieve River (Italy). Geomorphology 26, 253–277.

Rinaldi, M., 2003. Recent channel adjustments in alluvial rivers of Tuscany, Central Italy. Earth Surface Processes and Landforms, 28(6), 587-608.

Rinaldi, M., Casagli, N., Dapporto, S., Gargini, A., 2004. Monitoring and modelling of pore water pressure changes and riverbank stability during flow events. Earth Surface Processes and Landforms 29, 237–254.

Rinaldi, M., Darby, S.E., 2008. Modelling river-bank-erosion processes and mass failure mechanisms: progress towards fully coupled simulations. In: Habersack, H., Piégay, H., Rinaldi, M. (Eds), Gravel-Bed Rivers 6 - From Process Understanding to River Restoration. Series Developments in Earth Surface Processes, 11, Elsevier, Netherlands, 213-239.

Rinaldi, M., Luppi, L., Mengoni, B., Darby, S.E., Mosselman, E., 2008a. Numerical simulation of hydrodynamics and bank erosion in a river bend. Water Resources Research 44.

Rinaldi, M., Teruggi, L.B., Simoncini, C., Nardi, L. 2008b. Dinamica recente ed attuale di alvei fluviali: alcuni casi di studio dell'Appennino Settentrionale. Il Quaternario, 21(1B), 291-302.

Rossi Romanelli, L., Rinaldi, M., Darby, S.E., Luppi, L., Nardi, L., 2004. Monitoring and modelling river bank processes: a new methodological approach. In: Greco M., Carravetta A. & Della Morte R. (Eds), Proceedings River Flow 2004, Taylor & Francis Group, London, 993-998.

Rutherfurd, I.D., Grove, J.R., 2004. The influence of trees on stream bank erosion: Evidence from rootplate abutments. In: Bennett, S.J. and Simon, A. (Eds), Riparian Vegetation and Fluvial Geomorphology. American Geophysical Union, Washington, DC, pp. 141–152.

Schlichting, H., 1979. Boundary-Layer Theory. McGraw-Hill Book Company, New York.

Scozzafava, R.A., 2008. Metodi per la stima delle tensioni tangenziali esercitate da correnti fluviali ai fini della modellazione dei processi di erosione di sponda. Tesi di Laurea inedita, Corso di Laurea in Ingegneria per l'Ambiente ed il Territorio, Università degli Studi di Firenze.

Selby, M.J., 1982. Hillslope Materials and Processes. Oxford University Press, Oxford, UK.

Seminara, G., 2006. Meanders. Journal of Fluid Mechanics, 554, 271–297.

Simon, A., Wolfe, W.J., Molinas, A., 1991. Mass-wasting algorithms in an alluvial channel model. Proceedings of the 5th Federal Interagency Sedimentation Conference, Las Vegas, Nevada, 2, 8, 22–29.

Simon, A., 1995. Adjustment and recovery of unstable alluvial channels: Identification and approaches for engineering management. Earth Surf. Process. Landf. 20, 611–628.

Simon, A., Curini, A., 1998. Pore pressure and bank stability: The influence of matric suction, In Abt SR, Young- Pezeshk J, Watson CC (eds.), Water Resources Engineering '98, ASCE: Reston; 358-363.

Simon, A., Curini, A., Darby, S.E., Langendoen, E. J., 1999. Streambank mechanics and the role of bank and near-bank processes in incised channels. Incised River Channels, S. E. Darby and A. Simon, eds., John Wiley & Sons Ltd, Chichester, UK, Chapter 6, 123-152.

Simon, A., Curini, A., Darby, S.E., Langendoen, E.J., 2000. Bank and near-bank processes in an incised channel. Geomorphology 35, 193–217.

Simon, A., Collison, A., 2002. Quantifying the mechanical and hydrologic effects of riparian vegetation on streambank stability. Earth Surf. Process. Landf. 27, 527–546.

Simon, A., Thomas, R.E., Curini, A., Shields, F.D. Jr., 2002. Case study: Channel stability of the Missouri River, Eastern Montana. J. Hydraul. Eng. 128 (10), 880–890.

Simon, A., Langendoen, E.J., Collison, A., Layzell, A., 2003. Incorporating bank-toe erosion by hydraulic shear into a bank-stability model: Missouri River, Eastern Montana. Proceedings, EWRL-ASCE, World Water and Environmental Resources Congress, Cd-Rom, 11.

Simon, A., Pollen, N.L., 2006. A model of streambank stability incorporating hydraulic erosion and the effects of riparian vegetation. PROCEEDINGS of the Eighth Federal

Interagency Sedimentation Conference (8thFISC), April 2-6, 2006, Reno, NV, USA, 870-877.

Simon, A., Pollen, N.L., Langendoen, E. J., 2006. Influence of two woody riparian species on critical conditions for streambank stability: Upper Truckee River, California. J. Am. Water Resour. Assoc., 42, 99– 113.

Simons, D.B., Senturk, F., 1977. Sediment Transport Tecnology. Water Resources Pubblications. Forth Collins, Colorado.

Smith, J.D., McLean, S.R., 1977. Spatially averaged flow over a wavy surface, Journal of Geophysical Research, 82, 1735-1746.

Soares-Frazao, S., Le Grelle, N., Spinewine, B., Zech, Y., 2007. Dam-break induced morphological changes in a channel with uniform sediments: measurements by a laser-sheet imaging technique. Jour. Of Hydraulic Research 45 Extra Issue, 87-95.

Soil Conservation Service, 1977. Design of open channels. Engineering Div., Technical Release, No 25, Washington, D.C.

Spinewine, B., Capart, H., le Grelle, N., Soares Frazão, S., Zech, Y., 2002. Experiments and computations of bankline retreat due to geomorphic dam-break floods. Proceedings of River flow 2002, Louvain-la-Neuve, Belgium, September, Vol. 1, 651-661.

Spinewine, B., Zech, Y., 2007. Small-scale laboratory dam-break waves on movable beds. Journal of Hydraulic Research 45 Extra Issue, 73-86.

Steffler, P., 2000. Software River2D. Two dimensional depth averaged finite element hydrodynamic model. University of Alberta, Canada.

Steffler, P., Blackburn, J., 2002. River2D: Two-dimensional depth-averaged model of river hydrodynamics and fish habitats. University of Alberta, Edmonton, Canada.

Surian, N., Rinaldi, M., Pellegrini, L., Audisio, C., Maraga, F., Teruggi, L.B., Turitto, O., Ziliani, L., 2009. Channel adjustments in northern and central Italy over the last 200 years. In: James L.A., Tarhburn S.L., Whittecar G.R. (Eds), Management and Restoration of Fluvial Systems with Broad Historical Changes and Human Impacts, Geological Society of America Special Paper 451, 83-95.

Tarbuck, E.J., Lutgens, F.K., 2002. Earth: An Introduction to Physical Geography. 7th ed., Upper Saddle River, NJ, Prentice Hall.

Teruggi, L.B., Rinaldi, M., 2009. Analysis of planimetric channel changes along the Cecina River (central Italy). Amorosi A. (Ed.) International Proceedings 27th IAS

Meeting of Sedimentologists, Alghero, Italy, 20-23 September 2009. MEDIMOND, 27-30.

Terzaghi, K., 1923. Die Berechnung der Durchlassigkeistziffer des Tones aus Dem Verlauf der Hydrodynamichen Spannungserschei-nungen Akedemie der Wissenschaften in Wien. Matematisch-Naturwissen-Shaftliche Klasse. Sitzungsberichte. Abteilung II, V, 132(3/4), 125±138.

Thomas, H., Nisbet, T. R., 2006. An assessment of the impact of floodplain woodland on flood flows. Water and Environment Journal. Print ISSN 1747-6585.

Thorne, C.R., Tovey, N.K., 1981. Stability of composite river banks. Earth Surface Processes and Landforms 6, 469-484.

Thorne, C.R., Murphey, J.B., Little, W.C., 1981. Bank stability and bank material properties in the bluffline streams of northwest Mississippi. Appendix D. Report to the U.S. Army Corps of Engineers, Vicksburg District Office, on Stream Channel Stability, 258 pp.

Thorne, C.R., 1982. Processes and mechanisms of river bank erosion. In: Hey, R.D., Bathurst, J.C., Thorne, C.R. (Eds), Gravel-bed Rivers. Wiley, Chichester, pp. 227–271.

Thorne, C.R., Osman, A.M., 1988. Riverbank stability analysis. II: Applications. Journal of Hydraulic Engineering, 114(2), 151-172.

Thorne, C.R., 1992. Bend scour and bank erosion on the meandering Red River, Louisiana. In Lowland Floodplain Rivers: Geomorphological Perspectives, Carling PA, Petts GE (eds). John Wiley and Sons: Chichester; 95–115.

Thorne, C.R., Abt, S.R., 1993. Analysis of riverbank stability due to scour and lateral erosion. Earth Surface Processes and Landforms, 18 833-45.

Thorne, C.R., Reed, S., Doorkamp, J.C., 1996. A procedure for assessing river bank erosion problems and solutions. University of Nottingham, National Rivers Authority, R&D Report 28, 48 pp.

Thorne, C.R., 1998. Stream reconnaissance handbook. Geomorphological investigation and analysis of river channels. John Wiley & Sons, Chichester.

Thorne, S.D., D.J. Furbish, 1995. Influences of coarse bank roughness on flow within a sharply curved river bend, Geomorphology, 12, 241-257.

Tolhurst, T.J., Black, K.S., Shayler, S.A., Mather, S., Black, I., Baker, K., Paterson, D.M., 1999. Measuring the in situ erosion shear stress of intertidal sediments with the cohesive strength meter (CSM). Estuarine, Coastal and Shelf Science 49, 281–294.

Tolhurst, T.J., Black, K.S., Paterson, D.M., Mitchener, H., Termaat, R., Shayler, S.A., 2000. A comparison and measurement standardisation of four in situ devices for determining the erosion shear stress of intertidal sediments. Continental Shelf Research 20, 1397–1418.

Tolhurst, T.J., Jesus, B., Brotas, V., Paterson, D.M., 2003. Diatom migration and sediment armouring—an example from the Tagus Estuary, Portugal. Hydrobiologia 503, 183–193.

U.S. Army Corps of Engineers, 1983. Sacramento River and tributaries bank protection and erosion control investigation. California Sediment Transport Studies, Sacramento Dist., US Corps of Eng., Sacramento, CA.

U.S. Army Corps of Engineers, 2002. HEC-RAS River Analysis System. Hydraulic Reference Manual. Version 3.1. U.S. Army Corps of Engineers Hydrologic Engineering Center, Davis, CA, November 2002.

Van De Wiel, M.J., Darby, S.E., 2004. Numerical modeling of bed topography and bank erosion along tree-lined meandering rivers. In: Bennett, S.J. and Simon, A. (Eds), Riparian Vegetation and Fluvial Geomorphology. American Geophysical Union, Washington, DC, pp. 267–282.

Vardy, S., Saunders J.E, Tolhurst, T.J., Davies, P.A., Paterson, D.M., 2007. Calibration of the high-pressure cohesive strength meter (CSM). Continental Shelf Research 27 1190–1199.

Warner, R.F., 1992. Floodplain evolution in a New South Wales coastal valley. Australia: spatial process variations. Geomorphology 4, 447– 458.

Wasklewicz, T.A., Anderson, S., Liu, P.S., 2004. Geomorphic context of channel locational probabilities along the lower Mississippi River, USA. Geomorphology 63: 145–158.

Watts, C.W., Tolhurst, T.J., Black, K.S., Whitmore, A.P., 2003. In situ measurements of erosion shear stress and geotechnical shear strength of the intertidal sediments of the experimental managed realignment scheme at Tollesbury, Essex, UK. Estuarine, Coastal and Shelf Science 58, 611–620.

Wellmeyer, J.L., Slattery, M.C., Phillips, J.D., 2005. Quantifying downstream impacts of impoundment on flow regime and channel planform, lower Trinity River, Texas. Geomorphology 69, 1–13.

Wheaton, J.M., Pasternack, G.B., Merz, J.E., 2004a. Spawning habitat rehabilitation—I. Conceptual approach and methods. Journal of River Basin Management 2, 3–20.

Wheaton, J.M., Pasternack, G.B., Merz, J.E., 2004b. Spawning Habitat Rehabilitation—II. Using hypothesis development and testing in design, Mokelumne River, California, U.S.A. Journal of River Basin Management 2, 21–37.

Whipple, K.X., Hancock, G.S., Anderson, R.S., 2000. River incision into bedrock: mechanics and relative efficacy of plucking, abrasion and cavitation. Geological Society of America Bulletin 112: 490–503.

Whiting, P.J., Dietrich, W.E., 1989. The roughness of alluvial surfaces: An empirical examination of the influence of size and heterogeneity and natural packing, Eos Trans. AGU, 70(43), 1109.

Wiele, S.M., Graf, J.B., Smith, J.D., 1996. Sand deposition in the Colorado River in the Grand Canyon from flooding of the Little Colorado River. Water Resources Research 32, 3579–3596.

Wiele, S.M., Torizzo, M., 2005. Modelling of sand deposition in archaeologically significant reaches of the Colorado River in Grand Canyon, USA. In: Bates, P.D., Lane, S.N., Ferguson, R.I. (Eds.), Computational Fluid Dynamics: Applications in Environmental Hydraulics. John Wiley and Sons, pp. 357–394.

Wilson, C.A.M.E., Stoesser, T., Olsen, N.R.B., Bates P.D., 2003. Application and Validation of Numerical Codes in the Prediction of Compound Channel Flows. Proceedings of the Institution of Civil Engineers, UK, Water and Maritime Engineering, No. 153, pp. 117-128.

Wilson, G.V., Periketi, R.K., Fox, G.A., Dabney, S.M., Shields, F.D., Cullum, R.F., 2007. Soil properties controlling seepage erosion contributions to streambank failure. Earth Surface Processes and Landforms 32, 447-459.

Wynn, T.M., 2004. The Effects of Vegetation on Streambank Erosion. PhD Dissertation, Virginia Polytechnic Institute and State University, Blacksburg, Virginia.

Wynn, T.M., Henderson, M.B., Vaughan, D.H., 2008. Changes in streambank erodibility and critical shear stress due to subaerial processes along a headwater stream, southwestern Virginia, USA. Geomorphology, 97(3-4), pp 260-273.

Wu, R.S., Mao, C.T., 2007. The assessment of river ecology and Habitat using a two-dimensional hydrodynamic and habitat model. Journal of Marine Science and Technology, Vol. 15, No. 4, pp. 322-330.

Yu, H., Salgado, R., Sloan, W., Kim, J., 1998. Limit analysis versus equilibrium for slope stability. J Geotech Geoenviron Eng ASCE 124(1):1–11

Zech, Y., Soares-Frazão, S., Spinewine, B., le Grelle, N., 2008. Dam-break induced sediment movement: Experimental approaches and numerical modelling. Journal of Hydraulic Research 46, 176-190.